'Real-Time' Biomolecular Interaction Analysis

Novel Applications and Developments

A dissertation submitted for the degree of

Doctorate of Philosophy

by

John G. Quinn, B.Sc.,

1999

Under the supervision of Prof. Richard O' Kennedy,

School of Biotechnology,

Dublin City University,

Dublin 9, Ireland.

Declaration

I hereby certify that the material, which I now submit for assessment on the programme of study leading to the award of Doctor of Philosophy, is entirely my own and has not been taken from the work of others save to the extent that such work has been cited and acknowledged within the text of my work.

Signed: John Quinn Date: 3/March/99

Acknowledgements

I wish to thank Prof. Richard O'Kennedy for his constant support and guidance over the past few years. Special thanks to my friends at DCU and elsewhere for their unreserved camaraderie and common appreciation of base humour. I'm indebted to my family whose immense support (£,☺, 😐, ☛) made it possible for me to pursue this work. Finally, I reserve particular thanks for Lena, who I coerced into proof-reading this thesis, for her companionship (♥) and invaluable counsel.

Abstract

The work described in this thesis involves the application of direct 'real-time' biomolecular interaction analysis using existing SPR-based biosensors and the development of novel alternative SPR-based technologies. These systems were applied to the investigation of whole cell binding to an immobilised ligand. Solid-phase blood typing was demonstrated by employing monoclonal anti-A IgG and anti-B IgM as affinity ligands for the capture of washed whole red blood cells (RBC). Protein A affinity-capture of anti-A IgG was used as an alternative to direct immobilisation thereby facilitating surface regeneration.

A new non-'real-time' fibre optic-based system (BIACORE Probe) was evaluated using the same affinity-capture format and was successfully applied to direct whole blood typing. Non-'real time' analysis limited the data quality. Therefore, a similar 'real-time' fibre optic device was constructed. In addition, a miniature SPR-based biosensor employing a single platform optical configuration was developed with a view towards the production of a smaller, cheaper and portable alternative to the existing range of instruments.

Determination of kinetic rate constants using direct 'real-time' biosensors has proved more complex than suggested by early investigators and has lead to misleading conclusions from artifactual data. A model study, employing the interaction of CD4 and glutathione-s-transferase with specific monoclonal antibodies, investigated experimental and data analysis methods for the determination of reliable rate constants. In addition, novel assays for determination of the active analyte concentration without the requirement for a standard curve were examined.

Abbreviations

π	pie (i.e. 3.142)
χ^2	Chi squared (i.e. averaged squared residual per data point)
Δn	refractive index change
ΔT	temperature change
Δt	time difference
2D	two dimensional
A	blood group antigen A
ADC	analogue to digital converter
B	blood group antigen B
BGAA	blood group associated antigen
BIA	biomolecular interaction analysis
BSA	bovine serum albumin
bsAb	bispecific antibody
CCD	close circuit diode
CDR	complementarity determining regions of antibody
CF	correction factor
CM	carboxymethylated
Con A	concanavalin A
conc (c)	concentration
DNA	deoxyribonucleic acid
dsFv	disulphide-stabilised Fv antibody derivative
EDC	N-ethyl-N'-(dimethylaminopropyl) carbodiimide
EDTA	ethylenediaminetetra-acetic acid
ELISA	enzyme-linked immunosorbent assay
Fab	binding region of antibody above the hinge region
Fc	constant region of antibody molecule
FIA	flow injection analysis
FTIR	frustrated total internal reflection
Fv	variable binding region of antibody
GST	glutathione-s-transferase
HBS	hepes buffered saline
I/O	input/output
IgG	immunoglobulin class G
IgM	immunoglobulin class M

K_a	association affinity constant
k_a	association rate constant
K_d	dissociation affinity constant
k_d	dissociation rate constant
k_{obs}	observed rate constant
LED	light emitting diode
Lm	mass transport rate of analyte in bulk
Ln	natural logarithm
Log	logarithmic
Lr	Onsager coefficient of reaction flux
mAb	monoclonal antibody
max	maximum
MTL	mass transport limitation
MW	molecular weight
n	refractive index
NHS	N-hydroxysuccinimide
nm	nanometre
O	blood group antigen O
PBS	phosphate buffer saline
PC	personal computer
PDA	photodiode array
pH	log of the hydrogen ion concentration
R	regression coefficient
RBC	red blood cells
RD	reduced dextran
R_{eq}	equilibrium binding response
RI	refractive index
R_{max}	maximum binding response
RNA	ribonucleic acid
scFv	single chain Fv antibody derivative
SE	standard error
SPR	surface plasmon resonance
TE	transverse electric
TIR	total internal reflection
TM	transverse magnetic
UV	ultraviolet

V_H	variable region of heavy chain
V_L	variable region of light chain
X	immobilised ligand

Units

µg	microgram
(k)Da	(kilo) Daltons
µl	microlitre
µM	micromoles
°C	degrees Celcius
AU	arbitrary units
cm	centimetres
g	grams
h	hours
K	degrees Kelvin
kg	kilogram
l	litre
m	metre
M	molar
mg	miligram
MHz	megahertz
min	minute
ml	millilitre
mm	millimetres
mM	nanomolar
mol	molar
pg	picograms
rpm	revolutions per minute
RU	response units
sec, s	seconds
v/v	volume per unit volume
w/v	weight per unit volume

Publications

Reinartz, H.W., **Quinn, J.G.**, Zanker, K. and O'Kennedy, R. (1996). Bispecific multivalent antibody studied by 'real-time' interaction analysis for the development of an antigen-inhibition enzyme-linked immunosorbent assay, Analyst, **121**; 767-771.

Quinn, J.G., O'Kennedy, R., Smyth, M., Moulds, J., and Frame, T. (1997). Detection of blood group antigens utilising immobilised antibodies and surface plasmon resonance. J. Immunol. Methods, **206**; 87-96.

Liu, B., Smyth, M., **Quinn, J.G.**, Bogan, D. and O' Kennedy, R. (1996). Development of regenerable amperometric immunosensor for 7-hydroxycoumarin. Electroanalysis, **8**, 619-622.

Quinn, J.G., Patel, P., Fitzpatrick, B., Manning, B., Dillon, P., Daly, S., O'Kennedy, R. Alcocer, M., Lee, H., Morgan, M, Lang, K. (1999). The use of regenerable, affinity ligand-based surfaces for immunosensor applications. Biosensors and Bioelectronics. Submitted.

Presentations

Use of a bispecific antibody in sensor-based analytical systems. **Quinn, J.G.,** Reinartz, H.W and O'Kennedy, R. (1995). Abstract for Sensors and Signals III, Sept. 26-27th, Malahide, Co. Dublin, Ireland, p19.

BIACORE an optical biosensor. **Quinn, J.G.** and O'Kennedy, R. (1996). Irish Medical Devices Association, Hudson Bay Hotel, Athlone, April 24th.

'Real-time' biospecific interaction analysis: Sciences sixth sense. **Quinn, J.G.** and O'Kennedy, R. (1998). Area Section, Biochemistry Society, Dublin City University, Sept. 9-10th.

Courses

Laboratory-based training course on advanced analytical techniques (1995). Department of Food Chemistry and Biochemistry, University College, Cork, Nov. 27th.

Molecular Sensor Technology Euro-Course (1996). Advanced sensors workshop, Institute of Biotechnology, University of Cambridge, July 4-10th.

Table of Contents

Chapter 1

Introduction

1.0.0 Introduction

Molecular recognition forms the basis of all life, and the study and exploitation of these binding events is at the heart of both applied and fundamental biological research. Classical methods that allow the visualisation of biomolecular interactions provide end-point measurements and rely on various labels such as fluorophores, enzymes, or radioactive isotopes. However, direct detection technology for 'real-time' biomolecular interaction analysis has become available within the past decade (Vadgama and Crump, 1992; Robinson, 1993) and is routinely employed throughout the biological sciences. Many interactions naturally occur at interfaces, where one of the interactants is anchored to a natural support (e.g. cell membrane). Similarly, the new generation of instruments monitor molecular interactions occurring at interfaces that can be tailored to mimic natural environmental conditions (Chaiken *et al.*, 1992). Characteristically, these biosensing technologies combine mass sensitive transducers, biointerfacial chemistry and the specificity of a wide range of affinity ligands (Löfås *et al.*, 1991). The specificity of the biosensor is dictated by the choice of ligand to be immobilised and the biointerfacial layer provides a suitable environment for the interaction of the immobilised ligand with the target analyte. A non-invasive transduction system can detect the progress of the interaction without interfering with the binding event. Therefore, these three components will be discussed with particular emphasis on the elements that were explored in the following studies. A general review of current developments is presented and a specific introduction precedes each experimental chapter.

'Real-time' biomolecular interaction analysis provides answers to fundamental questions such as:

1. How strong are binding interactions during biomolecular recognition events?
2. What is the binding mechanism?
3. How fast do affinity pairs bind and dissociate?
4. How does molecular structure affect the biological function of macromolecules?
5. Where are the active binding sites located on the interacting biomolecules?
6. What is the concentration of the analyte?
7. What is the stoichiometry of the interaction?

Biomolecular interaction analysis can be applied to the study of any biomolecular interaction pair that express affinity for each other. A wide range of affinity ligands have been studied including antibodies, antibody fragments, genetically engineered antibody derivatives, lectins, membrane receptors, nucleic acids, gene fusion proteins, glycolipid hormone receptors, pesticides, viruses, bacteria, and cell-ligand interactions (Soderlind *et al.*, 1992; Bondeson *et al.*, 1993; Lowman and

Wells, 1993; Minunni and Mascini, 1993; Nice *et al.*, 1993; Soderlind *et al.*, 1993; Mani *et al.*, 1994; Nissim *et al.*, 1994; Scalice *et al.*, 1994; Nilsson *et al.*, 1995; Parsons and Stockley, 1997; Myszka, 1997, Fratamico *et al.*, 1998). Furthermore, 'real-time' biomolecular interaction analysis has proved to be a powerful tool for the discovery and/or selection of new affinity-based molecules from synthetic and natural sources. Many of these biomolecules are described in more detail is section 1.4.0. Considerable savings in time and reagent consumption make direct 'real-time' biosensors valuable bench-top analysers for both pure and applied biochemistry. *Figure 1.0.0* summarises the key advantages of 'real-time' biomolecular interaction analysis technology.

Figure 1.0.0. Diagram illustrating the key features of direct 'real-time' biosensor technology. Broken line (---) indicates optional peripheral technology.

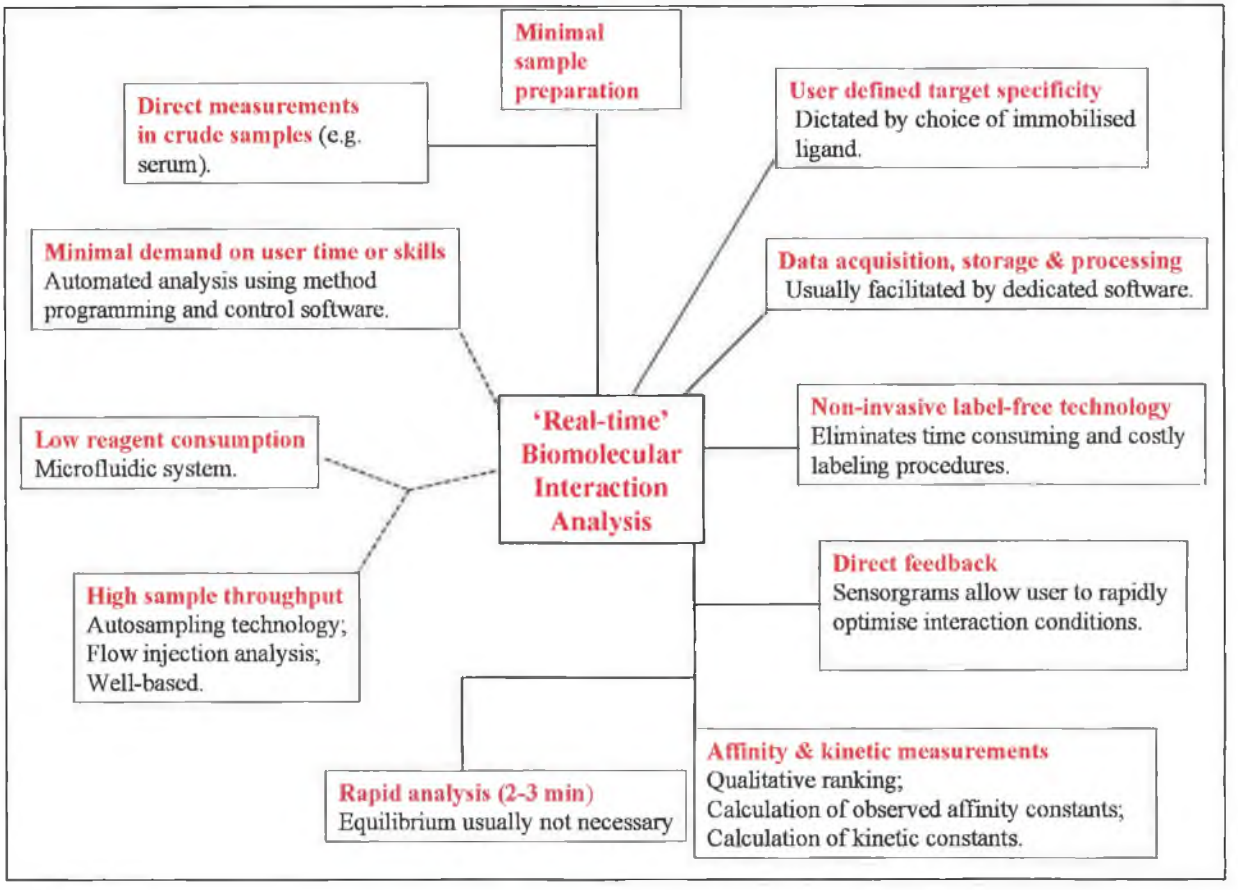

Typically, 'real-time' biomolecular interaction analysis involves the immobilisation of one partner of an affinity pair (e.g. antibody) onto the sensor surface and continuous monitoring of surface mass changes on exposure to a solution containing the other partner (e.g. antigen) (Stenberg *et al.*, 1991). Non-covalently associated analyte can be removed using chaotrophic solutions, allowing the functionalised surface to be used repeatedly (e.g. typically > 50 binding-regeneration cycles). A 'real-time' plot of the sensor response against time reveals a great deal of information (e.g.

specificity, concentration, kinetics) concerning the interaction. The main advantage of 'real-time' biomolecular interaction analysis is its ability to evaluate the kinetics of biomolecular interactions (Malmborg *et al.,* 1992; Fortune, 1993). Visual ranking of the rate of association and dissociation from 'real-time' interaction curves (sensorgrams) provides a rapid means of assessing interactions. More comprehensive characterisation requires calculation of the observed rate constants, while estimation of kinetic constants demands careful experimental design and data analysis.

1.1.0 Direct 'Real-Time' Biosensors.

Currently, there are several commercially available evanescent field-based biosensors. BIACORE AB (Uppsala, Sweden), have released six instruments. The BIACORE 1000/2000 series are fully automated SPR-based biosensors that consist of a disposable sensor chip, an optical detection unit, an integrated microfluidic cartridge, an autosampler, method programming and control software. Sample plugs are delivered to the sensor surface via a continuous buffer stream flowing across the surface. Dedicated BIAlogue software facilitates precise control of the integrated system including, data acquisition, processing, display and analysis (Fägerstam and O'Shannessy, 1993). Less expensive manually controlled alternatives include the BIAlite™ and the BIACORE X™. The latest additions are the BIACORE probe™ and BIACORE 3000™. The BIACORE Probe™ is a fibre optic SPR-based biosensor the enables 'dipstick'-type sampling. However, it is severely limited by non-'real-time' data acquisition. The BIACORE 3000™ is virtually identical to the BIACORE 2000™ but includes enhanced software for instrument control and data analysis. A number of other biosensing systems are available and include the IAsys (Affinity Sensors, Cambridge, U.K.), the IBIS (Intersens Instruments), the BIOS-1 (Artificial Sensing Instruments (ASI), Zurich) and the piezoelectric-1000 immunobiosensor (Universal Sensors Inc., Louisiana).

1.2.0 Transduction Technologies

Direct 'real-time' biomolecular interaction analyses imposes considerable demands on transduction technologies. The majority of biosensors that are capable of 'real-time' biomolecular interaction analysis can be described as generic evanescent wave-based mass sensors (Brecht and Gauglitz, 1995; Hutchinson, 1995) or direct mass sensors (i.e. piezoelectric transduction) and are reviewed in the following section. An evanescent field is an exponentially decaying electromagnetic field that is generated normal to the sensor surface and effectively probes refractive index changes within its penetration depth. Changes in refractive index are related to mass changes according to $dn/dc = 0.188$ ml/g, where n is the refractive index and c is the protein concentration. In addition, it is important to precisely control the temperature at the interaction surface since the refractive index at

the interaction surface increases with increasing temperature (i.e. temperature coefficient of refractive index for aqueous solutions is 1.25 x 10^{-4}/K (section 5.2.1.4)).

1.2.1 ***Evanescent Field and Transduction.*** Evanescent field (or evanescent wave) transduction techniques rely on total internal reflection. Total internal reflection occurs when light above a critical angle that is incident through a high refractive index material (e.g. glass) is reflected at the boundary with a low refractive index medium (e.g. sample medium). An electric vector component of the incident light generates an evanescent field normal to the surface that penetrates into the low refractive index material (e.g. aqueous solutions) by approximately one wavelength.

1.2.2 ***Principle of Surface Plasmon Resonance.*** Many of the sensors discussed earlier are based on the Kretschmann configuration for surface plasmon resonance (SPR). The principle of SPR is outlined in more detail in section 5.1.1 and, hence, a brief introduction will be presented. Consider the conditions for the generation of an evanescent wave, as outlined above (section 1.2.1). with a thin (~ 50 nm) metal layer deposited on the high refractive index material (e.g. glass slide). Light undergoing total internal reflection impinges on the metal surface. At a particular angle of incidence (or wavelength) the evanescent wave resonates with the surface plasmon (i.e. free oscillating electrons), resulting in the absorption of light and a corresponding minimum in the intensity of the reflected light (Yeatman, 1996). The position of the resonance minimum is sensitive to changes in the refractive index at the gold surface and can be located in 'real-time'. Hence, a plot of the resonance shift (expressed in arbitrary response units) against time allows changes in the refractive index within the penetration depth of the evanescent field (i.e. interaction surface) to be monitored. Gold is the preferred metal for SPR-based biosensing because it is chemically inert (less surface contamination) and generates strong plasmons that result in sharp reflectance minima (De Brunn *et al.*, 1992). Angle-dependent SPR can be generated using monochromatic light and wavelength-dependent SPR can be generated using polychromatic light and are both discussed in more detail in section 5.2.1.1.

1.2.3 Prism-Coupled Surface Plasmon Resonance. Prism-coupling of monochromatic light was first employed by Kretschmann (1969). The IBIS is an example of a simple Kretschmann configuration and employs vibrating mirror (scanner) optics to generate SPR on a gold-coated glass surface (*Figure 1.2.3.1*). This configuration is inexpensive as it eliminates the requirement for a two-dimensional photodiode array angle detector yet is highly sensitive to refractive index (< 2 x 10^{-6}). Briefly, laser light is directed into the prism by means of a vibrating mirror and the intensity of the reflected light is monitored by a large-area photodiode (Kooyman *et al.*, 1991). The vibrating mirror is supplied with an alternating current from a function generator and, thus, the angle of

incident light becomes time-dependent. During one cycle of the vibrating mirror, the light traverses the reflectance minimum twice and the position of the minima are time-resolved as t_1 and t_2. Hence, a change in the reflectance minimum results in a changing time span (Δt). A 'real-time' plot of the reflectance minimum angle against time is generated and can be used to monitor the progress of biomolecular interactions.

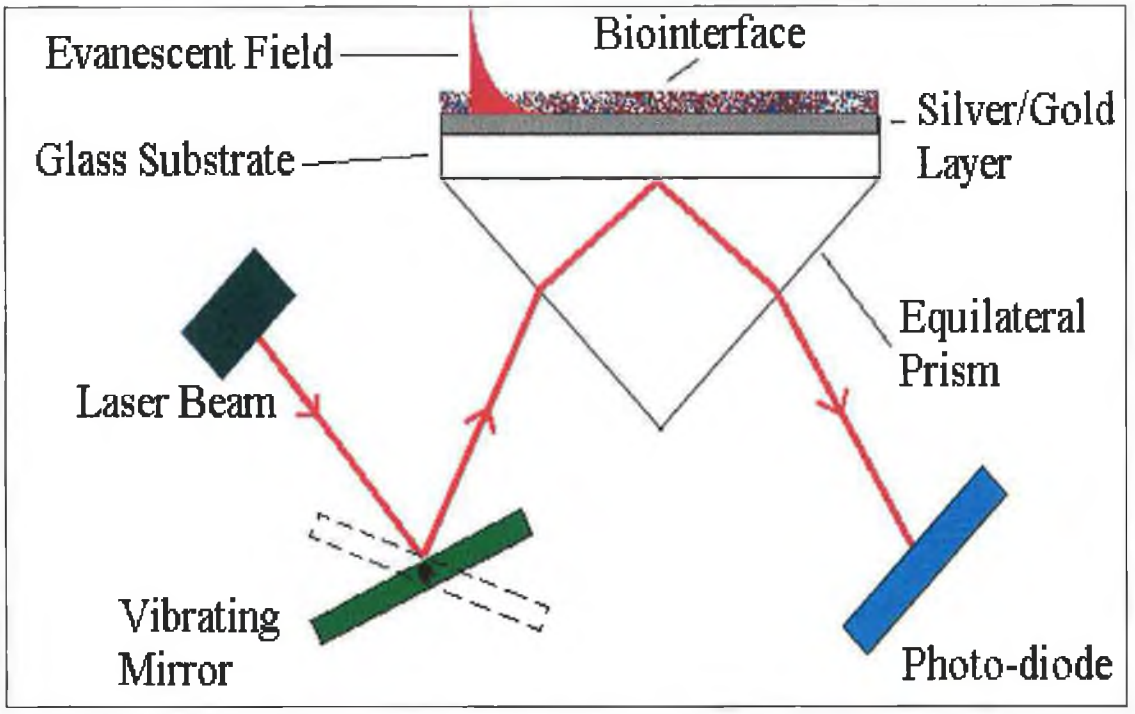

Figure 1.2.3.1 Schematic illustration of the vibrating mirror SPR configuration. The vibrating mirror employs the Kretschmann SPR configuration and generates SPR as described in section 1.2.3. The monochromatic light is supplied by a laser and the incident angle is rotated using a vibrating mirror. A simple photodiode determines the position of the resonance minimum as a function of time (i.e. position of the reflectance minimum is correlated to vibration rate of mirror).

A more convenient derivative of the Kretschmann configuration which eliminates the requirement for moving parts (e.g. vibrating mirror) was designed by Matsubara *et al.* (1988). A transverse wedge-shaped beam of light is focused onto a disposable sensor chip (*Figure 1.2.3.2*) and the reflectance minimum is monitored by a two-dimensional photodiode array. Computer interpolation algorithms are applied to the collected data to resolve the position of the reflectance minimum.

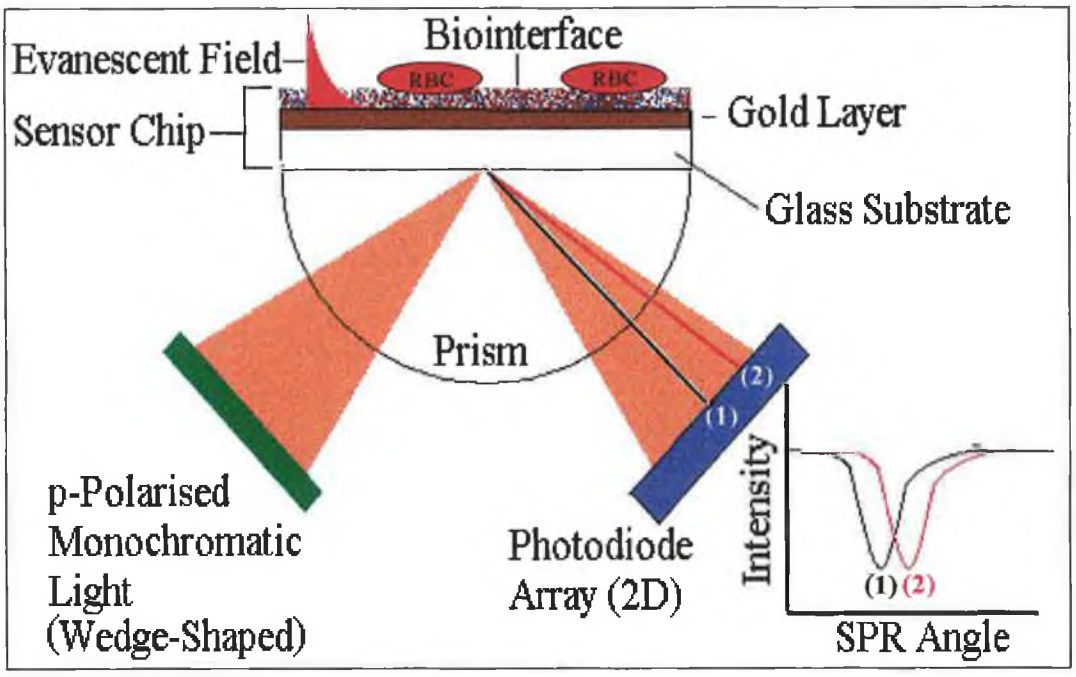

Figure 1.2.3.2. Schematic illustration of the Kretschmann SPR configuration employing a wedge-shaped beam of incident light. Light that is incident through the prism undergoes total internal reflection at the interface with the glass substrate. At a critical angle of incidence an evanescent wave that results from total internal reflection resonates with the surface plasmon of the gold layer. Thus, light is absorbed at this angle due to surface plasmon resonance and a corresponding minimum in the reflected light is detected by a photodiode array (1). The illustration shows the interaction of red blood cells with the sensing surface. This interaction changes the mass at the surface and, hence, causes a proportional change in the refractive index. This alters the resonance condition and is observed as a shift in the position of the reflectance minimum ((1) to (2)).

1.2.4 ***Miniaturised Single-Platform SPR.*** Texas Instruments have developed a miniature SPR device that interfaces with a personal computer. A schematic illustration of the device is shown in *Figure 5.2.3.1.* A light emitting diode is attached to the substrate and is enclosed within an adsorbing apertured box that is capped with a polarising film. P-polarised monochromatic light is directed through the aperture onto the SPR layer over a range of angles. The light undergoes total internal reflection and is directed by reflecting optics onto a linear photodiode detector array that resolves the position of the reflectance minimum. The sensor is connected to a controller electronics box that is interfaced with the computer. Dedicated software controls the device, data acquisition and analysis. This fully integrated miniaturised SPR system is economically produced and is capable of 'real-time' biomolecular interaction analysis. This transducer was modified to facilitate 'real-time' biosensing and is described in more detail in sections 5.2.3.5. It was envisaged that this device would offer a portable, inexpensive alternative to the large bench-top analysers currently available.

1.2.5 ***Waveguide-Based SPR.*** There are two basic optical configurations and these are based on fibre optic or planar waveguide technology. Both are governed by the same optical principles and can be configured to accommodate either angle-dependent SPR utilising monochromatic light or wavelength-dependent SPR employing a polychromatic light source.

(a) Fibre Optic SPR. Jorgenson and Yee (1993) constructed a fibre optic SPR device for refractive index sensing. White light was transmitted through a fibre optic cable and a grating was used to separate the light into a spectrum (miniature spectrometer), which was detected by a linear photodiode array. However, a section of the cable was striped of cladding and derivatised with a thin silver layer. White light transmitted through the modified fibre optic excited SPR over a range of wavelengths, resulting in a characteristic wavelength minimum in the SPR spectrum. Changes in the refractive index at the surface resulted in a proportional shift in the SPR minimum. An improved design employing a microfabricated mirror at the fibre tip allowed reflection of light back through the fibre to the detector, thus facilitating flowcell-free remote analysis. This configuration forms the basis of the BIACORE Probe™. However, the optical properties of materials (e.g. metal layer, fibre) are a significant function of wavelength and result in a non-linear response to refractive index changes. Ronot-Trioli *et al.* (1996) used a multimode fibre optic device employing monochromatic light. A laser source was rotated over a range of incident angles and at a specific incident angle the transmitted light intensity became attenuated due to SPR in the metal film. This fixed-wavelength angle-dependent configuration produced a linear response with respect to refractive index and was used to measure the refractive index change of aqueous solutions. However, these fibre optic SPR-based transducers were not interfaced with the appropriate hardware or software required to facilitate 'real-time' monitoring. Therefore, a fibre optic system employing polychromatic light that incorporated 'real-time' biosensing capability was constructed. This device was successfully applied to the visualisation of the interaction of whole red blood cells with immobilised antibody and is discussed in detail in sections 5.2.1.

(b) Planar Waveguide-based SPR. These are integrated optical sensors that combine the resonant coupling of guided light modes within planar optical waveguides with SPR at a gold-coated surface. Homola *et al.* (1997) used a prism to couple monochromatic light into and out of a waveguide possessing a narrow strip of gold along the optical path. The attenuation of transmitted light due to SPR was detected and was highly sensitive to the refractive index at the gold surface.

1.2.6 ***Fundamentals of Integrated Optical Waveguides.*** Integrated optical sensors are waveguiding devices that respond to changes in the refractive index and/or thickness of the biological overlayer (Sychugov *et al.*, 1997). They are flexible sensor platforms that support a wide variety of optical configurations (Flanagan *et al.*, 1988; Lin and Brown, 1997). Changes in the wave

propagation characteristics (e.g. phase velocity) that result from refractive index variations at the sensing surface are exploited as a means of detection (Lukosz, 1995). Waveguide films are typically produced by coating a glass substrate (low refractive index) with a thin (100-200 nm) sol-gel (e.g. SiO_2-TiO_2) layer of high refractive index (Jordan *et al.*, 1996). Monochromatic light is coupled into the waveguide and undergoes total internal reflection to generate an evanescent field at the waveguide surface. The propagation velocity of the guided light is dependent on the effective refractive index of the guided mode. A refractive index change (i.e. resulting from biomolecular interactions) within the penetration depth of the evanescent field leads to a change in the effective refractive index of the guided mode. Resonance occurs for both transverse electric and transverse magnetic polarisations of light. The refractive index difference between the waveguide and sample medium is maximised while minimising the waveguide thickness to generate high evanescent wave strength. Waveguide modes are guided by total internal reflection and surface plasmons are propagated at the metal-dielectric interface (Lukosz, 1991). In monomode waveguides, both transverse electric and transverse magnetic modes propagate but only the transverse magnetic mode excites surface plasmons. Additionally, surface plasmons are propagated over a very short distance (i.e. ~ 10 μm) whereas waveguide modes can be propagated over several centimetres and the sensitivity to refractive index is inversely proportional to the propagation distance (Lukosz *et al.*, 1991(b); Kang *et al.*, 1993).

1.2.7 ***Input/Output Couplers.*** These are integrated optical devices that incorporate a diffraction grating, which is imbossed (imprinted) onto the sol-gel surface, to facilitate direct input of laser light at an angle that excites a guided mode. Incouplers and outcouplers are fully opto-electronic devices that monitor the input coupling angle and output coupling angle, respectively. However, the interaction surface must cover the grating area (Lukosz *et al.*, 1991(a) and (b)) for outcouplers (Clerc and Lukosz, 1997) and the effective refractive index of the mode outside this region is irrelevant. Incouplers monitor the optimal incoupling angles for both transverse electric and transverse magnetic modes as a function of time through the use of cyclic rotations of the incident light angle as a function of time (*Figure 1.2.7.1*). The BIOS-1 employs an integrated optical scanner to determine the angle at which a guided mode is excited. The incident angle of the laser light is continuously varied (angle scanning) and the angle at which a guided mode is excited is detected by photodiodes at each end of the waveguide. Bier and Schmidt (1994) employed such an input grating coupler for 'real-time' biomolecular interaction analysis and demonstrated the detection of nanomolar concentrations of a pesticide using a competitive immunoassay format.

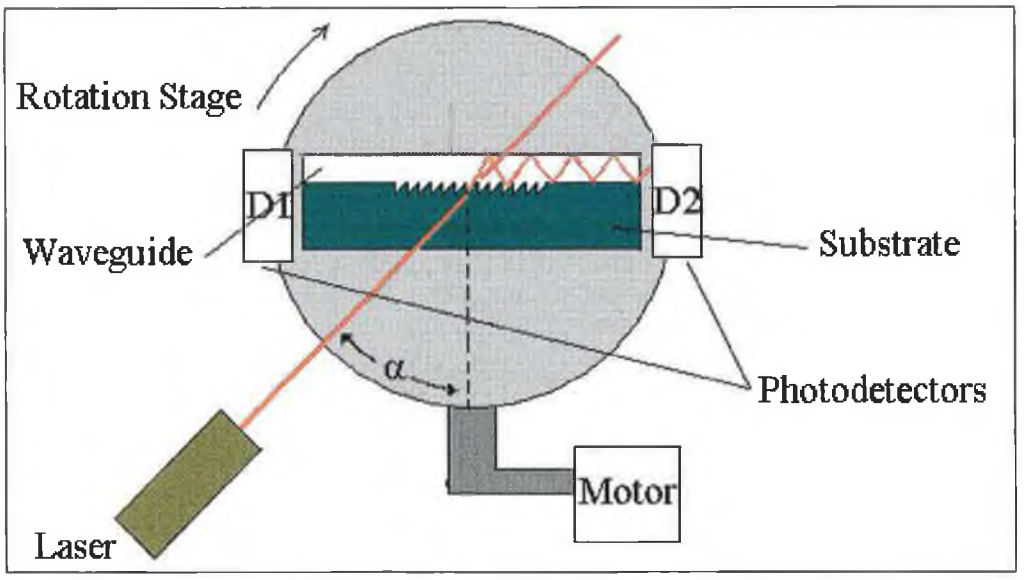

Figure 1.2.7.1. Schematic illustration (plane view) of an input-grating coupler. The waveguide substrate is rotated to give variable incident angles (α). A waveguide mode is excited by grating incoupling of laser light at a specific angle of incidence and can be detected at either end of the waveguide by a photodiode (i.e. D1 and D2). The angle at which this occurs is a function of the refractive index at the grating (i.e. sensing surface) and is time-resolved with respect to the rotation of the substrate.

The outcoupler uses a position-sensitive photodetector to determine changes in the outcoupling angles for both transverse electric and transverse magnetic components of the excited mode. The outcoupled transverse electric and transverse magnetic modes are focused by a lens onto a photodiode array, allowing measurement of the outcoupling angles with (sub millisecond) temporal resolution (*Figure 1.2.7.2*).

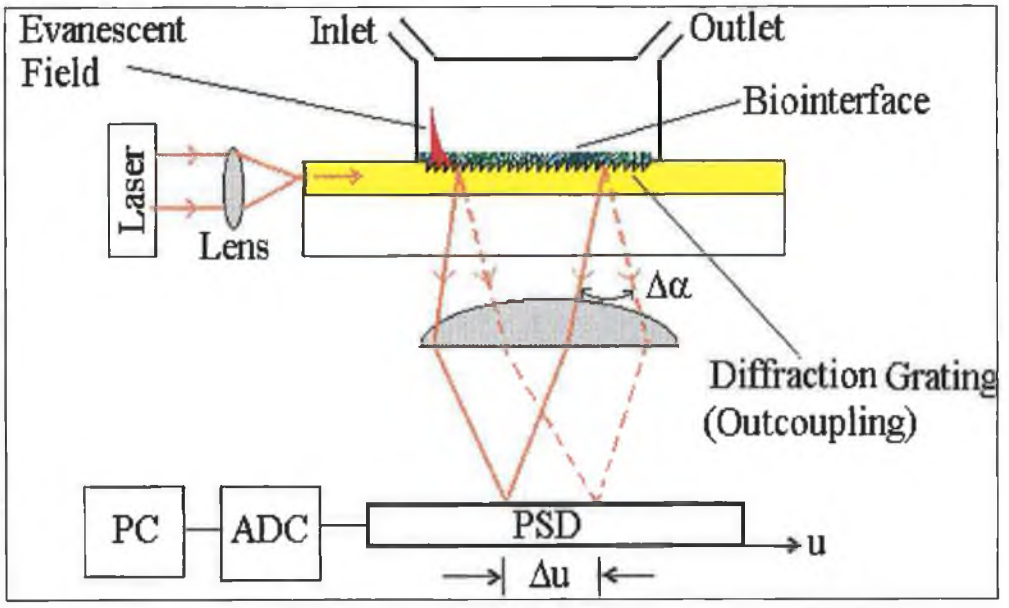

Figure 1.2.7.2. Schematic illustration of an output grating coupler. A lens focuses light into the waveguide and a diffraction grating outcouples both transverse electric and transverse magnetic polarisations of the guided mode onto a photodiode array (i.e. position sensitive detector). This finds the position (u) of the outcoupled light and can calculate the out-coupled angles ($\Delta\alpha$) as a function of the refractive index at the grating surface (i.e. biointerface). Abbreviations: personal computer (PC); analogue to digital converter (ADC); photosensitive detector (PSD); distance along the detector (U); outcoupling angle (α).

1.2.8 ***Mode Beat Interferometer.*** In common with most integrated optical-sensors, laser light is used to excite both transverse electric and transverse magnetic modes in a planar waveguide. Both modes follow the same path and interact with the exposed biosensing layer (10-20 mm in length). Time-dependent changes in the effective refractive index occur for both modes, resulting in a time-dependent phase shift between the transverse electric and transverse magnetic modes at the end of the waveguide. Several methods can be used to measure the phase variation, which is commonly measured as a function of time (Hartmann *et al.*, 1988). Lukosz *et al.* (1997) employed a Wollaston prism to focus the outcoupled transverse electric and transverse magnetic modes through a polariser to produce spatial interference fringes (mode beating) detectable by a linear CCD detector array. The spatial frequency of this pattern is proportional to the relative phase velocities of both surface waves, which are sensitive to refractive index changes. Klotz *et al.* (1997) simplified the optical configuration by using a channelled (strip)-surface waveguide that was compatible with many optical components developed for the telecommunications industry.

1.2.9 ***Mach-Zehnder Interferometer.*** The Mach-Zehnder interferometer normally employs light of the same polarisation but different mode number (i.e. TE_0 and TE_1) and is typically constructed as a strip monomode waveguide, thus enabling precise splitting and recombination of two light paths while minimising light scatter (Gabricius *et al.*, 1992). One path behaves as a reference while the evanescent field of the other interacts with the biomolecular interaction layer. This interaction changes the propagation velocity of the guided mode and results in a phase variation that causes interference when both paths are recombined. The interference can be interrogated which allows refractive index changes to be monitored. A Mach-Zehnder interferometer can be fabricated as a strip waveguide moulded into a glass substrate and a Y-junction can be used as a beam splitter and combiner. Kempen and Kuntz (1997) demonstrated a mass fabrication method suitable for commercial scale production of Mach-Zehnder interferometer sensor chips employing integrated diffraction gratings for incoupling/outcoupling of collimated light and, hence, reduced the requirement for expensive optical components. Drapp *et al.* (1997) combined the Mach-Zehnder interferometer sensor with a 3 x 3 mode coupler structure. Instead of recombining the two light beams of the interferometer in a simple Y-junction, mode coupling was used to exchange power from the two arms between the three outputs. A sensitive measure of the effective refractive index was possible by comparing the phase shift (e.g. $2\pi/3$) between all outputs.

1.2.10 ***Resonant Mirror.*** The resonant mirror (Cush *et al.*, 1993) is a composite resonant structure that is created by coating the base of a prism with a layer of silica (1 μm) and a thin (160 nm) high refractive index waveguiding layer (e.g. SiO_2-TiO_2) (*Figure 1.2.10*). Incident light is focused onto the prism-silica interface resulting in frustrated total internal reflection, which evanescently couples light into the waveguiding layer. Total internal reflection within the waveguide layer generates an evanescent field at the biointerface. Efficient coupling occurs for certain incident light angles where phase matching with the resonant guided modes in the waveguide is achieved. During resonance a 2π phase shift in reflected light occurs and causes constructive interference that produces sharp peaks of light at resonance. Changes in the angular position of the peaks can be monitored and is directly related to the refractive index change at the waveguide surface (i.e. sensing layer). The IAsys biosensor utilises this technique for 'real-time' monitoring of biomolecular interactions (Cush *et al.*, 1993).

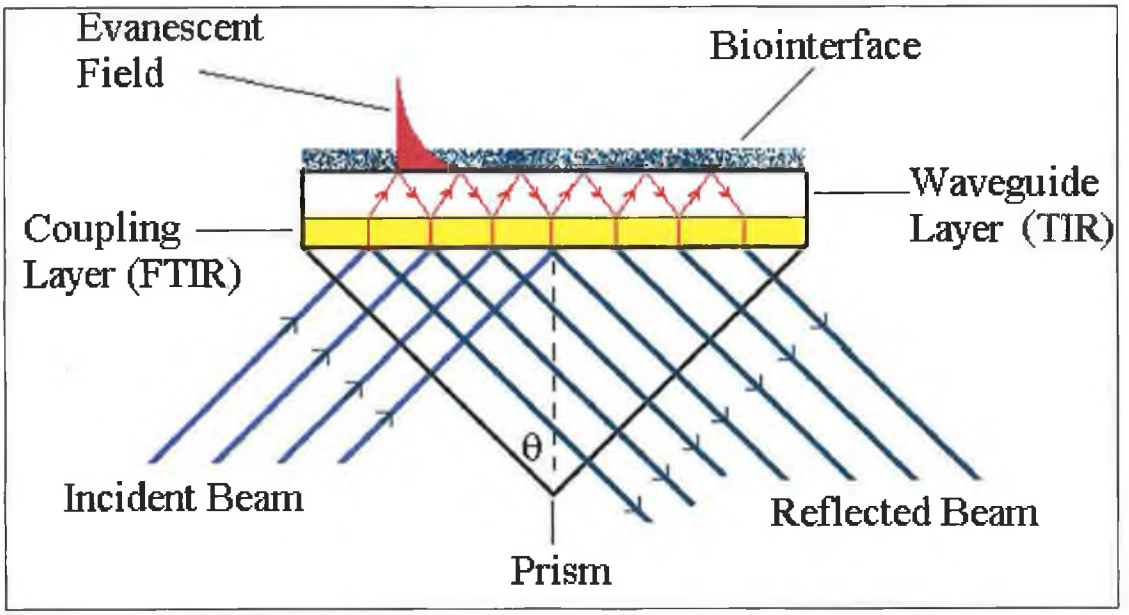

Figure 1.2.10. Illustration of the resonant mirror configuration. Monochromatic light, incident through a prism, undergoes frustrated totally internally reflected (FTIR) at the boundary with a low refractive index layer (e.g. silica). An evanescent field is generated and it couples light into the high refractive index waveguiding layer, where the guided mode gives rise to an evanescent field at the biointerface. The incident angle at which resonance between the evanescently coupled light and the waveguide mode (propagated by total internal reflection (TIR)) occurs is dependent on the refractive index at the biointerface. The resonance causes a 2π phase shift in the reflected light that results in constructive interference, which is observed as two sharp peaks (i.e. one for each polarisation) of light during resonance. The change in the angular position of the peaks can be related to the refractive index change at the biointerface.

1.2.11 ***Reflectometric Interference Spectroscopy.*** Reflectometric interference spectroscopy is a non-waveguide based technology that does not require the generation of an evanescent field. The progress of a biomolecular interaction on a glass surface generates a film of increasing optical thickness. White light that illuminates this interface is partially reflected at each interfacial layer (i.e. bulk-film and film-surface interfaces) and each reflected beam can be superimposed to give an interference pattern caused by the phase differences. The interference pattern allows 'real-time' monitoring of both the thickness and refractive index of the biomolecular interaction layer and is insensitive to bulk temperature fluctuations. Schmitt *et al.* (1997) modified a commercially available fibre optic-based miniature spectrometer to produce a cost effective reflectometric interference spectroscopic biosensor with a detection limit of 2 pg/mm^2. This system is particularly suitable for 'real-time' biomolecular interaction analysis involving low molecular weight analytes (Piehler *et al.*, 1996(a); Piehler *et al.*, 1997) and has been used for the determination of the affinity constants for monoclonal and recombinant antibodies.

1.2.12 ***Piezoelectric Transduction.*** Acoustic wave devices offer an inexpensive alternative for bioaffinity sensing. These devices are ultra-sensitive weighing devices based on the piezoelectric, electromechanical oscillator principle. Basic instrumentation is required in contrast with many optical transduction systems (Steegborn and Skládal, 1997). Piezoelectric materials interconvert electrical signals with acoustic waves and can be characterised as crystalline anisotropic solids that lack a center of symmetry in crystal structure. Mass changes that result from biomolecular binding events at a functionalised surface cause changes in the frequency and attenuation of the propagated wave. The sensitivity of these gravimetric sensors is related to the confinement of acoustic energy at the surface. Acoustic sensors are classified according to the wave characteristics and/or the device configuration.

(a) Bulk acoustic wave sensor (e.g. Quartz crystal microbalance)

(b) Surface acoustic wave sensor.

(c) Shear horizontal wave sensor (e.g. Acoustic plate mode).

1.2.12.1 *Bulk Acoustic Wave.* The simplest acoustic waves are plane waves such as the longitudinal and shear waves. These are dependent on the crystal symmetry and orientation of the piezoelectric material, usually a quartz crystal wafer. The bulk acoustic wave is commonly designed for shear wave operation. Typically, silver/gold electrodes are evaporated onto the top and bottom surfaces and the exposed electrode surface serves as the sensing layer. Applying a potential difference between the electrodes generates an alternating electric field that induces a standing shear wave as a result of mechanical oscillations of the crystal lattice. A displacement (e.g. acoustic evanescent field) is created parallel to the surface of the quartz crystal and the vibrational frequency of this wave is dependent on the physical properties of both the crystal and its environmental surroundings. It is vital that quartz crystal microbalance systems be designed to minimise acoustic losses incurred in aqueous phase operation. A wide variety of quartz crystal microbalance sensing configurations have been employed for biomolecular interaction analysis (Masson *et al.*, 1995; Sakai *et al.*, 1995; Sakai *et al.*, 1997). The evolution of appropriate oscillator circuitry for aqueous phase sensing has played a major role in these developments. Minunni and Mascini. (1993) demonstrated the ability of a quartz crystal microbalance system to visualise biomolecular interactions in 'real-time' with multiple surface regenerations. Universal Sensors, Inc. (Louisiana), have commercialised this system as the piezoelectric-1000 Immunobiosensor System. A piezoelectric detector for oscillating and monitoring the frequencies of two 5-15 MHz crystals is supplied along with PZ-Tools software for data acquisition, storage and analysis. A range of pre-coated quartz crystals are available and both static and flow injection analysis sampling configurations are supported.

1.2.12.2 *Surface Acoustic Wave Devices.* Metal electrodes are deposited on the surface of the piezoelectric material in the form of thin interdigitated transducers. The interdigitated transducers excite a two-dimensional shear longitudinal wave at the interface between the piezoelectric material and the environment. The excited surface acoustic wave is detected with a second interdigitated transducer whose operational frequency is dependent on the spacing between the fingers of the interdigitated transducer. Surface acoustic wave devices are unsuitable for liquid phase sensing because the acoustic wave is exponentially dampened due to leakage of energy into the liquid phase and the generation of leaky surface waves. However, if an elastically different solid layer covers the device, a horizontally polarised shear wave is generated on the top layer (i.e. Love wave). Love acoustic waveguide sensors possess a high sensitivity with minimal acoustic losses in liquid due to surface confinement of the acoustic wave.

1.2.12.3 *Shear Horizontal Wave Sensor.* Surface-generated bulk acoustic waves which are produced by the acoustic plate mode, are shear horizontal waves that propagate in the bulk of the piezoelectric material and show negligible acoustic dampening in liquid environments (Andle *et al.*, 1995). Multiple reflections of the wave between top and bottom surfaces generate a displacement at both surfaces. In common with the surface acoustic wave configuration, two interdigitated transducers that are separated by the biomolecular interaction surface are used to excite and collect acoustic waves. This is in contrast with the bulk acoustic wave system where the sensing layer is confined to the electrode covered crystal surface. Welsch *et al.* (1996) generated a shear horizontally polarised acoustic wave in $LiTaO_3$ at a fundamental frequency of 115 MHz. A low attenuation of the wave allowed the device to be used at its third harmonic (305 MHz) resulting in greater sensitivity. Both reference and biomolecular interaction delay lines were coated with chromium/gold layers to minimise buffer conductivity effects and silicone rubber was used to seal the electrical elements of the sensor. The phase shift was measured at a constant frequency and the background noise (i.e. bulk waves) was eliminated by taking a frequency spectrum as a function of time with a network analyser. Bender *et al.* (1997) showed that the use of a metal-coated interaction surface reduces the mass loading frequency by 40-50 % in an acoustic plate mode device. Nevertheless, the occurrence of spurious signals, often found during biomolecular interaction analysis in buffered solutions, was eliminated.

1.2.12.4 *Limitations of Piezoelectric Transduction.* The main limitations of the technology include the lack of an exact correlation between surface mass loading and frequency change during solution phase sensing and sensitivity to environmental conditions (e.g. viscosity at surface) (Barnes, 1991; Muratsugu *et al.*, 1993). Acoustic interactions with the protein layer or different

mass sensitivities for different boundary layers are possible causes and necessitate empirical optimisation for each piezoelectric sensing system. Mathematical expressions must be derived through careful consideration of the piezoelectric material (i.e. dimensions, density, shear modulus), operational mechanism and physical changes (i.e. viscosity, temperature) within the sensing layer during the progress of the biomolecular interaction. Zhang *et al.* (1997) attempted to describe the total frequency change of a piezoelectric biosensor in terms of a dual response: (a) mass loading and (b) viscosity dampening. It was shown that these two factors change simultaneously and a characteristic dampening vector can be applied to analyse the loading variation of the sensor in any situation.

1.3.0 Biomolecular Interaction Interfaces for Biosensing.

The construction of a suitable biointerface is a key component in biosensor design and has a critical influence on the biosensor's performance. Biomolecular interaction analysis requires the immobilisation of one of the interacting biomolecules onto a suitable biointerface. In general, it is prudent to mimic the native environment of the interactants as closely as possible. The ideal characteristics of a generally applicable biointerface are outlined below.

- The biointerface should be compatible with the transduction principle and tailored to optimise sensor performance.
- It should resist non-specific binding of biomolecules/cells.
- It should facilitate coupling of biomolecular ligands through reliable standard chemistries and allow precise control over the immobilisation yield.
- The binding sites of the immobilised biomolecules should be freely accessible in three-dimensional space.
- It should be chemically resistant to a wide variety of chaotrophs (e.g. extremes of pH, ionic strength or organic solvents.)
- The mass transfer rate within the sensing layer should approach bulk solution rates (i.e. viscosity of the sensing layer should be kept to a minimum).
- The volume/area of the biointerfacial layer should be sufficient to accommodate a statistically valid number of molecular binding events during analysis.

1.3.1 ***Non-Specific Binding.*** Adequate transduction technologies exist for the sensitive determination of mass. However, non-specific binding of molecules to a functionalised biointerface remains the main limitation. 'Real-time' biomolecular interaction analysis of complex samples (e.g. serum, urine and milk) invariably suffers from non-specific binding. Non-specific binding is the physisorption of sample components that do not possess specific interaction sites with the

immobilised ligand and often results from an inherent hydrophobic or ionic character of the interfacial chemistry. Generic transduction systems for mass detection cannot discriminate between non-specifically adsorbed protein and specifically bound analyte. Hence, the use of non-specific site blockers (e.g. bovine serum albumin), high ionic strength buffers, surfactants and spiking of samples with adsorbing molecules may be required.

1.3.2 Non-covalent Immobilisation.

1.3.2.1 Passive Adsorption. In general, any process involving an interface in contact with a protein solution will be influenced by protein adsorption (Horbett and Brush, 1987) and includes the design of biocompatible clinical implants, cell adhesion to surfaces, blood coagulation, solid-phase immunoassays, cell-surface receptor-ligand interactions and biosensor technology. However, adsorption characteristics vary considerably between different proteins as a result of different molecular properties such as size, charge, structure, amphipathicity, hydrophobicity, solubility and the physico-chemical composition of the surface. Binding forces such as van der Waals forces, hydrophobic interactions, hydrogen bonding and the electrostatic double-layer force mediate the physisorption process. This electrostatic double layer force (Müller *et al.,* 1997) is sensitive to pH and electrolyte concentration.

Passive physisorption processes do not discriminate between the active binding site of biomolecules and the framework structure and, therefore, cause significant losses in biological activity. Physisorption of biomolecules readily occurs onto hydrophobic surfaces whereas hydrophilic surfaces tend to resist protein adsorption. However, as soluble proteins possess hydrophilic surface groups and internal hydrophobic groups, the conformation of soluble proteins must alter in order to expose internal hydrophobic groups during the physisorption process. Random orientation of biomolecules on the surface together with subsequent conformational changes may cause steric hindrance and induce denaturation. Furthermore, physisorption is limited to the immobilisation of macromolecules and generally produces a heterogeneous monolayer that is subject to desorption. Despite these difficulties physisorption is a widely employed immobilisation technique since it is experimentally simple, fast and inexpensive. Entrapment is an equally simple technique and is used for the incorporation of molecules (e.g. fluorescent dyes, enzymes, and antibodies) into unheated sol-gel films (Wang *et al.*, 1993; Dave *et al.*, 1994; Lev *et al.*, 1995). However, it generally yields less than optimal results due to steric hindrance and poor diffusion of the sample medium within the microporous matrix of the sol-gel.

1.3.2.2 Affinity-Based Directed Immobilisation. Affinity-based immobilisation (affinity-capture) is a flexible technique that can be used in conjunction with more elaborate biointerfaces. Essentially, affinity-capture involves using non-reversible immobilisation of a high affinity ligand as a means of reversibly anchoring another ligand, which defines the specificity of the interaction of interest. In general, controlled orientation of the specific ligand can be achieved and impure, dilute sources may be used. However, these techniques commonly require replacement of the specific ligand after each interaction-regeneration cycle. Protein A and protein G are widely used for the reversible immobilisation of antibodies to biosensing surfaces (e.g. glass or gold) (Muramatsu *et al.*, 1987). Protein A from *Staphylococcus aureus* possesses three homologous Fc binding sites that bind the Fc region of IgG from a variety of mammalian species with high affinity ($\sim 10^9$ M^{-1}) (Goding, 1978; Langone, 1982; Jendeberg *et al.*, 1997). It is remarkably stable on exposure to extreme conditions of pH, temperature and denaturing agents and can be used repeatedly for over 200 binding-regeneration cycles (unpublished personal observations). Protein G from group G *Streptococci*, represents a more general and versatile IgG binding reagent (Björck and Kronvall, 1984; Åkerström et al., 1985; Åkerström and Björck, 1986) as it binds a greater range of IgG isotypes from a wider variety of mammalian species with higher affinity. However, native protein G also possesses a binding site for serum albumin. Recombinant protein G that has been genetically engineered to possess IgG-binding activity alone is commercially available. Typically, protein A/G is physisorbed onto the sensor surface from dilute solutions and the remaining surface binding sites are blocked with a non-specific protein (e.g bovine serum albumin, gelatin). In addition, binding of IgG to the protein A/G-coated surface occurs in a directed fashion, giving the desired orientation of the antigen-binding sites. Coating of surfaces with these 'anchor' proteins also confers hydrophilic properties to the surface that limit non-specific binding. However, the binding characteristics of such surfaces are subject to the limitations already outlined for direct physisorption and the use of protein A/G for affinity-capture is restricted to immunosensing applications. Nevertheless, this simple approach is extremely popular for biosensor applications.

Avidin is a tetrameric glycoprotein and has been incorporated into many biosensing formats owing to its four extremely high affinity ($\sim 10^{15}$ M^{-1}) binding sites for biotin (Ebersole *et al.*, 1990). Streptavidin possesses superior non-specific binding properties as it lacks both the carbohydrate moieties and alkaline nature of avidin. Nevertheless, both have been used to anchor biotinylated affinity ligands to interaction surfaces (Rehàk *et al.*, 1994; Hoshi *et al.*, 1995). Biotinylation of proteinaceous (e.g. antibodies, receptors, peptides, receptors) and non-proteinaceous (e.g. nucleic acids, phospholipids, organic haptens) affinity ligands is readily achieved by employing reactive biotin derivatives (e.g. biotin-NHS, biotin-hydrazide etc.) However, the avidin-biotin interaction is virtually irreversible and the random nature of protein biotinylation may impair biological function.

Similarly to protein A/G, the avidin bridging layer that is directly physisorbed onto the surface insulates the immobilised biomolecule from the substrate and, hence, preserves the biological activity of the biomolecule and reduces non-specific binding. Alternatively, a monolayer of streptavidin may be specifically attached to the surface via a layer of physisorbed biotinylated-BSA (Ahluwalia *et al.*, 1991; Abel *et al.*, 1996, Mooney *et al.*, 1996) or through covalent attachment (Caruso *et al.*, 1997) to a pre-formed self-assembled monolayer. In addition to exploitation of these naturally available affinity-capture strategies, novel non-biological anchoring systems have been developed. Gershon and Khilko (1995) described a stable chelating linkage for the reversible immobilisation of oligohistidine tagged proteins. N-(5-amino-1-carboxypentyl) iminodiacetic acid (NTA-ligand) was immobilised through covalent amine coupling to a dextran hydrogel. The NTA-ligand chelates metal ions such as Ni^{2+} leaving co-ordination sites available to bind oligohistidine-tagged ligands. The interaction with the tagged protein was stable and the surface could be regenerated under mild conditions with an EDTA solution.

1.3.3 Covalent Immobilisation.

1.3.3.1 Functionalised Self-Assembled Monolayers. Covalent immobilisation avoids many of the problems associated with physisorption processes and facilitates regeneration of the surface with minimal leaching of the biomolecule (Williams and Blanch, 1994). However, covalent immobilisation of biomolecules requires chemical modification of the biointerfacial substrates, which are commonly composed of glass or metals (see review of Lu *et al.*, 1996). Glass, quartz and silica surfaces can be treated with an alkylsiloxane (Matveev, 1994) and a variety of metals (e.g., gold, silver, copper, platinum) can be derivatised with alkanethiols or alkanedisulfides (Mrksich and Whitesides, 1995). These techniques allow the assembly of transparent monolayers of defined chemical composition. The exact nature of the interaction between alkanethiols and metal surfaces remains uncertain despite extensive investigations. However, it has been established that binding occurs through chemisorption of the surface-active thiol onto the metal surface and this exothermic reaction encourages the formation of a tightly packed monolayer. Van der Waals and hydrophobic interactions between adjacent alkyl chains stabilise the monolayer and, hence, longer alkyl chains create denser more stable monolayers.

The structure of self-assembled monolayers depends on the crystalline structure of the metal. Gold is commonly used and can be deposited by vacuum evaporation or sputtering onto a glass surface pre-coated with a thin layer of titanium or chromium. Mixed self-assembled monolayers are easily constructed since the molar ratio incorporated into the monolayer is the same as the mole ratio of the mixed thiol in solution assuming similar molecular weights. Preparation of mixed self-

assembled monolayers can be used to precisely control the chemical composition of the interaction surface and facilitates controlled immobilisation of biomolecules at the required density (Chidsey *et al.*, 1990; Bertilsson *et al.*, 1997). Rickert *et al.* (1996) applied this technique to immobilise synthetic peptides possessing the sequence specificity of a viral protein epitope. Self-assembled monolayers on gold are pseudo-crystalline assemblies that are stable for several months at room temperature and are generally characterised by a high packing density with few pinholes or defects (Wink *et al.*, 1997). However, they are significantly less stable than covalently bound silane monolayers on silicon/glass (Bain *et al.*, 1989). A wide variety of organosilanes are commercially available and include epoxy-, vinyl-, aminoalkyl-, sulfhydryl-, thiol-, haloalkyl- and amino-terminated alkoxysilanes. These compounds spontaneously react with surface silanol groups (e.g. present on the surface of glass or quartz) when evaporated under pressure or when immersed to form a covalently bound monolayer (Weetall, 1993). These monolayers are chemically inflexible and are less dense in comparison to alkanethiol monolayers on gold. Both aqueous and organic solvents have been successfully used for methoxy- and ethoxy-silanes whereas organic phase silanisation must be used when using chlorosilanes.

Silanisation and alkanethiol assembly both produce monolayers that effectively insulate the biomolecular interaction from the substrate and can be tailored to minimise non-specific binding and denaturation (Prime and Whitesides, 1991). The exposed functional group serves two main purposes: (a) It provides a reactive group that can be used for further derivatisation or to covalently cross-link biomolecules to the surface. (b) It should resist non-specific binding of unwanted sample components or facilitate conversion to a more appropriate hydrophilic functional group. Hydrophilic hydroxyl-, amino-, thiol- and carboxyl-terminated self-assembled monolayers are commonly used since a wide variety of suitable cross-linking chemistries exist (Mirsky *et al.*, 1997). Monolayers presenting densely packed carboxylic groups facilitate preconcentration and covalent coupling of biomolecules and the hydrophilic nature of such surfaces resists non-specific adsorption.

A similar carboxylated self-assembled monolayer was employed to generate a novel hydrophilic biointerface stabilised by ionic interactions (Frey *et al.*, 1995; Jordan and Corn, 1997). A monolayer of mercaptoundecanoic acid was assembled on gold and biotinylated poly(L-lysine) (positively charged) was reversibly adsorbed through ionic interactions with the negatively charged monolayer. Specific binding of avidin to the surface-bound biotin was observed. However, this biointerface is unlikely to be widely employed due to its dependence on ionic stabilisation, which is incompatible with commonly used buffers

Lu *et al.* (1993) derivatised silica slides with (γ-aminopropyl)trimethoxysilane (APTES) and further derivatised the exposed amino groups with N-succinimidyl-3-(2-pyridyldithio)propionate (SPDP), thereby introducing reactive disulphides. Hence, directed immobilisation of Fab fragments that possess hinge-region thiol groups was accomplished through thiol-disulphide exchange, resulting in a 2.7 fold increase in surface binding capacity relative to random physisorption. This technique is limited since it relies on the presence of a thiol group that is spatially separated from the active binding site. However, Mc Lean *et al.* (1993) avoided this restriction by genetically engineered a thiol side chain onto a biomolecular ligand at an appropriate attachment site, thereby controlling molecular orientation.

1.3.3.2 Supported Hydrogels. As described earlier, evanescent field-based optical transducers are widely employed for 'real-time' biomolecular interaction analysis. An extended hydrogel layer maximises the interaction volume probed by the evanescent field and, hence, dramatically increases the surface capacity in comparison to monolayer coverages (Liedberg *et al.*, 1993). Buckle *et al.* (1993) investigated the use of a variety of organosilanes and carboxymethylated (CM)-dextran for antibody immobilisation. Direct adsorption onto a bare glass substrate yielded 22 % of an equivalent active monolayer, silanisation for both covalent and non-covalent immobilisation averaged at 47 % active monolayer coverage and the CM-dextran gave > 900 % active monolayer coverage. Hydrophilic polymers such as poly(ethylenediamine) (Nakanishi *et al.*, 1996; Nakamura *et al.*, 1997), poly(ethyleneglycol), polysaccharides, poly(vinyl alcohol), poly(hydroxylethyl metacrylate), polyacrylamide and chitosan may form suitable hydrogels for biointerfacial construction. Piehler *et al.* (1996(b)) generated a self-assembled monolayer on glass substrates onto which a variety of hydrogels were grafted. Chitosan, poly(ethylenediamine), poly(oxyethylene), poly(acrylamide-coacrylic acid) and aminodextran were grafted onto a carboxylated self-assembled monolayer surface. Poly(oxyethylene) and aminodextran resulted in the lowest non-specific binding levels due to shielding of the silanised surface by the polymer chains. Highly cross-linked polymers possessing a high density of functional groups were prone to high levels of non-specific binding. Such hydrogels would undoubtedly suffer from diffusion limitations and steric hindrance effects. Predictably, an antibody-hapten interaction conducted on all surfaces revealed a significant decrease in the association rate of the free hapten as compared to a planar silanised surface.

CM-dextran hydrogels have been widely incorporated into biointerfaces as biomolecules attached to flexible dextran chains are freely accessible in three dimensional space, thus minimising steric hindrance (Löfås and Johnsson., 1990). This biocompatible surface preserves the biological activity of the biomolecule and minimises non-specific binding (Löfås *et al.*, 1993) thus obviating the

requirement for a blocking agent. As outlined above (section 1.3.3.1), a key advantage of using surface carboxylic groups is the ability to preconcentrate the ligand onto the surface through electrostatic attraction. A low ionic strength solubilisation buffer and a pH below the isoelectric point of the protein is required. This enables efficient coupling of the ligand from dilute solutions onto a pre-activated surface. A variety of well-defined surface chemistries can be used to couple the biomolecule via amine, thiol, disulphide or aldehyde groups. This biointerface is well established and is employed by the majority of direct 'real-time' biosensors currently available. A similar biointerface was assembled for the evaluation of biomolecular interactions using a novel miniature SPR transducer and is discussed in detail in section 5.2.3.4.2. This biointerface was selected to facilitate a high surface capacity thus maximising the sensor response. Stein and Gerisch (1996) demonstrated that a hydrophobic character can be generated in CM-dextran hydrogels by extensive covalent substitution with medium length alkyl chains. The hydrophobic surface was shown to bind phospholipid anchored cell adhesion molecules through hydrophobic interactions and these were further stabilised by specific covalent bonds. However, this amphiphilic surface may have few applications due to its high potential for non-specific binding to the hydrophobic interaction sites.

Hydrophilic polymers are unsuitable for the detection of cells (e.g. bacteria, mammalian cells), as cells cannot penetrate the hydrogel layer (BIACORE AB, 1995). This prevents them from interacting with the most powerful region of the evanescent field and results in lower sensitivity. Watts and Lowe (1994) found that planar functionalised aminosilanised surfaces yielded higher cell binding responses than dextranised surfaces for the detection of *Staphylococcus aureus*. In addition, hydrogels considerably increase the viscosity at the interaction surface, which makes them particularly unsuitable for piezoelectric-transduction systems (Dahint *et al.*, 1994). Renken *et al.* (1996) investigated the use of a hydrogel to improve the antigen-binding capacities and the non-specific binding characteristics of an acoustic plate mode sensor and found that the improvement in capacity was negated by the viscoelastic properties of the film. Furthermore, the high viscosity of hydrogels can alter the diffusion coefficient within the interaction layer and retard reaction kinetics.

1.3.4 Synthetic Membrane Structures

1.3.4.1 Langmuir-Blodgett Films. Langmuir-Blodgett films have been used in many biosensing formats (Nicolini *et al.*, 1995) and involve the transfer of a film-assembled at an air-water interface onto a solid substrate by spontaneous adsorption. Amphiphiles possess a water-soluble polar headgroup and a hydrophobic tail. These molecules (e.g. phospholipids and some proteins) form monolayers at an air-water interface that can be deposited onto a substrate surface by Langmuir-Blodgett transfer. Briefly, the amphiphile is dissolved in a volatile water immiscible

solvent and a drop from a syringe is placed onto the aqueous phase. The amount of amphiphile added must be optimised to ensure the development of a suitable film after solvent evaporation. The film is then compressed causing a thermodynamic change from a gas-analogue to a liquid-expanded state. Further compression leads to the formation of a liquid condensed state and finally, a non-compressible crystalline phase that is adsorbed onto the substrate using an immersion technique. The hydrophilic polar head-group spontaneously orientates towards the aqueous phase if the substrate is hydrophobic. Antibody films can be generated using this technique (Nicolini *et al.*, 1995) but tend to orientate randomly in the water subphase direction and/or in the gas phase direction causing denaturation. Dubrovsky *et al.* (1993) observed dramatic steric hindrance relative to molecular size. Anti-hapten antibody films retained 46 % of their total free hapten binding capacity but a thyroglobulin-hapten conjugate retained only 0.25 % and a soybean inhibitor of trypsin-hapten conjugate only 8 %. Furthermore, Langmuir-Blodgett transfer requires rigorous optimisation and high concentrations of antibody. Ahluwalia *et al.* (1991) compared physisorption and covalent cross-linking via aminosilanisation, avidin-biotin bridging and Langmuir-Blodgett films for antibody immobilisation and found that non-specific binding was significant for all immobilisation strategies studied.

1.3.4.2 *Supported Lipid Mono/Bi-layers.* Synthetic membranes were originally developed for modelling cell-cell interactions, cell-ligand interactions of the immune system and for the study of lateral diffusion of biomolecules. Many receptors require a membrane-like environment for optimal biological activity and, hence, a hybrid supported lipid bilayer may be assembled to mimic the native membrane. Receptors can be reconstituted in such synthetic membranes, thus avoiding solubilisation difficulties, protein denaturation and the associated decreases in biological activity. Supported lipid bilayers possess high stability, are easily prepared and are also readily functionalised with a range of non-amphiphilic biomolecules (Masson *et al.*, 1994, Cooper *et al.*, 1998). Liposomes are generated by extrusion of uncharged phospholipids into an aqueous buffer where spontaneous assembly of phospholipid bilayer vesicles occurs. If the initial phospholipid mixture is doped with an amphiphilic molecule, this will be incorporated into the liposomes. liposomes can be adsorbed onto a surface derivatised with a hydrophobic self-assembled monolayer to form a hybrid supported lipid bilayer. Alternatively, charged liposomes can adsorb onto a hydrophilic oppositely charged self-assembled monolayer to create an exposed hydrophobic fatty acid monolayer stabilised by ionic interactions. Re-exposure of this surface to liposomes establishes a supported phospholipid bilayer on the surface.

Mixed hybrid supported phospholipid bilayers can be generated from a mixture of biotin-labelled and unlabelled phospholipids and used to cross-link biotinylated non-amphiphilic ligands to the

surface via streptavidin (Fujita *et al.*, 1994). Alternatively lipid tagging of biomolecules by chemical or genetic manipulation is also a suitable means of anchoring soluble non-amphiphilic biomolecules to the synthetic membrane (Keinänen and Laukanen, 1994). Steinem *et al.* (1997) employed a quartz crystal microbalance biosensor to investigate the interaction of the lectin, peanut agglutinin, with a membrane receptor (ganglioside G_{M1})-doped supported lipid bilayer. BIACORE AB have designed an SPR chip coated with a hydrophobic self-assembled monolayer to enable the generation of a hybrid lipid bilayer (BIACORE™, 1995). User prepared liposomes, doped with the ligand of interest, are prepared and fused with the hydrophobic surface of the chip. The resulting bilayer is stable in aqueous buffer and to extremes of pH and ionic strength. Plant *et al.* (1995) generated a similar bilayer and found it to be stable on exposure to harsh regeneration solutions while complete removal of the phospholipid layer could be achieved using ethanol. In addition, non-specific binding to the membrane-like surface was negligible. Elender *et al.* (1996) produced a novel lipid bilayer on a glass substrate. The substrate was silanised to incorporate exposed epoxy groups for the covalent attachment of a dextran hydrogel. A lipid bilayer was constructed on top of the hydrogel by deposition of two phospholipid films using Langmuir-Blodgett transfer. It was speculated that the occurrence of membrane defects would be minimised due to the mobility of the bilayer over the lubricating hydrogel.

1.4.0 Affinity Ligands.

The development of 'real-time' biomolecular interaction analysis technology was prompted by the need to investigate and exploit biomolecular interactions. Originally developed for the characterisation of antibody-antigen interactions, a myriad of scientific papers now describe the study of a wide range of biomolecules. Furthermore, 'real-time' biomolecular interaction analysis technology has proved to be a powerful tool for the discovery and selection of an ever-increasing library of affinity-based molecules. Evanescent field-based biosensors are generic refractive index sensors and, hence, high molecular weight biomolecules elicit higher responses relative to low molecular weight biomolecules. However, the sensitivity afforded by current technology facilitates the detection of low molecular weight molecules (~ 200 Da). In addition, amplification systems based on high refractive index latex particles and colloidal gold have been successfully employed (Buckle *et al.*, 1993; Severs and Schasfoort, 1993) to increase immunoassay sensitivity. The investigations outlined in this dissertation include the study of antibody-antigen interactions and the detection of red blood cells using immobilised antibodies. Therefore, a review of antibody structure and production is presented. In addition, a brief description of non-immunological affinity ligands is included.

1.4.1 ***Polyclonal and Monoclonal Antibodies.*** Antibodies are serum proteins that are produced by B-lymphocytes in response to a foreign substance (i.e. antigen). A detailed review of antibody origin, structure and function was completed by Elgert (1996) but a brief description will be presented. Antibodies may be raised to almost all classes of substances including, proteins, polysaccharides, nucleic acids and complex particles (e.g. pollens, infectious agents and cells). They usually display high binding affinities for the target antigen and mediate many biological effector functions as part of the humoral immune system. Naturally occurring antibodies are bivalent antigen-binding molecules whose binding specificity is dictated by the choice of antigen used for immunisation. Initially, it was envisaged that antibody technology would be widely employed in therapeutic applications. However, such applications have been limited as compared to the diverse range of immunodiagnostic assay applications currently available. Traditionally, all antibody sera were purified from whole blood extracted from an animal that had undergone an immunisation procedure against the target antigen. These polyclonal antibody preparations are composed of many antibody isotopes with specificities for a range of epitopes located on the antigen surface. This heterogeneity limited the application of polyclonal antibodies in many areas. However, the development of monoclonal antibody (mAb) technology (Kohler and Milstein, 1975) has provided a source of homogenous antibody preparations of defined specificity. MAb are, as their name suggests, derived from a single clonal cell line known as a hybridoma. As a result, a homogenous population of antibodies with a single specificity for a defined epitope is produced. MAb have largely replaced polyclonal antibodies due to their homogeneity, reliable availability and negligible batch-to-batch variation.

Hybridomas are produced by cell fusion (e.g. somatic cell hybridisation) of antibody-secreting lymphocytes (extracted from an antigen-immunised mouse) with immortal myeloma cells. The heterogeneous population of hybridomas is diluted so that a single cell is aliquoted to each well of a 96-well microtitre plate. The cells grow and divide and secrete mAb into the media. The mAb contained in the media in each well is screened for antigen-binding activity using ELISA (Sedgwick and Holt, 1986) or preferably by 'real-time' biomolecular interaction analysis technology (Fägerstam and O' Shannessy, 1993). Selected hybridomas are cultured at larger scale and the mAb is isolated from the culture supernatant. Besides monospecific bivalent monoclonal antibodies (mAb), biomolecular monovalent antibodies (bsAb) capable of simultaneously binding two different antigens have been developed. These have found many therapeutic applications including drug targeting (Flavell *et al.*, 1991; French *et al.*, 1995(a); French *et al.*, 1995(b)), T-cell targeting (Chen *et al.*, 1992; Moreno *et al.*, 1995) and cytokine targeting (Robert *et al.*, 1996). BsAb have also been used to simplify ELISA formats (Görög *et al.*, 1989; Reinartz *et al.*, 1996), in immunohistochemical testing (Milstein and Cuello, 1984) and in biosensors formats (Turner, 1997).

1.4.2 ***Antibody Structure.*** A detailed understanding of antibody structure is required to appreciate recent developments and the future potential of antibody technology. Briefly, an antibody is a Y-shaped molecule (*Figure 1.4.2*) that possesses two identical antigen-binding sites.

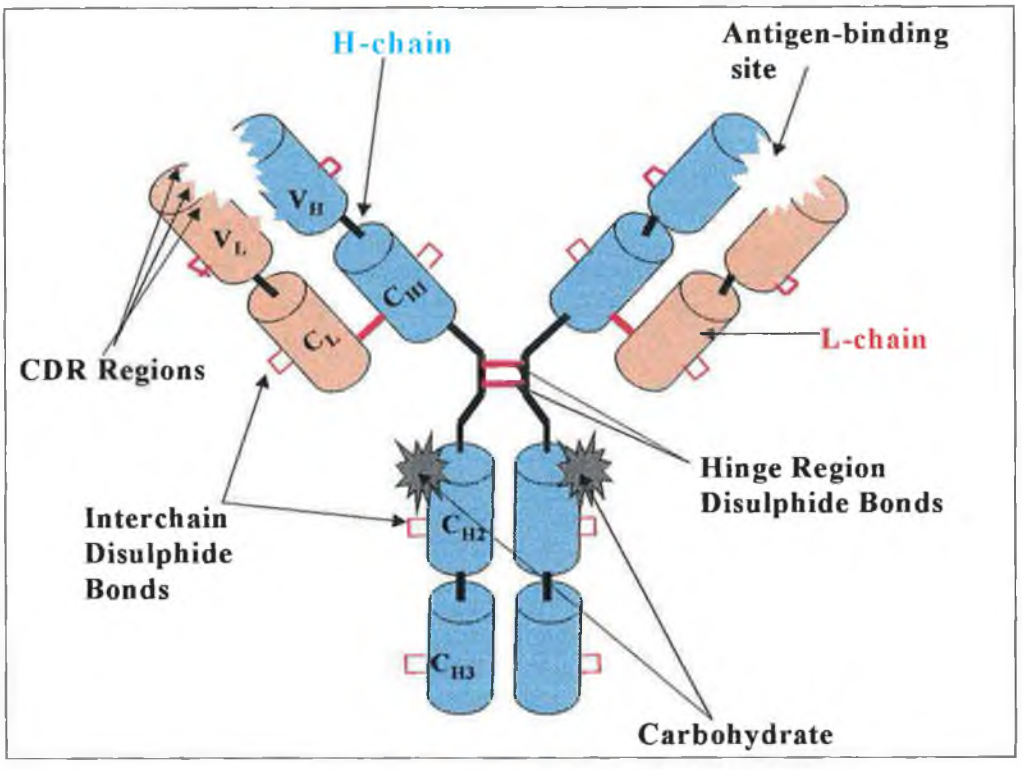

Figure 1.4.2. Illustration of antibody structure. The antibody is composed of four peptide chains that fold into domains which are stabilised by disulphide bonds. Both antigen-binding sites are formed by association of the variable region of the heavy chain (V_H) with the variable region of the light chain (V_L) and the amino acid residues that form the binding contacts with the antigen are located in the CDR regions. The hinge region is formed by disulphide bonds that link both heavy chains. Carbohydrate residues are commonly located along the constant domains but the biological role of these residues is uncertain.

Each binding site is formed from two polypeptide chains, one heavy (H) chain (50 kDa) and one light (L) chain (22 kDa) that are linked by a disulphide bridge. The variable region is composed of the variable heavy (V_H) and variable light (V_L) domains, which show amino acid variability between antibodies. X-ray crystallographic studies have found that six complementarity determining regions (CDR) form the strongest contacts with the antigen and define the antibody binding properties (Chothia *et al.*, 1989). The CDRs from both V_H and V_L domains associate in three-dimensional space to form the antigen-binding site (idiotype). Thus, the antigen-binding site is formed by a small number of segments of variable structure effectively grafted onto a scaffolding of an essentially invariant structure. Furthermore, studies indicate that the V_H region plays a greater role in antigen-binding than the V_L region (Noel *et al.*, 1996).

1.4.3 Antibody Engineering. The domain structure of the antibody molecule facilitates protein engineering and genetic engineering manipulations. Progress in antibody engineering has stemmed from the need to produce large quantities of clinical grade immunoreagents for *in vivo* therapeutics and the search for more efficient, cost effective reagents tailored for immunosensing applications (Sandhu, 1992). Gene technology has revolutionised the production of antibody fragments, as antibody genes can now be cloned directly from the lymphocytes of an immunised/non-immunised animal and expressed in baculovirus, animal, bacterial, insect and yeast cells (see review of Morrison, 1992) (*Figure 1.4.3*).

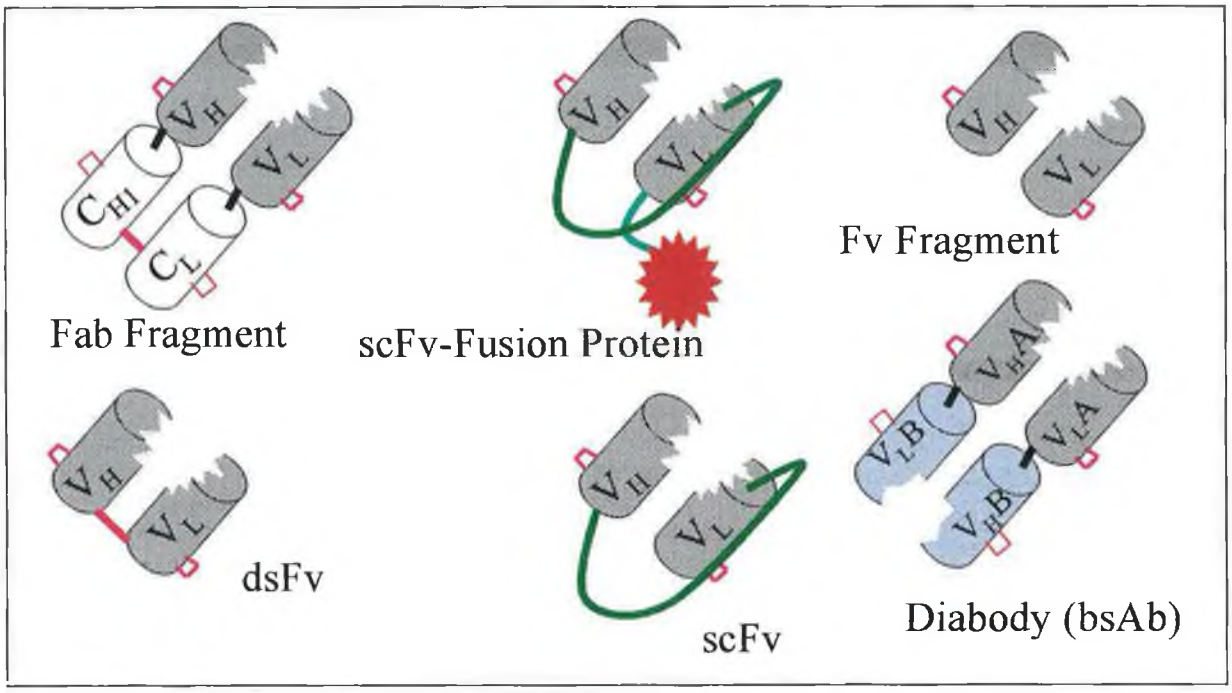

Figure 1.4.3. Illustration of truncated antibody derivatives. The six truncated antibody derivatives presented above can be produced recombinantly. Essentially, each derivative consists of an intact Fv region(s) but differ with respect to accessory linker peptides and domains (Note. See text for details). The isolated Fv fragment shown above is unstable in solution and, hence, the generation of Fab fragments is preferable. Alternatively, the Fv fragment can be stabilised by introducing a disulphide bond to cross-link both chains of the Fv domain (dsFv). However, the incorporation of a hydrophilic peptide to link both chains is more flexible (scFv). An additional functionality can be introduced by expressing the scFv in conjunction with a domain that possesses another biological activity (e.g. enzyme). Furthermore, the individual four chains that compose two whole Fv domains of two different parental antibodies can be co-expressed to form a bispecific antibody (diabody) that is capable of simultaneously cross-linking two different antigens.

Prokaryotic expression systems offer many advantages (Plückthun, 1990) such as rapid growth and well-characterised fermentation conditions both of which facilitate large-scale production. However, such expression systems commonly yield an inferior product (Samuelson *et al.*, 1996) as

a result of inappropriate post translational modifications and purification difficulties. Rapid progress in antibody technology has allowed the transfer of binding specificity from one antibody to another (Jones *et al.*, 1986), the alteration of antigen-binding characteristics (Roberts *et al.*, 1987) and the production of a range of truncated antibody derivatives (Killard *et al.*, 1995). The new generation of designer antibody molecules include Fv fragments, disulphide-stabilised Fv (dsFv), single-chain Fv (scFv), diabodies and fusion proteins possessing additional effector functions. Even synthetic peptides based on CDR sequences have been shown to bind antigen with high specificity (Levi *et al.*, 1993).

1.4.4 ***Advantages of Antibody Derivatives.*** Antibody derivatives offer a number of advantages over whole IgG for immunoassay and biosensing applications (Malmqvist, 1994).

(1) Reduction of non-specific binding. Whole IgG contains an Fc region that tends to non-specifically bind to non-antigenic components in crude samples. However, truncation eliminates unnecessary framework regions, thereby decreasing the number of potential non-specific binding sites.

(2) Monovalency. Monovalent antibody derivatives have been used to measure binding constants (George *et al.*, 1995) as monovalency prevents the formation of antigen-bridged complexes that result in an increase in binding avidity (MacKenzie *et al.*, 1996). Griffiths and Hall (1993) found a 10-fold higher dissociation rate constant for a monovalent antibody fragment in comparison to its bivalent parental Ab. The ability to regenerate a biomolecular interaction layer after a binding event is often the limiting factor in biosensor applications. High binding avidity resulting from multivalency is often responsible and may be reduced by employing monovalent antibody derivatives, which facilitate regeneration under mild conditions of pH, ionic strength and temperature.

(3) In contrast to polyclonal antibodies of animal origin and mAb from hybridoma technology, recombinant production promises to supply copious amounts of low cost, homogenous antibody derivatives.

(4) *De novo* selection of antibody genes from gene libraries allows the unrestricted generation of antibody derivatives against almost any substance (e.g. self-antigens) (Griffiths and Hall, 1993).

1.4.5 ***Sources and Structure of Antibody Derivatives.***

1.4.5.1 *Bifunctional Antibodies*: Bifunctional antibodies or, more correctly, bispecific antibodies (bsAb), can be produced by biological, genetic engineering and chemical methods (Nolan and O'Kennedy, 1990; Xiang *et al.*, 1992). Biological production of bsAb involves the generation of quadromas or triomas by somatic cell hybridisation and drug resistance selection techniques to eliminate the parent cells (Suresh *et al.*, 1986). Both quadromas and triomas produce

continuous cell lines that are clonal in origin and secrete bsAb. Quadromas are generated from the fusion of two different hybridoma cell lines (Milstein and Cuello, 1984). Triomas are produced by the fusion of a hybridoma cell line with spleen cells from an animal immunised against the second target antigen. Chemical methods for bsAb production (Cook and Wood, 1994; Coloma and Morrison, 1997) avoid the purification problems associated with the heterogeneous mixtures of parental and bsAb obtained from biological production systems. The most commonly used method involves limited pepsin hydrolysis of whole IgG to produce $F(ab)_2$ fragments. These are reduced to Fab fragments and recombined with Fab fragments of a different specificity by disulphide exchange to yield a hybrid $F(ab)_2$ bsAb (Brennan *et al.*, 1985). Alternatively, the cross-linking of the free thiols of both parental Fab species with O-phenylene-dimaleimide (Glennie, 1987) may be employed. This is a more flexible procedure that prevents parental antibody combinations and may be modified to produce trispecific $F(ab)_3$ antibodies (Tutt *et al.*, 1991; Schott *et al.*, 1993). However, the production of these multispecific derivatives is dependent on the number of hinge-region disulphide bonds present, a factor that varies between species. BsAb are more difficult to produce using recombinant technology because of problems inherent in the proper folding and association of V_H and V_L domains. However, Coloma and Morrison (1997) generated a novel recombinant tetravalent bsAb in which a scFv of one specificity was fused close to the hinge region or C-terminus of an antibody of a different specificity. A gene construct encoding the necessary gene segment was created and expressed by a transfectoma. Mack *et al.* (1995) simplified bsAb production by expressing a gene construct that encoded for two scFv derivatives connected via a peptide linker, thus reducing the number of domains and facilitating correct folding of the protein.

Pack and Plückthun (1992) described a novel technique for the production of functional dimeric Fv fragments in *Escherichi coli (E. coli)* that could easily be applied to the production of bsAb. A scFv gene construct was created and fused with genes encoding a mouse IgG hinge region, an amphiphilic helix (i.e. leucine zipper or four-helix bundle) and an optional cysteine-containing peptide. The constructs were expressed in *E. coli* and the translated product spontaneously dimerised to form the expected dimer. The incorporation of a disulphide stabilised bundle-helix produced stable dimers with equivalent binding characteristics to the parental antibodies whereas the leucine zipper approach yielded lower affinity dimers relative to the bundle-helix approach. A tetrameric mini-antibody was produced using a similar approach (Pack *et al.*, 1995) and, as expected, possessed greater antigen-binding avidity relative to the dimeric form.

1.4.5.2 *Fab fragments*. Whole antibodies can be proteolytically cleaved into two identical Fab fragments and one constant Fc fragment (Parham, 1983). Each Fab fragment contains the complete L-chain (V_L and C_L) and the first two domains of the H-chain (V_H and C_H), and possesses similar binding affinity to the parental antibody. However, antibodies from separate animal species and subtype differ in their susceptibility to proteolytic cleavage. Mouse IgG is typically cleaved with pepsin to yield $F(ab)_2$, but subtypes IgG_{2a} and IgG_{2b} are usually cleaved by papain to yield Fab. The bivalent $F(ab)_2$ fragment can be reduced with mercaptoethanol and acetylated with iodoacetamide in the absence of light to produce stable Fab fragments.

Fab fragments prepared by proteolysis are difficult to produce in high yield whereas recombinant Fab fragments are low cost homogenous antibody reagents of high purity. Scholthof *et al.* (1997) extracted the mRNA encoding the Fab fragment from a hydridoma secreting the mAb of interest. This was converted into complementary DNA, amplified (i.e. polymerase chain reaction) and inserted into a phagemid vector. Phage displaying the target Fab fragments were selected using magnetic beads coated with antigen. The encoding DNA was incorporated into an expression system that was designed to facilitate the production of soluble Fab fragments that could be recovered from the culture supernatant.

1.4.5.3 *Fv Derivatives*. The Fv fragment is the smallest antibody derivative that incorporates the whole antigen-binding site. The Fv fragment remained largely unavailable until recombinant DNA technology was applied. The genes encoding V_H and V_L domains of a given mAb are expressed separately in *E. coli* and associate non-covalently (Skerra and Plückthun, 1988). However, the stability of Fv heterodimers varies greatly despite their highly conserved framework regions. This instability has been shown by the dissociation of Fv heterodimers at high dilutions. However, the unstable association of V_H and V_L domains can be stabilised by engineering disulphide bonds into conserved framework regions (Brinkmann *et al.*, 1997; Reiter *et al.*, 1994). Cysteine residues can be genetically introduced at universal framework positions that do not interfere with the antigen-binding site. These disulphide stabilised Fv (dsFv) derivatives possess a lower tendency to aggregate and retain antigen-binding activity. Alternatively, the Fv derivative may also be stabilised by engineering an appropriate oligonucleotide into the Fv gene construct that, when translated yields a single polypeptide chain with a linker peptide bridging the two variable domains (Huston *et al.*, 1988; Savage *et al.*, 1993, de Haard *et al.*, 1998, Longstaff *et al.*, 1998).

1.4.5.4 *Minimal Recognition Units*. These are synthetic peptides that contain one or two CDR regions and have been found to bind antigen or inhibit binding of antibody (Levi *et al.*, 1993). However, due to the structural simplicity of these peptides, cross-reactivity (Arevalo *et al.*, 1993)

with similar recognition sequences is common. In addition, the selection of CDR-containing fragments of an antibody for peptide synthesis requires a detailed knowledge of the tertiary structure, which can be provided by X-ray crystallography (Williams *et al.*, 1989).

1.4.5.5 ScFv-Fusion Proteins. The specificity of antibodies can be combined with other effector functions in the form of a scFv-fusion protein (Chaudhary, 1989; Rodrigues *et al.*, 1995; Chowdhury *et al.*, 1998). These molecules obviate the need for chemical conjugation procedures (Yoshitake *et al.*, 1982; Fujiwara *et al.*, 1988) and, hence, simplify both immunoassay (Lindbladh *et al.*, 1993) and diagnostic histopathology (Spooner *et al.*, 1994). In principle, scFv-proteins may be constructed to incorporate the Fv region of any mAb and the effector protein of choice, offering the potential to produce a diverse range of molecules with novel effector functions. The construction of a scFv-fusion protein is similar in principle to scFv production. ScFv-fusion proteins have been constructed for drug targeting (Chaudhary *et al.*, 1989; Brinkmann *et al.*, 1993 (a) and 1993 (b)), for T-cell targeting (Traunecker *et al.*, 1991; Traunecker *et al.*, 1992; Katayose *et al.*, 1996) and as novel assay reagents (Hengsakul and Cass, 1997). Success in producing biologically active fusion proteins relies on the ability of the fused molecules to fold independently to allow reconstitution of biologically active domains. Fusion proteins possessing a high degree of structural complexity are less likely to succeed due to the limited ability of prokaryotic systems to the express complex eukaryotic proteins in their native conformation. A scFv-protein A fusion protein was created, and, when expressed, could form complexes with antibodies of different specificity and had the potential to create multivalent bispecific complexes (Ito and Kurosawa, 1993). Single-chain antibody derivatives have been expressed together with a hydrophobic lipid tag in order to facilitate directed incorporation into liposomes. The multivalent immunoliposome was passed over an antigen-coated surface and bound virtually irreversibly due to powerful avidity effects (Laukanen *et al.*, 1994).

Other affinity ligands have been engineered in a similar fashion to possess a tag intended to improve expression, facilitate purification and/or enable immobilisation through affinity-capture (Kipriyanov *et al.*, 1996). Hengsakul and Cass (1997) expressed the enzyme alkaline phosphatase fused with a streptavidin binding peptide. It was purified on a streptavidin affinity column and was shown to retain enzymatic activity.

1.4.5.6 Diabodies. Diabodies are composed of two antibody chains, each chain containing a V_H domain linked to a V_L domain by a short polypeptide linker (Gruber *et al.*, 1994; Mallender and Voss, 1994; Mack *et al.*, 1995). By employing a linker (5 residues) that is too short to allow pairing between the two domains on the same chain, the domains are forced to pair with complementary domains of another chain and, thus, two functionalised antigen-binding sites are

created. These dimeric antibody fragments can be designed as bivalent or bispecific molecules. Diabodies can be recombinantly produced in a similar manner to scFv. To produce a biomolecular monovalent diabody the V_H domain of one antibody is linked to the V_L domain of another on the same polypeptide chain to create two chains. These chains are co-expressed in the same cell and associate *in vivo* to form dimers with two antigen-binding sites (Holliger *et al.*, 1993).

1.5.0 ***Phage Display and Combinatorial Libraries.*** Gene libraries and phage selection technology provide powerful systems for the selection of antibody derivatives of defined specificity (Hoogenboom, 1997, Mc Call *et al.*, 1998). With further development these techniques may replace conventional hybridoma technology and obviate the use of animals (Marks *et al.*, 1992). However, antibodies derived from immunised animal sources result in much higher affinity antibodies relative to *de novo* approaches. The phage display approach, together with the possibility of creating large libraries of H- and L-chains, has resulted in the cloning of antibody genes derived from both immunised (Huse *et al.*, 1989) and non-immunised sources (Griffiths *et al.*, 1993). The phage particle is a convenient host for the display of large libraries of peptides or antibody fragments since it inherently couples the displayed protein with the encoding DNA. A phage display library is panned by selecting those phage displaying antibody fragments possessing affinity towards the immobilised target through the use of affinity chromatography. The DNA encoding a single antibody fragment can be isolated and amplified and the product expressed recombinantly in a soluble form.

Semi-synthetic gene libraries can be generated by taking genes encoding the antibody variable regions derived from an unimmunised animal (i.e. naive libraries) and subjecting them to mutagenesis using chemicals or error-prone PCR. The incorporation of a chain shuffling system further increases the size of the library and, hence, facilitates the selection of higher affinity antibodies. Monovalent (single copy) expression vectors that favour selection of antibody fragments based on high affinity binding to antigen (Lowman and Wells, 1993) are currently available. Baca *et al.* (1997) successfully used monovalent phage display for the selection of high affinity humanised Fab fragments from a library of human Fab fragments created by CDR transplantation and random mutagenesis of selected framework positions. The BIACORE analyser has been used for the selection of antigen binders in phage display and, unlike conventional panning techniques (Deng *et al.*, 1994; Malmborg *et al.*, 1996), binders were selected on the basis of association and dissociation rate constants.

1.6.0 Non-Immunoglobulin Affinity Ligands

1.6.1 *Synthetic Peptides.* Synthetic peptides offer an alternative to the use of complex biomolecular affinity ligands where the majority of the protein framework does not contribute to the recognition event but increases the probability of non-specific binding. These peptides are generally more stable, are of defined chemical composition and are readily synthesised. Their behaviour is easier to predict due to their structural simplicity but their affinity towards the target analyte is generally lower than antibody-antigen affinities. Short peptide sequences can be chemically synthesised in solution or on solid-phase. However, selection from phage display libraries (i.e. biological production) offers considerable advantages with respect to affinity selection (Houghten, 1993). In addition, specific functional groups can be introduced to facilitate directed controlled immobilisation. For example, a terminal thiol group can be introduced to facilitate self-assembly onto a gold surface (Van Den Heuvel *et al.*, 1993).

1.6.2 *Peptabody.* Multivalent biomolecules such as IgM are characterised by a low intrinsic affinity but compensate by forming multiple attachments with the antigen. Terskikh *et al.* (1997) mimicked this effect to produce a multivalent peptabody capable of binding a specific target with high avidity (*Figure 1.6.2*).

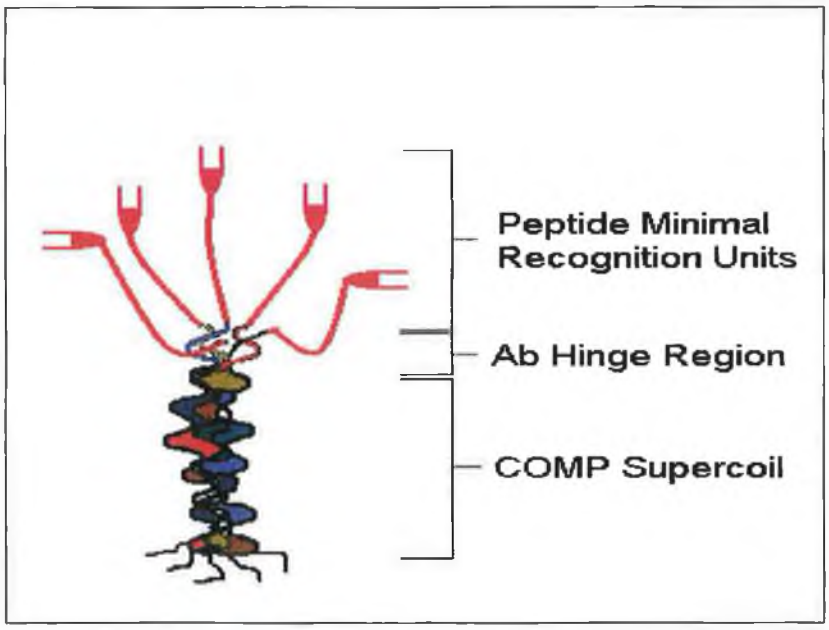

Figure 1.6.2. Illustration of a peptabody.

A fusion gene was engineered to encode a short polypeptide with affinity for a specific target analyte (selected from a phage display library), an antibody hinge region and the assembly domain of the cartilage oligomeric matrix protein (COMP), which spontaneously forms a five stranded α-

helix bundle. The gene construct was expressed by bacteria and produced a single protein chain that spontaneously assembled into a stable homopentamer. The 'peptabody' possessed an avidity equivalent to a typical native antibody and over 10^5-fold greater than the free peptide.

1.6.3 *Lectins.* Lectins are biomolecules capable of binding specific carbohydrate moieties with high affinity (Schwarz *et al.,* 1993) in a manner analogous to antibody-antigen interactions (Peacock *et al.,* 1990). They commonly possess two or more binding sites that require metal ions (e.g. Ca^{2+}, Mg^{2+}) for binding activity (Einspahr *et al.,* 1986). Lectins bind to complex carbohydrate structures with higher affinity relative to simpler structures and some can be use to distinguish complex structural features of glycoconjugates. Simple sugars can be used to competitively elute glycoconjugates (e.g. IgM) during affinity chromatography. However, the reduced affinity for simple sugars necessitates the use of high molar excesses (Merkle and Cummings, 1984). A vast collection of lectins have been discovered and purified from plant seeds but other sources include bacteria, moulds, lichens, sponges, fish, sera, eggs and animal cell membranes. Lectins have been used for the quantitative detection and/or purification of oligosaccharides, glycolipids, glycoproteins (Merkle and Cummings, 1984), cell-bound glycoconjugates (blood typing) and cells. Other applications include blood typing, mitogenesis of lymphocytes, cell agglutination and tissue typing. 'Real-time' biomolecular interaction analysis has been used for qualitative and quantitative analysis of lectin-oligosaccharide interactions (Shinohara *et al.,* 1994; Yamamoto *et al.,* 1994) and to characterise carbohydrate moieties of cells and biomolecules (Hutchinson,, 1994). Section 4.2.1 describes a feasibility study that investigated the binding of red blood cells to an immobilised lectin (concanavalin A) using 'real-time' biomolecular interaction analysis. Concanavalin A was chosen because it binds exposed glucose and mannose residues that are found in abundance on the surface of red blood cells.

1.6.4 *Nucleic Acids.* Techniques for the isolation and sequencing of specific genes have been rapidly advancing over the past decade. However, techniques that allow rapid identification and characterisation of protein-DNA interactions, DNA strand separation, DNA hybridisation and enzyme catalysed DNA manipulations have been limited. 'Real-time' biomolecular interaction analysis can be used for the study of DNA hybridisation (Watts *et al.*, 1995, Asensio *et al.*, 1998) and gene regulation (Bondeson *et al.*, 1993; Parsons *et al.,* 1995). A synthetic double stranded oligonucleotide encoding the operator site for the *Lac*-operon was immobilised and the binding constants for the interaction with the lactose repressor protein were determined. Nilsson *et al.* (1995) demonstrated the use of 'real-time' biomolecular interaction analysis for the analysis of routinely used molecular biology techniques employed for solid state gene assembly. Biotinylated nucleic acid (25-mers) was immobilised onto a streptavidin-coated hydrogel and the processes of

DNA strand separation, DNA hybridisation, enzyme catalysed DNA ligation and restriction were monitored in 'real-time'. Furthermore, immobilised single stranded DNA or RNA probes can be used to screen samples for the presence of a complementary sequence by observing the hybridisation interaction (Wood, 1993). 'Real-time' biomolecular interaction analysis technology is currently being adapted to facilitate the detection of point mutations by calculating kinetic and affinity parameters that can be related to hybridisation of base-pairs and DNA/RNA probes (Persson *et al.*, 1997).

1.6.5 *Receptors.* Membrane bound receptors are involved in a vast number of affector functions including cell-signalling processes, cell mobility and cell adherence mechanisms. Specific receptors have been associated with viral infection and the assimilation of bacterial toxins. Gangliosides are characterised by various carbohydrate moieties and act as receptors for a wide variety of molecules (e.g. bacterial toxins, peptide hormones). The ganglioside receptor, GM1, has been shown to behave as a receptor for cholera toxin, a variety of enterotoxins and *Salmonella* infection. Kuziemko *et al.* (1996) investigated the interaction between cholera toxin and a range of ganglioside receptors using a synthetic membrane biointerface.

1.6.6 *Mimetic Imprinted Polymers.* Molecular imprinted polymers are non-biological synthetic polymers capable of binding specific target molecules (Mayes and Mosbach, 1997). Briefly, a polymer solution possessing a variety of functional groups surrounds the analyte (print molecule) and spontaneously adopts a complementary association with the exposed functional groups. Polymerisation effectively captures this interaction forming a rigid highly cross-linked macroporous structure. Removal of the print molecule leaves binding sites possessing complementary steric and functional topography to the imprint species. Kriz *et al.* (1995) produced two molecular imprinted polymers using dansyl-L-phenylalanine and dansyl-D-phenylalanine as imprints. It was found that each bound both enantiomers, but the specific enantiomer used for imprinting was more strongly bound. This is of considerable significance as chiral drugs and their metabolites often possess different pharmacological and pharmacokinetic properties. With further development molecular imprinted polymer technology may facilitate the production of enantiomerically homogenous pharmaceuticals (Nicholls *et al.*, 1995). However, the time required to reach equilibrium and loading capacities must be improved. Nevertheless, replacement of biological affinity ligands would undoubtedly represent a major advance but it seems unlikely that these systems could match the high specificity and affinity that characterise natural affinity ligands.

1.7.0 ***Kinetics Analysis Employing 'Real-time' Interaction Analysis.*** Studies performed using several Fab-antigen complexes have revealed that combinations of several forces co-operatively determine the binding strength and specificity. These interaction forces include charge complementarity, hydrogen bonding, hydrophobic interactions, surface complementarity and, to a lesser extent, Van der Waals forces (Davies *et al.*, 1988). Despite the complexity and specificity of antigen recognition, cross-reactivity with molecules possessing a similar structure to the antigen may occasionally occur (Arevalo *et al.*, 1993). Affinity interactions are dynamic processes and measurement of the association rate constant (k_a) and the dissociation rate constant (k_d), which describe the kinetic properties of the interaction, facilitates a greater understanding of the binding event. ELISA-based techniques (Porstmann and Kiessig, 1992) are used to measure the true equilibrium constant (K_a) (Friguet *et al.*, 1985) and the k_d (Kim *et al.*, 1990). The k_d can also be determined by equilibrium dialysis (Lehtonen and Eerola., 1982) and is applicable to interactions involving low molecular weight molecules. The K_a represents the equilibrium binding properties of the interaction and is given by the quotient of the association rate constant and the dissociation rate constant. Hence, it does not give a comprehensive assessment of the biomolecular interaction.

'Real-time' biomolecular interaction analysis is a form of analytical affinity chromatography (Chaiken *et al.*, 1992). It is capable of continuous 'real-time' measurement and it can be used to determine kinetic constants (Malmborg and Borrebaeck, 1995; Edwards and Leatherbarrow, 1997). This kinetic information can be used as a basis for selection of affinity-ligands rather than using the equilibrium constant alone (Gruen *et al.*, 1994). 'Real-time' biomolecular interaction analysis has also been widely employed for the kinetic evaluation of a vast number of recognition molecules. Binding kinetics measured at interfacial layers differs from bulk solution measurements (Schuck and Minton, 1996) and is prone to many sources of interference. Furthermore, mass transport limitation may result from low mass transfer rates (i.e. low flow rates), a high concentration of surface binding sites and/or inherently fast reaction rates. Steric hindrance has been implicated in many of the deviations from the expected ideal pseudo-first-order interaction kinetic. Nieba *et al.* (1996) found that re-binding of analyte and bivalency effects can offset relative affinity parameters by as much as 500-fold. However, careful experimental design (Oddie *et al.*, 1997), correct model fitting and/or the use of short-chain dextrans may minimise such effects. An extensive evaluation of experimental techniques and data evaluation methods for the study of two model interactions is provided in chapter 3. In addition, a comprehensive introduction to the principles of kinetic evaluation is given.

1.8.0 Conclusions.

The evolution of biosensing technology continues unabated and promises to create a diverse generation of affordable biosensors. Brecht and Gauglitz (1997) suggested that parallel detection at over ninety-six interaction sites using imaging techniques may be possible in the future, allowing a vast improvement in sample throughput albeit at the expense of data quality. Miniaturisation of many of these optical sensors through microfabrication is feasible and may facilitate the production of low cost disposable sensor chips or sensor arrays. Integration of other technologies with 'real-time' biomolecular interaction analysis will expand the amount and quality of information attainable and current examples include micropreparative high-performance liquid chromatography (Nice *et al.*, 1994), mass spectroscopy (Krone *et al.*, 1997; Nelson *et al.*, 1997; Nelson and Krone, 1997) and electrochemistry (Tatsuma and Buttry, 1997). The technology has expanded to encompass a diverse range of applications. Current application developments include screening of ligands for orphan receptors, nucleic acid sequencing and the detection of point mutations by calculating kinetic and affinity parameters that can be related to hybridisation of base-pairs and DNA/RNA probes. The application of 'real-time' biomolecular interaction analysis technology to the study of DNA-protein interactions, elucidation of gene regulation systems and the study of cell signalling complexes (Schuster *et al.*, 1993) promises further exciting developments.

1.9.0 Overview of Dissertation. This dissertation describes the development of novel applications and the design of new 'real-time' biosensing technologies. A review of the published literature revealed that considerable ambiguity exists with respect to the kinetic evaluation of biomolecular interactions using current biosensor technology. Hence, methods of experimental and data analysis were evaluated for two model monoclonal antibody-antigen interactions. Furthermore, the detection of whole eukaryotic cells is largely unexplored. It was envisaged that solid phase detection and/or selection of whole cells could be monitored in 'real-time' using the BIACORE 1000™ system. In particular, solid phase blood grouping was demonstrated using immobilised blood group specific antibodies. In addition, two new SPR-based biosensors were developed to facilitate 'real-time' analysis of highly viscous red blood cell suspensions (> 50 % (v/v)) that could not be analysed using the BIACORE 1000™. These devices were constructed with a view towards providing a portable, inexpensive alternative to commercially available analysers.

Chapter 2

Materials and Methods

2.1 Reagents.

All reagents used were of analytical grade and were purchased from Sigma Chemical Co., Fancy Rd., Poole, Dorset BH12 4QH, England, unless otherwise stated. Phosphate buffer saline (PBS) was obtained as premixed tablets from Oxoid, Basingstoke, Hampshire, England, and dissolved in the recommended volume of distilled H_2O (dH_2O). When dissolved, these tablets prepare Dulbecco's A PBS, which contains 10 mM phosphate buffer and 0.14 M NaCl, pH 7.2-7.4. Bri-clone was purchased form BioResearch Ireland, Glasnevin, Dublin 9, Ireland. Dulbecco's modification of Eagles medium, fatal calf serum, HEPES, L-glutamine and non-essential amino acids were obtained from Gibco BRL, Trident House, Renfrew Rd., Paisley PA4 9RF, Scotland.

2.2 Plastic Consumables.

Sterile plastic disposables for cell culture (e.g. flasks, plates, pipettes etc.) were purchased from Corning-Costar Corporation, 45 Nagog Park, Acton, MA 01720, U.S.A. Eppendorf tubes and micropipette tips were purchased from Sarstedt Ltd., Sinnottstown Lane, Drinagh, Co Wexford, Ireland. 50-ml polypropylene centrifuge tubes were purchased from Greiner Labortechnik, Greiner GmBH, Maybachstrasse, PO Box 1162, D-7443 Frickenhausen, Germany.

2.3 *Equipment.*

The equipment used and its suppliers are listed below.

Equipment	**Supplier**
BIACORE 1000™	BIACORE AB, St. Albans, Hertfordshire AL13AW, England
BIACORE Probe ™	
CM5 chip and CM5 Probe	
Cone and plate viscometer	Browne's, Foxrock, Dublin
Daq-700 PCMCIA I/O card	National Instruments Corporation, National Instruments Corporation, 11500 N Mopac Expwy, Austin, TX 78759-3504
Fibre Optic Probe RS007	Ocean Optics, 1104 Pinehurst Rd., Dunedin, Florida, USA
Heraeus Biofuge A Microcentrifuge	Heraeus Instuments Inc., 111-A Corporate Blvd., South Plainfield, N.J. 07080, USA
Heraeus CO_2 Incubator	
Heraeus Labofuge 6000	
HB 2448K Laminar flow cabinet	Holten Laminair A/S, Gydevang 17, DK 3450 Allerod, Denmark
Laptop personal computer	Dell Computer Corporation, One Dell Way, Round Rock, TX 78682-2244. USA
Miniature S2000 spectrometer	Ocean Optics, 1104 Pinehurst Rd., Dunedin, Florida, USA
Nikon Diaphot phase contrast microscope	Nikon Corporation, 2-3 Marunouchi 3-chome, Chiyoda-ku, Tokyo, Japan.
Orbital incubator	Gallenkamp, Leicester, England
3015 pH meter	Jenway Ltd., Essex, England
RM6 Lauda waterbath	AGB Scientific Ltd., Dublin Industrial Estate, Dublin 11, Ireland
SB1 Blood tube rotator	Stuart Scientific, London, England.
Millipore glass filtration unit	AGB Scientific Ltd., Dublin Industrial Estate, Dublin 11, Ireland
Sentek pH Electrode (p56/BNC)	Sentek, Unit 6-7 Crittall Court, Crittall Drive, Braintree, Essex, England.
Sterile cell culture lab-wear	Browne's, Foxrock, Dublin, Ireland
Tiertek Multiscan Plate Reader	Flow Lab. Ltd., Woodcock Hill, Harefield Rd., Richmansworth, Hertfordshire WD3 1PQ, Emgland.
Tungsten-halogen lamp (LS-1)	Ocean Optics, 1104 Pinehurst Rd., Dunedin, Florida, USA
UV-160A spectrophotometer	Shimadzu Corp., Kyoto, Japan

2.4 *Characterisation of Macromolecular Interactions*

Anti-GST mAb and GST were both donated by Biotrin, (Mount Merrion, Dublin, Ireland). All data analysis was performed using BIAevaluation 3.0™ (BIACORE AB, St. Albans, Hertfordshire AL13AW, England) and Microsoft Excel™ software (Microsoft Corporation).

2.4.1 Production of Anti-CD4 IgG.

Frozen stocks of the OKT4 hybridoma cells were obtained from European Collection of Animal Cell Cultures (Salisbury, Wiltshire, UK.). The cells were cultured aseptically in a laminar flow cabinet, and incubated at 37 °C in a humid 5 % (v/v) CO_2 atmosphere. The cells were grown in Dulbecco's Modification of Eagle's Medium (DMEM) containing 20 % (v/v) FCS, 2 mM L-glutamine, 10 mM HEPES buffer, 0.5 % Bri-clone and 25 μg/ml gentamicin. 1 ml of frozen cell suspension was thawed in a waterbath at 37 °C and diluted with 9 ml of medium. The suspension was centrifuged for 10 min at 2,000 rpm. The cell pellet was then resuspended in 5 ml of medium and incubated in a 25 cm^3 tissue culture flask (T-25). When cells had grown to confluence in culture flasks they were taken into a suspension by gently washing the surface of the flask with medium using a sterile pasteur pipette. The suspension was poured into a sterile container and centrifuged for 10 min at 2,000 rpm. The supernatant was harvested and the pelleted cells were resuspended in 20 ml of fresh culture media. This suspension was used to seed new cultures and the supernatant was harvested as outlined above. The harvested supernatant was filtered (pore size of 0.22 μm) and 0.1 % (v/v) sodium azide was added as a preservative.

2.4.2 BIACORE Analyses (general operation)

Research grade CM5 sensor chips were employed unless otherwise stated. HBS buffer containing 10 mM HEPES, 150 mM NaCl, 3.4 M EDTA, and 0.005 % Tween 20 was used as constant running buffer. However, the Tween 20 and EDTA were omitted from the buffer during red blood cell analysis. The running buffer was filtered (pore size of 0.22 μm) and degassed using a milipore filtration apparatus (millipore sintered glass filtration unit) immediately before use. High volume samples (i.e. > 0.5 ml) were syringe-filtered (pore size of 0.22 μm) and precious low volume samples were centrifuged (13,000 RPM for 2 min using a Heraeus Biofuge) to remove any particulate matter.

2.4.3 Coupling Reaction

Standard amine coupling was employed for all studies. Activation of the carboxymethylated dextran-coated surface was carried out by mixing equal volumes of 100 mM N-hydroxysuccinimide (NHS) and 400 mM N-ethyl-N'-(dimethylaminopropyl)carbodiimide (EDC) (made up in ultrapure water

immediately before use) and injecting the mixture at 5 µl/min for 7 min. The ligand to be coupled was dissolved in 10 mM sodium acetate buffer and injected over the activated surface at 5 µl/min. Capping of unreacted sites was achieved by injecting 1 M ethanolamine, pH 8.5, for 7 min. The ligand concentration and the ligand contact time were varied in order to control the mass of ligand immobilised. In addition, the pH of the sample buffer (i.e. 10 mM sodium acetate buffer) was adjusted below the isoelectric point of the ligand to be immobilised.

2.4.4 Universal Standard Curve.

2.4.4.1 Determination of Active Concentration of Anti-CD4 IgG. CD4 (50 µg/ml in 10 mM sodium acetate buffer, pH 4.5) was immobilised (~ 7,700 RU) onto a CM5 sensor chip surface using conventional amine coupling. Three consecutive 30 sec pulses of 15 mM HCl were employed to remove non-covalently attached CD4. Neat OKT4 hybridoma supernatant (containing anti-CD4 IgG) was injected over the CD4-coated surface at 10 µl/min for 1 min and the surface was regenerated with two consecutive pulses (30 sec) of 15 mM HCl. This binding-regeneration cycle was repeated in triplicate. The CD4-coated surface denatured rapidly and, hence, a protein G-coated surface was employed for the determination of the total anti-CD4 IgG concentration.

2.4.4.2 Determination of the Total Anti-CD4 IgG. Protein G (50 µg/ml in 10 mM sodium acetate, pH 4.2) was immobilised (~ 1,000 RU) onto a CM5 sensor chip using conventional amine coupling. The surface was exposed to a 30 sec pulse of 15 mM HCl prior to commencing the analysis. Serial dilutions of OKT4 hybridoma supernatant and unused OKT4 media were prepared using HBS buffer as diluent. Dilutions from 1/8 to 1/256 were analysed. 25 µl of sample was injected at 15 µl/min and the surface was regenerated with a 30 sec pulse of 20 mM HCl and 10 mM NaOH. This procedure was repeated for each sample in triplicate

2.4.5 Flow Rate Method

Method for the determination of the total anti-CD4 concentration contained in the OKT4 hybridoma supernatant. The contribution of the contaminating bovine antibodies to the response was determined by analysing unused OKT4 culture media in parallel with the actual anti-CD4 IgG-containing hybridoma supernatant. The protein G-coated surface produced for the universal standard curve technique (section 2.4.4.2) was employed. OKT4 hybridoma supernatant was diluted (1/64) in HBS buffer and injected at 2 µl/min for 3 min. The surface was regenerated with a 30 sec pulse of 20 mM HCl and 10 mM NaOH. The sample contact time was kept constant at 3 min and the binding-regeneration cycle was repeated for injection flow rates of 5 µl/min, 10 µl/min, 25 µl/min and 50

µl/min. A 1/64 dilution of unused OKT4 culture media was prepared as a reference sample and was analysed in an identical manner. Four replicates were completed at each flow rate for all samples.

2.4.6 ***Contribution of Bovine Antibody to the Protein A Binding Response of Anti-CD4 Hybridoma Supernatant.*** Protein A (50 µg/ml in sodium acetate buffer, pH 4.3) was immobilised (~ 3,300 RU) onto a CM5 sensor chip surface. Unused OKT4 hybridoma medium was injected over the protein A-coated surface at 5 µl/min for 10 min and the surface was regenerated with a 30 sec pulse of 20 mM HCl. This binding-regeneration cycle was repeated for neat OKT4 hybridoma supernatant that contained anti-CD4 IgG. The above sequence was repeated for four replicates.

2.4.7 ***Protein A Affinity Chromatography.*** A 5 ml protein A-sepharose column was poured and equilibrated with 200 ml of PBS, pH 7.4, containing 0.3 M NaCl (running buffer). OKT4 hybridoma supernatant (200 ml) containing anti-CD4 IgG was sterile filtered (pore size of 0.22 µm). NaCl and Triton-100 were added to final concentrations of 0.3 M and 0.05 % (v/v), respectively. The pH of the supernatant was adjusted to pH 7.8 using a saturated HEPES solution, pH 8.0. The sample was added to the column and the flow rate was adjusted to 1 ml/min. The column was washed with 50 ml of running buffer after the sample had passed through the column. Affinity-captured antibody was eluted with 50 mM glycine, pH 2.4. 1 ml fractions were collected and immediately neutralised by adding saturated tris-HCl, pH 8.0, to a final concentration of 10 % (v/v). The optical density of each fraction was recorded at 280 nm and samples with an optical density > 0.05 were pooled. The final yield of antibody was 4.77 mg (i.e. 23.8 µg antibody per ml of hybridoma supernatant) assuming A_{280nm} (1 mg/ml) of 1.4. The affinity-purified antibody was dialysed against PBS (2 l) and sodium azide was added to 0.05 % (v/v). The sample was aliquotted (0.5 ml fractions) and stored at 4 °C.

2.4.8 ***Viscosity of Matrix.*** A dextran (M.W. 500 kDa) solution (20 mg/ml) was prepared using HBS buffer as diluent. A similar sample was prepared and 50 mg/ml BSA was added. The viscosity of both solutions was determined using a cone and plate viscometer (Model DV-I+) according to the manufacturer's instructions.

2.4.9 ***Reduced Dextran Biointerface***

2.4.9.1 *Preparation.* Dextranase (50 µg/ml in 50 mM phosphate buffer, pH 6.0) was injected over a blank CM5 sensor surface for 50 min at 5 µl/min. The dextranase was re-injected for a further 25 min. A reduced dextran (RD) chip was produced by incubating a CM5 chip in

dextranase solution (50 μg/ml in 50 mM phosphate buffer, pH 6.0) at 37 °C for 12 h. After incubation the chip was rinsed in H_2O and stored at 4 °C with desiccant.

2.4.9.2 *Preconcentration Test.* Bovine serum albumin (1 mg/ml in 10 mM sodium acetate buffer, pH 4.16) was injected over the dextranase-treated surface and a normal CM5 surface at 10 μl/min for 2 min and the pre-concentration responses recorded.

2.4.10 ***Determination of the Steric Hindrance Factor (n) for the CD4 Interaction.*** Anti-mouse Fc antibody (50 μg/ml in 10 mM acetate, pH 5.0) and protein G (50 μg/ml in 10 mM acetate, pH 4.2) were immobilised onto normal CM5 sensor surfaces and onto RD sensor surfaces using conventional amine coupling.

2.4.10.1 *Anti-Mouse Fc-Coated Surfaces.* Anti-CD4 IgG (10 μg/ml in HBS buffer) was injected for 2 min at 10 μl/min. CD4 (260 nM in HBS buffer) was injected over the surface at 10 μl/min for sufficient time (~ 3 to 8 min) to reach a stable response. The surface was regenerated with a 30 sec pulse of 20 mM HCl and 10 mM NaOH.

2.4.10.2 *Protein G-Coated Surfaces.* Anti-CD4 IgG (10 μg/ml in HBS buffer) was injected for 1 min at 10 μl/min. CD4 (260 nM in HBS buffer) was injected over the surface at 10 μl/min for sufficient time (~ 8 min) to reach a stable response. The surface was regenerated using a 30 sec pulse of 20 mM HCl.

2.4.11 ***Boundary Layer Steady State Affinity.*** Goat anti-mouse Fc IgG (50 μg/ml in sodium acetate, pH 5.0) was immobilised (~ 1,500 RU) onto a CM5 sensor chip surface using conventional amine coupling. CD4 samples were prepared by diluting a CD4 stock solution (100 nM CD4 dissolved in HBS, containing 0.3 M NaCl) in HBS buffer to final concentrations of 20 nM, 16 nM, 8 nM, 4 nM, 2 nM, and 1 nM. Purified anti-CD4 IgG (1.75 μg/ml in HBS buffer) was injected over the anti-mouse Fc-coated surface for 2 min at 5 μl/min. A CD4 sample was subsequently injected for 20 min at a flow rate of 5 μl/min. The surface was regenerated with a 30 sec pulse of 20 mM HCl. The above binding-regeneration sequence was repeated for each CD4 sample (random order). In addition, the CD4 sample was replaced with HBS to provide a suitable reference curve.

2.4.12 ***Solution Phase Steady State Affinity***. GST (2 μg/ml in 10 mM acetate, pH 5.0.) was immobilised (~ 2,784 RU) using conventional amine coupling. Equilibrium mixtures containing a fixed concentration of anti-GST IgG (11 nM) and serial dilutions of GST (i.e. final concentrations from 0.39 to 50 nM) were prepared in HBS buffer. The equilibrium mixtures were incubated at room temperature for 3 h. The concentration of free anti-GST IgG in each equilibrium sample was determined by constructing a calibration curve. Hence, serial dilutions of anti-GST IgG were prepared from 0.085 to 11 nM in HBS buffer. Equilibrium mixtures and standard anti-GST samples were analysed randomly (in triplicate) by injecting 25 μl over the GST-coated surface at 5 μl/min. The surface was regenerated after each sample interaction using 30 sec pulses of 20 mM HCl and 10 mM NaOH.

2.4.13 GST Saturation. Protein A (50 μg/ml in 10 mM sodium acetate, pH 4.3) was immobilised (~ 1,975 RU) onto a CM5 sensor surface. 12 μl of anti-GST IgG (10 μg/ml in HBS buffer) was injected over the protein A-coated surface at 10 μl/min. GST (200 nM in HBS buffer) was subsequently injected over the surface at 10 μl/min for 8 min and allowed to dissociate for a further 5 min. The surface was regenerated with a 30 sec pulse of HCl. The above binding-regeneration sequence was repeated for GST contact times of 6 min and 4 min.

2.4.14 ***Typical Kinetic Analysis (GST Interaction).*** Protein A (50 μg/ml in 10 mM sodium acetate, pH 4.3) was immobilised onto a RD sensor surface (~ 490 RU) using conventional amine coupling. Monoclonal anti-GST IgG (2.5 μg/ml in HBS buffer) was injected over the surface at 10 μl/min for 2 min. The baseline was allowed to stabilise for 5 min. GST (100 nM in HBS buffer) was injected for 2 min at 30 μl/min and allowed to dissociate for a further 5 min. The surface was regenerated using two 30 sec pulses of 20 mM HCl. A reference curve was obtained by replacing the GST sample with running buffer (HBS buffer).

2.4.15 ***Bulk Mass Transport Limitation for both GST and CD4 Interactions.*** Two CM5 sensor chips and a RD chip were coated with polyclonal anti-mouse-Fc IgG (50 μg/ml in 10 mM acetate, pH 5.0), protein A (50 μg/ml in 10 mM acetate, pH 4.3) and protein G (50 μg/ml in 10 mM acetate, pH 4.2), respectively.

The following binding-regeneration sequence was repeated on each surface at various antigen injection flow rates. Anti-GST IgG or anti-CD4 IgG was injected for 2 min, at a concentration of 10 μg/ml, with the exception of the protein A-coated surface, which required 2.5 μg/ml IgG to give a

comparable binding response. GST (100 nM in HBS buffer) or CD4 (20 nM in HBS containing 0.3 M NaCl) were injected for 3 min at a given flow rate and allowed to dissociate for a further 5 min. The surface was regenerated and the binding-regeneration sequence was repeated at different antigen flow rates (i.e. 5, 10, 20, 30 and 40 µl/min) in random order. The protein A-coated and protein G-coated surfaces were regenerated with a 30 sec pulse of 20 mM HCl, whereas the anti-mouse Fc IgG surface required 30 sec pulses of 20 mM HCl and 10 mM NaOH. In addition, a reference curve was produced by repeating the analysis with HBS buffer substituted for the antigen sample. Non-specific binding of GST and CD4 to each surface was determined by injecting both GST (100 nM in HBS buffer) and CD4 (20 nM in HBS buffer) over each surface in the absence of the specific antibody.

2.4.16 ***Determination of GST Saturation Response using Three Affinity-Capture Ligands.*** The surfaces prepared for the previous experiment were employed. These included two CM5-chips and a RD-chip coated with polyclonal anti-mouse-Fc IgG, protein A and protein G, respectively. The following binding-regeneration sequence was repeated on each surface for different GST contact times. 12 µl of anti-GST IgG (10 µg/ml in HBS buffer) was injected over the ligand-coated surface at 10 µl/min. GST (200 nM in HBS buffer) was subsequently injected over the surface at 30 µl/min for 8 min and allowed to dissociate for a further 5 min. The surface was regenerated and the above binding-regeneration sequence was repeated for GST contact times of 6 min and 4 min. The protein A-coated and protein G-coated surfaces were regenerated with a 30 sec pulse of 20 mM HCl, whereas the anti-mouse Fc IgG surface required 30 sec pulses of 20 mM HCl and 10 mM NaOH. GST (100 nM) was injected over each surface in the absence of anti-GST IgG to determine the non-specific binding response. Reference curves were produced by repeating the analysis with HBS buffer substituted for the GST samples.

2.4.17 ***Contact Time-Dependency.*** The contact time dependency of the GST interaction was determined from the data obtained from the saturation response study (section 2.4.16). This study was repeated for the CD4 interaction. Polyclonal anti-mouse-Fc IgG (50 µg/ml in 10 mM acetate, pH 5.0) was immobilised (~ 2,000 RU) onto a CM5 sensor chip. Purified anti-CD4 IgG (10 µg/ml in HBS buffer) was injected over the surface at 10 µl/min. CD4 (150 nM in HBS buffer) was subsequently injected over the surface at 30 µl/min and allowed to dissociate for a further 5 min. The surface was regenerated with 30 sec pulses of 20 mM HCl and 10 mM NaOH. This binding-regeneration cycle was repeated for CD4 contact times of 2, 3 and 8 min. Reference interaction curves were produced by repeating the analysis with HBS buffer substituted for the CD4 samples.

2.4.18 ***Optimisation of CD4 Interaction Conditions.*** Anti-mouse Fc IgG (50 μg/ml in 10 mM acetate, pH 5.0) was immobilised using conventional amine coupling (~ 11,000 RU). Purified anti-CD4 IgG (1.75 μg/ml in HBS) was injected at 10 μl/min for 1 min. A waiting period (5 min) was observed before injecting the CD4. CD4 (10 nM in HBS containing 0.3 M NaCl) was injected for two minutes at a given flow rate and allowed to dissociate for a further 5 min. The surface was regenerated with 30 sec pulses of 20 mM HCl and 10 mM NaOH. This binding-regeneration sequence was repeated for CD4 injection flow rates of 20, 30, 40, 50, 60, 70, 80, 90, 100 μl/min. The entire experiment was repeated with the CD4 sample substituted with HBS buffer to generate reference curves. All samples were analysed in random order.

2.4.19 ***CD4 Saturation.*** Anti-mouse Fc IgG (50 μg/ml in 10 mM acetate, pH 5.0) was immobilised using conventional amine coupling (~ 3,680 RU). Purified anti-CD4 IgG (10 μg/ml in HBS) was injected at 10 μl/min for 2 min. A 5 min waiting period was observed before injecting the CD4. CD4 (500 nM in HBS buffer) was injected for 3 minutes at 10 μl/min and allowed to dissociated for a further 5 min. The surface was regenerated with 30 sec pulses of 20 mM HCl and 10 mM NaOH.

2.4.20 ***Kinetic Analysis of GST Interaction Employing Protein A*** **Affinity-Capture.** Protein A (50 μg/ml in 10 mM acetate, pH 4.2) was immobilised (~ 1,970 RU) using conventional amine coupling. GST solutions were prepared using HBS buffer as diluent to final concentrations of 50, 60, 70, 80, 90 and 100 nM. The samples were analysed in random order according to the method outlined in section 2.4.14.

2.4.21 ***Analysis of GST Interaction Employing Protein A-Mediated Affinity-Capture and a RD Sensor Surface.*** Protein A (50 μg/ml in 10 mM acetate, pH 4.2) was immobilised (~ 490 RU) onto an RD sensor surface using conventional amine coupling. GST samples were prepared to final concentrations of 3.12, 6.25, 12.5, 25, 50, 100 nM GST in HBS buffer. Monoclonal anti-GST IgG (2.5 μg/ml in HBS buffer) was injected over the surface at 10 μl/min for 2 min and the baseline was allowed to stabilise for 5 min. A GST sample was injected for 2 min at 30 μl/min and was allowed to dissociate for a further 5 min. The surface was regenerated with a 30 sec pulse of 20 mM HCl. A reference curve was obtained by replacing the GST sample with running buffer (HBS buffer). The GST samples were analysed in triplicate in random order

2.4.22 ***Kinetic Analysis of the GST Interaction Employing Anti-Mouse Fc*** **Affinity-Capture.** Anti-mouse Fc IgG (50 μg/ml in 10 mM acetate, pH 5.0) was immobilised onto a CM5 chip (~ 11,000 RU) using conventional amine coupling. GST solutions were prepared to final concentrations of 50 nM, 60 nM, 70 nM, 80 nM, 90 nM and 100 nM using HBS buffer as diluent. The analysis was performed as outlined in section 2.4.14. However, the concentration of anti-GST IgG was increased to 10 μg/ml and the surface was regenerated with a 30 sec pulse of 20 mM HCl and 10 mM NaOH.

2.4.23 ***Kinetic Analysis of CD4 Interaction Employing Anti-Mouse Fc Affinity-Capture.*** Anti-mouse Fc IgG (50 μg/ml in 10 mM acetate, pH 5.0) was immobilised (~ 3,280 RU) onto a CM5 chip. Anti-CD4 IgG (10 μg/ml in HBS buffer) was injected over the surface at 10 μl/min for 2 min. CD4 (prepared in HBS buffer) was injected for 1 min at 100 μl/min and allowed to dissociate for a further 1 min. The surface was regenerated using a 30 sec pulse of 20 mM HCl and a 10 sec pulse of 10 mM NaOH. The above kinetic cycle was repeated for CD4 concentrations of 10, 20, 30, 40 and 50 nM. However, the 40 nM kinetic cycle was discarded due to poor quality data resulting from a response spike caused by an air bubble. This sample was not repeated due to the limited availability of precious CD4. A reference curve was produced by repeating the analysis with HBS buffer substituted for the CD4 samples. All samples were analysed in random order.

2.4.24 ***Analysis of Mass Transport Limited Interaction Curves.*** Anti-mouse Fc IgG (50 μg/ml in 10 mM acetate, pH 5.0) was immobilised (~ 3,280 RU) onto a CM5 chip by conventional amine coupling. Anti-CD4 IgG (10 μg/ml in HBS buffer) was injected over the surface at 10 μl/min for 2 min. CD4 (prepared in HBS buffer) was injected for 3 min at 30 μl/min and allowed to dissociate for a further 5 min. The surface was regenerated using a 30 sec pulse of 20 mM HCl and a 10 sec pulse of 10 mM NaOH. The above kinetic cycle was repeated for CD4 concentrations of 20, 40, 60, 80 and 100 nM in random order. The analysis was repeated with HBS buffer substituted for the CD4 samples to provide reference curves.

2.4.25 ***Analyte Saturation Front.*** Anti-mouse Fc (50 μg/ml in 10 mM acetate, pH 5.0) was immobilised (~ 11,270 RU) onto a CM5 sensor chip surface. Anti-CD4 IgG (16 μg/ml in HBS buffer) was injected over the surface for 2 min at 10 μl/min. CD4 (20 nM in HBS buffer containing 0.3 M NaCl) was injected over the surface for 3 min. The surface was regenerated using 30 sec

pulses of 20 mM HCl and 10 mM NaOH. This binding-regeneration sequence was repeated for CD4 injection flow rates of 5, 10, 20, 30, 40 and 50 μg/ml.

2.5 *Surface Plasmon Resonance Detection of Red Blood Cells*

All data analysis was performed using BIAevaluation 3.0™ and Microsoft Excel™ software (Microsoft Corporation).

2.5.1 ***Reagents.*** Hybridoma supernatants containing anti-A IgM, anti-A IgG and anti-B IgM were donated by Gamma Biologicals (3700 Mangum Road, Houston, Texas 770932, USA). Human blood samples were obtained from The Blood Transfusion Service Board (40 Pelican House, Mespil Road, Dublin 4, Ireland). Previously grouped EDTA anti-coagulated whole blood samples were obtained two days after bleeding and were stored for no longer than 3 days at 4 °C prior to analysis. The storage time was minimised because solid phase whole blood grouping is highly sensitive to the presence of free membrane-associated antigens that may result from degradation of the RBCs during storage. Furthermore, RBC samples were allowed to equilibrate at room temperature before use in order to permit them to recover from reversible deformation incurred during storage at 4 °C.

2.5.2 ***Washing RBCs.*** Rigorous washing procedures were employed to remove plasma that may contain free group A or group B blood group antigens since these substances competitively inhibit the antibody-cell binding interaction. After removal of the buffy layer (contains white blood cells), 1.0 ml of packed RBC were added to 50 ml centrifuge tubes. 49 ml of PBS (pH 7.4) were added, and the cells were gently suspended. The cells were centrifuged at 1000g for 5 min. The supernatant was discarded and the pellet was resuspended in 49 ml of fresh PBS. This washing procedure was repeated three times and the washed RBCs were mixed with CPD (89.0 mM trisodium citrate dihydrate, 16.2 mM sodium dihydrogen phosphate, 17.0 mM citric acid monohydrate, 0.14 M dextrose) in the ratio 10:1.4 and stored at 4 °C. Prior to analysis, cells were equilibrated at room temperature. The RBCs were washed as described above in the appropriate sample buffer [e.g. 10 mM HEPES containing 0.15 M NaCl, pH 7.4] and suspended at the required concentration. RBCs from different donors were treated separately. In addition, a single donor for a given blood group was employed for a given experiment (unless otherwise stated).

2.5.3 ***RBC Enumeration.*** RBCs were counted by diluting them in PBS and loading the sample onto an Improved Neubauer Haemocytometer. The cells were visualised on a Nikon phase

contrast ELWD 0.3 microscope and were counted manually. RBC concentrations were also described in terms of % (v/v). A packed RBC pellet was assumed to represent 100 % (v/v) RBCs and the appropriated dilutions were prepared from this sample.

2.5.4 ***BIACORE Analysis (general operation).*** The general operation of the BIACORE was as outlined in section 2.4.2. However, the Tween 20 and the EDTA were omitted from the HBS buffer during red blood cell analysis. Standard amine coupling was employed for the immobilisation of biomolecules and is described in section 2.4.3. Any deviations from these methods will be outlined when appropriate.

2.5.5. ***RBC Binding Studies Utilising Immobilised Concanavalin A.*** Washed RBCs were suspended in 10 mM HEPES containing 0.15 M NaCl, 1 mM $MnCl_2$, 1 mM $CaCl_2$, pH 7.4. This buffer was also used as the constant running buffer during the ConA-RBC binding experiment. Con A (100 μg/ml in 10 mM sodium acetate buffer, pH 4.5) was covalently immobilised (~ 7,594 RU) onto a CM5 sensor chip surface by conventional amine coupling. 50 μl of washed RBCs (1.0×10^9 cells/ml suspended in HBS buffer) were injected over the sensor surface at a flow rate of 5 μl/min. Running buffer was passed over the surface for 30 min to allow the RBCs to dissociate from the Con A surface. Regeneration of the surface was attempted using sequential pulses (5 μl/min for 1 min) of 10 mM NaOH, 20 mM HCl and 10 mM NaOH. Regeneration was unsuccessful and, hence, the above experiment was repeated employing competitive elution. 0.1 M alpha-D-mannopyranoside (dissolved in running buffer) was injected over the RBC-coated surface for 15 min at 5 μl/min.

2.5.6 ***RBC Binding Studies Utilising Immobilised IgM.***

2.5.6.1 *Anti-B IgM-Coated Surface.* Anti-B IgM (10 μg/ml in 10 mM sodium acetate buffer, pH 5.5) was covalently immobilised (~ 7,190 RU) onto a CM5 sensor chip surface. Washed group B RBCs were suspended in HBS buffer to final concentrations of 0.5×10^9, 0.5×10^9, 1.1×10^9, 1.5×10^9 and 2.1×10^9 cell/ml. 50 μl of the RBC sample was injected over the anti-B IgM-coated sensor surface at a flow rate of 5 μl/min. The surface was regenerated using two short pulses (i.e. 60 sec and 40 sec) of 20 mM NaOH. This binding-regeneration sequence was repeated for each RBC sample in order of increasing concentration. 50 μl of washed group A RBCs (2.5×10^9 cells/ml) were injected over the surface as a control.

2.5.6.2 *Anti-A IgM-Coated Surface.* Anti-A IgM (10 μg/ml in 10 mM sodium acetate buffer, pH 5.5) was immobilised (~ 4,600 RU) onto a CM5 sensor chip surface by conventional amine coupling. Washed group A RBCs were diluted to 1.1 x 10^9, 1.5 x 10^9, 2.2 x 10^9 cells/ml and 2.5 x 10^9 cells/ml in HBS buffer. The RBC samples were analysed as described in section *2.5.7.1.* 50 μl of group B RBCs (2.19 x 10^9 cells/ml) were injected over the surface as a control.

2.5.6.3 *Calibration Curve.* The anti-A IgM-coated surface produced in section 2.5.7.2 was employed. Washed group A RBCs were diluted to 0.33 x 10^9, 0.66 x 10^9, 0.9 x 10^9, 1.2 x 10^9, 1.5 x 10^9, 2.1 x 10^9 and 2.4 x 10^9 cells/ml in HBS buffer. 35 μl of the RBC sample was injected over the surface at 5 μl/min for 7 min. The surface was regenerated with two 1 min pulses of 20 mM NaOH. Each RBC sample was analysed in duplicate in order of increasing RBC concentration.

2.5.7 Protein A-Affinity Capture Format.

2.5.7.1 *Stability of Protein A-coated Surface.* Protein A (50 μg/ml in sodium acetate buffer, pH 4.3) was immobilised (~ 5,200 RU) using conventional amine coupling. 15 μl of anti-A IgG (1/400 dilution in HBS buffer) was passed over the protein A-coated surface at 5 μl/min. The surface was regenerated using a 1 min pulse of 10 mM HCl. This binding-regeneration cycle was repeated for 124 cycles.

2.5.7.2 *Reversible Capture of RBCs.* Protein A (50 μg/ml in sodium acetate buffer, pH 4.3) was immobilised (~ 4,400 RU) onto the dextran matrix using conventional amine coupling. 10 μl of anti-A IgG hybridoma supernatant (diluted 400-fold in HBS running buffer) was injected over the interaction surface at 5 μl/min. Washed blood group A RBCs (1.06 x 10^9 RBCs/ml in HBS running buffer) were injected over the surface at 5 μl/min for 5 min. The surface was subsequently regenerated using a 1 min pulse of 10 mM HCl.

2.5.7.3 *Calibration Curve*. The protein A-coated surface produced in section 2.5.7.2 was employed. Washed group A RBCs were diluted in HBS buffer to final concentrations of 0.13 x 10^9, 0.26 x 10^9, 0.40 x 10^9, 0.53 x 10^9, 0.66 x 10^9, 0.79 x 10^9, 0.92 x 10^9, 1.06 x 10^9, 1.19 x 10^9 and 1.32 x 10^9 cells/ml. Each sample was analyses in triplicate in order of increasing concentration as outlined in section 2.5.7.2.

2.5.7.4 *RBC Binding and Recovery.* Protein A (50 µg/ml in sodium acetate buffer, pH 4.3) was immobilised (~ 5,400 RU) onto a CM5 sensor chip surface using conventional amine coupling. 10 µl of anti-A IgG hybridoma supernatant (diluted 400-fold in HBS running buffer) was injected over the interaction surface at 5 µl/min. A 1 min pulse of 0.5 M NaCl was injected at 5 µl/min. Washed group A RBCs (1.0×10^9 RBCs/ml in HBS running buffer) were injected over the surface at 5 µl/min for 5 min. The flow rate was increased to 100 µl/min for ~ 1.5 min to elute bound RBCs. The remaining RBCs and anti-A IgG were recovered under non-lytic conditions using a 1 min pulse of 20 mM sodium acetate buffer, pH 4.0, containing 0.5 M NaCl.

2.5.8 Analysis of RBC Suspensions using BIACORE Probe™

This device uses a hand-held micropipette to aspirate the sample and bring it into contact with the sensing element within the pipette tip. 100 µl of each sample was aspirated during all analyses. The sensing element of the probe was exposed to PBS for 10 sec before and after sample aspiration during all BIACORE Probe™ experiments. Reliable binding measurements could thus be obtained despite bulk refractive index variations between sample solutions. The SPR response is a significant function of temperature and the sample temperature was not thermostatically controlled. However, a low background signal (± 5 RU) was observed during the course of this experiment as temperature variations within the laboratory were low (± 0.2 °C).

2.5.8.1 *Antibody Titration Curve.* Protein A (50 µg/ml in sodium acetate buffer, pH 4.3) was immobilised (~ 5.4 kRU) onto a CM5 sensor probe surface using conventional amine coupling Serial dilutions of anti-A IgG hybridoma supernatant were prepared from neat to 1/512. The anti-A IgG sample was exposed to the surface for 2 min. Regeneration of the surface was affected by a 30 sec pulse of 10 mM glycine, pH 1.7. Each sample was analysed in this manner for four replicates.

2.5.8.2 *RBC Binding Variation as a Function of Immobilised Antibody Concentration.* Protein A (50 µg/ml in sodium acetate buffer, pH 4.3) was immobilised (~ 5.7 kRU) onto a CM5 sensor probe using conventional amine coupling. The surface was exposed to anti-A IgG (1/20 dilution of hybridoma supernatant in PBS) for a given contact time. Washed group A RBCs diluted in PBS were aspirated and allowed to interact with the surface for 1 min. Bound RBCs were removed by shear force generated by a wash bottle filled with PBS. The remaining antibody was removed using two 30 sec exposures to 10 mM glycine, pH 1.7, followed by a 10 sec exposure to 0.5 % Triton-100 in PBS. The anti-A IgG functionalised surface was exposed to washed blood group O RBCs (50 % (v/v)) and washed group B RBCs (50 % (v/v)) to determine the non-specific binding

response. The above cycle was repeated for 100, 60 and 30 % (v/v) washed group A RBC samples and a range anti-A IgG contact times, thus giving different anti-A IgG coating concentrations.

2.5.8.3 *RBC Calibration Curve.* Protein A (50 µg/ml in sodium acetate buffer, pH 4.3) was immobilised (~ 5.7 kRU) onto the surface using conventional amine coupling. The surface was exposed to neat anti-A IgG hybridoma supernatant for 30 sec. Washed RBCs diluted in PBS were aspirated and allowed to interact with the surface for 1 min. The surface was regenerated as outlined in section 2.5.8.2. The above binding-regeneration cycle was repeated in triplicate for increasing concentrations of washed group A RBC (i.e. 10, 20, 40, 60, 80 and 100 % (v/v)).

2.5.8.4 *Effect of Non-Specific RBC Sub-Population.* Protein A (50 µg/ml in sodium acetate buffer, pH 4.3) was immobilised (6.2 kRU) onto the CM5 sensor probe. Washed group A RBCs were diluted to 80, 60, 40, and 20 % (v/v) in HBS buffer. A parallel series of RBC concentrations were prepared using 50 % (v/v) group O RBC in HBS buffer. Hence, the final concentrations of group A RBCs contained in these samples were the same as the first sample series but the total concentration of RBCs contained were 60, 70 and 80 % (v/v). The 80 % (v/v) group A RBC sample was omitted from the second series. Each sample was analysed in quadruplicate as described in section 2.5.8.2. The non-specific binding response was determined by repeating the analysis for 100 % (v/v) group O RBC.

2.5.8.5 *Donor Variation of RBC Binding Response.* The protein A-coated CM5 probe produced in section 2.5.8.5 was employed. Washed group A RBCs from 18 donors were suspended at 50 % (v/v) in HBS buffer and analysed (n = 4) as outlined in section 2.5.8.2. The non-specific binding response was assessed by repeating the analysis for 50 % suspensions of blood group O (10 donor samples) and blood group B (10 donor samples) RBCs.

2.5.8.6 *Determination of Plasma Binding Response.* Protein A (50 µg/ml in sodium acetate buffer, pH 4.3) was immobilised (~ 6.4 kRU) onto a CM5 sensor probe surface. Plasma was obtained from EDTA anti-coagulated whole blood. The plasma sample was aspirated and remained in contact with the surface for 2 min. The surface was regenerated using three consecutive 30 sec exposures to 0.1 M glycine, pH 1.77, 15 mM NaOH and 1% (v/v) Triton-X-100 in PBS, respectively. **(a)** This binding-regeneration cycle was repeated for 10 replicates for a single donor. **(b)** The above binding-regeneration cycle was repeated for 20 EDTA anti-coagulated plasma samples obtained from 20 separate donors

2.5.8.7 *Whole Blood Typing.* Protein A (50 µg/ml in sodium acetate buffer, pH 4.3) was immobilised (~ 5.7 kRU) onto the CM5 sensor probe surface using conventional amine coupling. The surface was exposed to neat anti-A IgG hybridoma supernatant for 1 min. Neat EDTA-anti-coagulated plasma was aspirated and allowed to interact with the surface for 2 min. EDTA anti-coagulated whole blood was aspirated and allowed to interact with the surface for 1 min. The surface was regenerated as outlined in *section 2.5.8.6* . The above binding-regeneration cycle was repeated employing group O whole blood to determine the non-specific binding response. In addition, the analysis was repeated with plasma substituted for the whole blood sample.

2.6 Fibre Optic SPR-based Sensor.

All data analysis was performed using BIAevaluation 3.0™ and Microsoft Excel™ software.

2.6.1 ***Sensor Construction.*** The sensing element (i.e. CM5 probe) was composed of a gold-coated (~ 50 nm layer) fibre optic with a mirror deposited at the tip. This sensing element is supplied with a carboxymethylated dextran (CM-dextran) hydrogel grafted onto the gold surface via an alkanethiol self-assembled monolayer and was obtained from BIACORE AB, St. Albans, Hertfordshire AL13AW, England. All other components were purchased from Ocean Optics, 1104 Pinehurst Rd., Dunedin, Florida, USA. A tungsten-halogen lamp (LS-1) was employed as a light source and was fitted to a fibre optic probe (RS00-7), that accommodates reflective mode operation. The sensing element was fitted to this fibre optic cable via a customised fibre optic connector that was fabricated 'in house'. A miniature S2000 spectrometer was connected to monitor spectral changes in the propagated light due to SPR. A National Instruments Daq-700 PCMCIA I/O card was required to acquire data from the spectrometer. Data acquisition, processing and display were performed using custom-written Labview software ('in house') and a laptop pentium class computer. All experimental work was performed in collaboration with Aiden Doyle (School of Physical Sciences, Dublin City University) and Shane O'Neill (School of Chemical Sciences, Dublin City University). Samples were exposed to the sensing surface by simply immersing the sensing element in the sample contained in a microfuge tube.

2.6.2 ***Temperature-Induced Response Drift.*** The BIACORE 1000™ was employed to determine the temperature coefficient of refractive index in HBS buffer. The system was primed with HBS running buffer and set to a flow rate of 5 µl/min. The thermostatically controlled temperature was adjusted from 25 °C to 20 °C. A change of 5 °C required approximately 1h to equilibrate. The changes in the baseline response (RU) and the temperature (°C) at the interaction surface were

recorded at intervals during this time. A calibration curve was constructed from the data and the slope was equal to the temperature coefficient of the refractive index.

2.6.3 ***Determination of Refractive Index of Standard Glycerol:Water Solutions.*** Serial dilutions of 50 % (v/v) glycerol in water were prepared. The refractive index of each sample was recorded in duplicate (room temperature of 24.3 °C) using an Abbé refractometer (Milton Roy Tabletop Refractometer 3L). A calibration curve was constructed from the data using Microsoft Excel™ software. This analysis was conducted in collaboration with Colm McAtamney (School of Physical Sciences, Dublin City University).

2.6.4 ***Sensor Calibration.*** Glycerol:water solutions were prepared from 5 to 50 % (v/v) glycerol in ultrapure water at 5 % (v/v) increments. The sensor was configured as outlined in section 2.6.1. The sensing element of the sensor was immersed in the glycerol sample for 1 min and the spectrum recorded. The sensing tip was then rinsed with ultrapure water and the procedure repeated for the remaining samples. A calibration curve was constructed from the data and a four-parameter equation fitted to the data using BIAevaluation software 3.0™.

2.6.5 ***Protein A Affinity-Capture Format***

2.6.5.1 *Immobilisation of Protein A.* The probe was incubated in PBS (numbered points) buffer before and after exposure to sample to eliminate bulk refractive index variations between solutions. The sensing element was immersed in activation solution (1:1 mixture of 0.4 M EDC and 0.1 M NHS in ultrapure water) for 7 min. The sensor was subsequently exposed to a protein A solution (50 μg/ml, in 10 mM sodium acetate buffer, pH 4.3) for 11 min to allow preconcentration of the positively charged protein onto the negative hydrogel. The surface was exposed to 1 M ethanolamine, pH 8.5, for 7 min to cap residual activated groups and this resulted in a final protein A-coating response of 8.8 AU.

2.6.5.2 *Protein A-IgG Interaction.* Rabbit IgG (4.0 mg/ml in PBS buffer) was serially diluted in PBS buffer to give final concentrations from 4,000 to 3.9 μg/ml. The sensing element was exposed to the sample for 2 min at room temperature. The sensing element was subsequently exposed to PBS buffer and the antibody binding response was recorded. The surface was regenerated by exposing the surface to 20 mM HCl for 30 sec to remove affinity-captured antibody. The above binding-regeneration cycle was repeated for each sample.

2.6.5.3 *RBC Detection.* Protein A (50 μg/ml in sodium acetate buffer, pH 4.3) was immobilised onto a CM5 sensor probe surface as described in section 2.6.5.1. Throughout the analysis, the probe was immersed in PBS buffer other than during exposure to the sample. The sensing element was exposed to neat hybridoma supernatant (serum-free) containing anti-A IgG_{2b} for 1 min. The probe was then exposed to 100 % (v/v) washed group A RBCs for 2 min giving a cell-binding response of 139.5 AU. The sensing element was regenerated with a 20 sec exposure to 20 mM HCl, a 15 sec exposure to PBS containing 0.1 % Triton-100 and a further 15 sec exposure to 20 mM HCl. This procedure was repeated for group A RBC concentrations of 20, 40, 63 and 90 % (v/v). Furthermore, the non-specific binding response was determined by exposing the protein A-coated sensing element to 100 % (v/v) group A RBCs for ~ 2 min in the absence of anti-A IgG.

2.7 Miniature SPR Sensor.

The miniature SPR transduction system was obtained from Texas Instruments (Dallas, Texas, USA). The system includes the SPR transducer, connector cables, power adapter, control box, flowcell and dedicated SPR-mini software. The system was installed according to the manufacturer's instructions. All data analysis was performed using BIAevaluation 3.0™ and Microsoft Excel™ software.

2.7.1 Sensor Performance Without a Disposable SPR Chip.

2.7.1.1 *Sensor Calibration.* Standard refractive index solutions were prepared by serially diluting 50 % (v/v) glycerol in ultrapure water. The refractive index of these solutions was determined by injecting the sample into a flowcell (supplied by manufacturers) fitted to the sensor and, thus, bringing it into contact with the sensing surface. After 1 min, the flowcell was flushed with 3 ml of water. A further set of glycerol:water solutions was prepared from 20 % (v/v) to 0.04 % (v/v). These solutions were analysed using the BIACORE 1000™. Each sample was injected over the sensor surface for 1 min at 5 μl/min. The response for each sample was recorded during sample injection. A calibration curve was constructed from the data obtained from both the miniature SPR biosensing system and the BIACORE 1000™ system.

2.7.1.2 *Surface Derivatisation.* The method outlined by Löfås and Johnsson (1990) was employed. Briefly, the gold layer of the miniature SPR sensor was immersed in 5 mM 11-mercapto-undecanol (dissolved in an 80 % (v/v) ethanol) and incubated at 30°C overnight. The resulting self-assembled monolayer was rinsed with ultrapure water and activated by exposure to 0.6 M epichlorohydrin (dissolved in a 1:1 mixture of 0.4 M NaOH and 2-methoxy ethyl ether) for 4 h at room temperature. The surface was rinsed with ethanol and incubated in 30 % (w/v) dextran (500

kDa) dissolved in 0.2 M NaOH for 15 h at room temperature. The surface was then rinsed in ultrapure water and immersed in 1 M bromoacetic acid dissolved in 2 M NaOH. After 4 h incubation at room temperature the surface was thoroughly rinsed in water and the device was stored at 4 °C with desiccant.

2.7.1.3 Preconcentration of BSA onto the CM-Dextran Biointerface. A flowcell was attached to the miniature SPR sensor and was primed with ultrapure water. A BSA solution (100 μg/ml in 10 mM sodium acetate, pH 4.5) was injected into the flowcell (volume of 10 μl) and preconcentration of the positively charged protein onto the negatively charged matrix was observed for 2 min. The preconcentrated protein was removed by injecting PBS into the flowcell to disrupt the ionic interactions. Ultrapure water was injected into the flowcell to return the signal to the initial baseline response.

2.7.2 ***Sensor Performance using Disposable SPR Chip.*** The gold layer of the miniature SPR sensor was removed by polishing with fine-grained sandpaper. A low volume (i.e. 5 μl/min) flow cell was custom fabricated ('in house') to facilitate docking of a CM5 SPR chip. Microscope lens oil was used to match the refractive indices of the glass slide and the epoxy plastic of the SPR transducer. The assembled device was then connected via a communications cable to the control box. A personal computer serial communications cable interfaced the control box with a computer running SPR-mini software. The sensor, complete with flowcell, was clamped so that the interaction surface was positioned along the roof of the flowcell (similar to BIACORE 1000™ configuration).

2.7.2.1 Sensor Calibration. Glycerol:water solutions were prepared by serially diluting a 40 % (v/v) glycerol solution with ultrapure water. The samples were manually injected into the flowcell and were exposed to the surface for > 30 sec. The samples were injected sequentially from low to high glycerol concentrations. A calibration curve of glycerol concentration against the refractive index was constructed.

2.7.2.2 SPR Chip Comparison. An SPR chip was fabricated 'in house' (Mark Hyland, NIBEC, University of Ulster, Co. Antrim, Ireland) and its performance was compared to that of the CM5 sensor chip. The miniature SPR biosensing system incorporating the CM5 sensor chip was assembled as described in *Figure 5.2.3.5.1*. The flowcell was primed with PBS buffer and the SPR minimum was recorded. This procedure was repeated using the 'in house' fabricated chip (i.e. planar chip).

2.7.3 Detection of Whole RBCs.

2.7.3.1 Immobilisation of Anti-Mouse Fc IgG. Anti-mouse Fc IgG IgG (100 μg/ml in 10 mM sodium acetate, pH 4.5) was immobilised onto a CM5 sensor surface by conventional amine coupling. The sensor was assembled as outlined in *Figure 5.2.3.5.1.* Ultrapure water was injected into the flowcell to give a steady baseline. The CM-dextran hydrogel was activated by injecting a 1:1 mixture of 0.4 M EDC and 0.1 M NHS, allowing a contact time of 6 min. The flowcell was flushed with water and polyclonal goat-anti-mouse Fc was injected. The antibody solution was incubated in the flowcell for 6 min to allow preconcentration and covalent coupling and the flowcell was then flushed with water. 1 M ethanolamine was injected to cap residual activated groups. After 6 min, the flowcell was rinsed with water and the final immobilisation response was recorded (i.e. $\Delta n \approx 0.00278$).

2.7.3.2 RBC Detection. PBS was injected over the goat-anti-mouse Fc-coated surface to obtain a steady baseline. Neat anti-A IgG hybridoma supernatant (containing 0.3 M NaCl), pH 7.4, was injected for a contact time of 2 min. The flowcell was flushed with PBS and washed group A RBCs (66 % (v/v)) were injected and remained in contact with the sensor surface for 3.5 min. The flowcell was flushed with PBS and the response due to cell binding was recorded. The surface was regenerated using a 1 min exposure to 20 mM HCl followed by a 40 sec exposure to 1 % (v/v) Triton-100. The above binding-regeneration sequence was repeated for washed RBC concentrations of 33 % (v/v) and 50 % (v/v). In addition, the non-specific binding response was observed by conducting the analysis with 66 % (v/v) group A RBCs in the absence of anti-A IgG.

Chapter 3

Characterisation of Macromolecular Interactions

Investigation of Experimental and Data Analysis Techniques

3.1 *Introduction.*

This chapter describes the investigation of methods of experimental and data analysis for the characterisation of molecular interactions. A wide variety of antibodies and antibody derivatives can be harvested from natural and synthetic sources for both diagnostic and therapeutic applications. The utility of these reagents depends primarily on their affinity, kinetic and stability properties. Characterisation of these reagents has primarily relied on enzyme-linked immunosorbent assays (Friguet *et al.*, 1985; Porstmann and Kiessig, 1992), affinity chromatography (Chaiken *et al.*, 1992), titration calorimetry (Wiseman *et al*, 1989), spectroscopy (Ward, 1985) and equilibrium dialysis (Lehtonen and Eerola, 1982). These techniques are based on the measurement of some property related to the concentration of the interactants or the immunecomplex and are restricted to equilibrium analysis with the exception of spectroscopy.

'Real-time' biomolecular interaction analysis (BIA) allows direct visualisation of the biomolecular interaction thereby facilitating qualitative affinity ranking, comparative estimation of observed rate constants and the determination of kinetic constants. If the affinity constant (K_a) is known, it is possible to predict the equilibrium concentration of the immunecomplex in a reaction. However, the equilibrium time of two antibodies possessing identical affinity constants may vary from a few minutes to several hours since the time required to reach equilibrium is a kinetic property of the interaction. Kinetic characterisation reveals the rate at which the immune complex both forms and dissociates, thus providing a stringent measure for tailoring and/or selecting reagents. A biomolecular interaction between a soluble analyte (A) and an immobilised ligand (X) can be described by the reaction scheme:

$$A + X \underset{k_d}{\overset{k_a}{\leftrightarrow}} AX \qquad [1]$$

where A = Analyte
X = Immobilised Ligand
AX = Complex
k_a = Association rate constant
k_d = Dissociation rate constant

also $$k_a/k_d = K_a = 1/K_d$$

where K_a = Equilibrium affinity constant
K_d = Equilibrium dissociation affinity constant

3.1.1 ***Pseudo-First-Order Kinetics***. The above interaction can be interpreted in terms of pseudo-first-order kinetics, where the rate of formation of complex is described by the differential equation

$$\frac{dC_{AX}}{dt} = k_a\,(C_A)_t\,[(Cx)_{tot} - (C_{AX})_t] - k_d\,(C_{AX})_t \qquad [2]$$

where C_{AX} = Molar concentration of complex at the interaction surface.

$(C_A)_t$ = Molar concentration of analyte at the interaction surface at time t.

$(Cx)_{tot}$ = Molar concentration of immobilised ligand.

$(C_{AX})_t$ = Molar concentration of complex at time t at the interaction surface.

and

$$(Cx)_t = (Cx)_{tot} - (C_{AX})_t$$

where $(Cx)_t$ = Molar concentration of available immobilised ligand.

The analyte concentration at the interaction surface can be approximated by the injected analyte concentration at any time.

$$(C_A)_i = (C_A)_t$$

where $(C_A)_i$ = Molar concentration of injected analyte sample.

$(C_A)_t$ = Molar concentration of analyte at the interaction surface at time t.

The validity of this assumption is dependent on continuous replenishment of the analyte during flow injection analysis and the absence of gradients in analyte concentration within the boundary layer (*Figure* 3.1.1).

Generic refractive index-based biosensors monitor these surface binding events, producing 'real-time' interaction curves where the rate of change of response (dR/dt) is directly related to the progress of the biomolecular interaction. Hence, equation [2] can be rewritten as

$$\frac{dR}{dt} = k_a\,(C_A)_i\,(R_{max} - R_t) - k_d\,R_t \qquad [3]$$

where R_{max} = Maximal response if all available ligand binding sites are occupied.

R_t = Biosensor response at time t.

Integration of equation [3] yields an integrated rate equation for a 1:1 pseudo-first-order interaction and is commonly used to determine R_{max}, k_a and k_d from interaction curves.

$$R_t = \frac{k_a (C_A)_i R_{max} (1 - exp[- k_a (C_A)_i + k_d] t)}{k_a (C_A)_i + k_d} \quad [4]$$

The apparent or observed kinetic rate constant, (k_{obs}), is given by the expression:

$$k_{obs} = k_a (C_A)_i + k_d \quad [5]$$

At equilibrium, equation 4 can be rearranged as follows

If $$\frac{k_a (C_A)_i R_{max}}{k_a (C_A)_i + k_d} = \frac{(C_A)_i R_{max}}{(C_A)_i + k_d / k_a} = \frac{(C_A)_i R_{max}}{(C_A)_i + K_d} = R_{eq} \quad [6]$$

then $$R_t = R_{eq} [1 - exp(-k_{obs} t)] \quad [7]$$

where R_{eq} is the equilibrium binding response.

R_{eq} values may be used to determine the affinity of a biomolecular interaction. Non-linear regression analysis of R_{eq} values over a range of analyte concentrations yields values for K_d and R_{max}. Ideally, the value of K_d obtained through this analysis should be comparable to the affinity constant determined from kinetic analysis. During the dissociation phase the analyte sample is no longer in contact with the surface (i.e. $(C_A)_i = 0$) and equation 3 reduces the following:

$$\frac{dR}{dt} = -k_d R_t \quad [8]$$

Integration of this differential rate equation gives

$$R_t = R_0 exp(-k_d t) \quad [9]$$

where R_0 is the sensor response at time t_0 (i.e. time at the onset of dissociation phase).

The analysis outlined above describes a biomolecular interaction that is governed by 1:1 pseudo-first-order kinetic behaviour. However, many investigations have demonstrated significant

departures from this model (Edwards *et al.*, 1995; Hall *et al.*, 1996; Karlsson and Fält, 1997; Schuck, 1996; Bowles *et al.*, 1997; Myszka, 1997; O'Shannessy and Winzor, 1996,).

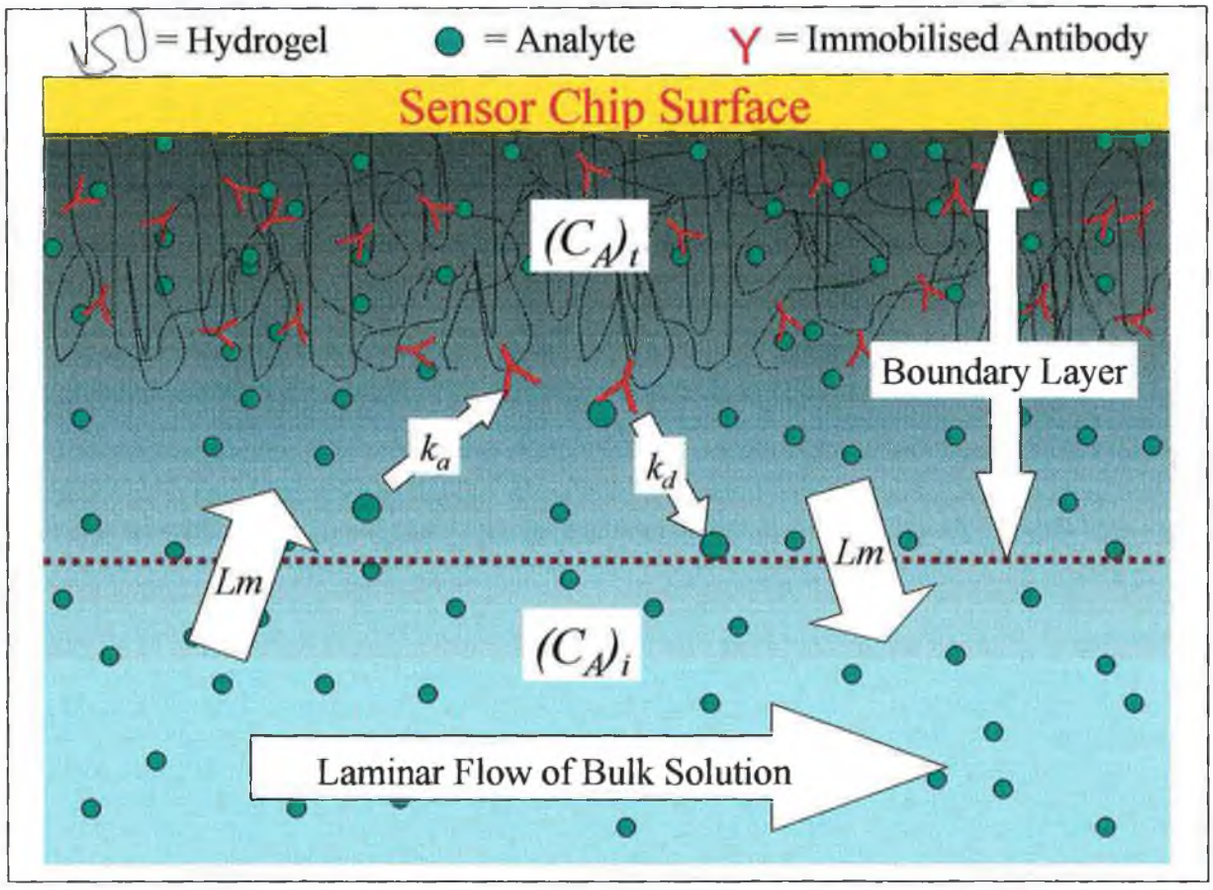

Figure 3.1.1. Schematic representation of an ideal biomolecular interaction. The immobilised antibody is depicted as a homogenous layer covalently attached to the dextran hydrogel. The background-shading gradient represents decreasing fluid velocity towards the surface. The analyte is flowing adjacent to the surface under laminar flow conditions. The bulk mass transfer coefficient (*Lm*) defines the flux of the analyte from the bulk into the boundary layer where $(C_A)_i$ and $(C_A)_t$ are the analyte concentrations inside and outside the layer, respectively. The 'true' kinetic constants define the rate of formation (k_a) and dissociation (k_d) of the antibody-analyte complex.

3.1.2 ***Factors that May Cause Deviations from Pseudo-First-Order Kinetic Behaviour.*** A review of the literature reveals that very few of the interactions studied conform completely to the pseudo-first-order interaction model. The many factors that cause deviations are listed below.

Table 3.1.2. Factors that cause deviations from pseudo-first-order behaviour.

1. Mass transfer limitation (MTL) from the bulk phase to the interaction surface (fluid dynamics).
2. MTL within the hydrogel due to increased viscosity.
3. Deviations from 1:1 interaction due to valency effects of ligand or analyte.
4. Immobilised ligand density (must be minimal to reduce the reaction flux and, thus reduce mass transport limitation).
5. Heterogeneity of immobilised ligand (e.g. steric hindrance effects due to random site attachment).
6. Heterogeneity of analyte (presence of sub-population with different binding properties).
7. Rebinding of dissociating analyte (particularly relevant for fast interactions).
8. Steric hindrance.
9. Protein-protein interactions.
10. Matrix effects (e.g. cross-linking, contraction, position of analyte within evanescent field).
11. Baseline drift (especially problematic for affinity-capture format).
12. pH and temperature effects.
13. Non-specific binding of analyte to functionalised surface.
14. Systemic error (refractive index offsets, microfluidic cartridge induced baseline jumps, air spikes).
15. Innate complex binding mechanism for the interaction.

3.1.3 Validity of Kinetic Constants from 'Real-Time' Biomolecular Interaction Analysis.

Considering the diversity of deviations that can occur during 'real-time' kinetic analysis, it is not surprising that the physical interpretation of extracted rate constants has become unclear (O'Shannessy and Winzor, 1996). This confusion may be avoided by examining the basic theory of reaction rates. The term 'intrinsic' rate constant is often used to describe rate constants obtained for a given biomolecular interaction in homogenous solution phase. However, kinetic theory implies that this 'intrinsic' rate constant is a function of the local interaction environment in conjunction with the intrinsic physical properties of the interacting molecules. The interaction of molecules possessing affinity towards each other can be described by simple reaction theory. The binding reaction results from molecular collisions possessing sufficient energy and the required orientation. Hence, the binding rate can be expressed as the sum of three factors.

Rate	=	**Collision Frequency**	x	**Energy Factor**	x	**Probability Factor**

The collision frequency depends on the concentration and diffusion rate of each interactant. Furthermore, the molecular weight and specific density of the interactants together with the physical properties of the local environment (such as temperature and viscosity) influence the diffusion rate and, hence, the binding rate. In addition, large molecules move more slowly due to frictional forces but the greater molecular size increases the collision frequency. The energy factor is given by the fraction of collisions that possess sufficient energy for binding to occur. This energy is supplied by the kinetic energy of mobile molecules combined with the alignment of atoms within the binding site at the time of collision. The probability factor is poorly understood but is dependent on the geometry of both interactants i.e. the fraction of surface area occupied by the binding site and the binding site topography. In general, closely related binding events will possess a similar probability factor.

It was recently suggested that all rate constants determined using 'real-time' interaction analysis are phenomenological in nature (O' Shannessy and Winzor, 1996). This is misleading as kinetic rates, being the product of the collision frequency, probability factor and the energy factor, are clearly a significant function of the local interaction environment and should be considered within this context. Hence, the question of the comparability of kinetic rates determined in solution and within a hydrogel is void. Reaction theory implies that kinetic rates will differ, even in homogenous solution phase, if the physical properties (e.g. viscosity, temperature) of each solution are not identical. Normally, the kinetic rate constant is considered independent of the concentration of the interacting molecules. This assumption is appropriate in homogenous solution phase where the viscosity is constant during the reaction. However, the accumulation of protein within the hydrogel during the course of an interaction may cause hindered diffusion, thereby decreasing the 'true' reaction rate constant in a concentration-dependent manner.

The validity of kinetic constants can be confirmed by comparing equilibrium constants determined from steady state analysis with those determined from kinetic analysis. In addition, the equilibrium affinity constants do not vary with environmental changes in viscosity or temperature, since both the association rate constant and the dissociation rate constants will be affected to the same degree. Consequently, equilibrium constants determined at steady state in solution or within a hydrogel should be comparable to those determined from kinetic experiments. Decreasing the surface binding capacity to the minimum reliable binding response (i.e. approximately 50 RU for the BIACORE 1000^{TM}) can reduce steric hindrance and viscosity effects.

3.1.4 ***Considerations for Experimental Design.*** Ideally, kinetic experiments should be conducted using a biointerface that mimics the physical properties of the application environment. Native immobilised ligands (e.g. membrane receptors) are generally supported in a directed manner that does not interfere with the binding site. Hence, a strategy that mimics the native anchorage mechanism is likely to avoid heterogeneous analyte binding effects. For example, the interaction of a membrane-bound receptor with a soluble ligand should be studied using a supported lipid bilayer biointerface. Experimental design is crucial to the attainment of high quality data that conforms to 1:1 pseudo-first-order behaviour. Furthermore, it is preferable to eliminate interferences when recording the interaction curves as opposed to accounting for these complex deviations during data analysis. The more important factors are discussed in more detail below.

3.1.5 ***Mass-Transfer Limitation.*** If the kinetic binding rate is very fast (e.g. $k_a > 10^7\ M^{-1}s^{-1}$) then the mass transfer rate becomes limiting and the maximal slope (*dR/dt*) of the association curve is given by:

$$\frac{dR}{dt} \approx \frac{D[C_x]}{d} \tag{10}$$

where D = Diffusion coefficient for the analyte in solution (m^2 /s).

$[C_x]$ = Concentration of analyte within the boundary layer (M).

δ = Thickness of boundary layer (m).

Figure 3.1.1 is a depiction of an interaction occurring under ideal conditions. Apparent kinetic constants for a MTL interaction are proportional to the sum of the diffusion coefficients of each binding partner (Karlsson *et al.*, 1994). The mass transfer coefficient, *Lm*, is primarily dependent on the flow rate (variable), dimensions of the flowcell (constant) and the diffusion coefficient (constant) of the analyte (Glaser, 1993; Christensen, 1997). Calculations predict that the boundary layer will be 10-fold (δ of 10 μm) higher than the hydrogel when *Lm* is 1×10^{-5} m/s and D is 1×10^{-11} m^2/s. *Lm* is proportional to the cube root of the flow rate and can be varied by a factor of approximately 5 between 1-100 μl/min. It is given by:

$$Lm = 1.21 \sqrt[3]{\frac{D^2 F}{h^2 b l}} \tag{11}$$

where D = Diffusion coefficient of the analyte (m^2/s).

F = Bulk flow rate (m^3/s).

h, b and l are the height, width and length of the flowcell, respectively (m).

Kinetic experiments demand that the rate of delivery of analyte exceeds the rate of consumption of analyte within the hydrogel. In other words, *Lm* must exceed the Onsager coefficient of reaction flux (*Lr*) by an order of magnitude in order to ensure MTL does not seriously limit the interaction. The reaction flux is given by the following:

$$Lr = k_a\,[\mathrm{C_X}] \tag{12}$$

If $Lm >> Lr$, the analyte concentration at the surface $(C_A)_t$ will be the same as the bulk analyte concentration $(C_A)_i$ and the interaction curve will reflect the 'true' kinetics of the interaction. A quantitative description of MTL is given by the expression:

$$\%\ MTL = \left(\frac{Lr}{Lm + Lr}\right)\frac{100}{1} \tag{13}$$

A value of < 10 % MTL is recommended for the determination of kinetic constants and is attained by lowering *Lr* and/or increasing *Lm*. *Lr* is lowered by decreasing the density of immobilised ligand [Cx] and *Lm* can be increased by simply using higher flow rates. The converse applies for the development of MTL applications (*Figure* 3.1.5).

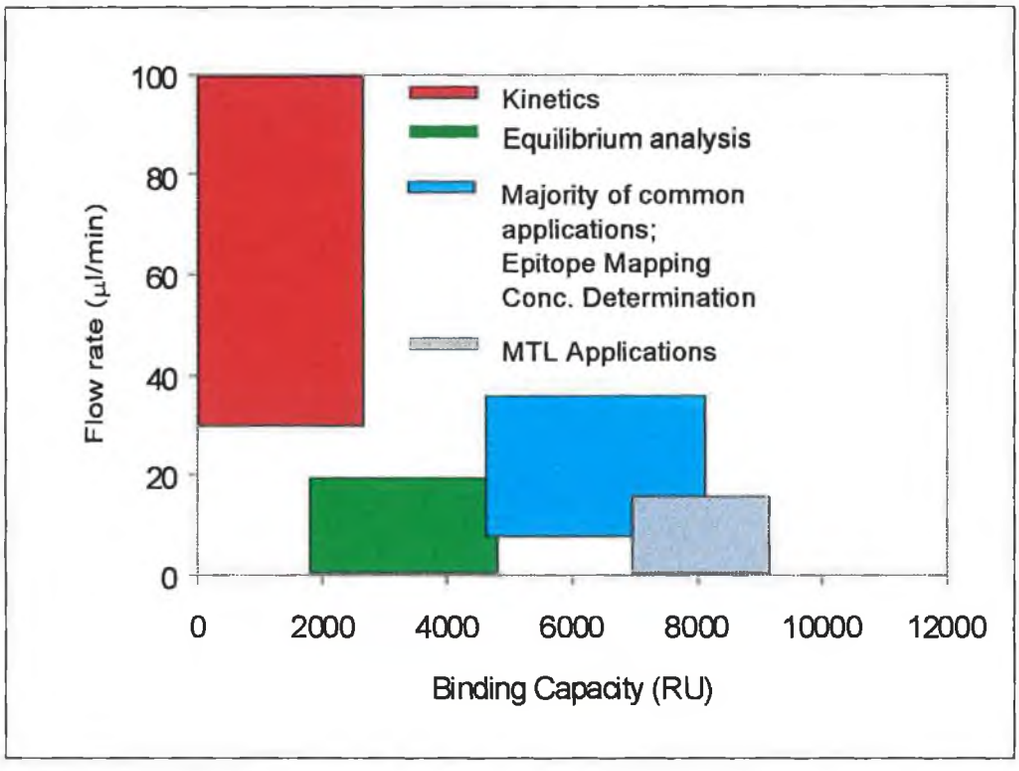

Figure 3.1.5. Guide to approximate binding capacities and flow rates for different interaction applications. In general, both affinity determination and mass transport limited applications require extremes of flow rate and binding capacity while the majority of other applications are far less demanding.

MTL causes deviations from ideal behaviour that distort both the association and dissociation phases of interaction curves. Deviations are particularly apparent as a curve in a dissociation phase derivative plot of $Ln(R_0/R_n)$ against time where R_0 is the sensor response at the beginning of the dissociation phase (Nieba *et al.*, 1996). Ideally, this transformation of the dissociation phase curve should reveal a straight line whose slope equals the k_d. A similar effect can be observed in the same transformation of the dissociation phase data of Parsons and Stockley (1997). In both cases, the value of k_d was concentration dependent and strongly suggested that rebinding of dissociating analyte was responsible. Rebinding of the analyte occurs when the mass transport rate from the hydrogel is insufficient to prevent recapture of the analyte and it affects interactions possessing high association rates to a greater degree. Increasing binding rates over the progress of the association phase have been observed by some investigators and were attributed to an apparent co-operativity factor, where the binding of one analyte molecule enhanced the binding rate of subsequent molecules (Fisher and Fivash, 1994). It was proposed (Schuck, 1996) that this apparent co-operativity could be accounted for by MTL, where the flux of the analyte to the surface is limiting. Under these conditions an inward moving saturation boundary may form and the observed response will reflect the position of the saturation front within the exponentially decaying evanescent wave. Moreover, the maximum k_a value that can be reliably determined depends on the mass transfer rate and the reaction rate. Karlsson and Ståhlberg (1995) reported cut-off values of k_a that can be reliably obtained for analytes of various molecular weights by direct analysis using the BIACORE 2000™. For instance, a cut-off k_a value of $3 \times 10^6 M^{-1}s^{-1}$ was estimated assuming an R_{max} of 50 RU, a flow rate of 20 µl/min, a molecular weight of 50 kDa and a ratio of 5 between the mass transport rate and the reaction flux (i.e. *Lm/Lr*).

3.1.6 ***Ligand Immobilisation.*** The term immobilisation is used in a loose sense as biomolecules are often covalently linked to a hydrogel environment that is dynamically mobile. It is important to consider that the immobilised ligand is assumed to be stationary, an overly simplistic approximation for ligands anchored to a dynamic hydrogel environment. Hydrogel immobilisation strategies restrict the mobility of the ligand in comparison to solution phase conditions but do not completely fix the ligands position. This fundamental difference implies that kinetic constants determined in solution phase can be expected to exceed those determined within a hydrogel environment. Random immobilisation of the ligand via amine coupling to a CM-dextran hydrogel can induce ligand heterogeneity, steric hindrance and matrix cross-linking. Furthermore, direct covalent attachment of the ligand to the hydrogel requires optimisation of regeneration conditions in order to remove the bound analyte while maintaining the binding activity of the immobilised ligand. Complete regeneration of the surface commonly requires harsh conditions that denature the immobilised ligand and cause a progressive loss in surface binding capacity.

Affinity-capture of the ligand may be more suitable for many applications as the ligand is replaced after each binding-regeneration cycle, thus avoiding exposure to denaturing conditions. In addition, the capture reagent can be chosen to accommodate directed immobilisation of the ligand, thereby limiting potential steric hindrance effects. Polyclonal anti-mouse antibodies are commonly employed to anchor monoclonal antibodies (ligand) via the Fc region. It is preferable to use an affinity-purified isotype-specific antibody directed against the Fc region in order to minimise the surface concentration of antibody required to achieve a given binding capacity. Otherwise, a high density of non-specific antibody will be present within the dextran matrix, hence, encouraging steric hindrance, matrix cross-linking, non-specific protein-protein interactions and diffusional limitations (Schuck, 1996). Preferably, directed immobilisation through a unique functional group (Ladbury *et al.*, 1995) or affinity-capture through the introduction of fusion tags (Gershon and Khilko, 1995; Nieba *et al.*, 1997) may be employed, but the availability of such reagents is limited.

3.1.7 ***Steric Hindrance.*** It has been suggested (Edwards and Leatherbarrow, 1997) that binding of an analyte to an immobilised ligand may hinder binding to an adjacent binding site, thereby accounting for biphasic association curves. It was proposed that only the early part of the interaction curve should be analysed to eliminate this effect. However, restricting data analysis to a subset of the complete interaction curve may yield inaccurate results. Injection of low concentrations of analyte for kinetic analysis has also been proposed to reduce steric hindrance effects, as these effects become greater when the interaction approaches saturation (O'Shannessy and Winzor, 1996). However, this measure will increase MTL leading to further complications. Consequently, it is preferable to reduce the analyte binding capacity (R_{max} < 100 RU) and to limit the concentration of the affinity-capture ligand in order to limit steric hindrance. In addition, steric hindrance can be minimised if a low molecular weight capture reagent such as protein A (MW 44 kDa) is used. This molecule can be used as a generic monoclonal antibody-capture system, since it possesses high affinity for many IgG subtypes from a range of vertebrate species. The protein A-antibody interaction is typified by low dissociation rates, and hence, limits baseline drift. In addition, regeneration of the surface is reproducible allowing hundreds of binding-regeneration cycles to be run without deterioration of the binding capacity. Furthermore, the antibody is captured via a single binding site, thus limiting steric hindrance and reducing cross-linking effects.

3.1.8 ***Applications under Mass Transport Limited Conditions.*** MTL is inherent in all biosensor configurations and imposes an upper limit on the 'true' kinetic association rate that can be resolved. However, MTL conditions can be exploited for the development of novel quantitative assays that offer many advantages over conventional assay techniques. A universal standard curve for the determination of active antibody concentrations was developed by Karlsson *et al.* (1993).

The technique employed low flow rates and high surface binding capacities in order to establish MTL conditions. The establishment of complete MTL was assessed by conducting the analysis on two surfaces with increasing densities of immobilised ligand, because MTL dominates when the binding rate is comparable for both surfaces. Under these conditions the binding rate (*dR/dt*) becomes independent of the 'true' reaction rate and is directly proportional to the concentration of the active analyte. Calibration curves for a variety of antibody-antigen interactions were superimposable yielding a universal standard curve for the determination of antibody concentration irrespective of the identity of the immobilised antigen.

An experimentally simpler technique was recently described that exploits the flow rate dependence of the binding rate under MTL conditions. Christensen (1997) derived a simple expression for the determination of the active analyte concentration from interaction curves obtained at different flow rates and subject to partial MTL conditions. When either MTL or kinetics is totally rate limiting, the concentration of analyte within the hydrogel is zero or equal to the bulk concentration ($[CA]_i$), respectively. However, a quasi-steady state where the average analyte concentration at the surface remains constant ($d[C_A])_t/dt = 0$) is a realistic approximation since interaction curves are a product of both kinetic and mass transfer influences. An expression for the average value of $[C_A]_t$ within the gradient was used to facilitate calculation of the active concentration of analyte $[C_A]_i$ and *Lr* from the following differential equation:

$$\frac{dR}{dt} = \frac{MW\ G\ Lm\ Lr\ [C_A]_i}{Lm + Lr} \qquad (14)$$

where *MW* = Molecular weight of the analyte (Da).
G = Response factor 10^9 units (RU) m^2/kg.
$[C_A]_i$ = Injected concentration of analyte (M).
Lr = Coefficient of reaction flux (s^{-1}).

(N.B. This expression assumes that dissociation is negligible during the initial association phase of the interaction curve.)

The molecular weight of the analyte must be known and the diffusion coefficient can be estimated from Stoke's law and the Einstein-Sutherland equation (Christensen, 1997). Variation of the sample injection flow rate causes a corresponding change in the mass transport coefficient (*Lm*), allowing estimation of the active concentration under partial MTL conditions.

3.1.9 ***Data Analysis***. Simple kinetic characterisation of interactions by visually ranking interaction curves is often sufficient for selecting reagents. More detailed kinetic characterisation involves determination of observed rate constants (k_{obs}) that are restricted within the context of the experimental system. Both of these methods are relatively insensitive to deviations from 1:1 pseudo-first-order behaviour and are reliable provided that MTL is not completely dominant. Determination of 'true' rate constants demands careful experimental design and data evaluation. In general, very few interactions conform completely to the simple 1:1 pseudo-first-order model, but a satisfactory fit to this model is more likely to provide a realistic approximation of the 'true' rate constants. O' Shannessy and Winzor (1996) suggested that all rate constants obtained from 'real-time' interaction analysis are apparent and phenomenological in nature. He proposed that the observed rate constant (k_{obs}) is a more appropriate description of sensorgram data because it is independent of bulk MTL and insensitive to many of the other factors listed in section 3.1.2.

If MTL effects cannot be completely eliminated experimentally, it may be possible to account for these affects during data analysis by incorporating expressions for MTL into the interaction model. Schuck (1996) accounted for observed deviations by developing a phenomenological two-compartment model for the analysis of partial MTL data. He showed that this model could be used to approximate 'true' kinetic constants from MTL data and extended the upper limit of k_a determination by two orders of magnitude. Early kinetic evaluation techniques relied on fitting the experimental data to an integrated form of the rate equation (equation 4) for a 1:1 pseudo-first-order model. However, partial MTL data is difficult to interpret using this analysis. Consequently, other researchers fitted heterogeneous binding curves to the sum of two smoothly decaying exponential functions (O'Shannessy and Winzor, 1996). Recent investigations have found that the contribution of each exponential function is difficult to resolve and that almost any binding response curve can be described in this way, leading to unreliable rate constants (Morton *et al.*, 1995).

In contrast to the above methods, software employing numerical integration algorithms to solve the differential form of the rate equations directly allows complex models (e.g. pseudo-first-order binding with mass transfer) to be fitted to experimental data. Global fitting of selected parameters of the algorithm produces a more robust data analysis. Essentially, rate constants are independent of concentration and may be constrained to a constant value during simultaneous analysis of a set of concentration-dependent binding interaction curves. However, very high quality data is required for this analysis as any deviations can lead to inaccurate fitting. Deviations from 1:1 pseudo-first-order behaviour have motivated other researchers to redefine the basic mechanism of reaction kinetics in order to account for an apparent co-operativity or isomerism of the molecular complex (Karlsson and Fält, 1997). This approach appears premature in the absence of any other evidence to confirm

such behaviour and the physical interpretation of such apparent rate constants is unclear. Complex reaction models have been developed for two-state, competitive and parallel interactions. These models possess additional variables that can cause data fitting to appear more accurate, but this does not necessarily imply that the model is more appropriate. A good fit to these models may imply that a particular mechanism is likely but should be confirmed or disproved using additional analytical techniques (Karlsson and Fält, 1997). In conclusion, a satisfactory fit to the simple pseudo-first-order model, with/without expressions to account for MTL, is preferable and is more likely to describe 'true' interaction kinetics (Roden and Myszka, 1996).

3.1.10 ***Overview of Chapter.*** Recently, some uncertainty has arisen with respect to the physical interpretation of rate constants obtained from 'real-time' biosensor analysis (O'Shannessy and Winzor, 1996). The purpose of this investigation was to provide a comprehensive assessment of the difficulties evolved while endeavouring to provide appropriate solutions. Knowledge of the active concentration of reagents for kinetic analysis is important for the estimation of 'true' affinity constants. Hence, two novel biosensor methods for the determination of the active concentration of anti-CD4 IgG, contained in hybridoma supernatant, were investigated. Equilibrium constants determined at steady state provide a very sensitive means of determining the accuracy of kinetic constants obtained from 'real-time' BIA. Hence, the equilibrium constants for two model interactions were determined by steady state solution phase and steady state boundary layer methods, respectively. These values were compared with those determined from kinetic studies. The influence of MTL, immobilisation techniques and the biointerface on interaction curves was investigated for both model interactions, with a view towards optimising experimental techniques. In addition, data analysis techniques for the extraction of approximate rate constants from MTL interaction curves were examined.

3.2 Results and Discussion

3.2.1 ***Novel Quantitative Assays Exploiting Mass Transport Limitation and Flow Injection Analysis.*** Conventional assays for the determination of protein concentration rely on spectroscopic and chemical techniques. These generic detection methods require the generation of a standard curve using pure standards of the protein of interest. Furthermore, they estimate the total protein concentration rather than the biologically active fraction. Consequently, affinity-based assay formats (e.g. ELISA) are superior as only the biologically active fraction is detected. Immunoassays allow accurate determination of the active analyte concentration contained in crude matrices. Despite these advantages, a standard curve must be constructed using known concentrations of analyte. Time consuming and expensive purification procedures such as affinity chromatography are required to obtain such samples. In addition, purification schemes commonly cause deterioration of the analyte's biological activity.

An ideal assay should facilitate sensitive estimation of the active concentration of the analyte in crude matrices without requiring a standard curve. Biosensor technology employing flow injection analysis (FIA) has facilitated the development of two assay methods that meet these demands.

(a) Universal standard curve. This method eliminates the requirement for a standard curve for each analyte by establishing MTL conditions, whereby the rate of analyte binding is directly related to the active concentration of the analyte. However, the applicability of the method is restricted to homogenous interactions involving analytes that share the same molecular weight and form (e.g. antibodies).

(b) Flow rate analysis. The bulk mass transfer coefficient (*Lm*) is dependent on the geometry of the flowcell (constant) and the bulk flow rate. Once MTL is established, the binding rate of the immobilised ligand becomes flow rate dependent. The binding rate recorded at different flow rates is related to *Lm* according to equation 15, allowing estimation of the active analyte concentration.

$$R_t = \frac{MW\ G\ Lm\ Lr\ [C_A]_i}{Lm + Lr}(t - t_0) + R_0 \qquad (15)$$

where

R_0 = Response at time zero

(Note: This expression is the integrated form of equation 14.)

Both methods assume that dissociation of the analyte during the early association phase of the interaction curve can be neglected. In addition, the bulk analyte concentration is assumed to be constant since it is continually replenished. If MTL is fully established, the binding rate will be constant giving a linear binding curve.

3.2.2 ***Universal Standard Curve.*** The binding rate of an antibody under conditions of high MTL is independent of the identity and concentration of the immobilised antigen. However, low flow rates and high surface capacities must be employed to establish these conditions (Karlsson *et al.*, 1993). This is difficult to achieve for interactions governed by low association rates ($< 10^5$ M^{-1} s^{-1}) because the flow rate can be lowered to a minimum of 1 µl/min and the maximum surface capacity attainable is dependent on the ligand. It is not uncommon to exceed binding capacities of 10,000 RU. However, many acidic proteins (e.g. hapten carrier proteins) are difficult to immobilise and hence, limit the surface binding capacity. The establishment of MTL conditions can be confirmed by obtaining the same binding rate over two surfaces that are coated with different concentrations of the antigen.

This method was applied to the determination of the active anti-CD4 IgG concentration contained in crude hybridoma supernatant. CD4 was immobilised (~7,700 RU) using conventional amine coupling and the interaction with anti-CD4 IgG was observed. Unfortunately, the immobilised CD4 proved to be unstable when exposed to mild regeneration solutions. A substantial (11-15 %) loss of surface binding capacity was observed after each binding-regeneration cycle. Consequently, determination of the total antibody concentration was performed using immobilised protein G. Protein G-antibody interactions are generally characterised by high association rates, which facilitates the establishment of MTL conditions. Furthermore, low dissociation rates and efficient regeneration, combined with the broad antibody specificity of protein G present a flexible format for antibody concentration determination. However, this broad specificity can lead to undesirable binding of contaminating antibodies contained in the hybridoma supernatant, thus necessitating reference curve subtraction. Both the OKT4 hybridoma supernatant and unused culture media (containing 5 % foetal calf serum) were serially diluted in HBS buffer and assayed for total antibody concentration. *Figure* 3.2.2 (a) is a plot of the binding rate against the dilution factor for both samples and *Figure* 3.2.2 (b) is the resulting universal standard curve for the determination of antibody concentration. The universal standard curve developed by Karlsson *et al.* (1993) was given by the simple expression:

$$Log\frac{dR}{dt} = m\ Log(C_A)_{(nM)} \tag{16}$$

where Slope (m) = 1.00.

The corresponding curve for the protein G-anti-CD4 IgG interaction was given by the following:

$$Log\frac{dR}{dt} = m\ Log(DF) \tag{17}$$

where m = 0.94.

DF = Antibody dilution factor.

The slope of both equations is dependent on the mass transfer coefficient (*Lm*) for each experiment. The corrected anti-CD4 IgG binding rates were converted into concentration values using equation 16 and were multiplied by 1/0.94 to account for the variation in *Lm* between experiments. The variation in *Lm* is due to the higher molecular weight of IgG_{3b} (160 kDa) as compared to other IgG isotypes (MW of 150-155 kDa). The average total anti-CD4 IgG concentration was found to be 19.74 ± 0.03 μg/ml. Therefore, the universal standard curve can be used to estimate the concentration of antibody samples analysed at different *Lm* values (i.e. flow rates) by simply using a correction factor to account for the variation in slope.

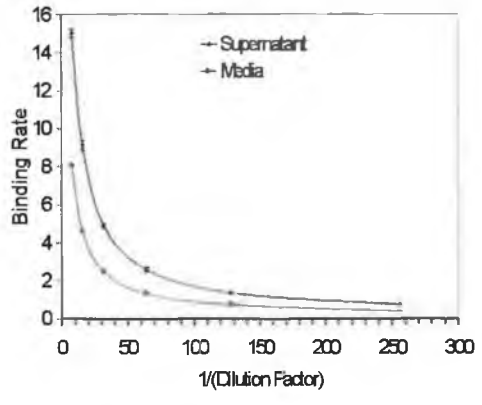

(a) Antibody binding rate.

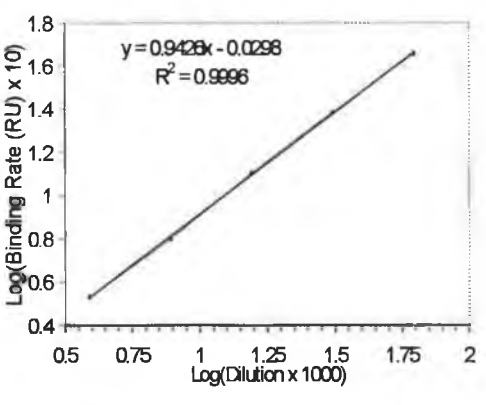

(b) Universal standard curve.

Figure 3.2.2. **(a)** Plot of the antibody-binding rate against the dilution factor. Serial dilutions of OKT4 hybridoma supernatant and unused OKT4 media were analysed under MTL conditions. 25 μl of sample were injected at 15 μl/min and the surface was regenerated with a 30 sec pulse of 20 mM HCl and 10 mM NaOH. The binding rates for all samples were recorded in triplicate and plotted against the dilution factor. **(b)** Universal standard curve for the determination of antibody concentration. The binding rates were calculated for the interaction of anti-CD4 IgG with a protein G-coated surface under MTL conditions. The binding rates of reference curves (unused OKT4 media) were subtracted from the values obtained for the OKT4 supernatant dilutions.

3.2.3 ***Flow Rate Method.*** Christensen (1997) showed that absolute MTL conditions are difficult to generate, since a variation of MTL from 5-95 % requires a 360-fold increase in the immobilised ligand concentration. In addition, a computer simulation model was developed to determine the conditions under which an analytical expression (equation 15) for the binding rate could be applied. The method is experimentally simple, requiring injection of the analyte (1-10 nM range) over the ligand-coated surface at different flow rates. The binding rate should be < 25 RU/sec in order to apply the analytical expression.

Firstly, the contribution of the contaminating bovine antibodies was determined by analysing unused OKT4 culture media in parallel with the actual anti-CD4 IgG-containing hybridoma supernatant. The flow rate-dependent binding rates were calculated for each curve by fitting a straight line to the linear association curves. The average binding rate for four replicates was plotted against the flow rate (*Figure* 3.2.3.1) and revealed that significant binding of contaminating antibodies contained in the cell culture media occurred, thus necessitating reference curve subtraction.

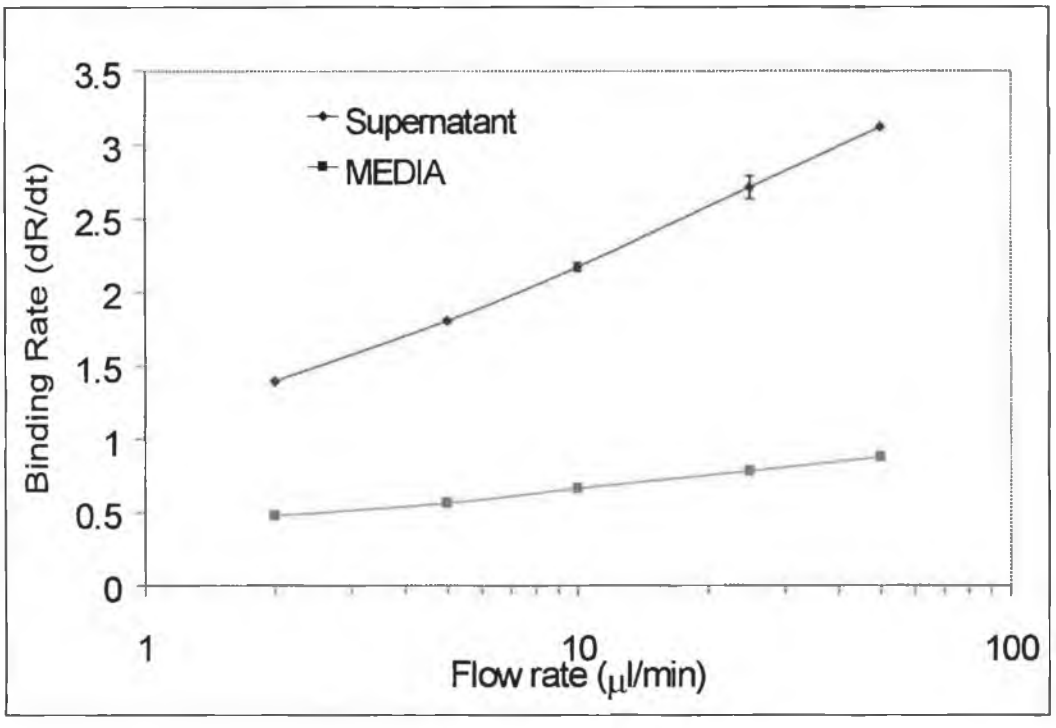

Figure 3.2.3.1. Plot of the sample injection flow rate against the binding rate. The antibody binding rate from the hybridoma supernatant and the unused media were determined by finding the slope of the interaction curves. The slope (i.e. binding rate) was plotted for each flow rate in triplicate. Non-specific binding to the surface was < 0.5 RU/s.

Christensen (1997) developed an empirical equation from computer simulations to correct the values obtained from the analytical expression in order to account for gradients in the analyte concentration at the surface. The correction factor (CF) is given by

$$CF = 1 + MTL\left(0.232\,(1 - MTL) - 0.117\,\sqrt[3]{\tau_R}\right) - 0.376\,\tau_R) \qquad (18)$$

where

Γ_R = $(D\,b.\,l)/F\,h.$

D = Diffusion coefficient of the analyte (4×10^{-11} m^2/s).

F = Bulk flow rate (m^3/s).

h, b and l are the height (5.0×10^{-5} m), width (5.0×10^{-4} m) and length (1.6×10^{-3} m) of the flowcell, respectively (m).

Γ_R describes the average time to pass through the flowcell relative to the time required to diffuse across the height of the flowcell and it becomes greater at lower flow rates. The correction factor accounts for deviations from the assumption that the concentration of antibody at the surface is constant, because boundary layer gradients in analyte concentration exist along the length of the flowcell. These deviations are more apparent at high MTL conditions due to the lower flow rates. The analytical expression (equation 15) for the determination of the anti-CD4 IgG concentration implies that a plot of the reciprocal of the binding rate ($1/dR/dt$) against the reciprocal of Lm ($1/Lm$) should yield a linear relationship, allowing $[C_A]$ to be calculated from the slope (*Figure* 3.2.3.2). The binding rates were corrected according to equation 18 and plotted together with the uncorrected values (*Figure* 3.2.3.2). However, the corrected binding rates were not significantly different (< 8 %) from the actual binding rates (*Table* 3.2.3). Consequently, the analysis was conducted by fitting the model directly to the interaction curves.

A set of corrected interaction curves for the interaction of anti-CD4 IgG with immobilised protein G is shown in *Figure* 3.2.3.3(a). The binding rate for each curve is virtually constant indicating the presence of MTL. The analytical expression was fitted directly to the actual interaction curves using a customised interaction model developed on BIAevaluation software. A robust analysis in which the active concentration was constrained to a constant value for all five curves (globally fit parameter) was completed. The linear fit expected from equation 15 yielded a good approximation of the data as evidenced by the low residual values (< ± 3 RU), and *Table* 3.2.3 is a summary of the results from this analysis. As expected the degree of MTL decreases as the flow rate increases. The anti-CD4 IgG concentration $[C_A]$ contained in the hybridoma supernatant was found to be 19.8 ±

0.94 μg/ml, which is almost identical to the value obtained using the universal standard curve method (19.74 ± 0.03 μg/ml).

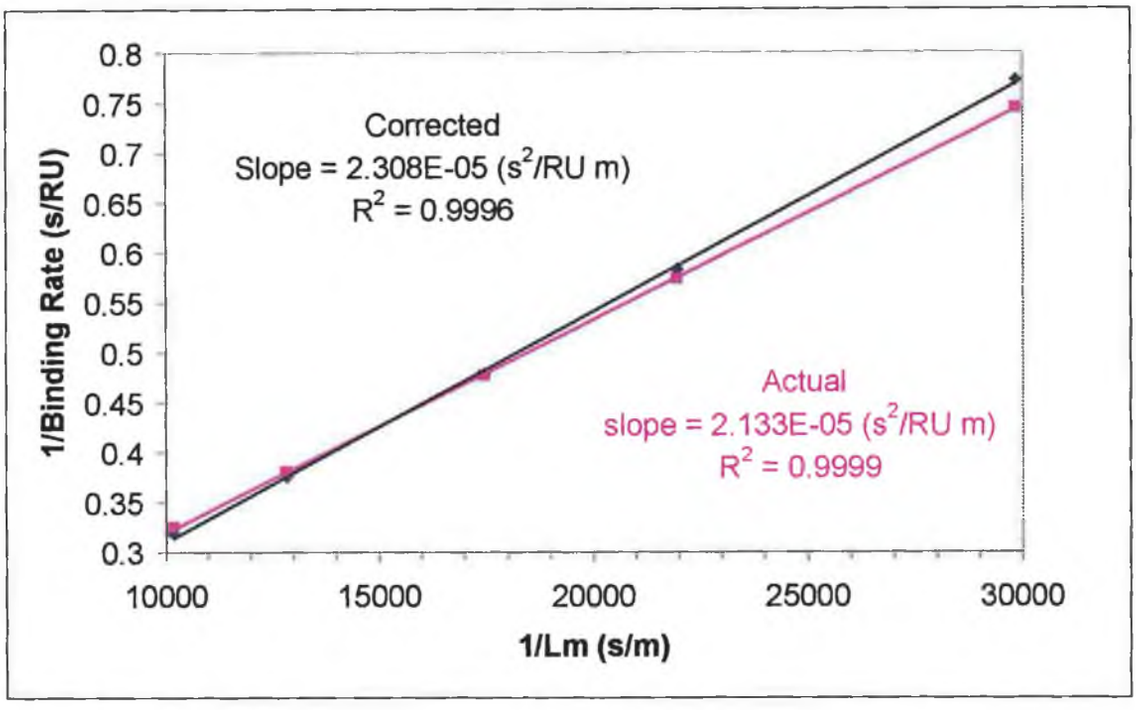

Figure 3.2.3.2. Plot of the reciprocal of the mass transfer coefficient (*Lm*) against the reciprocal of the binding rate (i.e. slope). The actual binding rates (—) and the corrected binding rates (—) are both plotted for comparative purposes. The slope and the regression coefficient for each curve were found by linear regression analysis.

The reliability of antibody concentrations determined from both the universal standard curve and the flow rate methods was confirmed by BIACORE 1000™ analysis combined with protein A-affinity chromatography. BIACORE 1000™ analysis showed that the contaminating antibody, which was contained in the hybridoma supernatant, contributed a mere 4.6 % to the total concentration of protein A affinity-captured antibody (*Figure* 3.2.3.4). Protein A affinity chromatography was employed to purify the anti-CD4 antibody resulting in a yield of 22.7 μg antibody/ml supernatant as determined by spectroscopy, assuming A_{280nm} (1 mg/ml) of 1.4. Accounting for 4.6 % contamination, the actual yield of anti-CD4 IgG (21.6 μg antibody/ml supernatant) agrees well with the estimates from both MTL-based assay methods.

Essentially, both assay methods are independent of the identity of the immobilised ligand, as they exploit MTL binding conditions to provide a condition where the analyte binding response is a function of concentration and molecular size. However, the flow rate method is a considerable

advancement over the universal standard curve method. In particular, relating the active concentration and the reaction flux to the mass transport coefficient provides a far more flexible method that can be applied to the determination of any macromolecular analyte. In contrast, the universal standard curve is limited to the assay of macromolecules possessing the same MW and morphology. In common with all direct 'real-time' biosensing applications, the applicability of both techniques is dependent on efficient regeneration of the surface. The active concentration of the anti-CD4 IgG could not be determined by either technique as immobilised CD4 was highly sensitive to regeneration. However, a general affinity ligand (i.e. protein G) was successfully employed to determine the total antibody concentration contained in the hybridoma supernatant. The biologically active fraction of all antibodies and antigens employed for kinetic analysis (section 3.2.6) was assumed to be 100 %. The kinetic analysis was concerned with the examination of experimental and data analysis methodologies and the absolute value of kinetic constants was inconsequential.

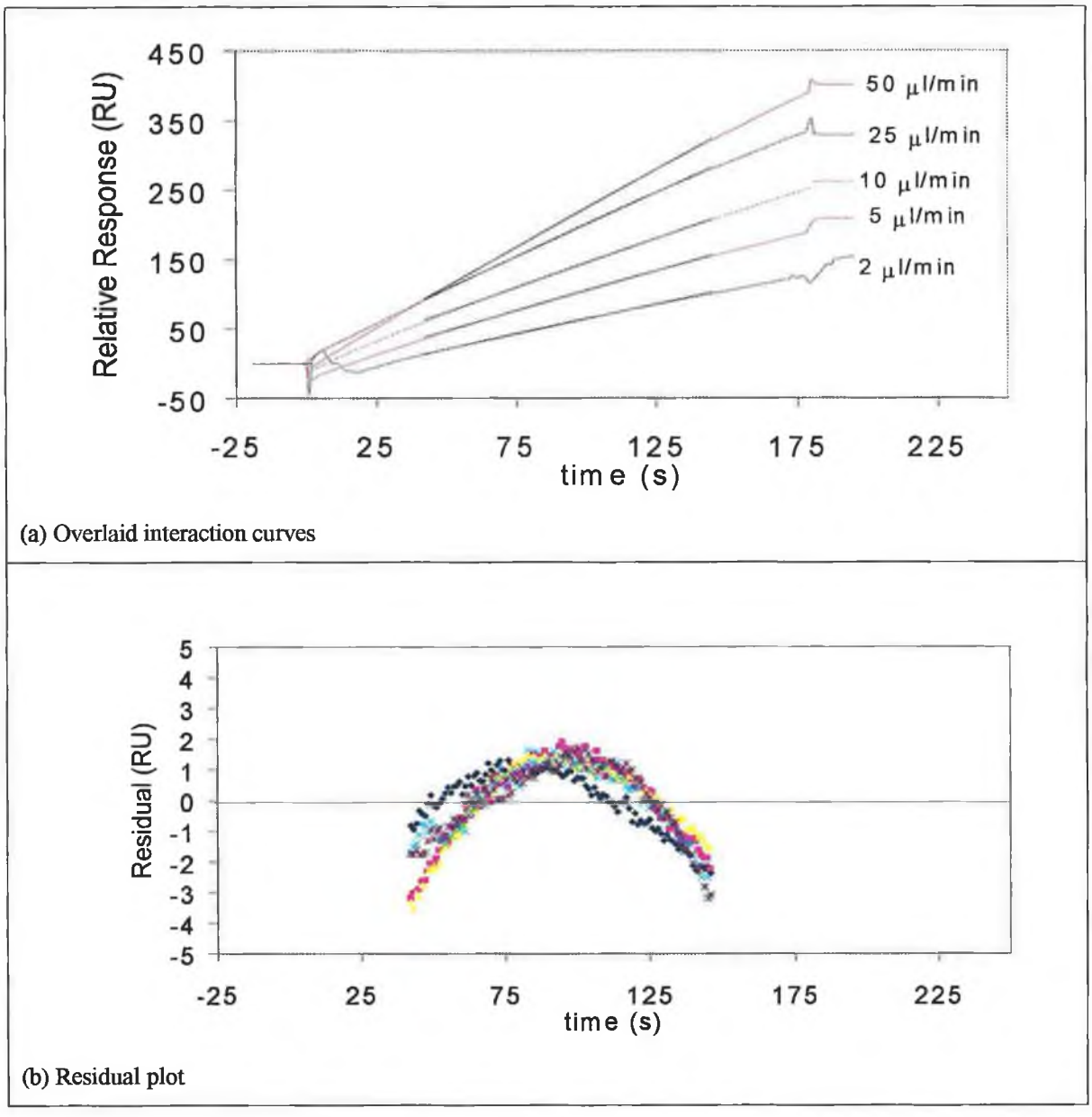

Figure 3.2.3.3. **(a)** Overlay of corrected sensorgrams for the interaction of anti-CD4 IgG with immobilised protein G (1,000 RU) under MTL conditions. OKT4 hybridoma supernatant was diluted 1/64 in HBS buffer and injected at different flow rates. Reference curves were completed using a 1/64 dilution of unused OKT4 culture media and were subtracted from the supernatant curves. Four replicates were completed at each flow rate and a single set is displayed above. The binding rate was calculated by finding the slope of a line fitted (superimposed dark lines) to the association phase of the interaction curves. **(b)** Plot of the residual response (RU) against time. The plot displays the difference between the actual curve and the fitted line at each data point.

Flow rate (μl/min)	*Lm* (m/s) x 10^{-6}	*dR/dt* (RU/s)	CF	$(dR/dt)_C$ (RU/s)	MTL %
2	3.35	1.344	0.9638	1.2953	93.2
5	4.55	1.742	0.9846	1.7152	91.0
10	5.73	2.096	0.9968	2.0893	89.0
25	7.78	2.631	1.0106	2.6589	85.6
50	9.81	3.076	1.0204	3.1387	82.5
***Lr* (m/s)**	$4.62 \pm 0.14 \times 10^{-5}$				
$[C_A]$ (M)	$1.84 \pm 0.008 \times 10^{-9}$				

Table 3.2.3. Results from global analysis of flow rate-dependent interaction curves using the customised interaction model developed on BIAevaluation software. The MW of anti-CD4 IgG was assumed to be 160,000 and the response factor (G) was 1×10^9. Values of *Lr* and $[C_A]$ were constrained to a single value for the curve set to give a robust global analysis (NB. Global analysis is where one or more parameters are constrained to a fixed value when fitting an expression to a set of interaction curves). *Lm* values were calculated from equation 11, MTL from equation 13 and the correction factor (CF) was calculated from equation 18. This procedure was repeated for a total of three sets of flow rate-dependent interaction curves giving an average *Lr* of $3.88 \pm 0.88 \times 10^{-5}$ m/s. Accounting for the dilution factor and MW, the antibody concentration $[C_A]$ was determined to be 19.8 ± 0.94 μg/ml.

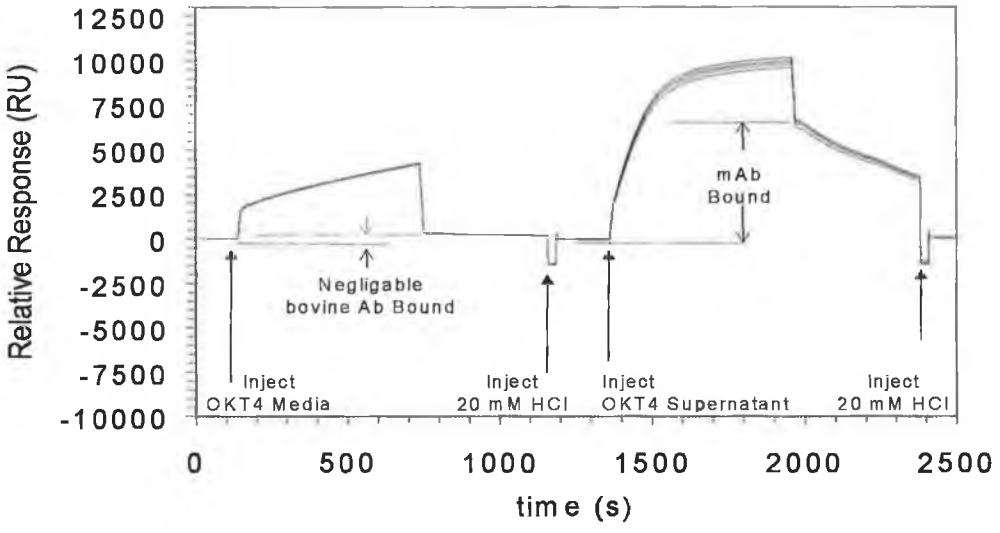

Figure 3.2.3.4. Overlay of sensorgrams for the detection of monoclonal anti-CD4 IgG contained in hybridoma supernatant. Unused OKT4 hybridoma media was injected over a protein A-coated surface to determine the binding response of contaminating bovine antibodies. After regeneration with a 30 sec pulse of 20 mM HCl, the supernatant was injected over the surface for 10 min. The surface was regenerated and the same binding-regeneration cycle repeated for four replicates. The bovine antibody binding response represents 4.6 % of the total anti-CD4 IgG binding response.

3.2.4 ***Reduced Dextran Biointerface.*** It has been suggested by several authors (Schuck, 1996) that hydrogel-based biointerfaces are responsible for many of the artefacts observable in interaction curves. It is important to consider the dynamic and complex nature of interactions that occur within a hydrogel. The assumption that the ligand is fixed, possessing a diffusion coefficient of zero, is incorrect. The diffusion coefficient (D) for molecules attached to the hydrogel can be expected to decrease by a factor of at least $1/\eta$ (since $D \cong 1/\eta$), where η is the viscosity within the matrix. Given a dextran concentration of 25 mg/ml within the hydrogel and an immobilisation concentration of 10 mg/ml, the viscosity within the hydrogel will be approximately twice that of water (Karlsson *et al.*, 1994). Therefore, kinetic constants in solution and within the matrix may differ by over 50 %.

The accuracy of this estimation was evaluated by finding the viscosity of dextran solutions. Dextran solutions exhibit Newtonian behaviour and the sample viscosity is a function of the molecular weight. Therefore, a dextran solution (20 mg/ml) was prepared in HBS buffer using a 500 kDa dextran preparation as employed for CM5 chip fabrication (Löfås et al., 1990). It was found that the viscosity was 3-fold higher than the viscosity of HBS buffer. Furthermore, doping the dextran solution with high concentrations (~50 mg/ml) of BSA had no detectable effect on the viscosity. These results imply that the diffusion coefficient is at least 3-fold lower within the matrix and that high protein concentrations (~ 5,000 RU) within the matrix do not significantly increase the viscosity. Both the hydrogel-bound ligand and the analyte are subject to these diffusional limitations and, hence, a 3-fold reduction in the association rate and dissociation rate constants as compared to homogenous solution phase may be expected.

Schuck (1996) proposed that additional factors affect the mobility of analytes within the hydrogel. Firstly, large molecules may be hindered at the gel-bulk interface in proportion to their molecular weight. This apparent partitioning coefficient of the analyte between the bulk and the hydrogel surface was estimated to be 0.15 for antibody molecules and exponentially dependent on the analyte's MW. Secondly, diffusion of the analyte within the matrix may be decreased in proportion with the reaction flux. The correction factor was estimated by $(1 + (Lr/k_d))^{-1}$. This factor is equal to the average time per second in which the analyte molecules are free (i.e. [bound]/free = $t_{trapped}/t_{free}$). However, this correction factor was found to be negligible (0.998) for a typical kinetic experiment given an antibody-coating concentration of 400 RU, a k_a of 2×10^5 $M^{-1}s^{-1}$ and a k_d of 5×10^{-4} s^{-1}. Other factors such as the inward moving analyte saturation front, steric hindrance and matrix cross-linking have also been associated with the use of a hydrogel (see section 3.1.2).

In view of these considerations, a reduced dextran sensor chip was produced to facilitate a comparison with the extended hydrogel biointerface for kinetic analysis of antibody-antigen interactions. Dextranase was used to digest the CM-dextran at the sensor surface to yield a reduced dextran (RD) sensor chip. *Figure* 3.2.4(a) is a sensorgram following the digestion over 1.25 hours. RD sensor chips were produced by incubating CM5 chips overnight in a solution of dextranase (50 μg/ml, in 50 mM phosphate buffer, pH 6.0). Pre-concentration studies were employed to confirm the depletion of surface-bound dextran, since the loss of negatively charged carboxylic groups causes a decrease in the pre-concentration capacity of the surface. *Figure* 3.2.4(b) is an overlay of sensorgrams monitoring the pre-concentration of BSA onto a normal CM5 sensor chip and the RD sensor chip. The 82 % decrease in pre-concentration suggested that the majority of the dextran had been removed. The residual pre-concentration effect may be attributed to dextranase resistant CM-dextran and/or the presence of carboxylic groups introduced onto the linker layer (self-assembled monolayer) during the chip fabrication process.

It is possible that the matrix may be resistant to complete digestion, because dextran and not CM-dextran is the natural substrate for dextranase. Considering that the hydrogel has been reported to contain 25 mg/ml of dextran, the expected decrease in response should approach 2,000 RU. A reduction of 1,100 was obtained, representing a loss of 13 mg/ml of dextran, and this implies that a further 12 mg/ml of dextran remained at the surface. Digestion of the hydrogel at the surface of the CM5 chip using 5 M NaOH removed 1,600 RU of dextran, causing a 97.4 % reduction in the preconcentration effect (section 5.2.3.4.2). This corresponds to a dextran concentration of 21 mg/ml and implies that approximately 34 % of the CM-dextran remains after dextranase digestion. Hence, the viscosity of the reduced dextran (RD) chip is considerably reduced and should lower matrix diffusional limitations.

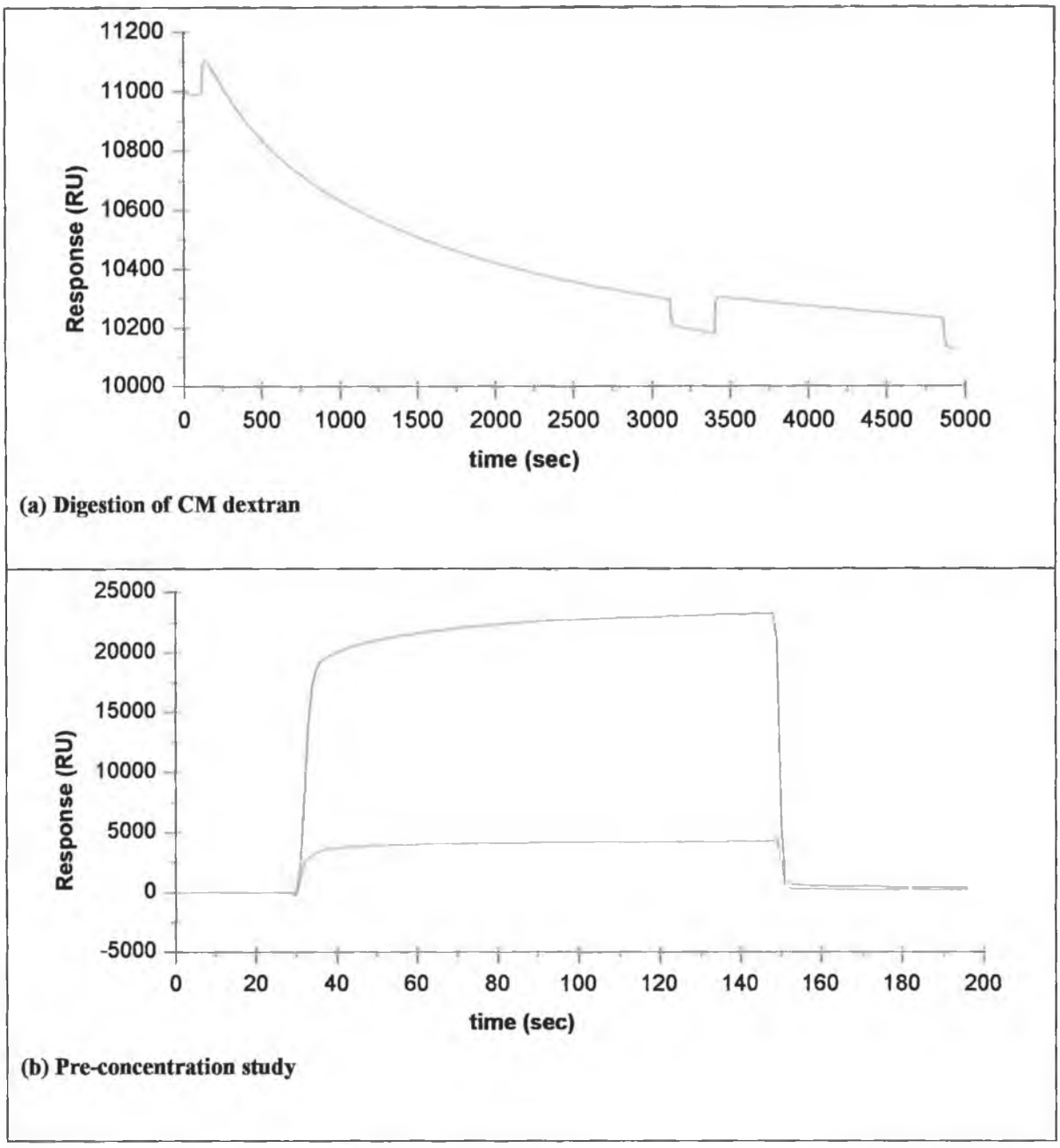

Figure 3.2.4. **(a)** Sensorgram following the digestion of surface bound carboxymethylated (CM) dextran. Dextranase (50 μg/ml, in 50 mM phosphate buffer, pH 6.0) was injected over a blank CM5 sensor surface for 50 min at 5 μl/min. The dextranase was re-injected for a further 25 min as the digestion curve had not reached a plateau. A final digestion response of ~ 860 RU was observed although the digestion level had not reached a plateau. **(b)** Overlay of sensorgrams for the pre-concentration of BSA onto both the CM5 sensor chip and the RD chip. Bovine serum albumin (1 mg/ml in 10 mM sodium acetate buffer, pH 4.16) was injected over both surfaces at 10 μl/min for 2 min. The pre-concentration responses at the plateau points of both the CM5 sensor chip surface and the RD sensor chip surface were ~ 23,100 RU and ~ 4,200 RU, respectively.

3.2.5 ***Characterisation of Molecular Interactions at Equilibrium.*** The affinity constant (K_a) for an equilibrium mixture is defined as the quotient of the association rate constant (k_a) and the dissociation rate constant (k_d). Hence, prior knowledge of the affinity constant can be used to assess the reliability of kinetic constants determined using direct 'real-time' biosensing. The affinity constant is a sensitive index, since relatively small changes in the kinetic constants have a large effect on the calculated affinity constant. Steady state affinity constants for the interaction of anti-CD4 IgG with CD4 and anti-GST IgG with GST were determined by boundary layer and solution phase techniques, respectively. The values obtained were compared with affinity constants determined for these interactions from kinetic experiments (section 3.2.6).

3.2.5.1 ***Boundary Layer Steady State Affinity.*** The anti-CD4 antibody was affinity-captured in order to avoid model complexity arising from the binding of a bivalent analyte. In any case, immobilisation of CD4 was unsuitable due to its sensitivity to mild regeneration conditions. Affinity-capture of anti-CD4 IgG_{3b} was necessary as attempts to optimise regeneration conditions for direct immobilisation of the antibody were also unsuccessful due to the antibody's sensitivity to regeneration conditions. The steady state affinity for a surface interaction is related to concentration according to equation 6 (section 3.1.1) but is rearranged here in terms of the affinity constant (K_a) and is given by the following expression:

$$R_{eq} = \frac{K_a.(C_A)_i.R_{max}}{K_a.n.(C_A)_i + 1} \qquad (19)$$

where n = Steric hindrance factor and represents the average number of ligand sites occupied per analyte molecule bound.

Other symbols have their usual meaning.

The steric hindrance factor (n) was experimentally determined for both the CM5 sensor chip and the RD sensor chips (see section 3.2.4). Anti-mouse Fc and protein G-coated surfaces were used for affinity-capture of the antibody. In addition, a variety of coating concentrations were employed in order to determine the effect of ligand density on steric hindrance. *Table 3.2.5* shows that steric hindrance effects clearly influence the saturation response for all formats, with the exception of the low-density (3,680 RU) anti-mouse Fc-coated CM5 surface. This surface was chosen for the equilibrium analysis as it had a high % R_{max} value of 99 % which confirmed the absence of serious steric hindrance effects.

The results showed that protein G affinity-capture reduced the binding capacity by ~ 40 %. This was not unexpected as protein G anchors the antibody via the Fab arm close to the antigen-binding

site. The RD chip gave a maximum % R_{max} of 68 % for a coating density of 1,670 RU. In this case, the reduced % R_{max} may be attributed to the proximity of the interacting molecules with the planar surface (RD chip), resulting in poor orientation of a sub-population of the CD4 binding sites. Furthermore, reduced access to binding sites due to overcrowding may account for the observed reductions in % R_{max} (86 %) for high coating concentrations (11,000 RU of anti-mouse Fc).

	Surface density (chip type)	*Anti-CD4 Captured (RU)*	*CD4 Bound at Saturation (RU)*	*Ideal Saturation Response (R_{max})*	*% of Ideal R_{max}*	*n*
Anti-Mouse Fc surface	11,000 RU (CM5 chip)	468	251	292	86%	0.86
	3,680 RU (CM5 chip)	601	370	375	99%	0.99
	1,670 RU (RD chip)	228	97	142	68%	0.68
Protein G-surface	1,000 RU (CM5 chip)	650	221	406	54%	0.54
	262 RU (CM5 chip)	266	99	166	60%	0.60
	277RU (RD chip)	650	220	406	54%	0.54

Table 3.2.5. Determination of the steric hindrance factor (n) for the interaction of CD4 and anti-CD4 IgG. Anti-mouse Fc antibody and protein G were employed as affinity-capture ligands. Both were immobilised onto CM5 sensor chips and onto the reduced dextran (RD) sensor chips. The concentration of the immobilised ligand was varied in order to evaluate the effect of ligand concentration on steric hindrance. The actual surface concentration (mg/ml) can be estimated by dividing the surface density (RU) by 100. The MW of both CD4 and anti-mouse Fc Ab were taken to be 50 kDa and 160 kDa, respectively.

A set of corrected sensorgrams obtained for the interaction of CD4 with affinity-captured anti-CD4 IgG is shown in *Figure* 3.2.5.1(a). A plateau was reached after a short 20 min exposure to the affinity-captured anti-CD4 IgG since the association rate of the interaction was very fast ($k_a \sim 1 \times 10^6$ s^{-1}). The equilibrium response (R_{eq}) values were plotted against the CD4 concentration and the 'boundary layer' steady state affinity model was fitted to the data yielding a K_a value of 3.04×10^8 M^{-1} (*Figure 3.2.5.1*(b)). This 'boundary layer' affinity constant should describe solution phase equilibrium mixtures even if hydrogel diffusional effects are present, as the association and dissociation rate constants will be slowed by the same factor.

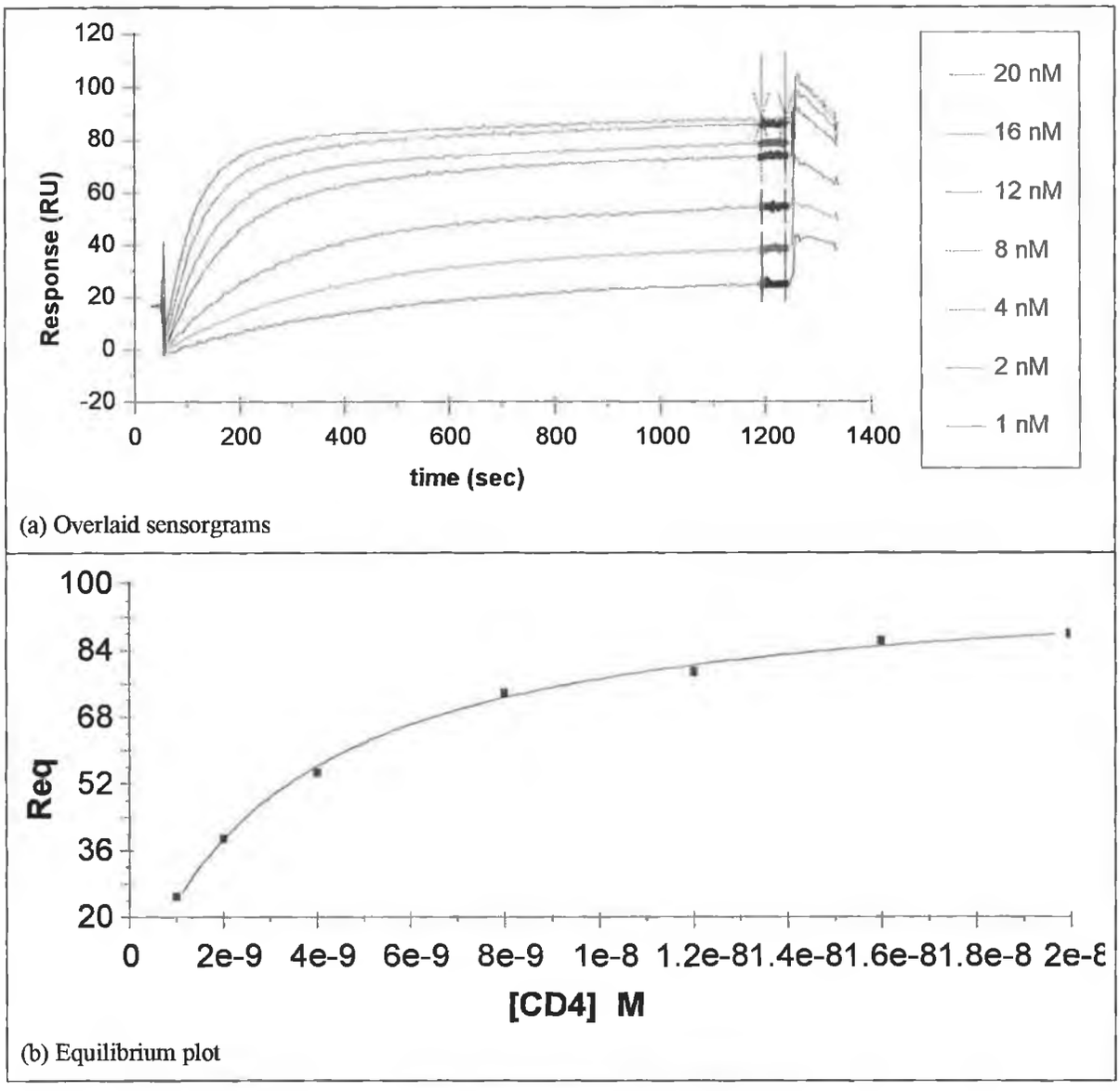

Figure 3.2.5.1 **(a)** Overlay of corrected sensorgrams for the interaction of CD4 with affinity-captured anti-CD4 IgG. Goat anti-mouse Fc IgG was immobilised (1,500 RU) onto a CM5 sensor chip surface and purified anti-CD4 IgG was captured, giving an average binding response of ~ 460 RU. Steric hindrance was avoided by employing low (< 90 RU) binding capacities. CD4 samples and a HBS reference sample were injected over the surface for 20 min at a flow rate of 5 µl/min. The sensorgram obtained for the HBS reference sample was subtracted from the other curves to compensate for dissociation of anti-CD4 IgG. The response curves were normalised to zero response directly after the injection point. This eliminated the contribution of bulk refractive index differences due to variable buffer composition. The equilibrium response (R_{eq}) values were obtained by reading the response at the plateau region of each binding curve, as illustrated by the arrows. **(b)** Plot of R_{eq} against CD4 concentration. The R_{eq} values obtained from the equilibrium response curves were plotted against the molar concentration of CD4. The boundary layer steady state affinity model (equation 19) was fitted to the data, assuming a steric hindrance factor (n) of 1.0, to give a K_a value of 3.0×10^8 M^{-1}.

3.2.5.2. ***Solution Phase Steady State Affinity***. Solution phase conditions allow the 'true' equilibrium constant (K_d) to be determined. Serial doubling dilutions of GST were titrated against a fixed concentration of anti-GST IgG. The mixtures were allowed to reach equilibrium and each was assayed for free anti-GST IgG using a BIACORE quantitative assay. A standard curve for the determination of free IgG was generated by employing immobilised GST and standard solutions of anti-GST IgG (*Figure* 3.2.5.2 (a)). A general 4-parameter equation was fitted to the data and used to determine the concentration of free anti-GST IgG and is given by:

$$R = R_{Hi} - \frac{R_{Hi} - R_{Lo}}{1 + \left(\frac{Conc}{A_1}\right)^{A_2}} \qquad (20)$$

Where R_{Hi} = Response at infinite concentration.

R_{Lo} = Response at zero concentration.

$Conc$ = Analyte concentration (M).

A_1 = Fitting constant.

A_2 = Fitting constant.

(Note. A_1 and A_2 are mathematical fitting parameters whose absolute value is inconsequential.)

The overlaid interaction curves for the binding of free antibody contained in the equilibrium samples are shown in *Figure* 3.2.5.2(b). The concentration of GST was plotted against the free anti-GST IgG concentration and fitted to the solution affinity model. The resulting equilibrium plot is shown in *Figure* 3.2.5.2(c). The solution affinity model is given by:

$$B_{free} = \frac{B - A - Kd}{2} + \sqrt{\frac{(A + B + Kd)^2}{4} - A\,B} \qquad (21)$$

Where B_{free} is the free concentration of anti-GST IgG.

A and B are the total concentrations of GST and anti-GST IgG, respectively.

K_d is the equilibrium dissociation constant.

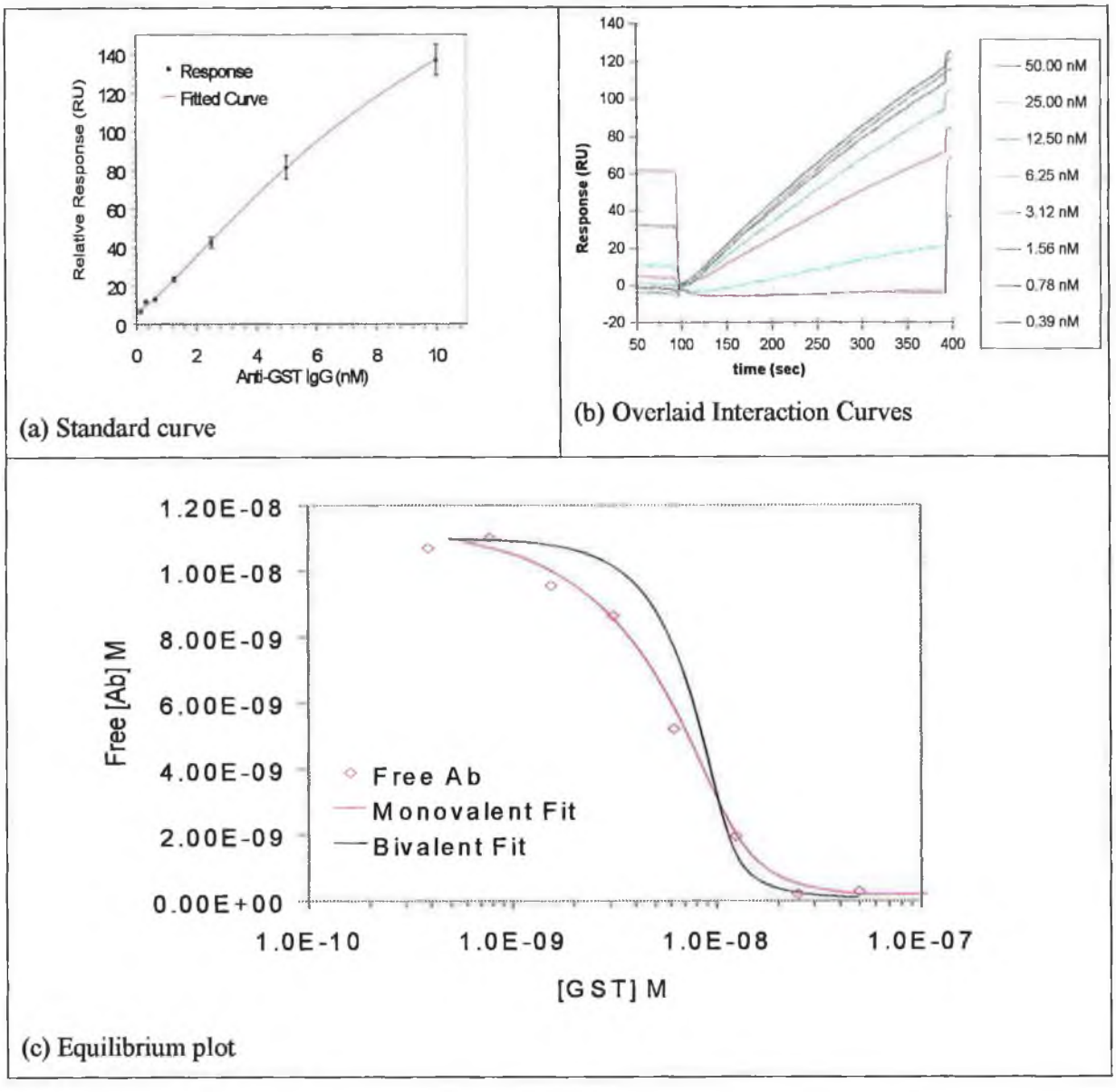

Figure 3.2.5.2. (a) Calibration curve for the determination of free anti-GST IgG contained in equilibrium mixtures. GST (2 μg/ml in 10 mM acetate, pH 5.0.) was immobilised (2,784 RU) using conventional amine coupling. Standard anti-GST IgG solutions and equilibrium mixtures were analysed randomly by injecting 25 μl at 5 μl/min. The surface was regenerated using a 30 sec pulse of 20 mM HCl and 10 mM NaOH. (b) Interaction curves for the interaction of the equilibrium mixtures with immobilised GST. Equilibrium mixtures containing anti-GST IgG (11 nM) and serial dilutions of GST (as shown above) were assayed. Variations in the bulk refractive index were subtracted by normalising the curves to zero response immediately after the injection point. (c) Plot of the GST concentration against relative response. The relative response values for binding of free anti-GST IgG to the surface were calculated from the standard curve. The solution phase equilibrium model (equation 21) was fitted to the data assuming a 1:1 interaction to give a K_d value of 6.83 x 10^{-10} M. A bivalent interaction model (equation 22) was also fitted but failed to describe the data.

The use of a BIACORE concentration assay for the determination of free anti-GST IgG as an alternative to the conventional ELISA approach (Friguet *et al.*, 1985) has several advantages. Conventional ELISA-based methods require an incubation period (< 30 min) in a 96-well microtitre plate that is pre-coated with the antigen. This extended incubation period allows the mixture to re-equilibrate, resulting in over-estimation of the free antibody concentration and under-estimation of the affinity constant. The BIACORE quantitative assay limits this effect due to short sample contact times and continuous replenishment of the equilibrium sample over the GST-coated surface. Dissociation of the equilibrium complex, which releases interfering free antibody, was further minimised by using high flow rates to decrease the thickness of the boundary layer.

The model described (equation 21) assumes that the anti-GST IgG is monovalent. However, a direct antibody assay ought to detect free antibody and monovalently occupied antibody, while excluding the fully occupied $[GST]_2$-IgG complex. In this case, the free antibody concentration will be overestimated, resulting in underestimation of the affinity constant. Consequently, the model was amended to account for the distribution of the analyte between the two antibody binding sites. The probabilities of the analyte occupying one or both binding sites are described by a standard binomial distribution (Piehler *et al.*, 1997) and the concentration of antibody with at least one free binding site can be expressed as:

$$B_{free} = B - \frac{\left[\frac{B - A - Kd}{2} + \sqrt{\frac{(A + B + Kd)^2}{4} - A\,B}\right]^2}{B} \qquad (22)$$

(Note. The notation has its usual meaning.)

The model assumes that the sensor response is equivalent for the free antibody and monovalently occupied antibody. Despite this oversimplification, this equation should approximate the data better than the 1:1 interaction model. In practice, the bivalent model proved inappropriate and completely misfitted the experimental data (*Figure* 3.2.5.2(c)). This suggested that steric hindrance prevented both antibody binding sites from being occupied simultaneously. Consequently, saturation experiments were conducted and confirmed that affinity-captured anti-GST IgG binds to GST monovalently. Approximately half (54.1 ± 0.7 %) of the expected saturation response was found assuming a MW of 50 kDa for the GST and 150 kDa for IgG (*Table 3.2.5.2*). Therefore, only free anti-GST IgG was detected by the BIACORE assay. Hence, the 1:1 solution affinity model fitting was appropriate, giving a K_d value of 6.83×10^{-10} M. The experiment highlights the value of fitting interaction models to experimental data since the affinity constant plus valuable information concerning steric hindrance were obtained.

Anti-GST IgG (RU)	*GST (RU)*	*Expected R_{max} (RU)*	*% R_{max}*	*Average % R_{max} (RU)*
416	142 (8 min)	260	54.61	54.1 ± 0.7
412	142 (6 min)	257	55.14	
416	137 (4 min)	260	52.69	

Table 3.2.5.2. Table of values for the saturation of affinity-captured anti-GST IgG with GST. Protein A was immobilised (1,975 RU) and anti-GST IgG was affinity-captured. A saturating concentration of GST (200 nM in HBS) was injected over the surface at 30 µl/min for 8 min. The surface was regenerated as before and the saturation experiment was repeated for GST injection times of 6 min and 4 min. The interaction curves for all three GST interactions reached a stable plateau indicating surface saturation allowing reliable estimation of R_{max}. Protein A has been shown to be a suitable capture reagent as it provides directed immobilisation of the antibody via the Fc region thereby avoiding steric hindrance of the antigen-binding sites.

3.2.6 ***Kinetic Analysis***. Kinetic analysis of both the GST interaction and the CD4 interaction was carried out using affinity-capture of the IgG to avoid surface heterogeneity. Moreover, using this format, the interaction of soluble antigen with an immobilised antibody can be considered as a monovalent binding system that can be described by the 1:1 pseudo-first-order interaction model. A review of published data reveals that the influence of the affinity-captured ligand on the interaction curve has not been adequately investigated. Moreover, visual inspection of published results (Karlsson and Fält, 1997) suggested that the affinity-capture ligand might be responsible for some of the deviations from ideal behaviour. Consequently, three different affinity-capture ligands were used to anchor the monoclonal antibody. Polyclonal anti-mouse Fc IgG, protein A and protein G were immobilised using conventional amine coupling. Reproducible affinity-capture and effective regeneration were optimised for the interaction of the monoclonal anti-GST IgG with each capture ligand. *Figure* 3.2.6 is an overlay plot that illustrates the basic methodology.

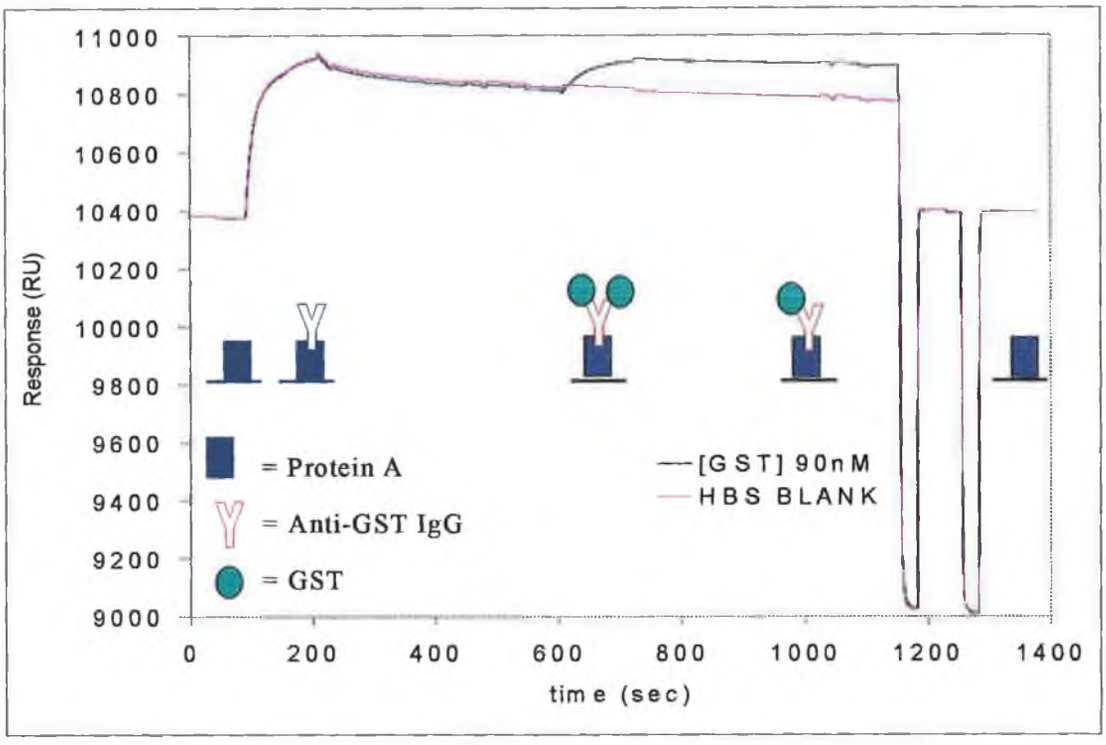

Figure 3.2.6. Overlay of interaction curves for a typical kinetic experiment. Protein A was immobilised onto an RD chip surface (490 RU) using conventional amine coupling. The binding interactions are depicted by the illustrations. Monoclonal anti-GST IgG (2.5 μg/ml) was injected over the surface at 10 μl/min for 2 min and was affinity-captured (~ 410 RU) by the immobilised protein A. The downward baseline drift after this interaction is due to dissociation of the bound antibody. The baseline was allowed to stabilise for 5 min before injecting GST (100 nM in HBS buffer) for 2 min at 30 μl/min. A reference curve was obtained by replacing the GST sample with running buffer (HBS buffer). The downward drifting baseline results from the accumulative dissociation of both the antibody from the immobilised protein A and GST from the antibody. Therefore, the reference curve was subtracted from the GST binding curve in order to eliminate the contribution of dissociating antibody. This process of reference curve subtraction is essential when affinity-capture is employed. Finally, the surface was regenerated using two 30 sec pulses of 20 mM HCl.

Figure 3.2.6.1

and

Accompanying Legend

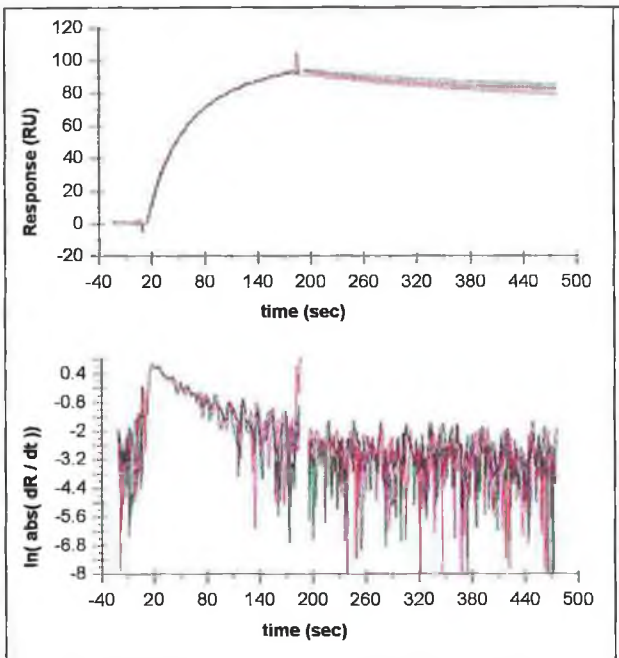

(a) Anti-mouse Fc-coated surface (GST-interaction)

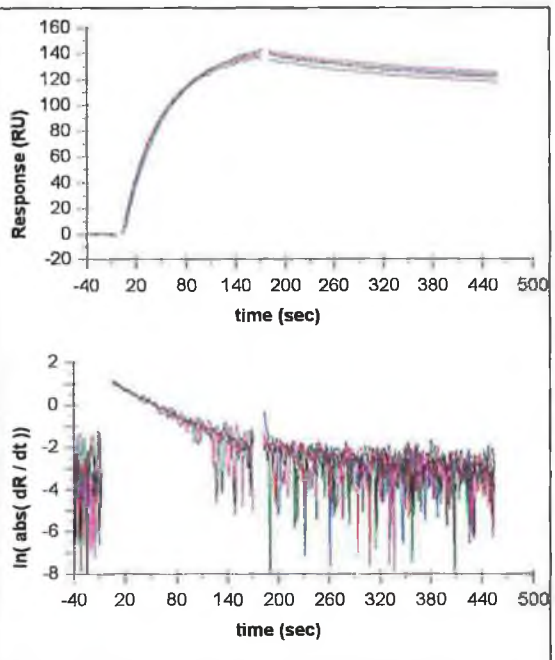

(b) Protein A-coated surface (GST interaction)

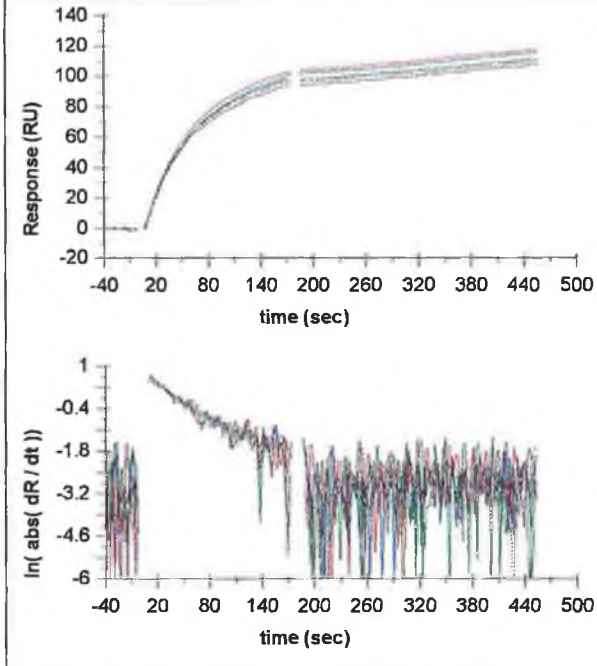

(c) Protein G-coated surface (GST interaction)

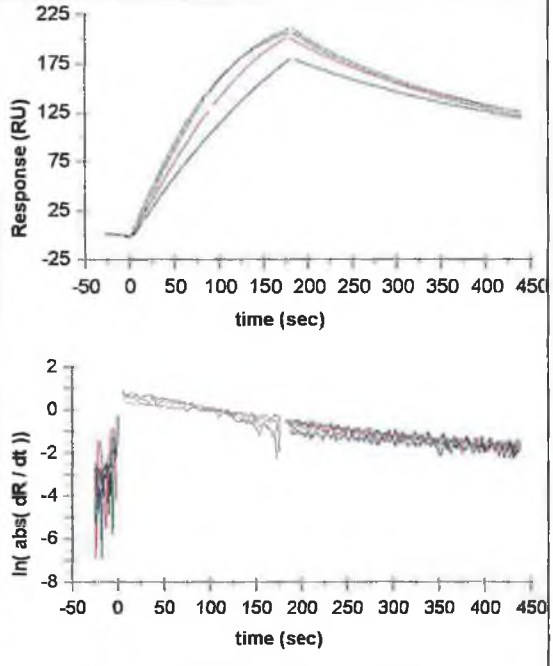

(d) Anti-mouse Fc-coated surface (CD4 interaction)

3.2.6.1 ***Bulk Mass Transport Limitation***. Prior to kinetic analysis it was important to determine the precise experimental conditions required to eliminate MTL. The presence of bulk MTL is easily detected, as the binding response curves will exhibit flow rate-dependent binding rates. Non-MTL binding response curves generated for different flow rates should appear superimposable upon visual inspection. In addition, a transformation of the curves as the natural log of the absolute slope against time (Ln(abs(*dR/dt*)) against time) should reveal a linear association phase. These transformations appear noisy for regions of the binding response curve that have a low slope. *Figure 3.2.6.1*(a), (b) and (c) are binding response curves at various flow rates, for the interaction of GST with affinity-captured anti-GST IgG over anti-mouse IgG, protein A and protein G-coated sensor surfaces, respectively. The binding response curve is virtually independent of flow rate for this interaction on all three surfaces. However, the choice of affinity-capture ligand greatly influences the interaction curves, as evidenced by the variable dissociation phase curves for each affinity-capture ligand. The anti-mouse Fc-coated surface reveals a slight increase in the dissociation rate with increasing flow rate, which is indicative of steric hindrance (Edwards *et al.*, 1995) or rebinding of dissociating ligand (Nieba *et al.*, 1996). At high flow rates the dissociation rate increases, as rebinding is less likely. The analysis of the dissociation phase can be restricted to 2-3 min of the post-injection phase to reduce rebinding since a large fraction of GST binding sites are occupied. This supports the suggestion of Schuck (1996) that diffusional limitations within the hydrogel can effect the interaction curves. Essentially, high viscosity within the matrix, resulting from the high dextran concentration (21 mg/ml) and high protein concentration (~ 118 mg/ml), decreases the mass transport rate and encourages rebinding effects.

In support of this model, the protein A-coated and protein G-coated surfaces did not exhibit divergence in the dissociation phase. This may be attributed to lower matrix diffusional limitation or lower thermodynamic stress resulting from lower protein densities (protein A and protein G surface concentrations were 19.7 mg/ml and 3.27 mg/ml, respectively) at these interaction surfaces. However, the protein G-coated RD chip surface exhibited pronounced deviations from ideal behaviour. The superimposable curves indicate the absence of bulk MTL but the association phase is heterogeneous, indicated by a slight curve in the association phase of the derivative plot. Moreover, the unusual positive dissociation phase slope suggests an increase in surface mass. Clearly, this is impossible as the surface is no longer exposed to the GST sample and the expected dissociation of affinity-captured GST and IgG should yield a negative slope. However, the apparent increase in mass may result from non-specific GST-GST interactions that cause an increase in the protein concentration within the most sensitive region of the evanescent field through matrix contraction. This effect was not observed for the CD4 interaction conducted on both the CM5 and RD chip surfaces, thus directly implicating GST as the causative agent. The interaction of CD4 with

affinity-captured anti-CD4 IgG, employing an anti-mouse Fc-coated CM5 surface, contrasts strongly with the previous GST studies. Firstly, visual inspection of the overlaid interaction curves reveals that MTL is present, since both binding and dissociation phases are flow rate-dependent. Secondly, non-linear association phase curves for the derivative plot indicate a heterogeneous association profile resulting from MTL.

3.2.6.2 ***Determination of Saturation Response.*** Having determined the influence of flow rate on the interaction curves, potential steric hindrance effects of the three affinity-capture formats were examined. An extensive CD4 saturation study employing protein G and anti-mouse Fc immobilised onto both CM5 and RD chip surfaces was completed for affinity characterisation (see section 3.2.5). Briefly, protein G immobilised onto either the CM5 chip or the planar RD chip surface were shown to induce steric hindrance. In addition, steric hindrance was also observed for the CD4 interaction conducted using an anti-mouse Fc-coated RD-chip and for the CM5-chip when a high concentration of anti-mouse Fc was immobilised.

A similar GST saturation experiment was conducted using the three surfaces prepared for the flow rate experiment (*Figure 3.2.6.2*). The average saturation response as a percentage of the ideal (% R_{max}) was greater for the protein A-coated surface (*Table* 3.2.6.2). An average % R_{max} value of 49.3 ± 1.4 % was obtained for the protein A surface and this was lower than the value (54.1 ± 0.7 %) obtained during optimisation of solution phase steady state affinity measurement (section 3.2.5.2). Furthermore, this observation confirmed that anti-GST IgG bound GST monovalently as opposed to bivalently and suggested that steric hindrance of the second binding site, due to the orientation of a bound GST molecule, was occurring. The access radius of a typical antibody is approximately 11 nm and, hence the bound GST molecule must be capable of bridging this distance when bound to the antibody binding site. Experimental evidence implies that monovalent binding occurs irrespective of whether the interaction takes place in homogenous solution phase (Table 3.2.5) or within the hydrogel environment. In addition, both the anti-mouse Fc-coated and protein G-coated surfaces failed to produce a stable plateau during GST saturation experiments. Characteristic saturation curves for the protein A and anti-mouse Fc-coated surfaces are shown in *Figure* 3.2.6.2.

	Anti-GST IgG (RU)	GST (RU)	% R_{max}
Anti-Mouse Fc-Coated (11,800 RU)	354 (4 min) 354 (6 min) 351 (8 min)	106 101 110	45 43 47 **45 ± 1.1**
Protein A-coated (1,975 RU)	421 (4 min) 411 (6 min) 414 (8 min)	137 130 146	49 47 52 **49.3 ± 1.4**
Protein G-coated (327 RU)	316 (4 min) 300 (6 min) 295 (8 min)	97 90 91	46 45 46 **45.6 ± 0.3**

Table 3.2.6.2. Table of binding responses and saturation values for the interaction of GST with affinity-captured anti-GST IgG using three different affinity ligands. A saturating concentration of GST (200 nM in HBS) was injected over each surface at 30 µl/min for 4 min. The surfaces were regenerated and the saturation experiment was repeated for GST injection times of 6 min and 8 min. The interaction curves for the protein A-coated surface reached a stable plateau indicating surface saturation and allowed reliable estimation of R_{max}. The other surfaces failed to reach a plateau and resulted in lower R_{max} values (R_{max} is the ideal saturation response assuming bivalent occupation). The response values were recorded immediately before and after the GST injection pulse. The average % R_{max} values were approximately 4 % lower for the protein G-coated and anti-mouse Fc-coated surfaces than for protein A-coated surface. Non-specific binding of GST (100 nM) was < 1.0 RU.

The protein A-coated surface yielded a curve that reached a satisfactory plateau and the slope (0.0112 RU/sec) at the plateau was 3.8 fold lower than that obtained for the anti-mouse Fc-coated surface (0.0427 RU/sec) over the last 1.25 min of the injection phase. Therefore, bivalent occupation is highly unlikely, because a low degree of hindered bivalent occupation would be observed as an increasing binding response that fails to plateau. As expected the protein A format closely approximated ideal behaviour (*Figure 3.2.6.2*), indicating that the apparently faster dissociation rate for the anti-mouse Fc surface is artifactual. The % R_{max} of 50.3 % and the existence of a plateau confirmed that saturation was reached for the protein A-format. In contrast, the lower % R_{max} of 45.8 % combined with the failure to reach a plateau for the anti-mouse Fc format suggested

that steric hindrance of free antibody binding sites was occurring. Therefore, the faster apparent dissociation rate may be attributed to steric thermodynamic stress imposed on a fraction of bound GST molecules. One might argue that diffusional limitations within the anti-mouse Fc-coated matrix should increase rebinding and thus slow the dissociation rate relative to the protein A format. However, rebinding is highly unlikely as the majority of GST binding sites are occupied at saturation. In addition, viscosity experiments on dextran solutions that mimic the hydrogel showed that high protein concentrations (50 mg/ml BSA (~5,000 RU)) have little effect on viscosity (section 3.2.4). Therefore, the diffusion coefficient within the anti-mouse Fc-matrix may not be significantly different from the protein A-coated surface. Nevertheless, the occupation of a much greater specific volume within the anti-mouse Fc-coated matrix may induce overcrowding (Edwards *et al.*, 1995) and result in steric hindrance of binding sites. Earlier studies (section 3.2.6.1) showed that the apparent dissociation rate increased with increasing flow rate. This is consistent with the proposed model, as the effective mass transfer coefficient will vary with flow rate and hence, change the dissociation profile.

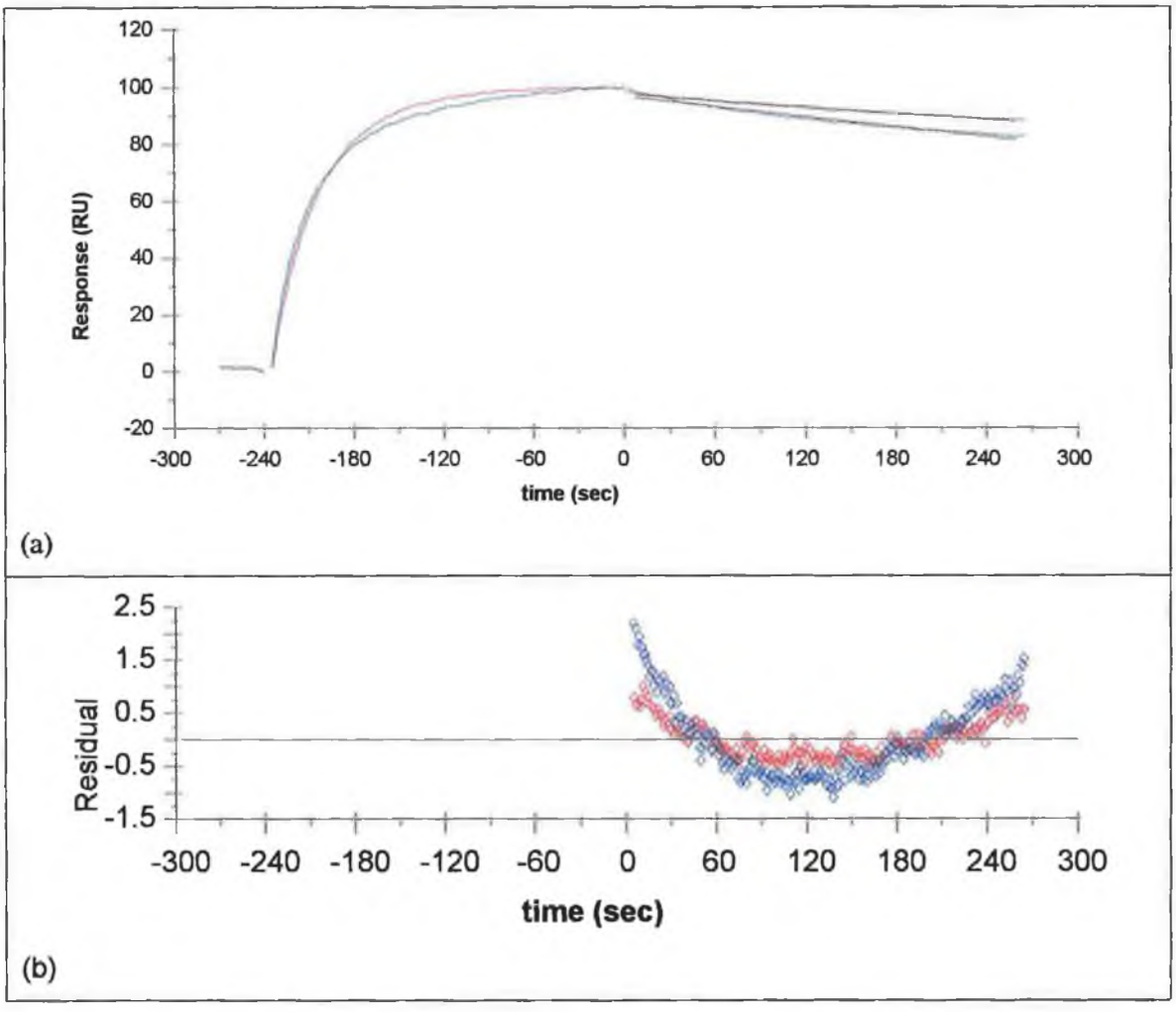

Figure 3.2.6.2. **(a)** Overlay plot for the saturation study conducted on protein A-coated and anti-mouse Fc-coated surfaces. GST (200 nM) was injected at 30 µl/min for 4 min over each surface. After reference curve subtraction, both curves were normalised with respect to each other. The final % R_{max} values for the protein A-coated and anti-mouse Fc-coated surface were 50.3 % and 45.8 %, where the concentrations of anti-GST captured were 414 RU and 357 RU, respectively. Therefore, similar R_{max} values can be assumed. The lower % R_{max} together with the lack of a plateau suggests that steric hindrance is present for the anti-mouse Fc-coated surface. **(b)** A 1:1 pseudo-first-order model was fitted to the dissociation phase of both interaction curves and the residual plot reveals the difference between the actual curves and the fitted curves at each data point.

Figure 3.2.6.3

and

Accompanying Legend

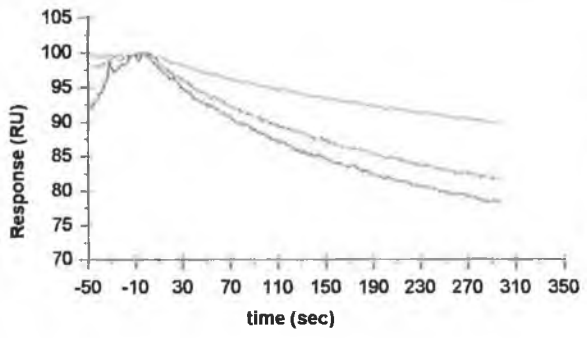

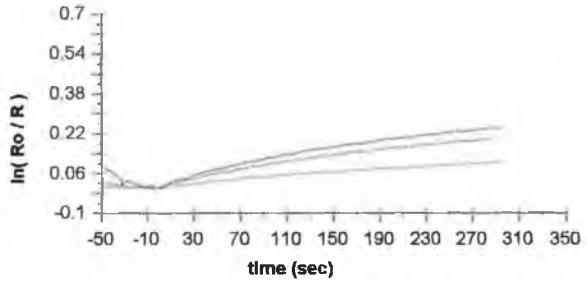

(a) Anti-mouse Fc-coated sensor surface

(GST interaction)

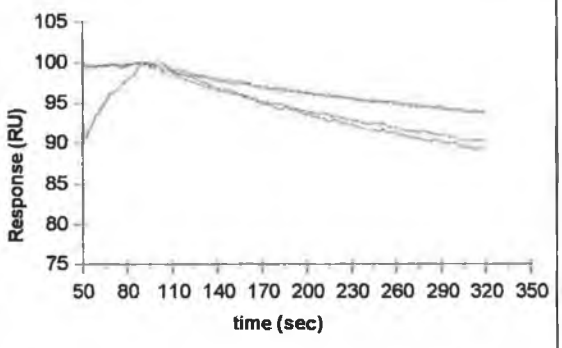

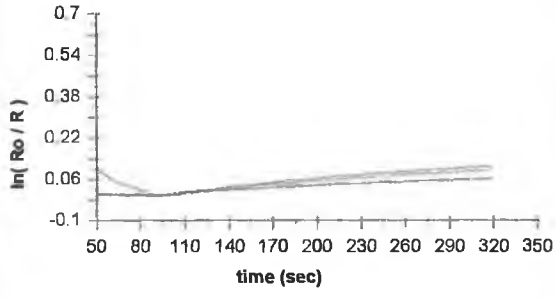

(b) Protein A-coated sensor surface

(GST interaction)

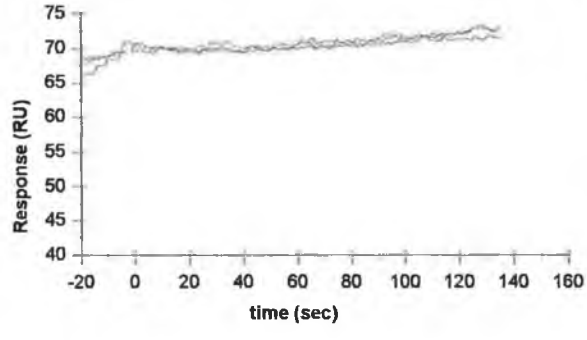

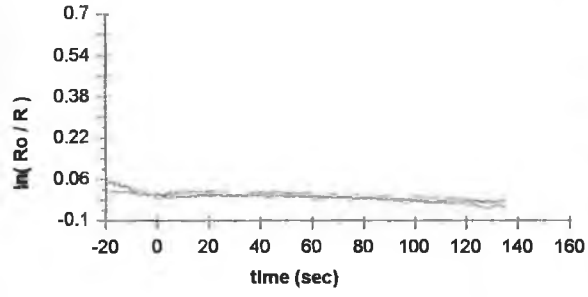

(c) Protein G-coated sensor surface

(GST interaction)

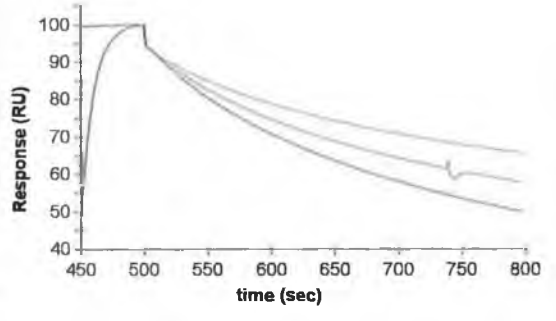

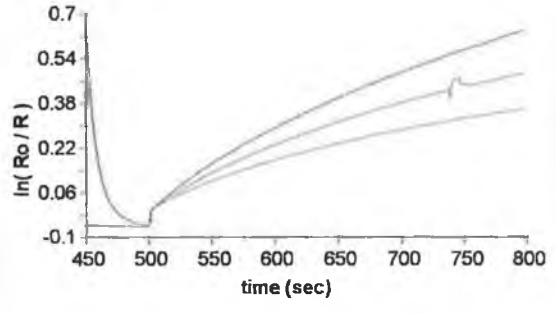

(d) Anti-mouse Fc-coated sensor surface

(CD4 interaction)

3.2.6.3 ***Contact Time-Dependency***. Deviations from 1:1 pseudo-first-order behaviour should be observable as a contact-time dependent variation in the dissociation rate. Overlay plots for model interactions conducted at different contact times are shown in *Figure* 3.2.6.3. At saturation, all available binding sites should be occupied, resulting in a plateau in the association phase interaction curve. Prolonged exposure of the surface to excess antigen should not affect the plateau or the dissociation phase and should result in superimposable dissociation phase curves. Close examination of the dissociation phase curves as a function of analyte contact time revealed marked deviations for the anti-mouse Fc-coated surface. In addition, the dissociation rates for both the GST and CD4 interactions on this surface were much slower after long contact times and was particularly apparent for the CD4 interaction. Furthermore, the derivative plots ($Ln(R_o/R)$ against time) for the dissociation phase of the interaction curves were curvilinear although the degree of the curvature varied with each surface (*Figure* 3.2.6.3). A dramatic divergence in the dissociation phase was observed for the CD4 interaction and may have resulted from 'overcrowding' effects within the hydrogel that were amplified by the high k_d for the interaction. Consider that the protein concentration within the anti-mouse Fc-coated matrix is very high (exceeds 120 mg/ml) and results in 'overcrowding' effects. This condition may be further exaggerated over time by constant rearrangement of the matrix in order to facilitate binding of the analyte to the remaining sterically hindered binding sites. Thus, steric hindrance would increase as a function of time, thereby accounting for the observed contact time-dependent dissociation phase. Although this mechanism is consistent with the experimental results other mechanisms cannot be dismissed.

Karlsson and Fält (1997) employed immobilised polyclonal anti-mouse Fc (4,300 RU) for affinity-capture of anti-myoglobin antibody and interpreted similar myoglobin dissociation phase deviations as evidence for a two-state interaction. Clearly, this is not consistent with the results presented here, since the GST interaction conducted on both the protein G-coated and protein A-coated surfaces did not suffer from this effect. These results emphasise the need to exercise caution when drawing conclusions on the basis of model fitting data alone and highlight the value of repeating kinetic experiments employing different formats. As stated earlier, the faster apparent dissociation rates for the anti-mouse Fc format may be attributed to steric thermodynamic stress imposed on a fraction of bound GST molecules. This mechanism may also account for the extreme contact-time dependency of the CD4 dissociation phase when employing the anti-mouse Fc-coated surface. Consequently, the protein A-coated CM5 sensor chip was found to be the most suitable for kinetic analysis of the GST interaction. In addition, a low surface binding capacity (< 200 RU) and a high flow rate of 30 µl/min were selected in order to ensure that the binding response curve was a function of the reaction flux and not a function of the bulk mass transport coefficient.

3.2.6.4 ***Optimisation of CD4 Interaction Conditions***. Having identified many potential problems, the experimental conditions required for kinetic evaluation of the CD4 interaction were investigated. The results obtained for the CD4 interaction contrast with the GST interaction, since the CD4 interaction is characterised by high kinetic rate constants and requires higher flow rates and lower surface capacities to eliminate MTL. The anti-CD4 IgG_{3b} did not possess adequate affinity for protein A during preliminary experimental optimisation. Therefore, an anti-mouse Fc IgG-coated surface was employed for affinity-capture, despite the sub-optimal performance outlined earlier (*Figure 3.2.6.3*). The saturation response was determined to be 98 % of the expected bivalent response in agreement with earlier studies (*Table 3.2.5*). This value is validated by the presence of a steady plateau for the saturation curve (*Figure* 3.2.6.4(c)). The absence of overcrowding effects for the saturation curve may be due to the low surface concentration of anti-mouse Fc (3,680 RU) and a favourable binding conformation of the immunoglobulin-like CD4 molecules. Interestingly, both CD4 and GST are approximately the same MW (50,000 Da), but exhibit contrasting binding behaviour.

The occupation of both CD4 binding sites highlights the limitations of the GST interaction and suggests that monovalent binding to bivalent antibodies may be more prevalent than one would expect. A maximum flow rate of 100 µl/min was selected for kinetic evaluation of the CD4 interaction since overlaid interaction curves showed that the interaction was significantly influenced by the flow rate at lower values (*Figure* 3.2.6.4(a)). Analysis of the derivative plot (*Figure* 3.2.6.4(b)) for the dissociation phase revealed a slight divergence with increasing flow rate. However, divergence did not occur between the curves at the highest flow rates (90 and 100 µl/min) but the plot remained slightly curvilinear as opposed to an ideal linear relationship. This curvature may result from 'overcrowding' as a high concentration of anti-mouse Fc was immobilised onto this interaction surface. Nevertheless, the results demonstrate that a flow rate of 100 µl/min is required to reduce MTL and that slight deviations may occur due to steric hindrance.

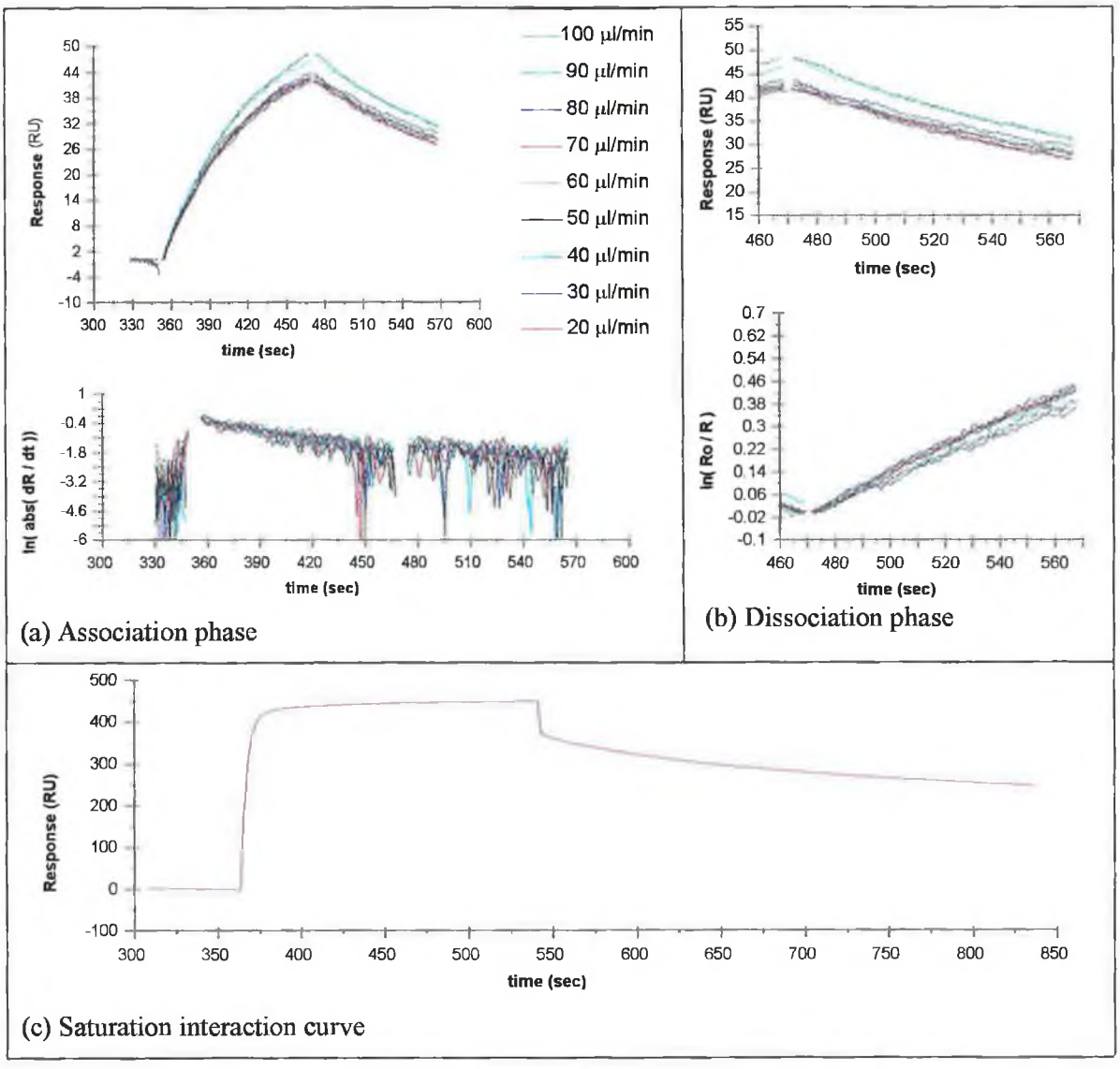

Figure 3.2.6.4. Overlay of binding-progress curves for the interaction of CD4 with affinity-captured anti-CD4 IgG at various flow rates. Anti-mouse Fc was immobilised using conventional amine coupling (~11,000 RU). A 1 min pulse of anti-CD4 IgG (1.75 µg/ml in HBS) was injected at 10 µl/min, giving an average response of 150 RU. A 2 min pulse of CD4 (10 nM in HBS containing 0.3 M NaCl) was injected and was followed by regeneration. This cycle was repeated for increasing CD4 injection flow rates of 20, 30, 40, 50, 60, 70, 80, 90, 100 µl/min as indicated above. A reference curve was subtracted from each working curve to account for baseline drift and bulk refractive index variations. (a) Overlaid binding response curves and derivative plot of ln (abs(dR/dt) (i.e. ln (abs(dR/dt)) against time. (b) Overlay of isolated dissociation phase curves and derivative plot of Ln (dR_0/R) against time. (c) Interaction curve for saturation of the anti-CD4 IgG. Anti-mouse Fc was conventionally immobilised (3,680 RU). Anti-CD4 IgG (10 µg/ml in HBS buffer) and CD4 (500 nM in HBS) were injected consecutively at 10 µl/min for 5 min and gave binding responses of 601 RU and 370 RU, respectively.

3.2.6.5 ***Kinetic Analysis of GST Interaction Employing Protein A Affinity-Capture.*** The GST interaction was kinetically evaluated using the simple 1:1 pseudo-first-order interaction model and a typical analysis is presented in *Figure* 3.2.6.5. BIAevaluation software generates rate equations based on the selected model and parameter values that best fit the experimental data. The 1:1 pseudo-first-order model is defined in terms of two integrated rate equations. The dissociation phase is fitted according to equation 9 and the value of k_d is then used to evaluate the association phase according to equation 4. BIAevaluation 3.0™ software employs the Marquardt-Levenberg curve-fitting algorithm to optimise parameter values by iterating from initial starting values for each parameter until the sum of the squared residuals between the actual curve and calculated curve are minimised. The parameters are defined as constants or variables and can be fitted locally or globally. Global fitting constrains the value to a constant for a set of overlaid interaction curves. The goodness of fit is described by the statistical value χ^2, which is the average squared residual per data point. A perfect fit should give a value close to the mean square of the signal noise (χ^2 of 0.25) but values < 10 are often acceptable. Furthermore, the standard error (SE) quoted for each parameter is an estimate of how sensitive the fitting is to changes in that parameter.

The entire interaction curves were analysed (*Figure* 3.2.6.5) and revealed a moderate association rate constant (average k_a of 2.23×10^5 $M^{-1}s^{-1}$) and a low dissociation rate constant (average k_d of 4.72×10^{-4} s^{-1}) that together result in a high affinity constant (K_a of 4.75×10^8 M^{-1} or K_d of 2.13×10^{-9} M). Nieba *et al.* (1996) found that K_d values determined in solution phase can be as much as 50-fold *higher* (lower apparent affinity) than the K_d determined from kinetic analysis as a result of a combination of rebinding and avidity effects. However, the solution phase K_d (6.83×10^{-10} M) for the GST interaction (section 3.2.5.2) was only 3-fold *lower* than the kinetically determined value. Conformity of the experimental data to the simple model, together with the solution phase equilibrium study, confirmed that 'true' kinetic constants can be determined using biosensor analysis and that the hydrogel biointerface does not invariably cause serious deviations which is in agreement with previous findings (Parsons and Stockley, 1997). Moreover, the study emphasises the dependency of kinetic analysis on the method of antibody capture, thus urging the development of more generally applicable and reliable affinity-capture formats. Ideally, antibodies and other ligands should be reversibly attached to the matrix via a unique functional group (or moiety) that is distant from the binding site. In addition, the technique should not rely on prior immobilisation of bulky proteins that may induce 'overcrowding' and the linkage should be resistant to leaching effects. Such strategies are not widely available, although a few recombinant proteins have been produced that possess an affinity tag (oligohistidine) that can bind to the matrix via a metal chelating linkage (Gershon and Khilko, 1995).

Figure 3.2.6.5

and

Accompanying Legend

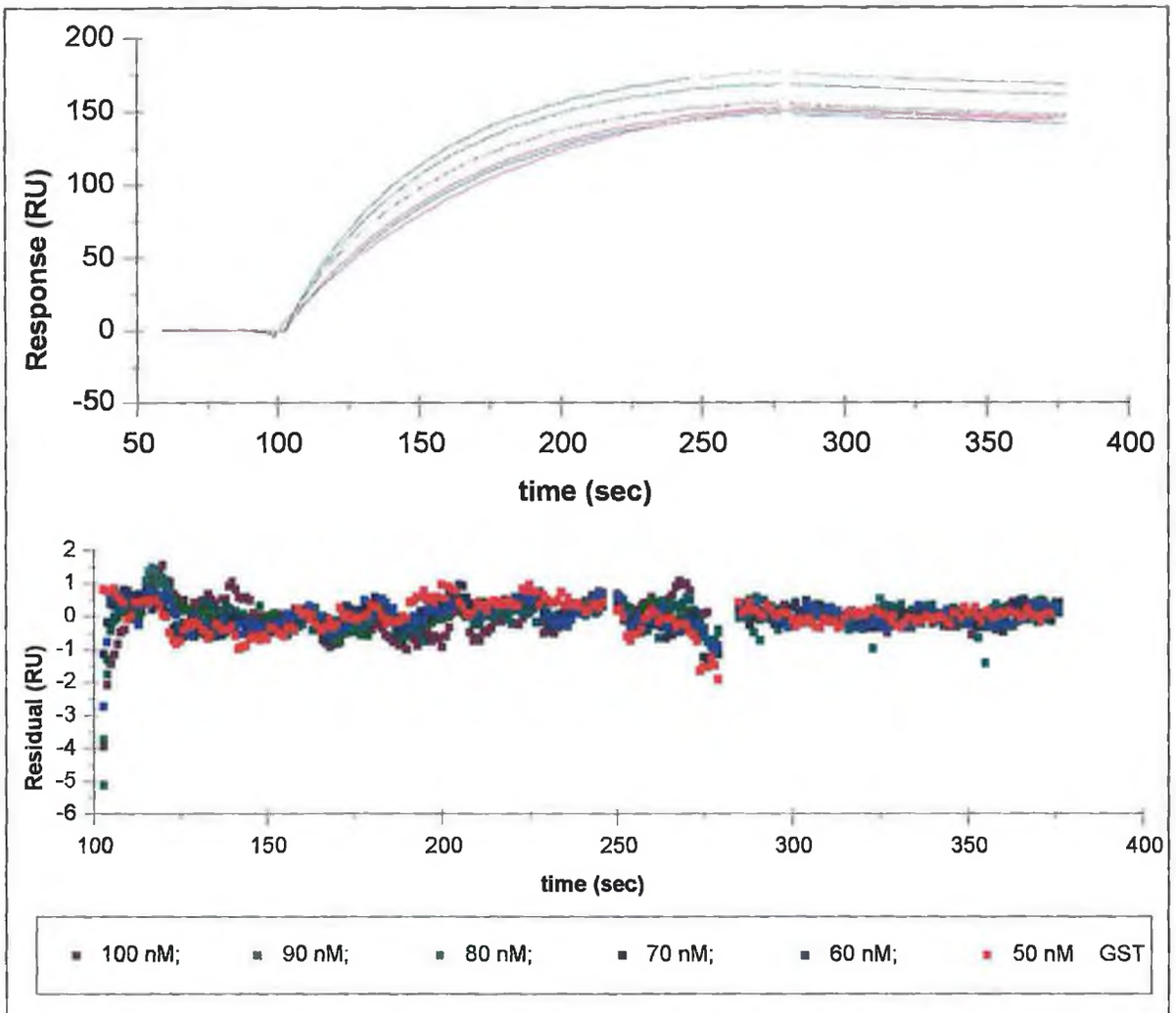

(a) Overlay of binding response curves and corresponding residual plot.

Conc (nM)	k_a (1/Ms)	SE (k_a)	k_d (1/s)	SE (k_d)	R_{max} (RU)	SE (R_{max})	K_a (1/M)	K_d (M)
100	1.95e5	5.06e2	4.62e-4	5.31e-6	182 (*164*)	0.162	4.23e8	2.36e-9
90	2.11e5	5.72e2	4.59e-4	5.54e-6	176 (*162*)	0.161	4.60e8	2.17e-9
80	2.27e5	6.89e2	5.08e-4	6.05e-6	162 (*168*)	0.163	4.47e8	2.24e-9
70	2.15e5	7.39e2	4.78e-4	6.31e-6	165 (*162*)	0.180	4.50e8	2.22e-9
60	2.53e5	8.58e2	4.66e-4	6.13e-6	166 (*167*)	0.178	5.44e8	1.84e-9
50	2.37e5	9.78e2	4.61e-4	6.39e-6	173 (*166*)	0.249	5.14e8	1.95e-9
$\chi^2 = 0.275$								

(b) Table of Results.

3.2.6.6 Analysis of GST Interaction Employing Protein A Affinity-Capture and a RD Sensor Surface. The influence of the hydrogel on the protein A affinity-capture format for kinetic characterisation of the GST interaction was investigated by employing a reduced dextran sensor chip (RD chip). The RD chip was produced and characterised as outlined in section 3.2.4. Protein A was employed as the affinity ligand. The response curves for the GST interaction are shown in *Figure* 3.2.6.6.

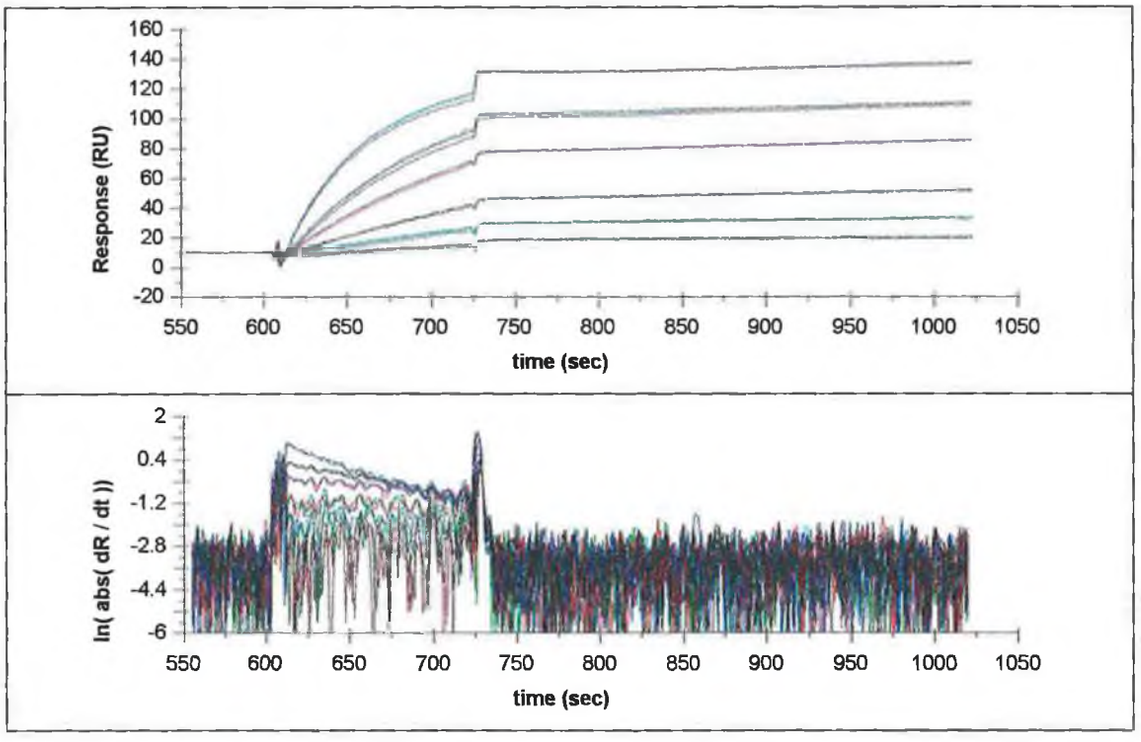

Figure 3.2.6.6. Overlay of interaction curves and derivative plot of ln (abs(dR/dt)) against time. Protein A was immobilised onto an RD chip surface (490 RU) using conventional amine coupling. Monoclonal anti-GST IgG (2.5 μg/ml) was injected over the surface at 10 μl/min for 2 min and was affinity-captured (~ 410 RU) by the immobilised protein A. The baseline was allowed to stabilise for 5 min before injecting GST for 2 min at 30 μl/min. A reference curve was obtained by replacing the GST sample with running buffer (HBS buffer). Reference curves were subtracted from the working curves in order to eliminate the contribution of dissociating antibody. The analysis was conducted in triplicate. The association curves displayed above increase with respect to concentrations of 3.12 nM, 6.25 nM, 12.5 nM, 25 nM, 50 nM, 100 nM GST in HBS buffer.

The protein A-coated RD surface did not perform as expected as can be observed from the positive dissociation rates after termination of the sample injection. This behaviour was also observed for the GST interaction using a protein G-coated RD chip (*Figure* 3.2.6.1), but was absent for the CD4 interaction on both CM5 and RD chip surfaces (results not shown). Therefore, the deviations are particular to the GST interaction and probably result from GST-GST self-association when at very

high local densities at the reduced dextran surface (thin layer). Self-association of GST would increase the protein concentration within the most sensitive region of the evanescent field through cross-linking of available dextran chains, thus accounting for the positive dissociation rates. The derivative plot (*Figure* 3.2.6.6) indicated that the association phase of the sensorgram did conform to 1:1 pseudo-first-order behaviour and was analysed assuming a k_d value of 4.72 x 10^{-4} s^{-1} (from *Figure* 3.2.6.5). The fit yielded a χ^2 value of 0.097, residual values of ± 0.6 RU and a k_a of 1.9 x 10^5 m^{-1} s^{-1}. This k_a value is 15 % lower than the value obtained for the same analysis employing the CM5 chip and suggests that the lower mobility of captured anti-CD4 IgG at the RD chip surface is responsible. Changes in the mobility (i.e. diffusion coefficient) of the captured antibody will effect the collision frequency for the reaction, and cause a proportionate change in the reaction rate. In principle, knowledge of the diffusion coefficient within the reaction environment may allow estimation of kinetic rates in homogenous solution phase from rate constants determined within hydrogel layers. Furthermore, it was demonstrated (section 3.2.5) that the RD chip surface results in steric hindrance of the interaction. Consequently, a hydrogel biointerface constructed using a short chain (~ 70 kDa) dextran at a low surface concentration (~ 5 mg/ml) may be a suitable compromise between the extended CM5-hydrogel and the planar interaction surface.

3.2.6.7 ***Kinetic Analysis of the GST Interaction Employing Anti-Mouse Fc Affinity-Capture.***
The analysis was conducted similarly to the previous experiments (*Figure* 3.2.6.6). A moderate association rate constant (k_a of 2.37 x 10^5 $M^{-1}s^{-1}$) and a low dissociation rate constant (k_d of 4.03 x 10^{-4} s^{-1}) resulted in a high affinity constant (K_a of (5.97 x 10^8 M^{-1} or K_d of (1.68 x 10^{-9} M). These values are very similar to those determined for the protein A-CM5 chip surface (*Figure* 3.2.6.5), giving a 6 % higher k_a and an 18 % lower k_d. The lower k_d value is consistent with deviations observed during the flow rate (section 3.2.6.1) and saturation experiments (section 3.2.6.2). The residual plot (*Figure* 3.2.6.7(a)) shows obvious deviations from the ideal 1:1 pseudo-first-order interaction model but the magnitude of the residuals was low (± 2 RU). The low residuals combined with a low χ^2 value of 0.646 indicated a good fit. The result table (*Figure* 3.2.6.7(b)) shows that R_{max} decreased by 7 % while k_a increased with decreasing GST concentrations. The experimentally calculated R_{max} values also show a decreasing trend of ~ 4 % but, more significantly, are almost 30 % higher. The discrepancy between the calculated and experimentally expected R_{max} values may be related to 'overcrowding' effects. However, despite the observed deviations from ideal behaviour, the kinetic constants determined from this analysis approximated those determined for the 'ideal' analysis employing the protein A-coated CM5 sensor chip (*Figure* 3.2.6.5). The agreement between both analyses may be attributed to the low kinetic rates characterising the GST interaction as non-ideal behaviour (MTL effects) is exaggerated by faster kinetic rates (*Figure* 3.2.6.3(d)).

Figure 3.2.6.7

and

Accompanying Legend

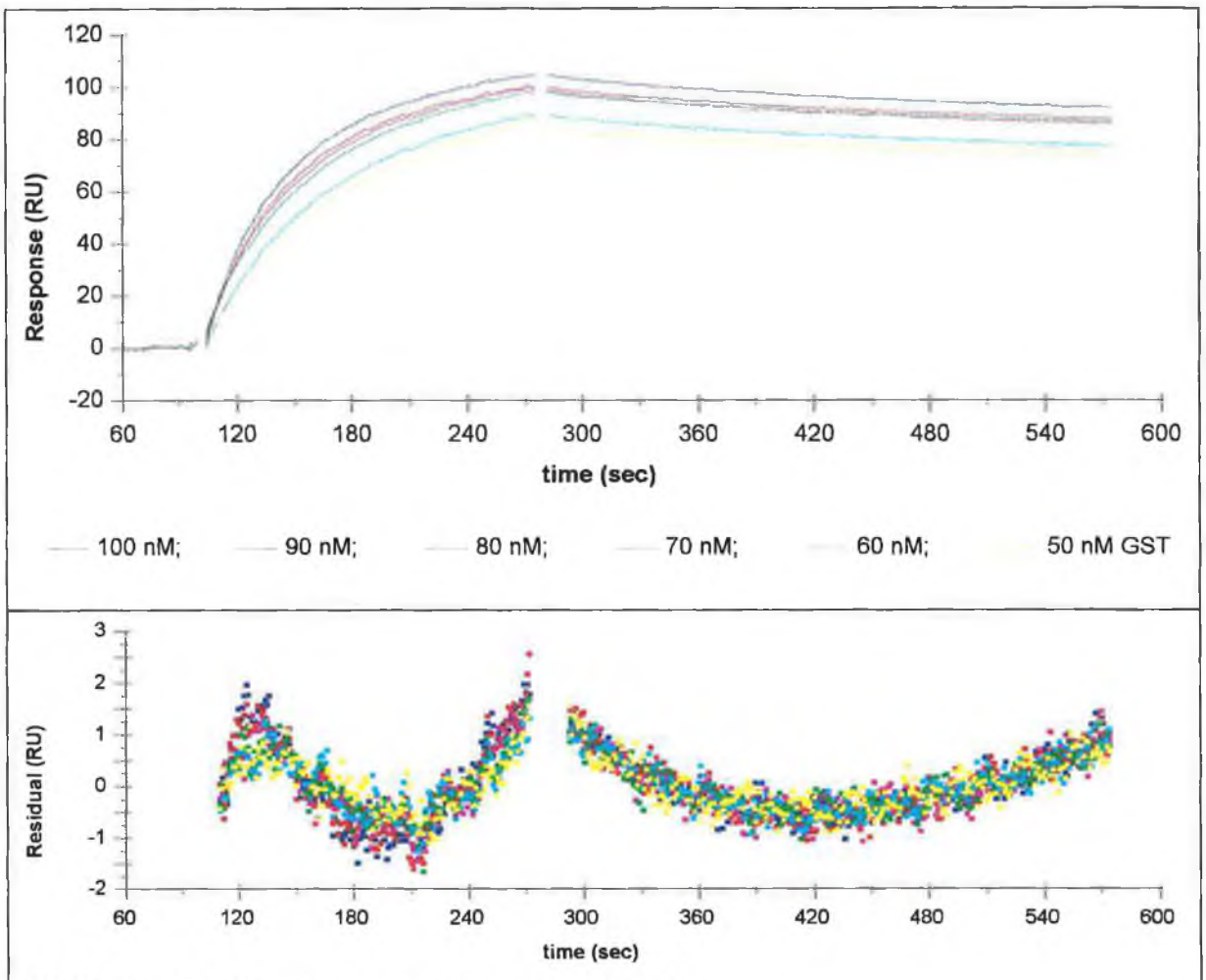

(a) Overlay of binding response curves and residual plot.

Conc (nM)	k_a (1/Ms)	SE (k_a)	k_d (1/s)	SE (k_d)	R_{max} (RU)	SE (R_{max})	K_a (1/M)	K_d (M)
100	2.16e5	1.53e3	3.88e-4	3.91e-6	100 *(145)*	5.89	5.62e8	1.78e-9
90	2.3e5	1.72e3	4.02e-4	4.26e-6	97 *(144)*	4.92	5.78e8	1.73e-9
80	2.3e5	1.89e3	4.29e-4	4.36e-6	96 *(143)*	7.86	5.42e8	1.85e-9
70	2.39e5	2.13e3	3.83e-4	4.28e-6	95 *(143)*	8.46	6.32e8	1.58e-9
60	2.49e5	2.46e3	4.14e-4	4.50e-6	94 *(128)*	2.52	6.08e8	1.64e-9
50	2.6e5	2.98e3	4.00e-4	4.99e-6	93 *(126)*	3.60	6.59e8	1.52e-9
$\chi^2 = 0.646$								

(b) Table of Results

3.2.6.8 ***Kinetic Analysis of CD4 Interaction Employing Anti-Mouse Fc Affinity-Capture.*** The CD4 interaction is characterised by high kinetic association and dissociation rates (*Figure* 3.2.6.3(d)) and, hence, requires an extremely high flow rate (100 µl/min) and a low surface capacity (R_{max} of > 80 RU) to eliminate MTL. The final concentration of protein within the hydrogel was reduced, by immobilising a low concentration of anti-mouse Fc-IgG (3,280 RU) in order to prevent 'overcrowding' effects, as observed with the GST interaction (*Figure* 3.2.6.2(d)). These experimental conditions were sufficient to reduce deviations from the simple 1:1 pseudo-first-order interaction model, as can be observed from the residual plots for the analysis (*Figure* 3.2.6.8(a) and (b)). The data appears 'noisy' in comparison to earlier analyses, since the data collection rate was increased 10-fold (10 points/sec) in order to increase the reliability of the data over a shortened injection period. The R_{max} values calculated from the fitting agree well with those expected from the experimentally calculated values (Italics). A χ^2 value of 0.53 confirms a good fit of the calculated and experimental curves. Furthermore, the standard errors for the k_a, k_d and R_{max} were low indicating that the fitting was robust and, hence, the kinetic rates were reliable.

Simultaneous fitting to the association and dissociation phases resulted in a slight increase in the residuals compared with separate fitting. Consequently, the results (*Figure* 3.2.6.8 (c)) are quoted for separate fitting though the kinetic parameters were almost identical (e.g. < 5 % variation in average k_a) for both analyses. The increase in fitting error for simultaneous fitting resulted from slight variations in the alignment of the injection 'start' and 'stop' points for the curve set. Despite low residual values, the k_a increased with decreasing CD4 concentration and hence, indicates steric hindrance effects. The misleading goodness of fit (χ^2 of 0.53) is a consequence of fitting parameters locally as opposed to more stringent global fitting, but it facilitates the identification of systemic deviations. A rapid association rate constant (average k_a of 1.24 x 10^6 M^{-1} s^{-1}) and a high dissociation rate constant (average k_d of 4.25 x 10^{-3} s^{-1}) resulted in a moderate affinity constant (K_a of 2.98 x 10^8 M^{-1}) for the CD4 interaction. However, the ka values obtained for the individual curves varied by 50 % and may be attributed to steric hindrance effects and the instability of the flow rate at the maximum rate (i.e. 100 µl/min). However, the affinity constant was similar to that determined by boundary layer equilibrium analysis (K_a of 3.04 x 10^8 M^{-1}) (section 3.2.5.1). The agreement of the values for the affinity constant determined by both methods further validates kinetic constants determined by 'real-time' interaction analysis. Interestingly, the GST and CD4 interactions exhibit contrasting kinetic behaviour but share a similar affinity constant (K_a for GST interaction was 4.75 x 10^8 M^{-1}). This valuable information allows prediction of the behaviour of these reagents when applied to diagnostic or therapeutic applications, thus reducing time-consuming and expensive optimisation procedures.

The kinetic analysis presented thus far has clearly shown that the design of a successful kinetic experiment is not a trivial matter as it requires detailed exploratory experiments in order to optimise experimental conditions. In addition, deviations may still occur despite rigorous investigation but do not necessarily invalidate the analysis. These experimental considerations include the immobilisation strategy, surface regeneration, flow rate, surface binding capacity, analyte concentration range and elimination of non-specific binding. However, there exists an upper limit to the association rate that can be reliably determined using this technology. This upper limit is dictated by MTL and is dependent on the limitations of instrument performance (i.e. sensitivity and flow rate range) and the physical characteristics of the analyte (i.e. diffusion coefficient, MW and morphology). The bulk mass transport coefficient (*Lm*) describes the flux of the analyte to the interaction surface and is dependent on the physical characteristics of the analyte, the geometry of the flow cell and the flow rate (equation 11). In order to obtain reliable kinetic constants *Lm* must significantly (5 to10-fold) exceed the reaction flux (*Lr*).

Figure 3.2.6.8

and

Accompanying Legend

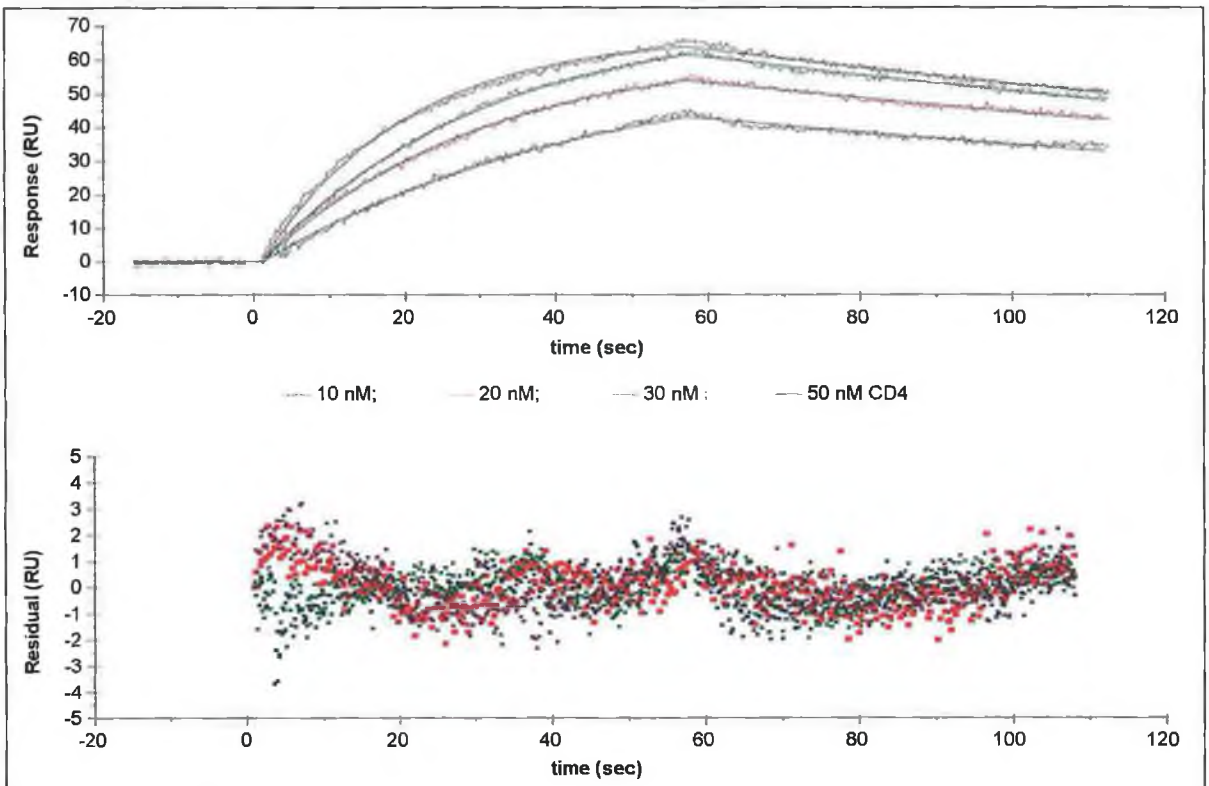

(a) Overlaid binding curves and corresponding residuals for simultaneous fitting of k_a and k_d.

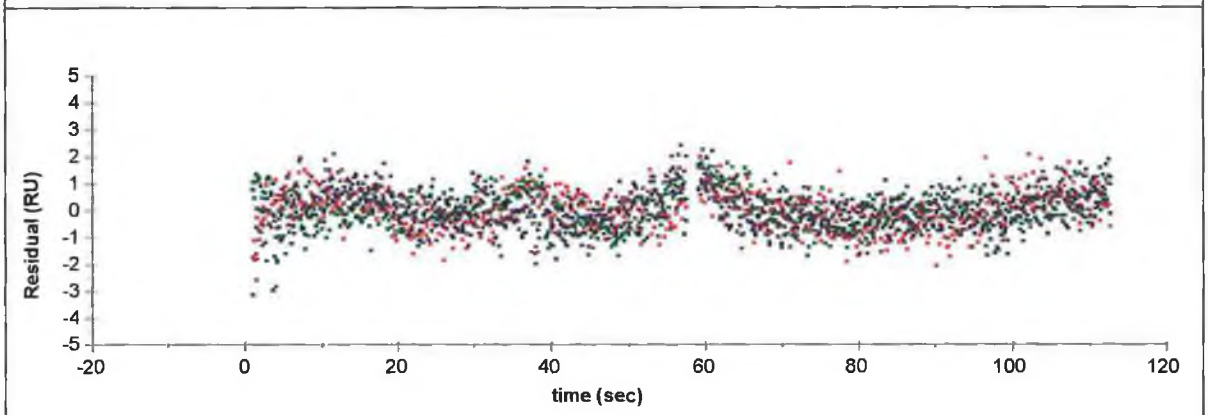

(b) Residual plot for separated fitting of k_a and k_d.

Conc (nM)	k_a (1/Ms)	SE (k_a)	k_d (1/s)	SE (k_d)	R_{max} (RU)	SE (R_{max})	K_a (1/M)	K_d (M)
10 nM	1.76e6	3.39e4	4.04e-3	5.51e-5	77 *(77)*	0.87	4.42e8	2.26e-9
20 nM	1.31e6	1.51e4	4.26e-3	4.43e-5	74 *(76)*	0.39	3.09e8	3.24e-9
30 nM	1.05e6	8.73e3	4.24e-3	3.90e-5	82 *(77)*	0.27	2.47e8	4.05e-9
50 nM	8.61e5	5.88e3	4.47e-3	3.81e-5	72 (80)	0.16	1.93e8	5.19e-9
$\chi^2 = 0.530$								

(c) Table of results for separate fitting of k_a and k_d

3.2.6.9 ***Analysis of Mass Transport Limited Interaction Curves.*** The analysis of fast interactions where MTL cannot be reduced to negligible levels relies on the incorporation of MTL correction components. The MTL model accounts for the changing analyte gradient at the surface by introducing a second exponential expression into the analysis. This model simultaneously fits the k_a and k_d to a set of interaction curves according to numerical integration (Morton *et al.*, 1995) of the following rate equations. The rate equations are presented using the notation employed in BIAevaluation software. The rate of change of the analyte concentration at the surface is described by the differential equation:

$$\frac{dA}{dt} = k_t\,(Conc - A) - (k_a * A * B - k_d * AB) \qquad (23)$$

where:

A	=	Concentration of analyte at the surface.
k_t	=	Mass transfer constant.
$Conc$	=	Concentration of analyte in solution.
B	=	Concentration of binding sites.
AB	=	Concentration of complex.

Assuming a 1:1 interaction:

$$B_{[time = 0]} = R_{max}$$

then

$$\frac{dB}{dt} = -(k_a * A * B) - k_d * AB \qquad (24)$$

Given initial condition $AB_{[time = 0]} = 0$

then

$$\frac{dAB}{dt} = (k_a * A * B - k_d * AB) \qquad (25)$$

MTL binding data were generated for the interaction of CD4 with affinity-captured anti-CD4 IgG by reducing the flow rate to 30 µl/min and increasing the surface capacity to ~ 250 RU. However, the concentration of anti-mouse Fc immobilised to the matrix was minimised (3,400 RU) to limit steric hindrance effects. Initially the simple 1:1 pseudo-first-order interaction model without the MTL correction component was fitted to the set of interaction curves. The overlaid curves and the residual plot are shown in *Figure* 3.2.6.9. As expected, the residual plot for this analysis demonstrates patterned deviations from the calculated curves due to MTL. In addition, the value of k_a determined from this analysis was 3-fold lower than the 'true' value.

Figure 3.2.6.9

and

Accompanying Legend

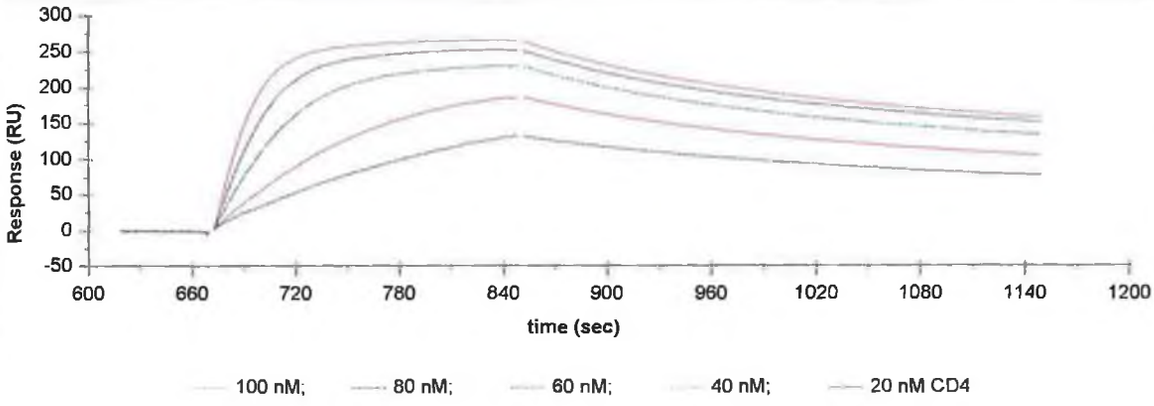

(a) Overlaid sensorgrams

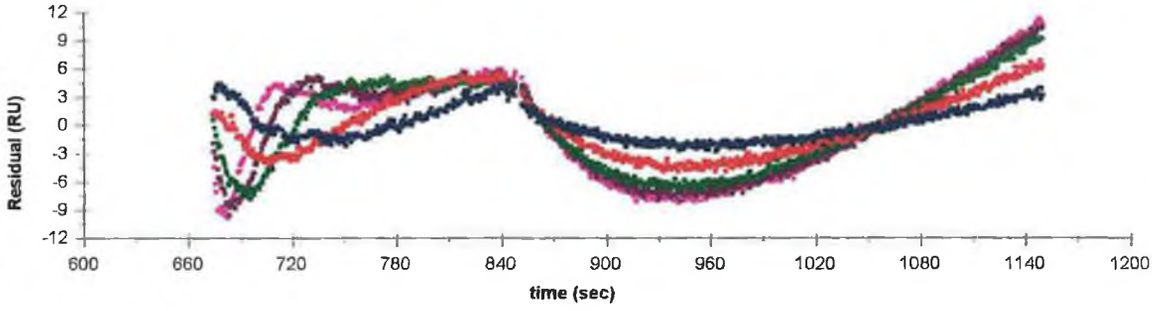

(b) Without compensation for MTL (k_a, k_d and R_{max} fit locally)

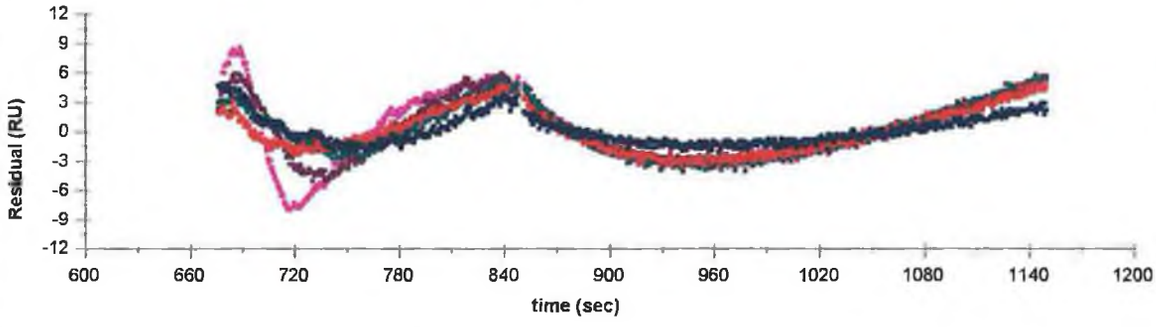

(c) With compensation for MTL (k_a, k_d and R_{max} fit locally)

Conc (nM)	k_a (1/Ms)	SE (k_a)	k_d (1/s)	SE (k_d)	R_{max} (RU)	SE (R_{max})	K_a (1/M)	K_d (M)
100	2.04e5	7.48e3	2.65e-3	1.02e-5	267 *(370)*	0.11	3.91e8	2.56e-9
80	8.86e5	5.52e3	2.49e-3	8.28e-6	255 *(356)*	0.13	3.56e8	2.81e-9
60	7.38e5	4.02e3	2.55e-3	7.83e-6	238 *(341)*	0.17	2.90e8	3.45e-9
40	4.55e5	2.69e3	2.59e-3	8.66e-6	222 *(381)*	0.474	1.76e8	5.68e-9
20	6.52e5	7.13e3	2.66e-3	1.43e-5	183 *(378)*	1.02	2.46e8	4.07e-9
$\chi^2 = 7.04$								

(d) Table of Results

The MTL model described above was fitted to the MTL interaction curves and this yielded the residual plots and results table shown in *Figure* 3.2.6.9. Application of the mass transfer model resulted in lower residuals with a patterned deviation and the resulting average k_a value represents 40 % of the actual value (1.24 x 10^6 $M^{-1}s^{-1}$). The k_d was found to be approximately 40 % higher due to rebinding of dissociating analyte. However, the R_{max} values did not correspond with the experimentally expected values and wide deviations in the other parameters were apparent with the exception of the k_d values, thus invalidating the kinetic constants obtained. The use of this model improved the apparent correspondence of the derived rate constants with the 'true' rate constants but did not give a complete description of the MTL interaction curves.

3.2.6.10 ***Analyte Saturation Front.*** The residual plots for the MTL CD4 interaction indicated that an inward moving saturation boundary may be present during the course of the interaction. The existence of an analyte saturation front was speculated (Schuck, 1996) in an attempt to account for increasing binding rates of interaction curves. It was proposed that, under MTL conditions, the analyte flux from the bulk would cause the outer region of the matrix to be saturated initially and the saturation front would move inwards as the interaction progressed. This effect would cause an apparent increase in the binding rate due to higher evanescent field strength closer to the surface. The form of the association phase curve would be dependent on the velocity of the analyte saturation front and the decay constant of the evanescent field. A slight ascent in the dissociation phase would be expected from redistribution of the analyte front within the matrix, immediately after a non-saturating injection of analyte.

Consequently, a further experiment was conducted where the CD4 interaction was studied under MTL in order to visualise this effect. The overlaid interaction curves were collected for the interaction of CD4 with affinity-captured CD4 at increasing flow rates (3.2.6.10(a)). As expected, an increasing binding rate (sigmoidal curve) was observed during the early association phase of the interaction. However, visual inspection of the curves and the derivative plot (3.2.6.10(b)) revealed that the increasing binding rate was less pronounced at low flow rates. In addition, a positive dissociation phase slope was found for the lower flow rates (*Figure* 3.2.6.10(c)). However, the high k_d (4.24 x 10^{-3} s^{-1}) combined with rebinding effects may mask the true upward drift of the baseline, which results from redistribution of the analyte saturation front. This evidence suggests that an inward moving saturation front was present and was exaggerated at high flow rates. High flow rates increase the bulk mass transfer rate, thus causing a proportional increase in the mass transfer rate within the hydrogel and, hence, an increase in the velocity of the inward moving front. This may result in more acute deviations of the interaction curves as observed in *Figure* 3.2.6.10(a). In

conclusion, an apparent co-operativity was not observed for the CD4 interaction under kinetic rate-limiting conditions and this implies that the positive binding rate is an artefact, resulting from diffusional limitations and not a co-operative binding mechanism as suggested by other investigators (Fisher and Fivash, 1994).

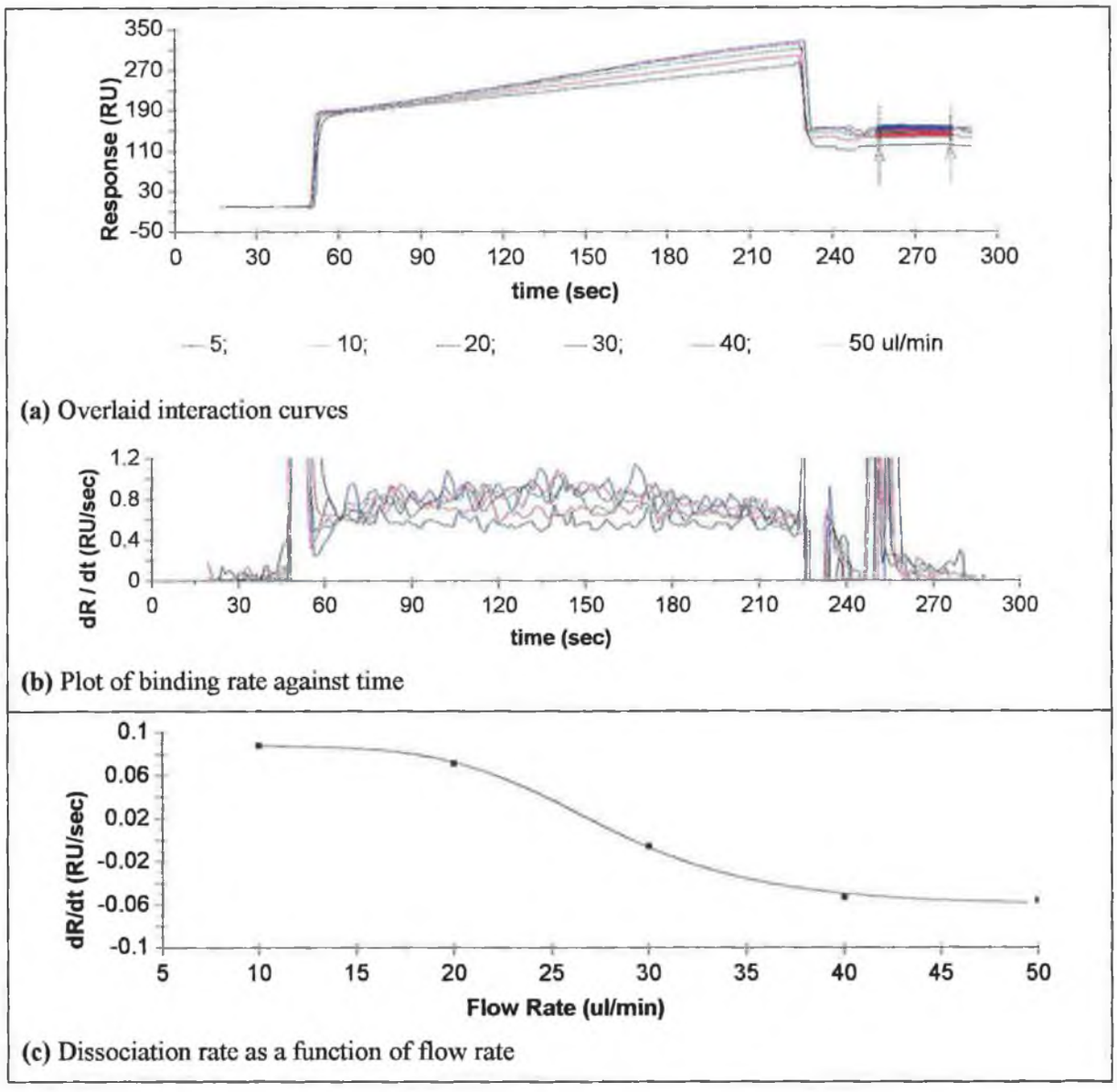

Figure 3.2.6.10. Interaction of CD4 with affinity-captured anti-CD4 IgG under MTL conditions. Anti-mouse Fc was immobilised (11,270 RU) onto a CM5 sensor chip surface and anti-CD4 IgG (16 μg/ml) was injected over the surface for 2 min at 10 μl/min, giving an average response of 985 RU (corresponding to a surface capacity of 625 RU). CD4 (20 nM in HBS buffer containing 0.3 M NaCl) was injected over the surface for 3 min. This cycle was repeated for different CD4 injection flow rates (colour coded in units of μg/ml). (a) Overlaid sensorgrams for the interaction. (b) Derivative plot of the binding rate against time. (c) Plot of the dissociation phase slope (evaluated for the data selection given by the *'heavy line'* in (a)) against the CD4 injection flow rate.

3.2.6.11 The Phenomenological Two-Compartment Model. The observed deviations for the MTL interaction curves shown in *Figure* 3.2.6.9 are due to bulk diffusional limitations and hindered diffusion within the matrix. However, these processes are extremely difficult to accurately model, as evidenced by the failure of the MTL model to describe the interaction curves. For an ideal interaction, a plot of the observed rate constant (k_{obs}) against the analyte concentration should give a straight line with a slope equal to the k_a and the k_d given by the intercept. However, Hall *et al.* (1996) showed that if the analyte concentration at the surface is not equal to the bulk analyte concentration the concentration dependence of k_{obs} becomes curvilinear (*Figure* 3.2.6.11). Computer simulations developed by Schuck and Minton (1996) showed that such plots are sometimes almost linear even in the presence of high MTL. In addition, a two-compartment phenomenological description of the transport process was employed for the derivation of expressions that approximate the 'true' kinetic rates without analysing the transport process. The transport process was highly simplified and described mass transport from the bulk to the sensor surface, as opposed to the diffusion/reaction model (see section 3.1.5). The expressions provide approximate rate constants that depend on the 'true' rate constants, the effective transport rate and the concentration of free surface binding sites (see Schuck and Minton, 1996, for a detailed description of the derivation). The corrected observed rate constant can be described as a function of the analyte concentration (A) according to the expression:

$$k_{obs(A)} = \frac{k_a(A + K_d)}{1 + \frac{k_a R_{max}}{k_t^*}\left(1 + \frac{A}{K_d}\right)^{-1}} \qquad (26)$$

where k_{obs} = Observed rate constant.

k_t^* = Effective transport rate constant.

Other symbols have their usual meaning.

The affinity constant for the CD4 interaction is known to be 3.3 x 10^{-9} M (reciprocal of K_a) from steady state analysis (section 3.2.5.1) and the R_{max} value can be estimated from the average concentration of antibody captured for each interaction curve. Substitution of these values into the above expression allowed accurate estimation of k_a from a plot of k_{obs} against the CD4 concentration without knowledge of the k_d. Furthermore, the k_d can be calculated from the product of the approximated k_a multiplied by the equilibrium K_d. Hence, the k_d can be estimated while avoiding the interpretation of heterogeneous dissociation phases. The observed rate constants for the interaction curves were estimated independently of the dissociation phase by fitting the following integrated rate equation (integrated form of equation 7) to the association phase of the data:

$$R_t = R_{eq} * (1 - exp(-k_{obs}*(t-t_0))) \qquad (27)$$

The observed rates were plotted against the CD4 concentration and two fitting models were applied (*Figure 3.2.6.11*). *Figure 3.2.6.11(a)* shows a relatively linear relationship with respect to high CD4 concentration values but tails off rapidly at the lower CD4 concentration. In addition, the curve implies that the deviation between the 'true' k_a and the apparent k_a increases for lower analyte concentrations. Clearly, if the lowest concentration had been omitted a seemingly ideal linear relationship would be observed. However, a linear fit to this plot (*Figure 3.2.6.11(a)*) gave a 2-fold underestimation (5.84 x 10^5 M^{-1} s^{-1}) of the 'true' k_a. Hence, the two-compartment model was fitted to the data set (*Figure* 3.2.6.11(b)) giving an apparent k_a of 1.0 x 10^6 M^{-1} s^{-1}, which is a good approximation of the 'true' k_a (1.24 x 10^6 $M^{-1}s^{-1}$). Schuck and Minton (1996) demonstrated that the two-compartment model does not provide a good approximation for exclusively MTL data, as the resulting plot of k_{obs} against the analyte concentration will be linear thereby limiting the applicability of the two-compartment model to partially MTL data. However, the analysis extends the range of reaction rates that can be determined by 'real-time' biomolecular interaction analysis by one or two orders of magnitude. Consequently, kinetic characterisation of fast interactions (k_a of > 1 x 10^7 $M^{-1}s^{-1}$) that were previously outside the range of this technology (Hall *et al.*, 1996) may be possible.

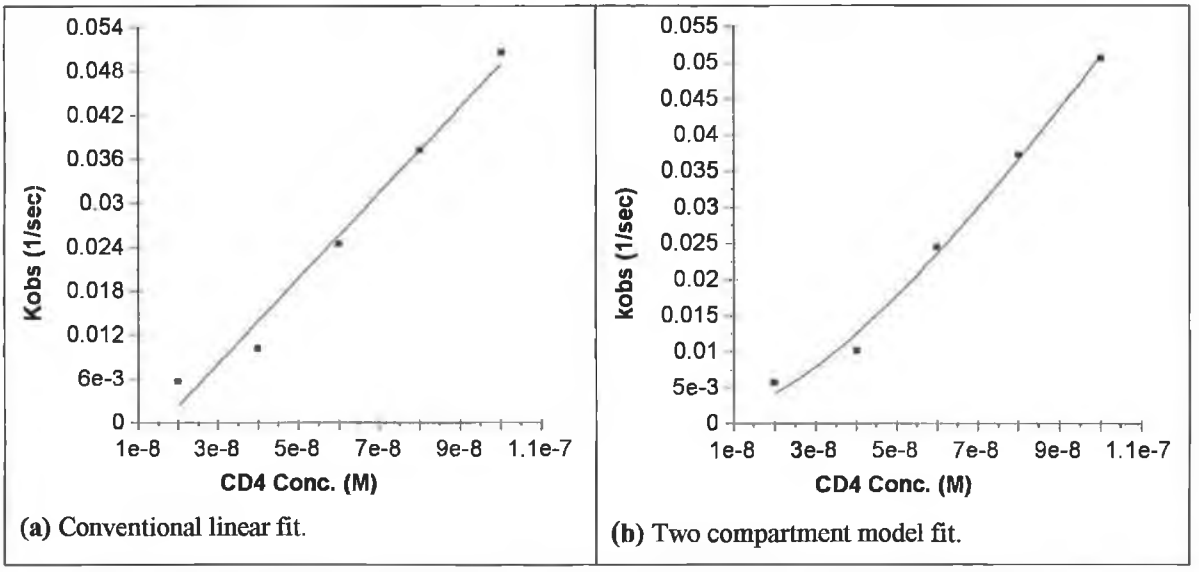

(a) Conventional linear fit.

(b) Two compartment model fit.

Figure 3.2.6.11. Model Fitting. The observed rate constants (k_{obs}) were determined by fitting equation 27 to the association phase of the interaction curves in *Figure* 3.2.6.9 and were plotted against the CD4 concentration. (a) A conventional linear fit was applied to the data giving a k_a (i.e. slope) of 5.84 x 10^5 M^{-1} s^{-1}. (b) The two-compartment model for the association rate (equation 26) was compiled and fitted using BIAevaluation software. The R_{max} was experimentally determined to be 260 RU and the K_d was previously determined from steady state analysis (section 3.2.5.1) to be 3.3 nM. Hence, both parameters were fitted as constant values. The analysis revealed an approximate k_a of 1.0 x 10^6 $M^{-1}s^{-1}$.

3.3 Conclusions.

This investigation focused on the investigation of experimental methods and data analysis techniques for the attainment of valid kinetic constants. The determination of the active concentration of reagents intended for kinetic analysis improves the reliability of rate constants. However, the active anti-CD4 antibody concentration could not be determined as immobilised CD4 was unstable when exposed to typical regeneration conditions. However, determination of the total anti-CD4 antibody concentration was successfully completed using three methods that correlated well. The universal standard curve and flow rate methods employed immobilised protein G, and protein A affinity chromatography was used to validate both of these techniques. For the above methods the average anti-CD4 IgG concentration contained in the hybridoma supernatant was found to be 19.74 ± 0.03 μg/ml, 19.8 ± 0.94 μg/ml and 21.6 μg/ml (assuming A_{280nm} (1 mg/ml) of 1.4), respectively. Hence, the concentration of biomolecules can be obtained within crude matrices without the requirement for a standard curve.

The design of a successful kinetic experiment is not a trivial matter, requiring detailed exploratory experiments in order to optimise experimental conditions. Kinetic analysis of both the GST interaction and the CD4 interaction was carried out using affinity-capture of the IgG, thus avoiding surface heterogeneity. Moreover, the interaction of soluble antigen with an immobilised antibody was considered as a monovalent binding system and was described by the 1:1 pseudo-first-order interaction model. However, the choice of affinity-capture ligand has a significant effect on kinetic analysis. Protein G affinity-capture anchored the antibody via the Fab arm, close to the antigen-binding site, and induced 40 % steric hindrance. In addition, high concentrations of protein at the surface produced a similar effect, causing 14 % steric hindrance. Reduced access to binding sites due to overcrowding may account for this observation. A reduction (66 %) in the concentration of dextran within the hydrogel resulted in ~ 30 % steric hindrance for a previously unhindered interaction. It is probable that the hydrogel layer is very thin and that the proximity of the interacting molecules to the surface results in poor orientation of a sub-population of the CD4 binding sites. In addition, the reduced dextran surface may have restricted the mobility of captured anti-GST IgG, thus accounting for a 15 % lower k_a compared with the extended hydrogel environment. In principle, knowledge of the diffusion coefficient of the interactants within a given reaction environment may be used to predict the rate constant from rate constants determined within the hydrogel.

The steady state affinity constant was found for both the CD4 interaction and the GST interaction. Steady state analysis of the CD4 interaction within the hydrogel environment revealed that

equilibrium is reached after 20 min, indicating a fast reaction rate. A BIACORE quantitative assay was employed for solution phase equilibrium analysis of the GST-anti-GST antibody interaction. The assay allowed rapid determination of the free anti-GST antibody concentration contained in equilibrated reaction mixtures and avoided perturbation of equilibrium. A bivalent solution phase affinity model proved inappropriate, completely misfitting the experimental data. Furthermore, saturation experiments confirmed that anti-GST IgG binds GST monovalently as opposed to bivalently. Therefore, monovalent binding was observed irrespective of whether the interaction occurred in homogenous solution phase or within the hydrogel environment.

Protein A affinity-capture yielded kinetic data that closely approximated ideal behaviour for the GST interaction indicating that directed immobilisation via the Fc region is a suitable immobilisation strategy. Despite having similar affinity constants, the CD4 interaction contrasted with the GST interaction. It was characterised by higher kinetic rate constants and required a higher flow rate (100 µl/min) and a lower surface (< 80 RU) capacity to eliminate MTL. The GST interaction was described by a moderate association rate constant and a low dissociation rate constant and, hence, yielded a high affinity constant (K_d of 2.13 x 10^{-9} M). In addition, the steady state solution phase K_d (6.83 x 10^{-10} M) for the GST interaction was only 3-fold *lower* than the kinetically determined value. Furthermore, the affinity constant for the CD4 interaction, as determined from kinetic analysis was almost identical to that determined by boundary layer equilibrium analysis. Affinity constants determined at steady state are very sensitive to small changes in the kinetic constants since such changes have a large effect on the calculated affinity constant. Hence, the agreement of the kinetically determined affinity constants with the solution phase and the boundary layer equilibrium constants confirmed that kinetic constants can be reliably determined using biosensor analysis and that the hydrogel biointerface does not invariably cause deviations.

'Overcrowding' effects may be responsible for many of the deviations commonly observed from interaction curves including the heterogeneous dissociation profile of overlaid contact-time dependent interaction curves. Overcrowding may become exaggerated over time by constant rearrangement of the matrix in order to facilitate binding of the analyte to sterically hindered binding sites. This mechanism may also account for the extreme contact-time dependency of the CD4 dissociation phase observed when the anti-mouse Fc-coated surface was employed. In addition, GST-GST self-association may be responsible for an apparent increase in mass during the dissociation phase of interaction curves. The interactions depend on high local densities of GST at the reduced dextran surface and prevent kinetic analysis of the dissociation phase. In addition, the existence of an inward moving analyte saturation boundary under MTL conditions was

demonstrated for the CD4 interaction and became exaggerated at high flow rates. This observation eliminates the ambiguity regarding the inappropriate application of a positive co-operativity factor as suggested by other investigators. However, kinetic constants for the GST interaction conducted on the non-ideal anti-mouse Fc-coated surface approximated those determined for the 'ideal' analysis (employing the protein A-coated CM5 sensor chip) despite deviations from ideal behaviour.

The application of MTL interaction models for the analysis of partially MTL interaction curves did not prove successful since wide variations in many of the fitted parameters invalidated the analysis. The model improved the apparent correspondence of the derived rate constants with the 'true' rate constant but did not give a complete description of the MTL interaction curves. However, a two-compartment phenomenological description of the transport process was successfully employed, giving a good approximation of the 'true' rate constant. The analysis has the potential to extend the range of reaction rates that can be determined by 'real-time' biomolecular interaction analysis by one or two orders of magnitude.

In conclusion, kinetic analysis of biomolecular interactions is complicated by MTL, steric hindrance, matrix cross-linking and surface heterogeneity effects. It is difficult to determine, with certainty, which of these effects is responsible for observed deviations from ideal pseudo-first-order behaviour. Nevertheless, the protein A affinity-capture format produced ideal binding progress curves for the interaction of GST with anti-GST monoclonal antibody, while protein G and polyclonal anti-mouse Fc-coated surfaces gave curves that did not conform to the pseudo-first-order interaction model. It is worth noting that without the benefit of experimental comparisons one could easily mistake the observed deviations as an inherent property of the interaction. Consequently, it is prudent to investigate alternative formats when performing kinetic analysis.

Chapter 4

Surface Plasmon Resonance Detection of Whole Red Blood Cells

4.1. Introduction

This chapter describes solid phase detection of whole red blood cells (RBCs) using immobilised blood group-specific antibodies and surface plasmon resonance sensing. However, the main findings may be applicable to general solid phase detection and/or selection of other cell types. In addition, many of the principles involved have been well established for general solid phase cell-selection over the past 30 years. Consequently, a brief introduction to the principles of blood grouping and solid phase cell selection will be presented.

4.1.1 ***Blood Grouping.*** There are many blood group antigens present on the surface of human RBC membranes. However, the ABO and Rhesus blood grouping systems are of greatest importance as they determine blood type compatibility for transfusion purposes (Dacie *et al.*, 1968). Four different antigen systems are of significance, namely the A, B and H antigens in the ABO system and the D antigen in the Rhesus system. The A and B antigens are not primary gene products but are defined by the enzymatic attachment of acetylgalactosamine (group A antigen) or galactose (group B antigen) to the H antigen (group O antigen) precursor. The H antigen is present on virtually all RBCs and the *A* and *B* gene products (i.e. transferase enzymes) add sugars to the H antigen giving the A and B phenotype. In addition, there are variations in the copy number of A antigens present on RBCs due to different catalytic properties of acetylgalactosamine transferase. The A_1 and A_2 gene products code for acetylgalactosamine transferases that differ with respect to a few amino acid residues, resulting in different catalytic properties. Consequently, individuals expressing the A_1 gene product will possess blood group A_1 antigens and those expressing the A_2 gene product will possess blood group A_2 antigens. Typical expression levels of both A and B antigens are shown in *Table 4.1.1* (see Reid and Lomas-Francis, 1997, for a complete review of blood group antigens).

A Antigen (copies/cell)		B Antigen (copies/cell)	
A_1	810,000 -1,170,000	B	610,000 - 830,000
A_2	240,000 - 290,000	A_1B	439,000 approximately
A_1B	460,000 - 850,000		
A_2B	120,000 approximately		

Table 4.1.1. Typical expression levels of blood group antigens A and B.

Antibodies possessing affinity towards blood group antigens are naturally present in human serum (predominantly IgM) without previous exposure to the corresponding RBC antigen. These include anti-A, anti-B and anti-H. It is believed that residues resembling blood group-associated antigens (BGAA) are widely found in nature and give rise to the corresponding antibodies. However, blood transfusions and passage of foetal cells into the mother's circulation during pregnancy also give rise to blood group-specific antibodies (predominantly IgG). Blood group-specific IgG is referred to as incomplete since it is usually unable to bridge the distance between two red blood cells. This is thought to be due to charge repulsion between RBCs in close proximity as a result of the abundance of sialic acid residues in the membrane. However, high concentrations of soluble protein, such as BSA, or high ionic strength negate these charge effects facilitating IgG-mediated agglutination. Blood group-specific IgM is the active component of most commonly used blood-grouping reagents. It is capable of binding BGAAs with high avidity due to its decavalency and causes complete agglutination of RBCs.

4.1.2 ***Blood Grouping Technology.*** Whole blood is usually taken into tubes containing an anti-coagulant solution and may be stored at 4 °C for 1-2 weeks. Metal chelators such as citrate and EDTA are commonly used anti-coagulants but heparin is also popular. There are a number of techniques employed for blood grouping and all rely on solution phase agglutination. The anti-coagulated whole blood sample is simply mixed with the blood-grouping antibody resulting in agglutination and accelerated sedimentation of the clumped cells. Non-reacted cells will not sediment and the optical density of the sample will remain constant, whereas a positive test can be identified by a decrease in the optical density of the sample. The tile technique (Dacie *et al.*, 1968) is commonly employed for rapid assessment of blood type (emergency cases). It involves mixing whole blood with a particular anti-BGAA antibody preparation and visual ranking of the agglutination reaction. Controls are incorporated by including analysis of known blood group A, B and O blood types. Large-scale blood grouping analysis is performed by dedicated automatic or semi-automatic bench-top analysers (e.g. Quatro QASAR system from Quatro biosystems, Manchester, U.K.) These systems usually employ optical interrogation of agglutination reactions occurring within the wells of a microtitre plate. Dedicated image analysis software can discriminate between the agglutinated samples and the non-agglutinated samples by the appearance of an acquired image. These systems offer attractive features such as low sample consumption, high throughput (100 samples per hour) and minimal demands on operator time.

4.1.3 ***Cell Selection.*** The irreversible agglutination of cells may not be considered a disadvantage in conventional blood grouping where samples are disposed after analysis. However, these technologies do not support cell recovery thereby limiting the flexibility of the technology. Solid phase techniques that allow recovery of intact cells present more flexible formats with the potential for cell detection and/or isolation. The determination and isolation of specific cell types in a viable unaltered state is required for therapeutic techniques such as bone marrow transplantation and for basic research. A variety of aqueous phase cell separation techniques are routinely employed and include density gradient centrifugation (Bøyum, 1984), dielectrophoresis (Cheng *et al.*, 1998), complement-mediated lysis (Ray, 1989) and fluorescence activated cell sorting (Vaughan and Millner, 1989). Ideally, the method should facilitate the recovery of viable, unaltered cells (Hubbard *et al.*, 1983) with high yields (> 10^8 cells). However, these techniques rely on differing physical properties of the target cell sub-population or the use of a labelled antibody with specificity for a membrane-associated antigen. In principle, it is much simpler to isolate cells at a solid-liquid interface by immobilising a specific affinity-capture ligand.

4.1.4 ***Immunoadsorbent Affinity Chromatography.*** The isolation of cells using affinity chromatography has been investigated over the past thirty years with varying degrees of success. Efficient separation of viruses, bacteria, cellular organelles, and even whole cells has been developed (Kataoka *et al.*, 1987). These techniques are generally rapid and can yield pure target cell preparations. However, non-specific binding and the recovery of bound cells remain the main limitations of the technique. There are two modes of operation:

(a) ***Positive Selection***: The targeted cell sub-population within the sample is captured onto the solid phase through specific interactions of membrane-associated antigens with the immobilised ligand. After washing away non-adherent cells, the specifically selected cells are recovered.

(b) ***Negative Selection***: The solid phase is designed to adsorb all cells with the exception of the target sub-population. This technique is of limited application since it is often difficult to create a functionalised solid phase that retains all cells other than the target sub-population.

Positive selection is more demanding than negative selection as a compromise must be reached between cell binding avidity, which enables efficient retention of specifically captured cells during wash steps and recovery. Negative selection merely requires an excess of the immobilised ligand to generate maximum binding avidity, thus facilitating the recover of the non-adherent sub-population from the supernatant. The optimum ligand-coating density is a function of the cell receptor density, degree of capping, hydrodynamic conditions and the affinity of the specific receptor-ligand interaction, and hence must be determined empirically for each application. Solid phase cell

selection can be accomplished using a variety of solid phase supports that can be categorised as affinity column-based or planar surface-based.

4.1.4.1 Column-Based Separation. The affinity ligand is immobilised onto the chromatography matrix and captures the target cells as the sample is passed through the column. After washing the column, the retained cells are recovered from the matrix by repeated aspiration of the gel using a Pasteur pipette (Ghetie and Sjöquist, 1984). Column separation can be effective even when the interaction of the target cells with the affinity ligand merely retards their mobility relative to non-interacting cells. Originally designed for macromolecular affinity chromatography, matrix supports based on dextran, agarose and polyacrylamide are popular due to their hydrophilic character, which discourages non-specific binding of cells (Mishell and Mishell, 1984). However, physical entrapment of cells within these matrices can occur thus lowering the purity of the recovered cells. Blocking procedures based on the occupation of potential non-specific binding sites by a hydrophilic non-descript protein (i.e. bovine serum albumin (BSA)) has often proved helpful. In addition to conventional affinity matrices, plastic and glass beads have proven particularly useful for cell isolation as the surface area of the solid phase that is exposed to the cell sample is maximised and the potential for cell entrapment is minimised.

4.1.4.2 Affinity Panning. Panning refers to cell selection employing a functionalised planar surface. A wide variety of materials have been used (Mosier, 1984) including glass (e.g. glass slides) and polystyrene surfaces (e.g. petri dishes). Many investigators have employed direct physisorption of the affinity ligand followed by blocking of remaining sites with a non-specific protein (e.g. BSA). The contact area is considerably lower than that obtained for column chromatography thus limiting the selection capacity. In addition, panning requires high cell binding avidity to enable the selective removal of non-adsorbed cells by washing. This necessitates the use of high affinity-capture ligands and/or high coating densities. Recovery of adsorbed cells is frequently problematic due to high cell binding avidity resulting from multiple interactions between the cell and the ligand-coated surface. However, this technique does not require specialised equipment, hydrogels or immobilisation strategies and has been successfully applied for the selection of a wide variety of cell types. Anti-mouse antibody has been used for the isolation of B-cells (possess surface immunoglobulin molecules) from mouse lymphocyte preparations (Mage, 1984). Antibody-coated polystyrene tissue culture dishes have been used for the selection of a variety of separations including T-lymphocyte sub-populations, bone marrow neutrophils and lectin-binding T-cells (Hubbard *et al.*, 1983).

4.1.4.3 *Cell Recovery from Solid Phases.* Recovery of absorbed cells is often difficult as the use of chaotrophic conditions must be avoided when viable cells are to be recovered. Mechanical agitation (e.g. scraping of surface or aspiration of gel) and competitive elution (e.g. solution phase excess of ligand) are the most commonly employed techniques. In practice, a combination of both techniques is often required for efficient recovery of target cells. However, mechanical agitation induced by scrapping or aspiration of the hydrogel often lowers the yield of intact viable cells. Competitive elution requires an excess of free ligand that competes for binding sites with the immobilised ligand. For example, sugar-specific lectins are available which can be used to isolate cell sub-populations. The lectin, *Helix pomatia*, more commonly known as hemagglutinin, binds mature T-cells via specific glycoproteins and does not bind to B-cells. The lectin recognises specific sugar residues of the glycoprotein and, hence, a solution excess of these sugars should competitively elute the target cells (Hellström *et al.*, 1984). However, high solution concentrations are required to force the equilibrium in favour of cell release due to the high number of binding interactions between a single cell and the functionalised surface.

4.1.5 ***Behaviour of Cells at Interfaces.*** Many cell types are naturally adherent and include various immortal cell lines, macrophages, and fibroblasts. Macrophages are readily separated from lymphocyte preparations by incubating the cell sample at 37 °C in a petri dish. Macrophages adhere to the surface allowing the non-adherent lymphocytes to be recovered (Mosier, 1984). However, solid phase cell selection may not be appropriate for some applications as the surface-binding event can trigger undesirable metabolic and phenotypic changes (Kataoka *et al.*, 1987). Furthermore, membrane-associated antigens tend to diffuse laterally and cluster at the interface with the solid phase causing an increase in binding avidity. However, minimising the cell contact time with the functionalised matrix or surface will limit the degree of capping thus facilitating efficient recovery.

4.1.6 ***Dynamics of Cell Binding and SPR Detection.*** Solid phase blood grouping using SPR sensing allows the optimisation of both biointerfacial chemistries and of conditions for solid phase cell selection. Detailed information concerning the progress of surface binding events can be obtained from interaction curves. The 'real-time' binding response originates from the evanescent wave that arises under conditions of surface plasmon resonance and that probes the refractive index of the solution close to the sensor surface (section 5.1.1). This evanescent wave decays exponentially with distance from the surface, and the effective penetration depth is about 190 nm (Liedberg *et al.*, 1993). The relatively large RBCs cannot penetrate the 100 nm thick hydrogel layer resulting in decreased sensitivity. In addition, the fractional coverage of the sensor surface that arises when cells bind (*Figure 4.1.6*) will further decrease the expected response.

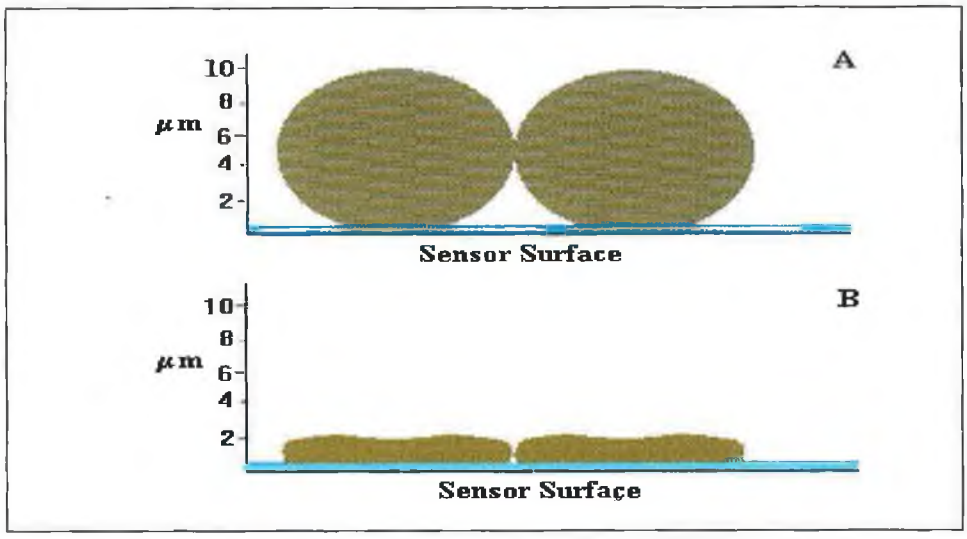

Figure 4.1.6. Diagrammatic representation of the fractional coverage of the sensor surface when cells are immobilised. The shaded region along the horizontal axis represents the evanescent field penetration depth, and hence, mass changes outside this region are not detectable. Diagram A shows a low fractional coverage of the surface for spherical cells of diameter 10 μm. Diagram B shows RBCs bound to the cell surface. A much greater coverage of the surface is possible due to the biconcave disc morphology of the RBC, which increases the total volume of cells inside the penetration depth of the evanescent field. This model assumes that the RBCs are bound at their flattened surface.

Furthermore, it was thought that the large RBCs would cause blockages within the narrow (50 μm) channels of the microfluidic cartridge employed in the BIACORE 1000™. The microfluidics system was designed to minimise mass transport limitation in kinetic studies and not for the accommodation of large particles. However, detection of whole cells binding to a functionalised CM-dextran surface has been documented for prokaryotic (Watts and Lowe, 1994) and eukaryotic cells (BIACORE AB, 1995). The normal RBC is a biconcave disc with a diameter of 7.8 to 8.3 μm and is 1.7 μm thick (Lessin and Bessis, 1978) under isotonic conditions. However, these dimensions change considerably in hypotonic or hypertonic solutions. Within the cardiovascular circulation system, RBCs traverse blood vessels of varying diameters and flow rates and exhibit a variety of dynamic transitions of form. The construction of the microfluidics system did not hinder the analysis of physiological concentrations of RBC (e.g. < 40 % (v/v)). Clearly, the viscoelastic properties of RBCs (Blackshear and Anderson, 1977) are significant for the delivery of high RBC cell densities to the flowcell via the microfluidic system without causing blockages within the system. Cell deformation is dependent on the applied force, cell size, morphology, area/volume ratio, membrane mechanical properties and cytoplasmic viscosity. However, poor signal quality was commonly observed at high RBC densities (~ 40 % (v/v)). It is probable that the analysis of less

deformable cells would be hindered to a greater extent by flow disturbances. The ability of immobilised ligands to capture free RBCs and generate a SPR response is dependent on many factors (*Table 4.1.6*).

Table 4.1.6. List of constraints that determine the SPR response when RBCs are captured onto the sensor chip surface by an immobilised ligand.

1. Repulsion and attraction of charged groups on the CM-dextran or the cell surface.
2. Average refractive index of RBC.
3. Density of the immobilised ligand at the interaction surface.
4. Distance of the cell from the sensor surface (i.e. Position of the cell within the evanescent field).
5. Affinity/avidity of the ligand for a specific membrane receptor on the RBC surface.
6. Accessibility of the immobilised ligand to the BGAA on the RBC surface.
7. Density of the receptor on the cell surface.
8. Fluid viscosity, ionic strength, pH, temperature.
9. RBC concentration of the sample.
10. Flow rate.
11. Presence of essential trace elements (ligand dependent; e.g. Mn^{++} , Ca^{++} are essential for Con A-carbohydrate binding activity).
12. Duration of sample pulse and dimensions of the flowcell.

The maximum cell binding response is limited by the fractional coverage of the sensor surface, the presence of an impenetrable hydrogel and fluid dynamic effects. The SPR detector measures the average SPR response over a 0.8 mm^2 surface; a surface coverage less than 100 % will give a correspondingly reduced response. Spherical cells of diameter 10 μm with a refractive index of 1.37 would reduce the surface coverage significantly and a response of approximately 1,500 RU would be expected (BIACORE AB, 1995). If the cells are not spherical, the fractional coverage of the surface may be increased and the expected minimum response will be higher (*Figure 4.1.6*). The deformable biconcave disc morphology of the RBC facilitates an increased fractional coverage of the sensor surface in comparison to spherical cells. This combined with the high refractive index of RBCs (i.e. 1.39 (Hladky and Rink, 1982)) increases the expected response significantly.

4.1.7 ***Overview of Chapter.*** The use of SPR-based biosensors for the study of whole cell-ligand interactions is largely unexplored. Hence, a series of preliminary investigations employing covalently immobilised monoclonal anti-A IgM and monoclonal anti-B IgM were completed. It was envisaged that the antibody would reversibly capture the target RBCs from suspension, effectively demonstrating solid-phase blood grouping. Affinity-capture of the specific antibody was employed to anchor anti-A IgG to the hydrogel as an alternative to direct immobilisation. Furthermore, a fibre optic SPR-based sensor was employed for the analysis of concentrated RBC samples and viscous whole blood since viscous samples cause flow disturbances within BIACORE 1000™'s fluid delivery system. A summary of the experimental aims is presented.

1. Determine feasibility of whole cell detection using SPR-based biosensors.
2. Examine the ability of immobilised antibodies, which recognise BGAA, to specifically retain RBCs of the respective blood group.
3. Optimise the detection format to enable effective regeneration thus allowing multiple cell-binding interactions to be performed on a given sensor surface.
4. Elucidate the relationship between cell binding, sample concentration and binding response.
5. Assess the effect of the immobilised antibody concentration on the RBC binding response and the RBC binding variation between individual donors.
6. Explore the potential of SPR technology to facilitate blood grouping using whole blood samples.
7. Develop a simple model to describe the dynamics of RBC adsorption that accounts for experimental observations.

4.2 *Results and Discussion*

Previously grouped whole blood samples were obtained from the Blood Transfusion Service Board two days after bleeding and were stored for no longer than 3 days at 4 °C prior to analysis. The storage time was minimised as solid phase whole blood grouping is highly sensitive to the presence of free membrane-associated antigens that may result from degradation of the RBCs during storage. Furthermore, RBC samples were allowed to equilibrate at room temperature before use in order to permit them to recover from reversible deformation incurred during storage at 4 °C.

4.2.1 ***RBC Binding Studies Utilising Immobilised Concanavalin A.*** Surface plasmon resonance detection of cell adsorption was demonstrated for the capture of RBCs from suspension onto a concanavalin A (Con A)-coated sensor surface. This study was performed to assess the feasibility of detecting whole RBC using the BIACORE 1000™. The use of lectins as molecular probes (Skibo *et al.*, 1988(a); Skibo *et al.*, 1988(b)), as specific agglutination reagents (Peacock *et al.*, 1990), as mitogenic agents (Skibo *et al.*, 1988(c)) and in biosensor applications (Blake and Goldstein, 1982) is well documented. Con A was selected for use in a preliminary model study due to its ability to bind glycoproteins (high copy number per cell) through exposed mannose and glucose residues (Blake and Goldstein, 1982). Con A can bind RBC membrane glycoproteins with high avidity, thus capturing cells from suspension onto the sensor chip surface. Con A exists as a dimer at pH 5.8, as a tetramer above pH 6.8 and as higher aggregates above pH 7.0. It requires Ca^{++} and Mn^{++} ions in order to maintain binding activity and possesses one carbohydrate-binding site per monomer.

In order to maximise the cell binding response in BIACORE 1000™, the concentration of the immobilised ligand must be high enough to ensure that sufficient binding avidity is generated to overcome shear forces within the flow cell. Therefore, a high concentration of Con A was immobilised (~ 7,594 RU) using conventional amine coupling (*Figure 4.2.1.1*). Specific affinity-capture of RBCs onto the Con A-coated surface was demonstrated (*Figure 4.2.1.2*) and shows an exponential decay towards a steady state response. The cell binding response accelerated during the initial binding phase and reached a plateau after 15 min. The acceleration in the cell binding response may result from a contraction of the hydrogel in which bound cells are drawn closer to the surface (i.e. more sensitive region of the evanescent field) or from a co-operative binding effect. Binding of a cell to the smooth surface may increase the probability of a free cell being retained due to the collision of a free cell with the bound cells (see section 4.2.5.4). In addition, bound cells (~ 1,390 RU) appeared to be anchored strongly to the surface as < 7 % dissociation occurred after 30 min.

However, regeneration of the surface was not satisfactory. The interaction curve showed that the first regeneration pulse (10 mM NaOH) resulted in an apparent increase in mass (~ 40,000 RU) at the surface. It is possible that membrane fragments resulting from cell lysis may have penetrated the hydrogel, thus occupying the more sensitive region of the evanescent field (i.e. closer to the surface). Moreover, three successive regeneration pulses failed to regenerate the surface (< 30 % reduction in apparent mass). As expected, subsequent cell binding-regeneration cycles showed that the accumulation of residual cellular material at the surface caused a dramatic decrease in the cell binding capacity.

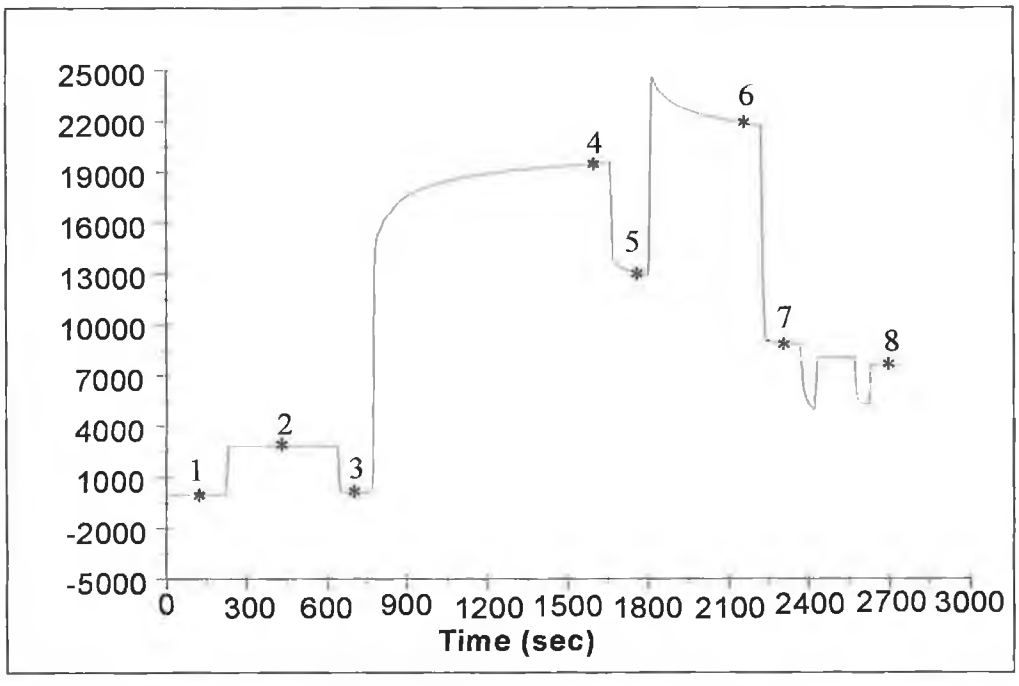

Figure 4.2.1.1. A sensorgram from a typical immobilisation sequence in which Con A is coupled to the sensor chip. Stage (8) is particular to the immobilisation of Con A. The numbered points refer to the following stages in the immobilisation procedure:

(1) Baseline for the unmodified sensor chip surface with eluent buffer.

(2) The pulse of NHS/EDC gives an increase in the SPR signal due to its higher bulk refractive index over HBS running buffer.

(3) Baseline after activation.

(4) Total Con A adsorbed to the surface as a result of both preconcentration and covalent coupling.

(5) Total covalently attached Con A.

(6) Deactivation of unreacted NHS-esters using 1 M ethanolamine-hydrochloride adjusted to pH 8.5 with NaOH. Deactivation also removes any residual non-covalently attached Con A.

(7) Total Con A remaining after deactivation.

(8) Immobilised ligand after a 1 min pulse of 20 mM NaOH (This pulse dissociates ConA tetrameric complexes leaving dimeric Con A complexes covalently attached to the matrix).

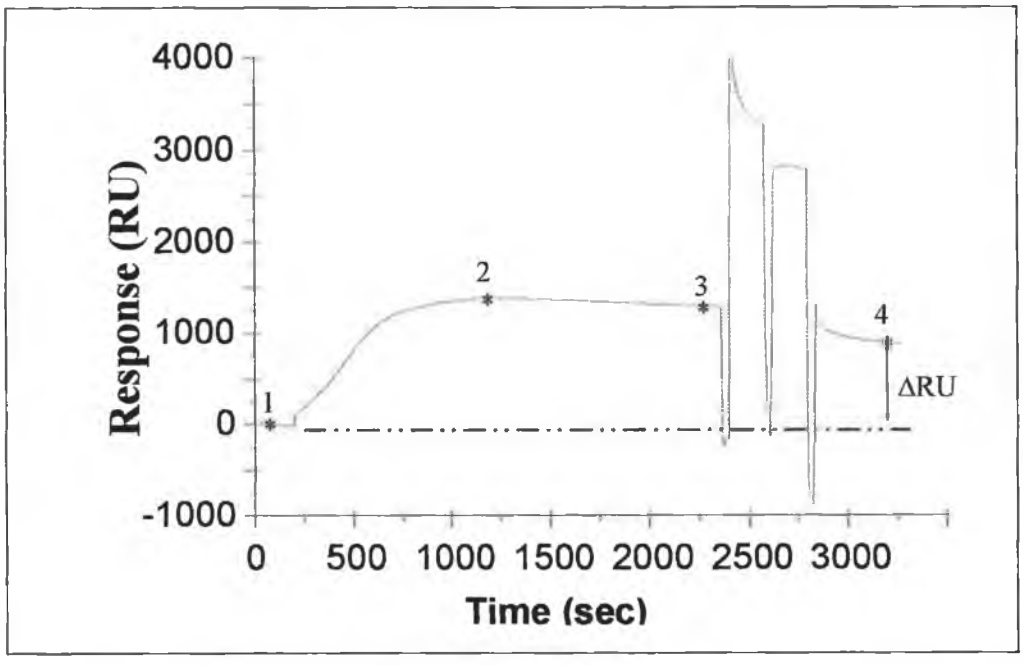

Figure 4.2.1.2. Binding of RBCs to a Con A-coated surface as measured on the BIACORE 1000™ system. Con A was covalently immobilised onto the sensor chip surface (~ 7,000 RU) and 50 µl of washed RBC (1.0 x 10^9 cells/ml) suspended in HBS buffer were injected over the sensor surface at a flow rate of 5 µl/min. The numbered points refer to the following stages in the interaction sequence. 1. Baseline for the Con A-coated sensor surface with eluent buffer. 2. Total RBC adsorbed after 15 min. At this point the RBC sample injection over the sensor chip surface has been discontinued. 3. Dissociation phase. Running buffer was passed over the surface for 30 min allowing the RBC to dissociate from the Con A surface. 4. Baseline after sequential pulses (5 µl/min for 1 min) of 10 mM NaOH, 20 mM HCl and 10 mM NaOH, respectively. A considerable amount of cellular debris remains on the surface (ΔRU).

Competitive elution of bound RBC using alpha-D-mannopyranoside proved unsuccessful. RBCs (1 x 10^9 cells/ml) were passed over the Con A-coated surface (5 µl/min for 15 min) and were competitively eluted using 0.1 M alpha-D-mannopyranoside (5 µl/min for 15 min), resulting in approximately 16 % removal of the total cellular mass at the surface (results not shown). Efforts to optimise regeneration conditions were unsuccessful as complete regeneration of the surface while maintaining the biological activity of Con A was not possible. The failure to regenerate the surface suggested that the concentration of immobilised Con A must be reduced to decrease cell binding avidity. This is a common difficulty and has been observed in many solid phase cell binding studies (see section 4.1.4.3). However, further optimisation of this format was not pursued as the goal of demonstrating RBC detection was achieved.

4.2.2 ***RBC Binding Studies Utilising Immobilised IgM.*** Solid phase blood grouping was accomplished by immobilising blood group-specific antibody and monitoring the SPR response as RBCs were passed over the sensor surface. RBC binding was found to be specific as RBC binding did not occur during control cycles. These controls involved injecting blood group A cells (2.5×10^9 RBC/ml) over the anti-B IgM-coated surface (50 µl at 5 µl/min) (*Figure 4.2.2.1*) and injecting blood group B cells (2.1×10^9 RBC/ml) over the anti-A IgM-coated surface (50 µl at 5 µl/mim) (*Figure 4.2.2.2*). However, the non-specific binding potential of RBCs may be reduced as shear forces within the flow cell may negate any non-specific reactions. In addition, charge repulsion between the negatively charged CM-dextran matrix and the negatively charged RBC may help to prevent non-specific binding. Furthermore, the absence of a detectable non-specific binding response may be due to an apparent 'invisibility' caused by a low fractional coverage of the sensor surface over which the response signal is averaged. *Figure 4.2.2.2* shows that the RBC binding response was not significantly different for RBC concentrations of 2.2×10^9 cells/ml and 2.5×10^9 cells/ml, suggesting that the response may be approaching saturation. The maximum binding response represents 68 % occupation of the total volume immediately outside the hydrogel (see section 4.2.4.8). A free volume of only 32 % suggests that considerable deformation of the bound RBC may occur to enable such high coverage.

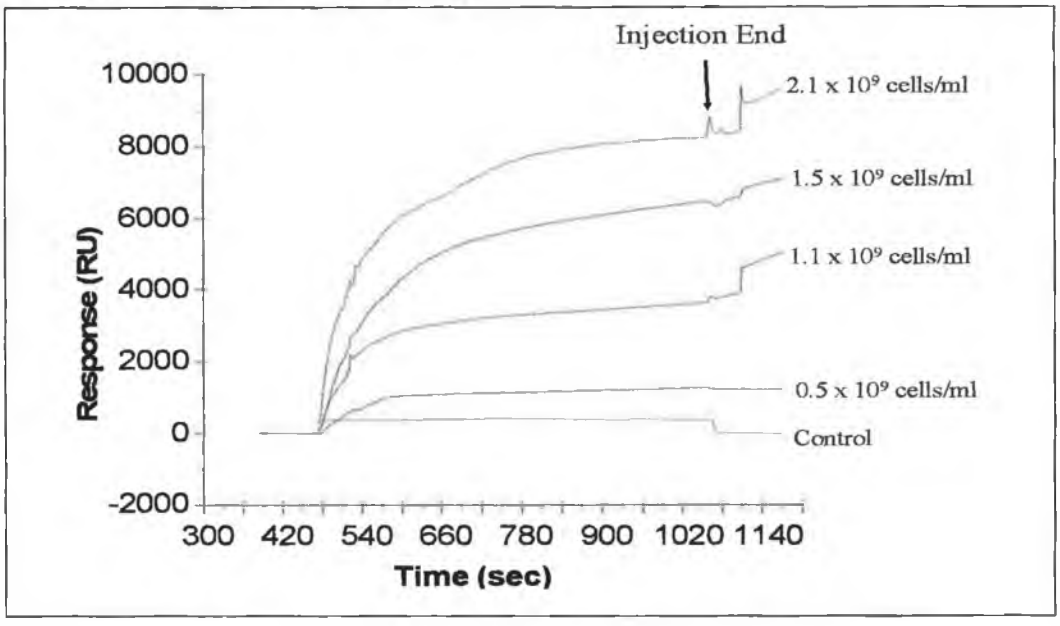

Figure 4.2.2.1. Binding of four increasing concentrations of blood group B RBCs to an anti-B IgM-coated surface. Anti-B IgM was covalently immobilised (7,196 RU) onto the sensor chip surface and 50 µl of washed group B RBCs, suspended in HBS buffer, were injected over the sensor surface at a flow rate of 5 µl/min. Sampling was performed in order of increasing RBC concentration. The surface was regenerated using two short pulses (i.e. 60 sec and 40 sec) of 20 mM NaOH. 50 µl of group A RBCs (2.5×10^9 cells/ml) were injected over the surface as a control ('Control') and did not give a detectable binding response.

The copy number of BGAAs per cell varies between individuals. Hence, the maximum response of a given blood type at a constant concentration will vary for different donors making binding response comparisons between experiments difficult. For this reason, a single donor for each blood type was employed during each experiment. The interaction curves displayed in *Figure 4.2.2.1 and 4.2.2.2* show that cell binding rapidly approached an approximate steady state at lower RBC densities but required 10-15 min sample contact time at higher concentrations. This approximate steady state will be referred to as a pseudo-steady state and is discussed in more detail in section 4.2.5. The curves are characterised by a rapid exponentially decaying association phase and the binding rate is proportional to the cell concentration. The association curve gradually approaches a pseudo-steady state.

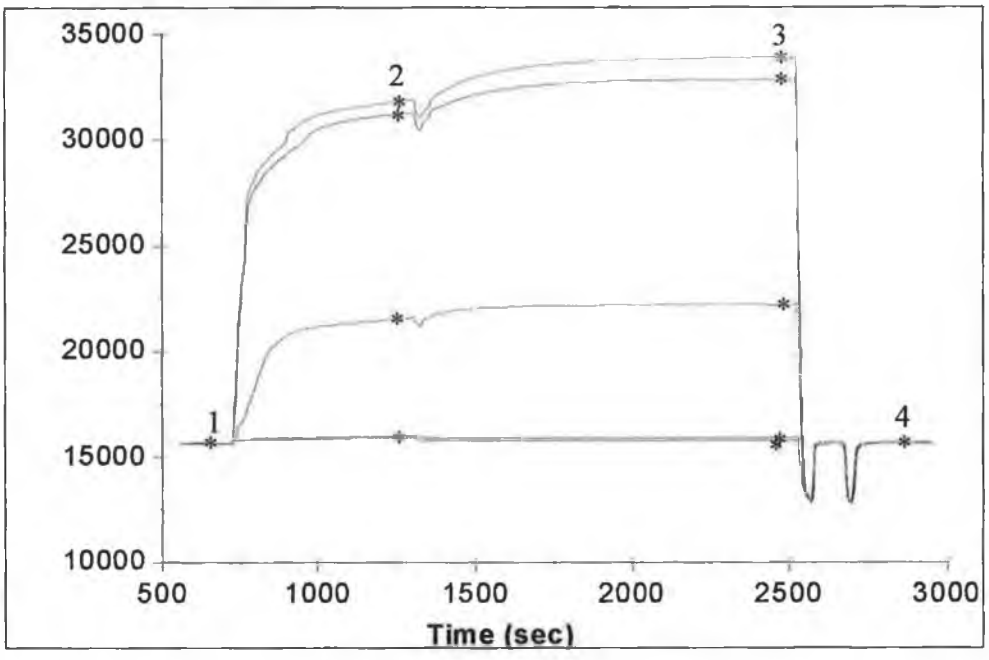

Figure 4.2.2.2. Binding of blood group A RBCs to the anti-A IgM-coated surface (4,600 RU immobilised). Washed group A RBCs were suspended in HBS buffer and analysed as described in *Figure 4.2.2.1*. The final RBC sample concentrations were 1.1 x 10^9 cells/ml (——), 1.5 x 10^9 cells/ml (——), 2.2 x 10^9 cells/ml (——) and 2.5 x 10^9 cells/ml (——). 50 µl of group B RBCs (2.19 x 10^9 cells/ml) were injected over the surface as a control (——) and did not give a detectable cell binding response. The numbered points refer to the following stages in the sequence. 1. Baseline for the anti-A IgM-coated sensor surface with eluent buffer. 2. Total RBCs adsorbed after 10 min. At this point the RBC sample injection over the sensor chip surface has been discontinued. 3. Dissociation phase. Running buffer was passed over the surface for 20 min to allow the RBCs to dissociate from the IgM-coated surface. An apparent increase in mass occurred after discontinuation of the sample pulse, possibly due to deformation of the cells at the surface resulting in an increase fractional coverage of the surface. 4. Baseline after regeneration using two short pulses (i.e. 60 sec and 40 sec) of 20 mM NaOH. Complete regeneration of the surface was achieved in contrast with the Con A-RBC experiment (*Figure 4.2.1.2*).

In theory, approximately 12,300 RBCs can be bound to the sensor surface at saturation. This estimate assumes the RBCs have a diameter of 8 μm and that the space occupied by a single cell may be approximated by a square of equivalent dimension. Furthermore, *Figure 4.2.2.2* shows that the RBC binding response can exceed 16,000 RU (2.5 x 10^9 RBC/ml). The high binding response suggests that deformation of bound cells may be occurring at the surface (see section 4.2.4.7). In addition, the positive dissociation phase and the heterogeneous association phase observable in *Figures 4.2.2.1* and *4.2.2.2* provide further evidence for surface deformation. These effects were commonly observed during RBC binding studies. Deformation is probable as RBCs making contact with a surface can deform to the dacryocyte (teardrop) morphology *in vivo* (Lessin and Bessis, 1978).

The performance of this solid phase blood grouping format can be evaluated by constructing a calibration curve for the RBC binding response. The reproducibility, sensitivity and dynamic range, as determined from a calibration curve, are a reliable means of characterising the detection system. Hence, anti-A IgM was immobilised (9,645 RU) and group A RBCs were injected (5 μl/min for 7 min) over the sensor surface. Dissociation of bound RBCs from the sensor surface proceeded slowly, which is indicative of high avidity between the multivalent IgM and the captured RBCs.

Figure 4.2.2.3(a) is a calibration plot for the analysis conducted on a single sensor chip surface. The plot indicates an approximately exponential increase in the binding response with respect to the RBC concentration. This acceleration of the binding response may be attributed to a steric co-operativity effect at low surface coverage. The poor agreement between replicates is due to the decrease in the cell binding capacity caused by a combination of antibody denaturation, stripping of BGAA from cells and the accumulation of residual cellular material. *Figure 4.2.2.3*(b) shows that < 1,000 RU of residual cellular mass accumulated during the course of the experiment, which suggests that acute denaturation of the immobilised IgM and antigen stripping are the dominant causes. Inefficient regeneration severely restricted the number of cell binding-regeneration cycles (i.e. < 20) that could be reliably performed. Clearly, a more effective regeneration technique was required in order to maximise the number of sequential cell binding-regeneration cycles that can be run on a given antibody-coated surface.

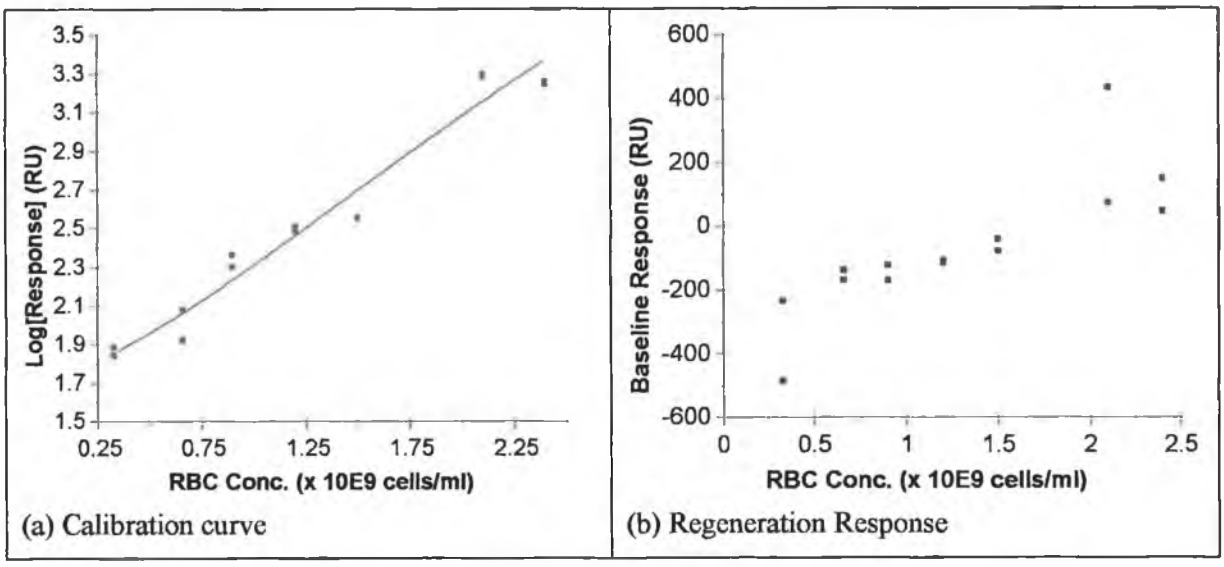

Figure 4.2.2.3. Washed group A RBCs at varying concentrations were analysed in order of increasing concentration over the IgM-coated sensor surface at 5 µl/min for 7 min. Regeneration of the surface after each cell binding-regeneration cycle was accomplished using two 1 min pulses of 20 mM NaOH. (a) Calibration plot for the interaction of group A RBCs with covalently immobilised anti-A IgM. The relative binding responses for duplicate sample analyses are shown. A 4-parameter equation was fitted to the data (see section 3.2.5.2) (b) Regeneration profile for the calibration curve. Ideal regeneration of the surface should consistently result in a baseline response of ~ 0 RU. Sub-optimal regeneration resulted in excessive removal of mass when the RBC binding response was low (i.e. regeneration removed a fraction of immobilised anti-A IgM as indicated by the negative values) and insufficient removal when the RBC binding response was high. Furthermore, the outlying points indicated poor reproducibility between replicates.

4.2.3 ***Protein A Affinity-Capture Format.*** The previous studies (*section 4.2.2*) demonstrated that immobilised antibodies are capable of reversibly binding RBCs. However, a limited number of binding-regeneration cycles were possible due to an accumulative loss in cell binding capacity after each cycle. This was attributed to denaturation of the immobilised antibody and antigen stripping. Consequently, protein A affinity-capture of the specific antibody was introduced to avoid these difficulties. Protein A is extremely stable when repeatedly exposed to regeneration solutions and can bind IgG subtypes from many animal species (Goding, 1978; Langone, 1982).

4.2.3.1 *Stability of Protein A-Coated Surface.* The regeneration efficiency of the protein A-coated surface was investigated prior to cell binding analysis. Protein A was immobilised (5,200 RU) using conventional amine coupling. *Figure 4.2.3.1* shows the relative binding response of anti-A IgG hybridoma supernatant (diluted 400-fold in HBS running buffer) to this surface for 124

binding-regeneration cycles. The protein A-coated surface is extremely stable to regeneration with 10 mM HCl as evidenced by the insignificant loss of IgG binding activity (approximately 5 %). Furthermore, accumulation of residual antibody did not occur as the baseline response remained stable throughout the analysis. These encouraging results indicated that the protein A format may provide a successful alternative to direct covalent attachment of the antibody to the dextran matrix and may facilitate surface regeneration.

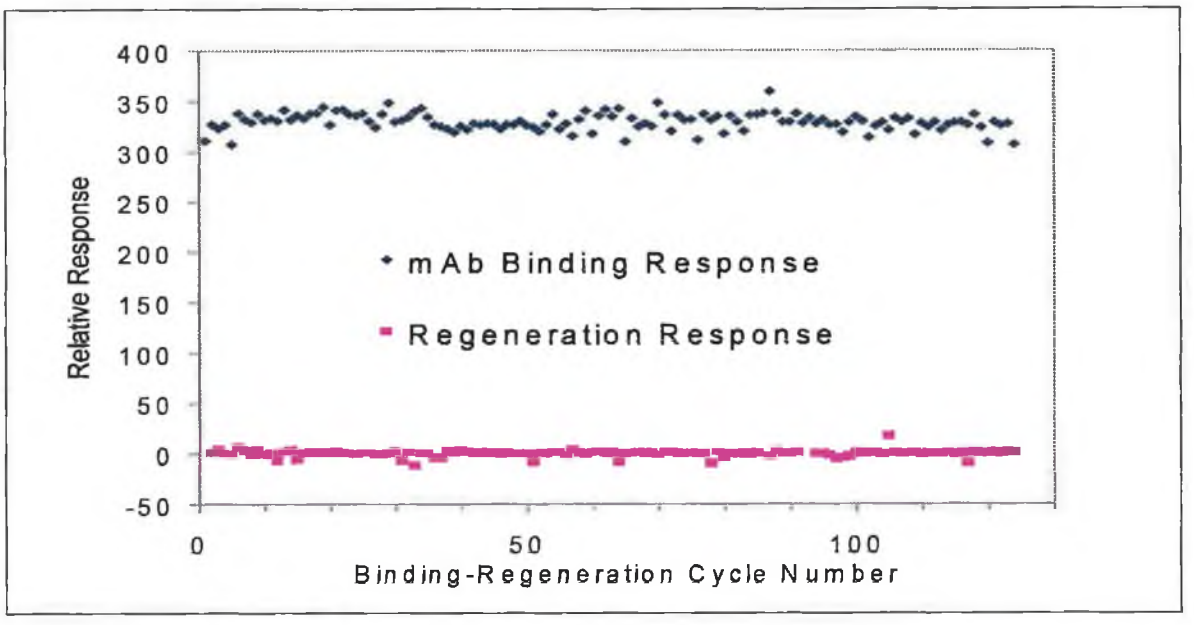

Figure 4.2.3.1 Binding response and regeneration profile of 124 binding-regeneration cycles for the interaction between immobilised protein A and anti-A IgG. 15 µl of anti-A IgG was passed over the protein A-coated surface at 5 µl/min and the surface was regenerated after each binding cycle using a 1 min pulse of 10 mM HCl.

4.2.3.2 *Reversible Capture of RBCs.* Protein A was immobilised onto the CM-dextran matrix as before and anti-A IgG hybridoma supernatant was injected over the surface. Group A RBCs were injected over the surface at 5 µl/min for 5 min. Non-covalently bound material (IgG and RBCs) was subsequently removed using a 1 min pulse of 10 mM NaOH. This procedure was repeated in triplicate for increasing RBC concentrations. *Figure 4.2.3.2.1* is a typical interaction curve and shows that both the antibody and RBC association curves are approximately linear. The concentration of affinity-captured anti-A IgG (~ 276 RU) and the sample contact time were minimised to prevent high cell binding avidity. This proved effective as the RBC binding response was low (~ 1,156 RU) in comparison to previous studies under similar conditions. However, the low response may be partially attributed to donor variation, as it was not possible to obtain blood samples from a single donor throughout the investigation. Dissociation of bound cells can be observed immediately before regeneration. Hence, the concentration of anti-A IgG is sufficient to

capture RBCs from solution but they may dissociate from the surface as a result of fluid dynamic shear forces. Regeneration of the surface was non-ideal as 21 % of the total mass (i.e. RBC debris) remained at the surface. A calibration curve was constructed for increasing group A RBC concentrations that were analysed as outlined in *Figure 4.2.3.2.2* in triplicate.

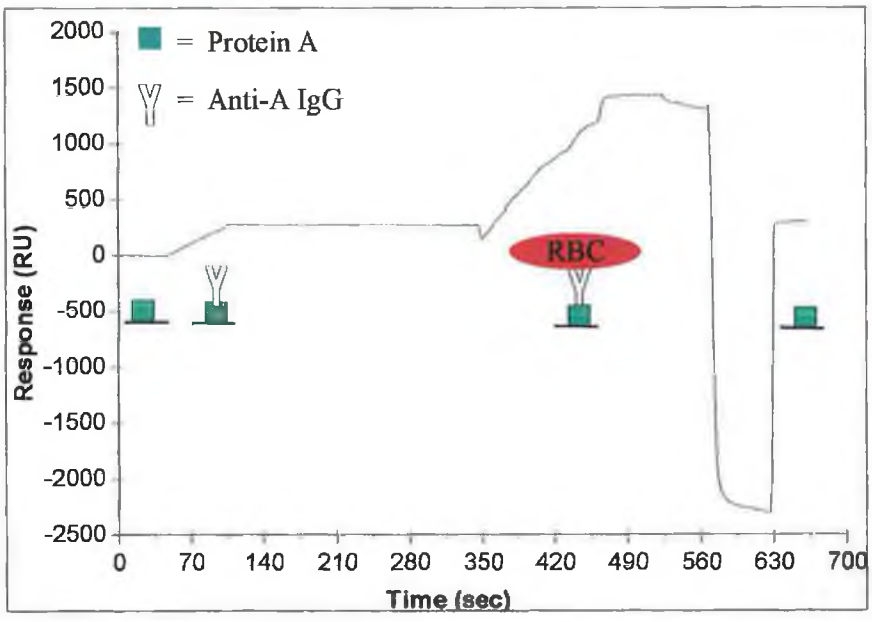

Figure 4.2.3.2.1. Protein A was immobilised (~ 4,400 RU) onto the dextran matrix using conventional amine coupling and 10 µl of anti-A IgG hybridoma supernatant (diluted 400-fold in HBS running buffer) was injected over the interaction surface at 5 µl/min giving a binding response of 276 RU. Washed group A RBCs (1.06×10^9 RBCs/ml in HBS running buffer) were injected over the surface at 5 µl/min for 5 min giving a cell-binding response of 1,156 RU. The surface was subsequently regenerated using a 1 min pulse of 10 mM HCl. However, 21 % of the total adsorbed mass remained.

As a control, group A RBCs (1.75×10^9 cells/ml) were passed over the protein A surface, in the absence of anti-A IgG for 2 min at 5 µl/min and this gave a low non-specific response of 11 RU. The low non-specific binding response agrees with previous observations (*section 4.2.2*). A single set of interaction curves for each RBC concentration is shown in *Figure 4.2.3.2.2* (a). Visual inspection of the curves reveals that the binding curves become increasingly erratic at high RBC concentrations. In particular, air spikes caused the SPR signal to fail at high RBC concentrations. This occurred frequently when analysing concentrated RBC suspensions and may be attributed to turbulent fluid dynamic effects within the flowcell. In addition, these spurious effects were more common when the integrated microfluidic cartridge was approaching its life expectancy (~ 6 months). It was impossible to eliminate these effects as the flow disturbances within the flowcell arise from the innate viscosity and turbulence of concentrated RBC samples.

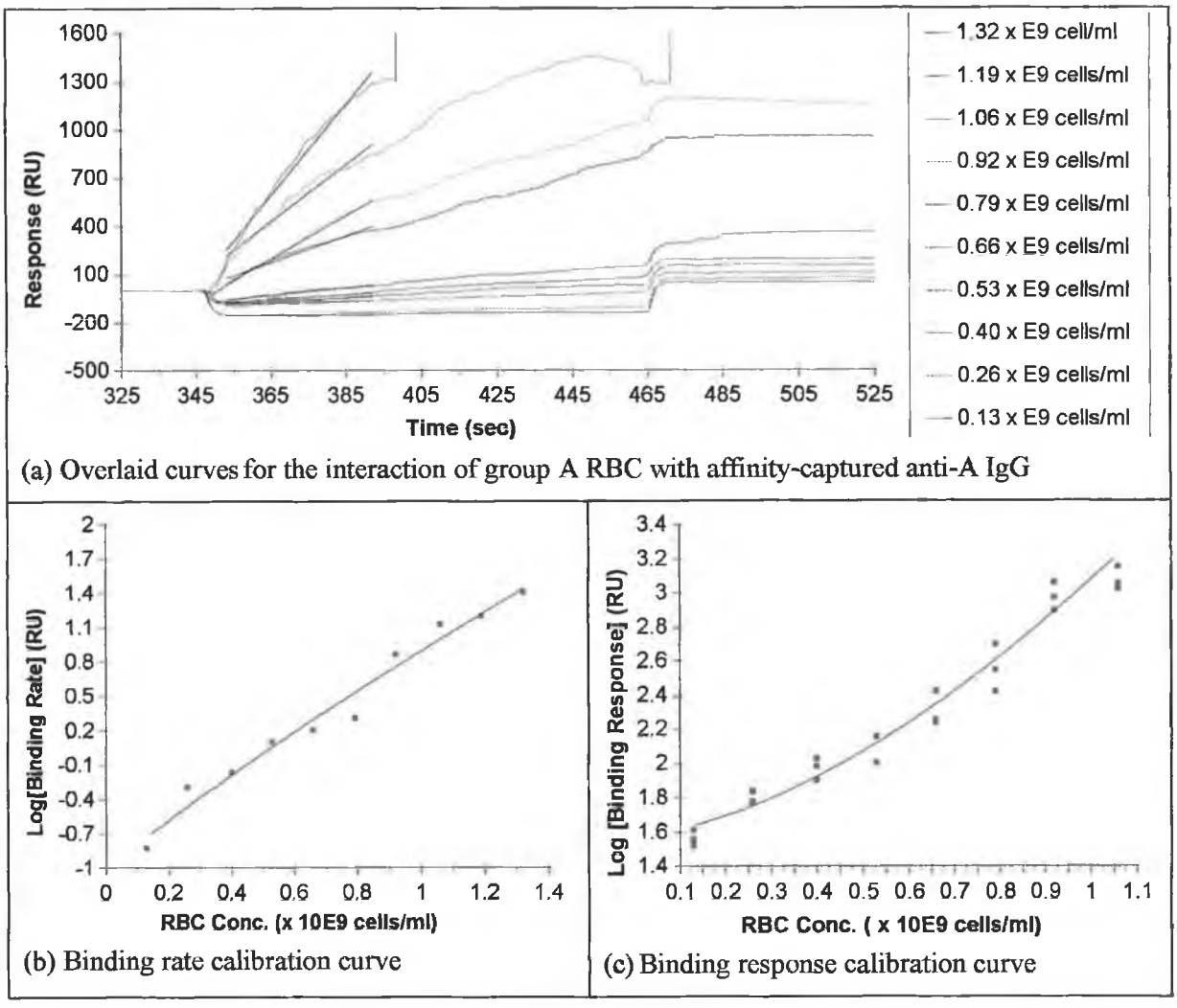

Figure 4.2.3.2.2. (a) Overlaid interaction curves for the binding of group A RBC to affinity-captured anti-A IgG. The analysis of increasing concentrations of RBCs was conducted as outlined in *Figure 4.12.2.* A single set of interaction curves for each RBC concentration is shown. The initial binding rate for each curve was approximated by the slope of a line fitted to each curve. A linear fitting model was applied using BIAevaluation software. (b) Calibration curve constructed for the cell-binding rates as a function of sample concentration (c) Calibration curve of the RBC binding response against sample concentration. A 4-parameter equation was fitted to both calibration curves (see *section 3.2.5.2*).

However, a sufficient portion of the interaction curve was recorded to allow measurements to be taken. The initial binding rate for each curve was approximated by the slope of a line fitted to the data using BIAevaluation software. Visual inspection shows that the curves conform well to a linear association rate at lower RBC concentrations (i.e. lower binding rates). A calibration curve of the log of the cell binding rate against concentration (*Figure 4.2.3.2.2*(b)) shows that the binding rate increased exponentially with RBC concentration as the 4-parameter fitting reveals an approximately linear dependency. A plot of the log of the cell binding response against the RBC concentration

(*Figure 4.2.3.2.2*(c)) shows a curvilinear relationship using the 4-parameter fitting but the data could also be approximated by a conventional linear fitting (r^2 = 0.96). A similar pattern of deviations from linearity can be observed for both curves. These deviations may reflect the complex nature of the forces acting within the bulk and at the surface (section 4.2.5). However, RBC binding responses were low (R_{max} = 1300 RU) and conformity to a linear fit demonstrates that the surface did not approach the maximum response previously observed under similar experimental conditions (13-15 kRU) (*Figure 4.2.2.1* and *Figure 4.2.2.2*).

The agreement of RBC binding responses between replicates (n = 3) was poor (*Figure 4.2.3.2.2*(c)), indicating deterioration of the surface binding capacity. Further analysis of the experimental data revealed that the anti-A IgG binding response progressively decreased throughout the course of the analysis (*Figure 4.2.3.2.3*(a)). In addition, substantial accumulation of residual material (< 5,000 RU) (*Figure 4.2.3.2.3*(b)) occurred, thus accounting for the 60 % reduction in the antibody binding response. Hence, a decrease in cell binding avidity may be expected due to the lower number of potential surface contact points. This implies that cells will be bound less tightly, resulting in a decreased capacity to withstand the shear forces within the flow cell. These results demonstrate that sub-optimal surface regeneration seriously hinders solid-phase cell binding studies. Clearly, dilute NaOH and/or HCl solutions are not sufficient to remove cell debris at the surface. Consequently, a two-step regeneration process may be more effective. Bound RBCs may be eluted by hydrodynamic shear force generated by high flow rates and any remaining cells plus affinity-captured antibody may be removed using mild acid elution under hypertonic conditions.

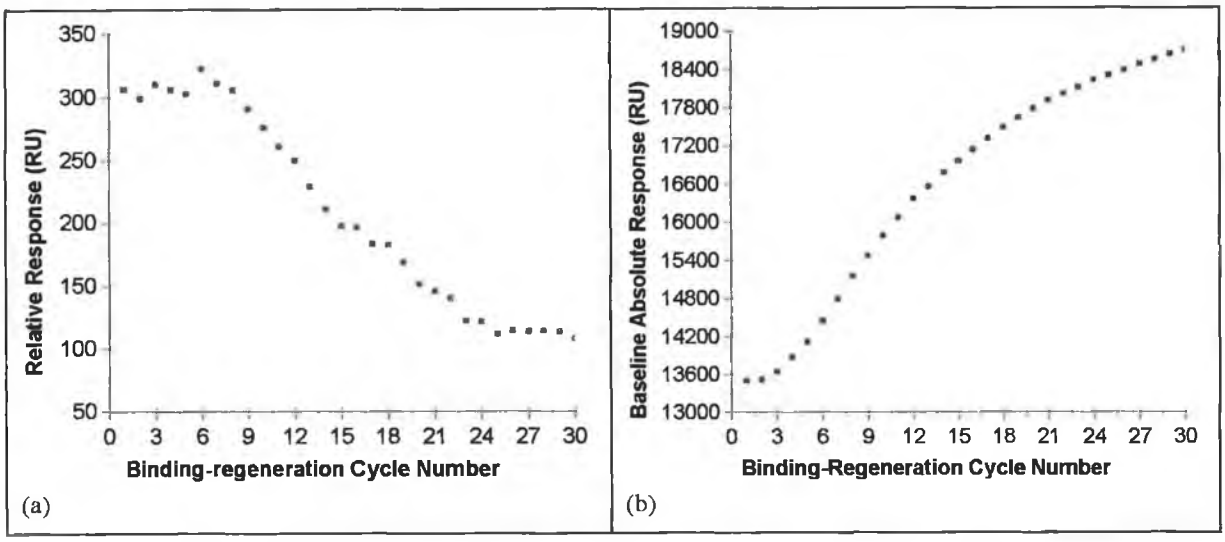

Figure 4.2.3.2.3. (a) Decreasing anti-A IgG affinity-capture response as a function of the interaction cycle number. (b) Increasing baseline response as a function of the interaction cycle number. The primary results and experimental details are outlined in *Figure 4.2.3.2.1* and *Figure 4.2.3.2.2*

4.2.3.3 *RBC Binding and Recovery.* Regeneration conditions employed during the previous experiments resulted in cell lysis which causes the release of intracellular biomolecules and membrane fragments; this may have contributed to the poor regeneration performance previously observed. However, elution of bound cells while maintaining cell integrity would eliminate these difficulties. In addition, the ability to recover viable cells would expand the potential of the technique to include cell isolation. The technique could be further optimised for cell recovery by minimising the cell contact time, thus avoiding excessive cell-binding avidity and undesirable metabolic changes in the target cells (occurs during solid phase isolation of lymphocytes). However, the implementation of this technique for the selection of other mammalian cells was not attempted due to the size limitations of the microfluidic cartridge.

The concentration of specific antibody, the copy number of the membrane-associated antigens, the conformation of the cell at the surface and the cell contact time dictate the cell-binding avidity. Hence, a low anti-A IgG binding response (431 RU) was employed. A high RBC binding response was observed (9,500 RU) and the interaction curve is shown in *Figure 4.2.3.3.* This response is far greater than the binding responses previously observed under similar conditions (*Figure 4.2.3.2.2*(a)) and may be attributed to donor variation (i.e. variable expression levels of the blood group A antigen). A low concentration of immobilised anti-A IgG was sufficient to anchor the cells to the surface and, hence, it was possible to elute 82 % of captured cells without inducing cell lysis by simply increasing the flow rate to 100 µl/min. The remaining cells and antibody were removed under non-lytic conditions using 20 mM sodium acetate buffer, pH 4.0, containing 0.5 M NaCl.

Regeneration of the surface without lysing the cells avoided exposing the surface to cell lysis products. Moreover, residual membrane fragments were not generated thus preserving the cell binding capacity of the surface. The combination of shear force and non-lytic pH elution proved successful in that 99 % of the bound RBCs and affinity-captured antibody were eluted. Consequently, a similar elution approach may be recommended for conventional solid phase cell selection.

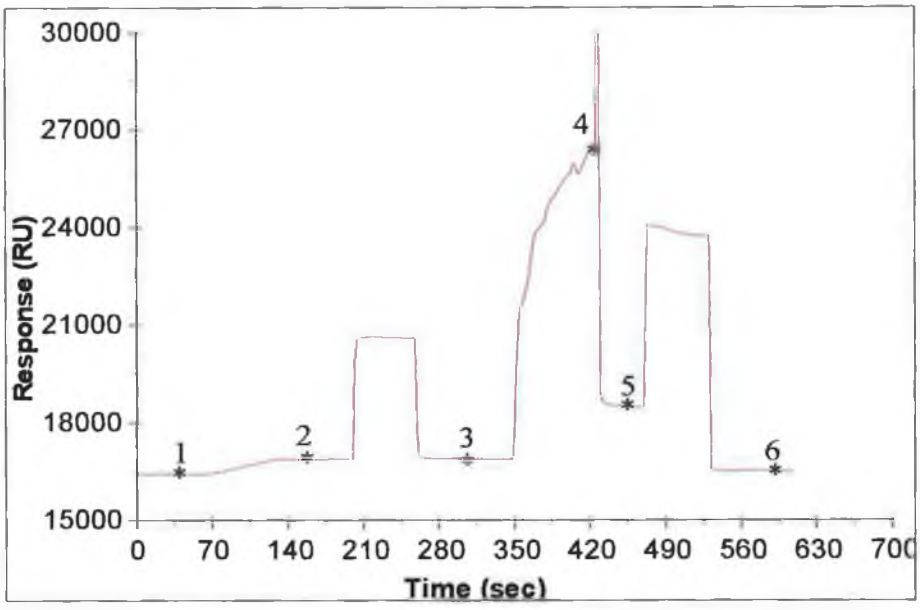

Figure 4.2.3.3. Protein A was immobilised (~ 5,400 RU) onto the dextran matrix using conventional amine coupling giving a stable baseline (**1**). 10 µl of anti-A IgG hybridoma supernatant (diluted 400-fold in HBS running buffer) was injected over the interaction surface at 5 µl/min giving a binding response of 431 RU (**2**). A 1 min pulse of 0.5 M NaCl was injected to determine whether baseline 'jumps' would occur due to matrix contraction under high ionic strength conditions. A low apparent increase in mass (~ 31 RU) occurred (**3**). Washed group A RBCs (1.0 x 10^9 RBCs/ml in HBS running buffer) were injected over the surface at 5 µl/min for 5 min giving a high cell binding response (~ 9,506 RU). The response spike is due to flow disturbances (**4**). The flow rate was increased to 100 µl/min and ~ 82 % of bound RBC were successfully eluted (**5**). The remaining RBCs and anti-A IgG were recovered under non-lytic conditions using a 1 min pulse of 20 mM sodium acetate buffer, pH 4.0, containing 0.5 M NaCl (**6**). This two-step regeneration procedure successfully removed 99 % of bound mass (i.e. RBCs and IgG).

4.2.4 ***Analysis of RBC Suspensions Using the BIACORE Probe™.*** The BIACORE Probe™ is a fiber optic SPR-based biosensor and represents a departure from the integrated analyser approach to biosensor design. A hand-held micropipette uptakes the sample, bringing it into contact with the sensing surface. The disposable fibre optic sensing surface (*Figure 4.2.4*), which employs the same hydrogel-based biointerface as the CM5 chip, is fitted to the pipette. Standard ligand

immobilisation chemistries can be applied. 'Real-time' data acquisition is not supported, but a touchpad control interface enables a single point measurement to be recorded. Furthermore, the sample temperature is not thermostatically controlled and can lead to significant signal drift if the temperature fluctuates ($> \pm 0.5$ °C) within the laboratory (N.B. the SPR response is significantly affected by temperature due to the thermal expansion of matter). A similar device was assembled ('in house') to enable 'real-time' monitoring of RBC-binding interactions and is described in detail in *chapter 5*.

Earlier studies using the BIACORE 1000™ demonstrated that immobilised antibodies are capable of reversibly binding RBCs from suspension. However, the occurrence of spurious signals, especially at high RBC concentrations (> 40 % (v/v)), proved to be a considerable limitation. It was expected that the use of the BIACORE Probe™ would avoid sampling difficulties as highly viscous samples (100 % (v/v) RBC) can be aspirated without cell damage. However, manual sampling demands strict time keeping and disciplined technique to ensure sampling reproducibility. Packed RBC samples were prepared by centrifugation and may be expected to contain > 5 % fluid (Chaplin and Mollison, 1952). These samples were used to prepare RBC concentrations in terms of % (v/v) rather than employing specific RBC counts (N.B. 100 % (v/v) RBC $\approx 11.6 \times 10^9$ cells/ml).

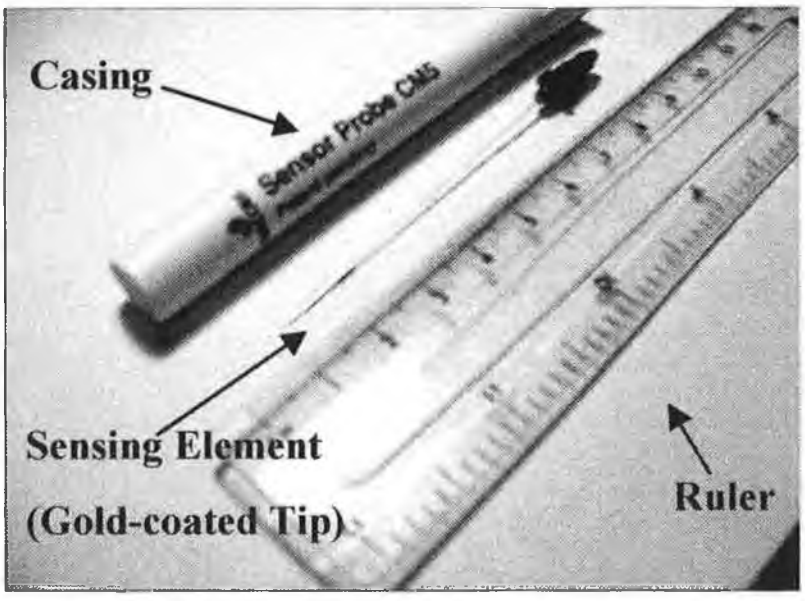

Figure 4.2.4 Digital image of the fibre optic CM5 sensing tip of the BIACORE Probe. The casing and ruler are shown as a reference scale.

4.2.4.1 *Calibration Curve for Protein A-anti-A IgG Interaction.* The previously established protein A affinity-capture format was applied. Protein A was immobilised and a titration curve for the interaction of anti-A IgG is shown in *Figure 4.2.4.1*. The protein A-coated surface was

regenerated repeatedly, allowing a large number of binding-regeneration cycles (> 40) to be completed. Very little variation in the background signal was observed (± 5 RU) during the course of this experiment since temperature variations within the laboratory were low (± 0.2 °C). The standard error recorded for each concentration (n = 4) was relatively low in view of manual control of the analysis.

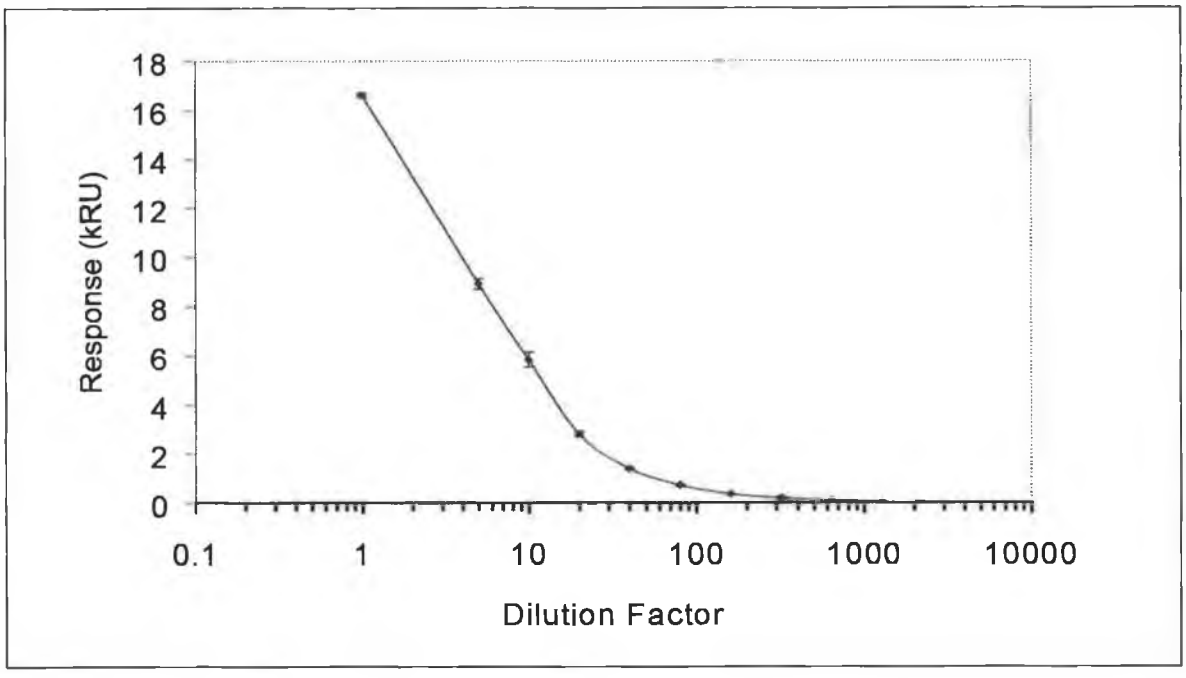

Figure 4.2.4.1. Calibration curve. Protein A was immobilised (~ 5.4 kRU) onto the CM5 sensor probe surface using conventional amine coupling and serum free hybridoma supernatant containing anti-A IgG was exposed to the surface for 2 min (n = 4). Regeneration of the surface was affected by a 30 sec pulse of 10 mM glycine, pH 1.7. The surface was exposed to PBS for 10 sec before and after sample analysis. Reliable binding measurements could thus be obtained despite bulk refractive index variations between sample solutions. The SPR response is a significant function of temperature and the sample temperature was not thermostatically controlled. However, a low background signal (± 5 RU) was observed during the course of this experiment since temperature variations within the laboratory were low (± 0.2 °C).

4.2.4.2 RBC Binding Variation as a Function of Immobilised Antibody Concentration.

Variation in the cell binding response with respect to the immobilised antibody concentration and the RBC concentration is shown in *Figure 4.2.4.2.* The probe surface reached a steady state binding response of ~ 13 kRU. Clearly, the effect of hydrogel exclusion was not overly limiting and this suggested that the cells deformed to occupy a large fraction of the volume immediately adjacent to the hydrogel. As expected, it was found that higher antibody levels at the surface promoted higher RBC retention, presumably due to increased binding avidity. A threshold contact time was required

to allow sufficient binding avidity to be generated to overcome resistive forces. Fluid dynamic shear forces were not as significant as observed during BIACORE 1000™ analysis, since flow injection analysis was not employed. However, sedimentation of the suspended RBCs, shear forces generated by the initial plunge into the sample and charge repulsion may all influence the binding response.

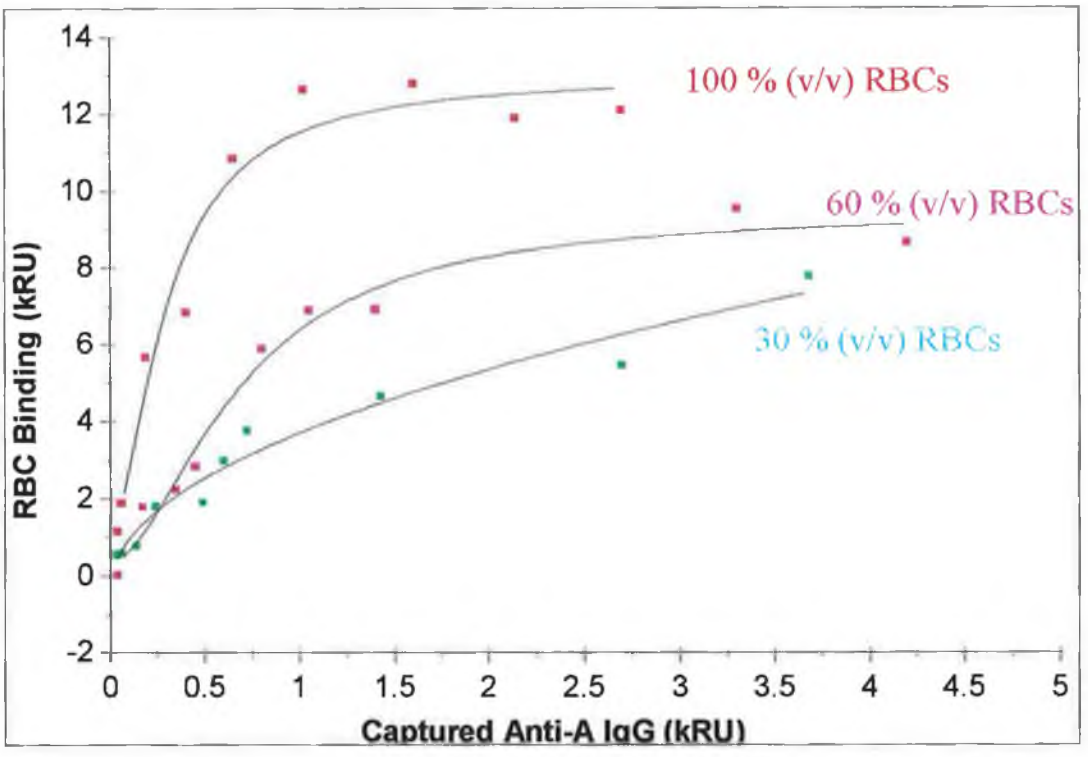

Figure 4.2.4.2. RBC binding response as a function of the captured anti-A IgG concentration as determined by BIACORE Probe™ analysis. Protein A was immobilised (~ 5.7 kRU) onto the surface using conventional amine coupling, as outlined for immobilisation of Con A (*Figure 4.2.1.1*). The surface was exposed to anti-A IgG (1/20 dilution of hybridoma supernatant in PBS) for a given contact time. Washed RBCs diluted in PBS were aspirated and allowed to interact with the surface for 1 min. Bound RBCs were removed by shear force using a wash bottle filled with PBS. The remaining antibody was removed using two 30 sec exposures to 10 mM glycine, pH 1.7, followed by a 10 sec exposure to 0.5 % Triton-X-100 in PBS. Neither blood group O RBCs (50 % (v/v)) nor group B RBCs (50 % (v/v)) were retained on the sensor surface (< 0.05 kRU) after washing. The above cycle was repeated for 100, 60 and 30 % (v/v) group A RBC samples employing variable anti-A IgG contact times, thus resulting in different antibody coating concentrations. (Note. The sensor tip was exposed to PBS before and after sample analysis in order to provide a baseline response from which the actual binding response could be reliably measured. This was consistently employed when recording binding measurements throughout the following studies).

It is important to emphasise that the probe was washed (i.e. three aspiration and dispensing cycles using PBS) after cell binding to remove weakly associated cells. Therefore, the cell binding response represents cells that are bound with sufficient avidity to withstand the shear forces generated by buffer aspirations during the washing step. Neither blood group O RBCs (50 % (v/v)) nor group B RBCs (50 % (v/v)) were retained on the sensor surface (< 0.05 kRU) after washing. Conventional pH elution of bound cells resulted in the accumulation of residual membrane fragments at the surface, as previously observed during BIACORE 1000™ analyses (*Figure 4.2.3.2.3*(b)). The lack of non-specific binding may be due to a combination of the hydrophilic properties of the dynamic hydrogel, charge repulsion and shear forces during washing. However, repeated cell binding-regeneration cycles resulted in stabilisation of the baseline response, presumably due to blocking of potential non-specific binding sites. Permanently bound residual cellular material may block non-specific binding sites or modify the exposed probe surface with membrane fragments, thereby conferring resistance to further non-specific adsorption. In addition, this surface was stable to conventional regeneration conditions.

Almost complete recovery of bound cells was accomplished by shear force elution employing a powerful buffer stream from a wash bottle, thus avoiding the accumulation of residual material. The captured antibody was then eluted using 10 mM glycine, pH 1.7. Replacement of the antibody layer after each binding-regeneration cycle was performed to avoid possible losses in the cell binding capacity that may result from antigen stripping. The possible accumulation of membrane fragments from residual cells that may have resisted shear elution was limited by including a 30 sec exposure to a detergent solution (0.5 % Triton X-100 in PBS). This sampling procedure was followed for subsequent analyses.

4.2.4.3 RBC Calibration Curve. A sigmoidal RBC titration curve for the interaction of increasing concentrations of RBCs with affinity-captured anti-A IgG is shown in *Figure 4.2.4.3*. The standard errors for replicates were higher at high RBC concentrations but remained acceptable for cell binding analysis. In contrast to the BIACORE 1000™ studies, packed RBC suspensions (i.e. 100 % (v/v) RBC) could be analysed, allowing a complete calibration curve to be constructed. The dynamic range for the sigmoidal calibration curve is very low (< 1 order of magnitude). The sigmoidal curve indicates that the binding response accelerates with respect to RBC concentrations less than 50 % (v/v) and decelerates at higher concentrations. In addition, the cell binding response reaches a plateau at high RBC concentrations due to saturation of the surface. The initial acceleration phase may be due to a variety of factors including steric co-operativity effects (i.e. at low surface coverage the collision of free cells with bound cells enhances the probability of retaining the free cell (section 4.2.5)). This region of the curve accounts for the approximate

exponential increase in response with increasing RBC concentration observed in *Figures 4.2.2.1*, 4.2.2.3 and *4.2.3.2.2.*

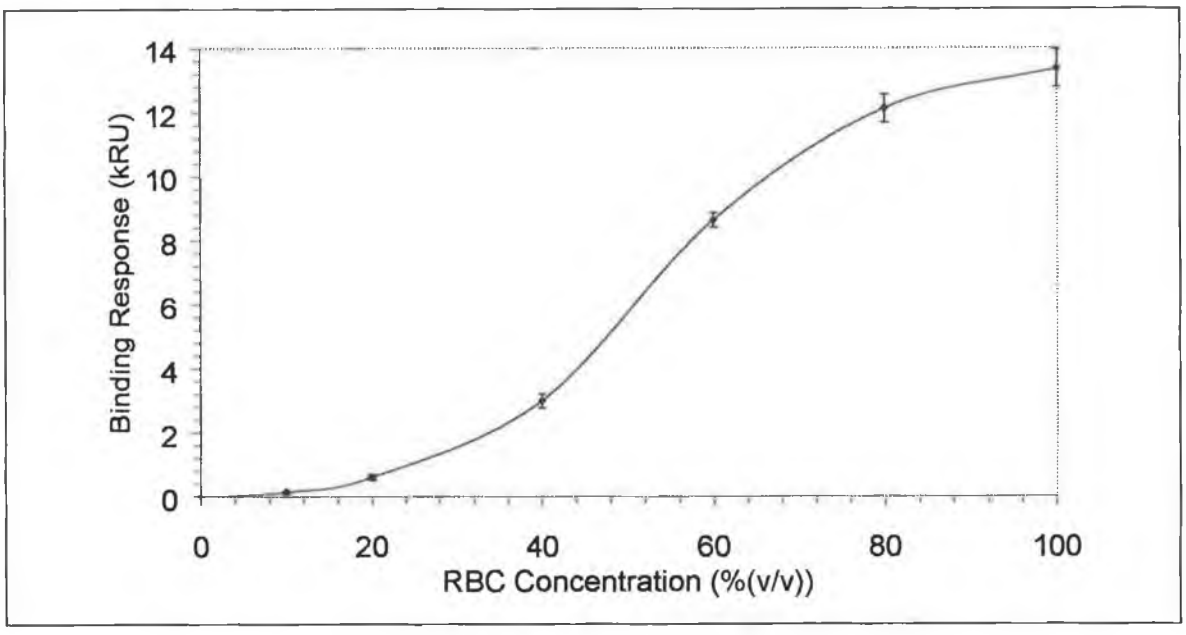

Figure 4.2.4.3. Calibration curve for the interaction of RBCs with affinity-captured anti-A IgG employing the BIACORE Probe™. Protein A was immobilised (5.7 kRU) onto the surface using conventional amine coupling. The surface was exposed to neat anti-A IgG hybridoma supernatant for 30 sec, resulting in the capture of ~ 3.5 kRU of antibody. Washed RBCs diluted in PBS were aspirated and allowed to interact with the surface for 1 min. The surface was regenerated as outlined in *Figure 4.2.4.2.* The above binding-regeneration cycle was repeated in triplicate for increasing group A RBC concentrations from 10-100 % (v/v).

4.2.4.4 *Effect of Presence of Non-Specific RBC Sub-Population.* The RBC binding response increases non-linearly with increasing cell density. If spatial separation of cells due to charge repulsion influences the cell-binding response, then the presence of a non-specific sub-population should increase the binding response. This was examined by analysing group A RBC suspensions prepared with and without group O RBCs. A series of group A RBC suspensions was prepared using PBS as diluent. A parallel series of samples was prepared using 50 % group O RBCs in PBS as diluent. The final group A RBC concentration was the same as the first sample series but the total concentrations of RBCs contained in the samples were 60, 70 and 80 % (v/v), respectively. The samples were analysed (n = 4) and the cell binding responses are shown in *Figure 4.2.4.4.* The presence of a non-specific sub-population extended the dynamic range for detection of the target RBC population. This effect may be attributed to charge repulsion and the proportional decrease in the free space within the mixed RBC samples as compared to the homogenous population. The sensitivity is sufficient for analysis of physiological concentrations of RBCs (~ 40 % (v/v)).

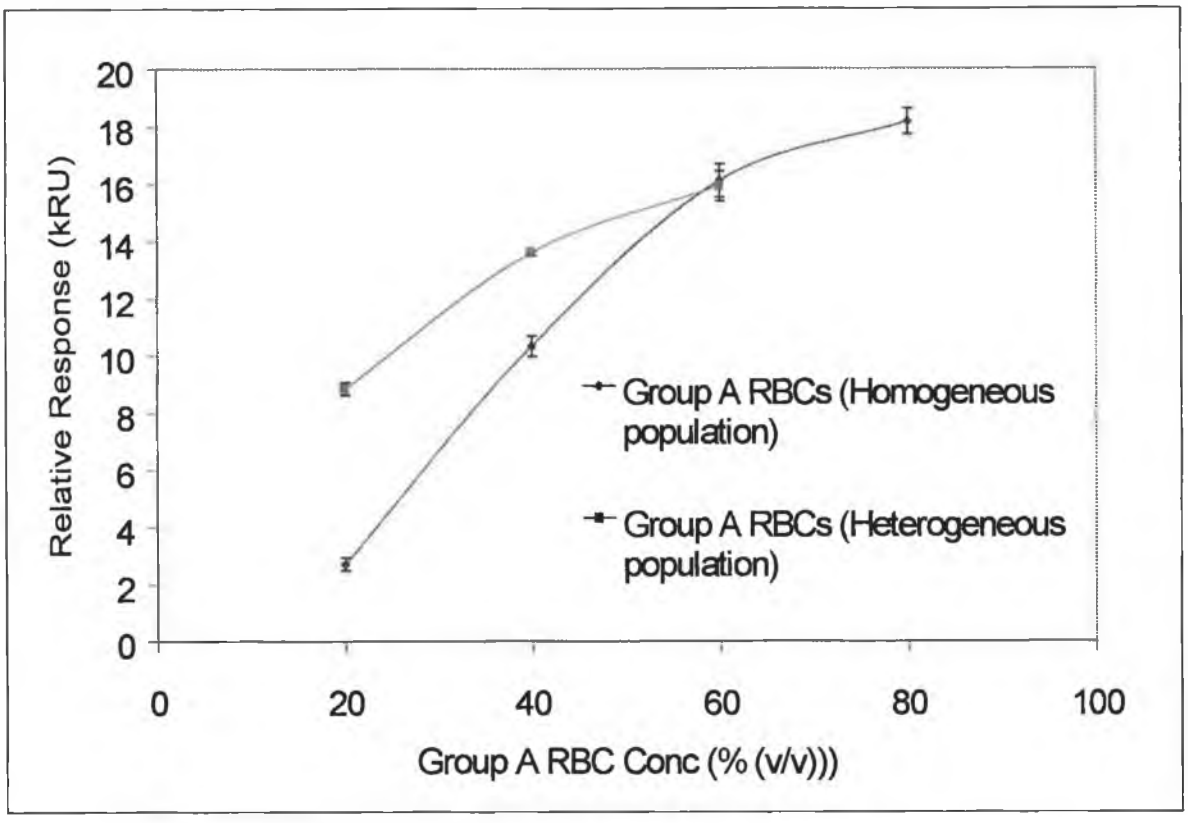

Figure 4.2.4.4. Plot of the RBC binding response against the RBC concentration for the determination of the effect of a non-specific sub-population on the binding response. Protein A (~ 6.2 kRU) was immobilised onto the CM5 sensor probe. Washed group A RBCs were diluted to 80, 60, 40, and 20 % (v/v) in HBS buffer. A parallel series of RBC concentrations were prepared using 50 % (v/v) group O RBC in HBS buffer. Hence, the final concentration of group A RBC contained in these samples was the same as the first sample series, but the total concentration of RBCs contained were 60, 70 and 80 % (v/v), respectively. The 80 % (v/v) group A RBC sample was omitted for the second series. The samples were analysed in quadruplicate as described in *Figure 4.2.4.2.* The analysis was also repeated for 100 % (v/v) group O RBC, resulting in a non-specific binding response of 0.09 kRU.

4.2.4.5. *Donor Variation of RBC Binding Response.* Washed group A RBCs (suspended at 50 % (v/v) in HBS buffer) from 18 donors were analysed and the results of the analysis are presented in the bar chart (*Figure 4.2.4.5*). Significant donor variation (~ 2-fold) in the RBC binding response occurred for both blood group AB and group A samples from eighteen individuals. This variation may be attributed to the diversity of possible genotypes for the A-antigen and, hence, the variable copy number of antigen per cell (section 4.1.1). However, all donor samples analysed gave a reliable binding response. The non-specific binding response was assessed using 50 % (v/v) suspensions of blood group O RBCs (n = 10) and blood group B RBCs (n = 10) in HBS buffer. These samples were analysed in an identical manner to the group A and AB donor

samples and resulted in an average binding response of < 0.01 kRU. The protein A-coated probe was found to be stable for at least 100 cell binding-regeneration cycles without deterioration of the RBC binding response. In any case, reduction in the antibody capture response can be offset by increasing the anti-A IgG sample concentration or increasing the sample contact time.

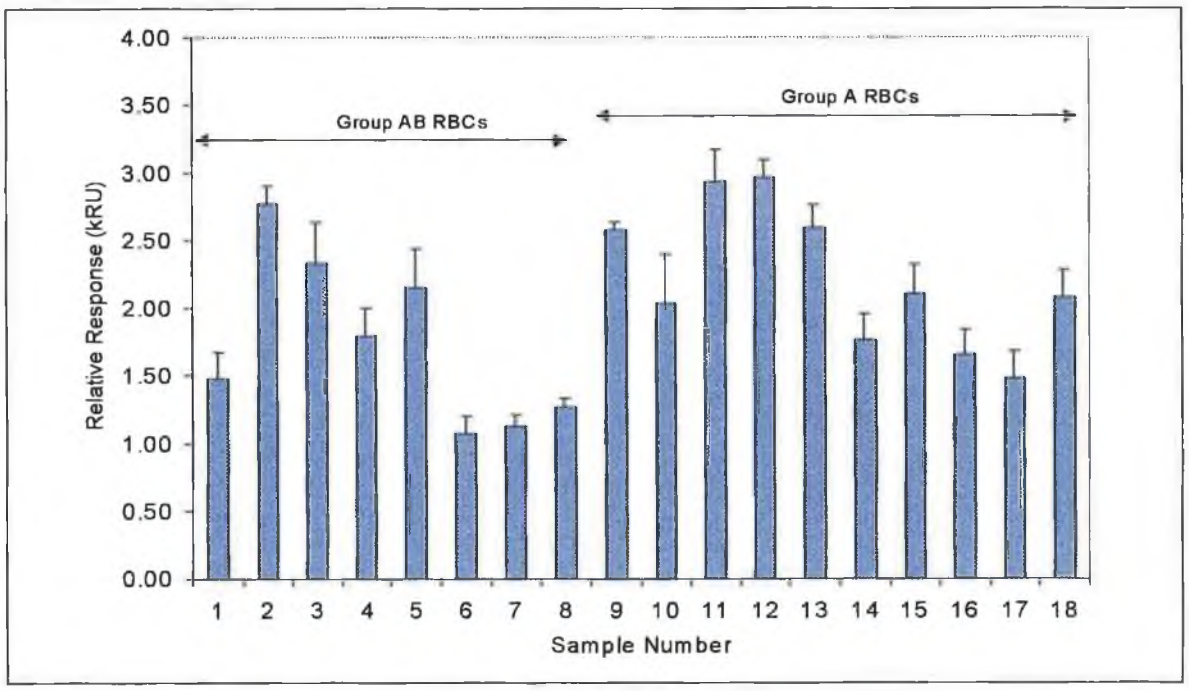

Figure 4.2.4.5. Bar chart illustrating the variation in the RBC binding response for individual donors. Washed group A RBCs from 18 donors were suspended at 50 % (v/v) in HBS buffer and analysed (n = 4) as outlined in *Figure 4.2.4.3* and the results of the analysis are presented above. The non-specific binding response was assessed using 50 % suspensions of blood group O (n = 10) and blood group B (n = 10) giving responses of < 0.01 kRU.

4.2.4.6 *Whole Blood Grouping.* The experimental results presented thus far using the BIACORE 1000™ and the BIACORE Probe™ were performed using washed RBC preparations. However, such tedious washing procedures are not compatible with large-scale blood grouping. However, the analysis of whole blood samples is complicated by non-specific binding of anti-coagulated plasma components to the CM5 sensor probe. Consequently, the degree of non-specific binding of anti-coagulated plasma to a protein A-coated CM5 sensor probe was examined, in terms of the reproducibility of the response for a single donor and binding variation between donors. Non-specific binding of plasma from a single donor to the probe was found to be reversible and reproducible (*Figure 4.2.4.6.1(a)*). A stable response of ~ 13 kRU was observed over 10 binding-regeneration cycles. Furthermore, successful regeneration of the surface was accomplished. The experiment was repeated for 20 donor samples (*Figure 4.2.4.6.1(b)*) and showed that both the

plasma binding response and regenerability of the surface were consistent between donors. Consequently, whole blood grouping was performed as outlined earlier (*Figure 4.2.4.2*) but with an additional plasma-blocking step.

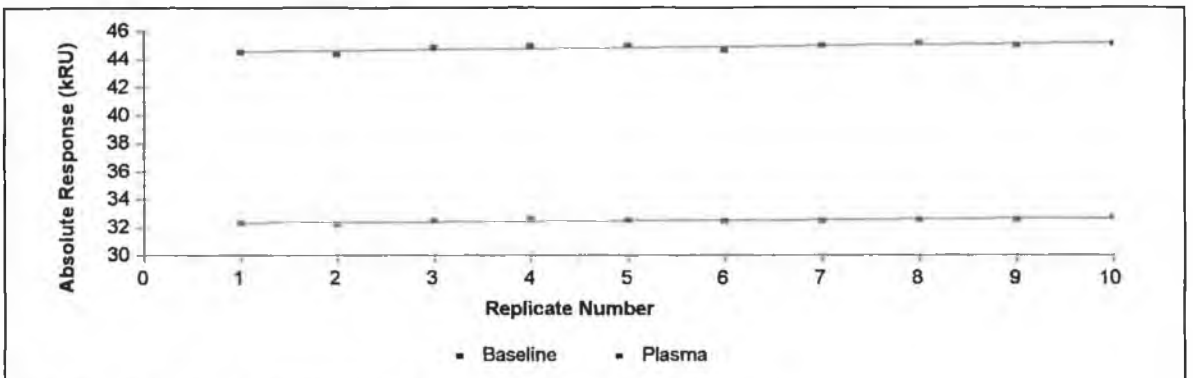

(a) Baseline slope of 0.0357 and plasma binding slope of 0.665

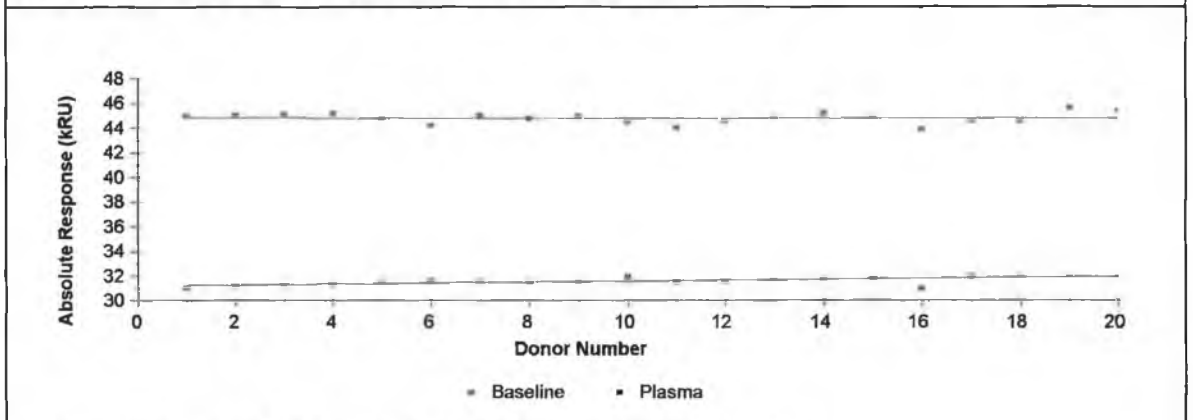

(b) Baseline slope of 0.0386 and plasma binding slope of -0.0026.

Figure 4.2.4.6.1. Binding and regeneration response profiles for a single donor and multiple donors. The analysis was conducted on a protein A-coated (6.4 kRU) CM5 sensor probe surface. The plasma sample was aspirated and remained in contact with the surface for 2 min. The bound plasma components were removed using three consecutive exposures (30 sec) to 0.1 M glycine, pH 1.77, 15 mM NaOH and 1 % Triton-X-100 in PBS, respectively. **(a)** Binding and regeneration response profile for 10 replicates of the above binding-regeneration cycle using EDTA anti-coagulated plasma obtained from a single donor. **(b)** Binding and regeneration response profile for 20 EDTA anti-coagulated plasma samples obtained from 20 separate donors.

Whole blood grouping was performed as illustrated in *Figure 4.2.4.6.2*(a). Manual readings were recorded at 5 sec intervals during the interaction, allowing a semi-'real-time' interaction curve to be plotted. Anti-A IgG was affinity-captured onto the surface and non-specific binding sites were blocked by exposure to pooled anti-coagulated plasma. The semi-'real-time' interaction curves indicate that the non-specific binding interaction approaches equilibrium after a 2 min exposure.

Group A anti-coagulated whole blood was allowed to interact with the blocked surface for 1 min. The surface was regenerated as outlined in *Figure 4.2.4.6.1*. A reference curve was obtained by repeating the above analysis but replacing the whole blood sample with a pooled plasma sample. *Figure 4.2.4.6.2*(b) is an overlay of the final section of the complete interaction curve. As a control, the above analysis was completed for group O whole blood and the interaction curve derived from this analysis is shown together with the group A RBC binding response curve and the plasma reference curve. Both negative controls (i.e. group O whole blood and neat plasma) samples resulted in a binding signal of ~ 1 kRU. The agreement between both controls suggests that non-specific binding of group O whole blood is mainly due to the adsorption of plasma components as opposed to non-specific cell adsorption. Plasma components may have adsorbed to the surface as the blocking response had not reached absolute saturation. However, the exposure time during the blocking step was sufficient to reduce non-specific binding to an acceptably low level. Moreover, the group A whole blood binding response (3,5 kRU) was significantly greater than the negative controls, thus substantiating the specific retention of group A RBCs. Furthermore, the analysis demonstrated that solid phase whole blood grouping can be accomplished within a short (5 min) sample analysis time.

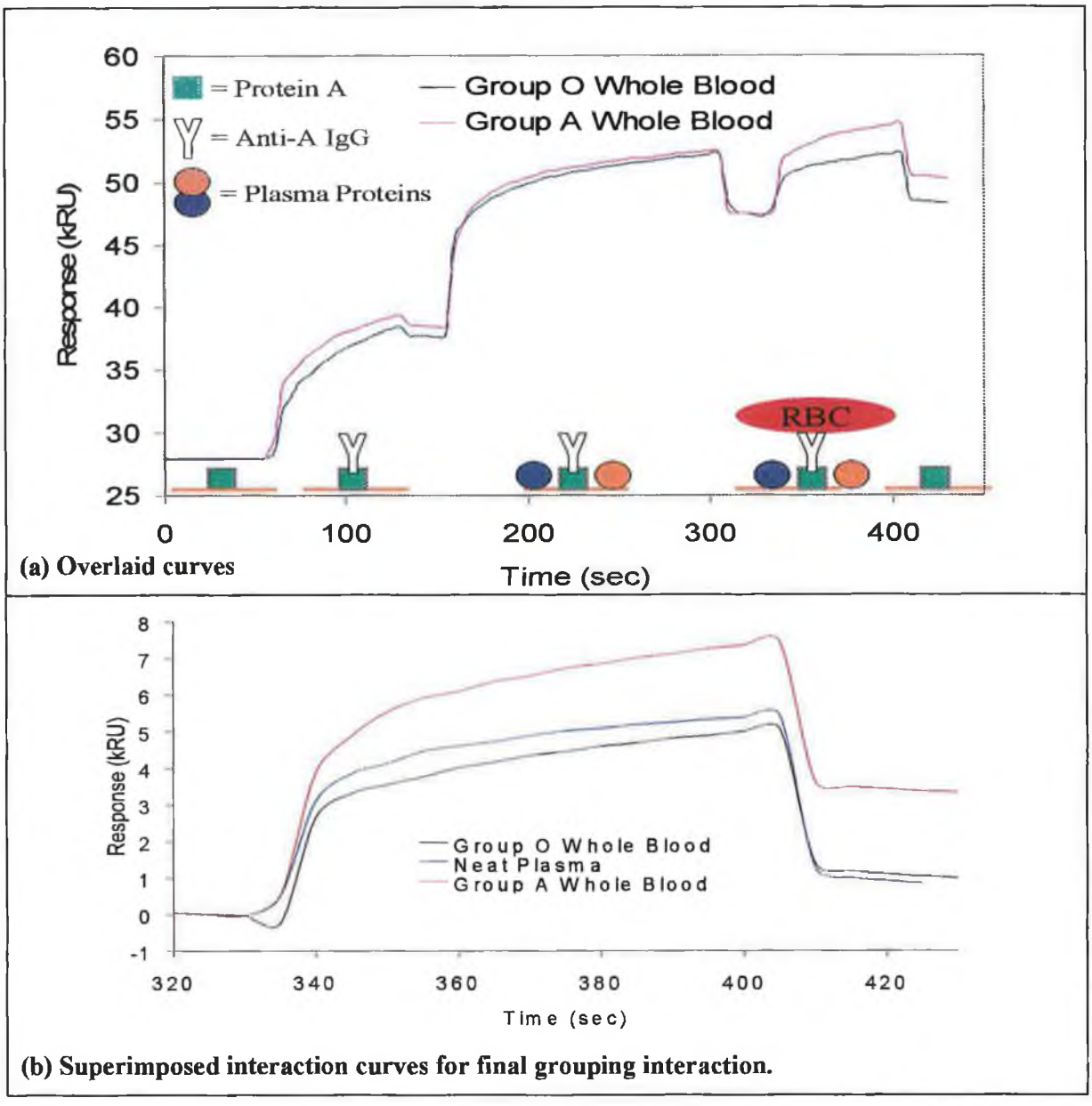

Figure 4.2.4.6.2. **(a)** Overlaid sensorgrams for semi-'real-time' monitoring of the whole blood typing interaction cycle. Protein A was immobilised (~ 5.7 kRU) onto the surface using conventional amine coupling. The surface was exposed to neat anti-A IgG hybridoma supernatant for 1 min, resulting in the capture of ~ 9.5 kRU of antibody. Neat EDTA-anti-coagulated plasma was aspirated and allowed to interact with the surface for 2 min. EDTA anti-coagulated whole blood was aspirated and allowed to interact with the surface for 1 min. The surface was regenerated as outlined in *Figure 4.2.4.6.1* (Note. the probe was briefly incubated in PBS before and after each sample to allow reliable binding response measurements to be recorded). As a control the above binding-regeneration cycle was repeated employing group O whole blood. **(b)** Overlay of the final section of three normalised (with respect to initial baseline) sensorgrams for the whole blood typing interaction as outlined in (a). Neat plasma and group O whole blood were employed as negative controls to determine the non-specific binding response.

4.2.4.7 Conformational Changes of Captured RBCs. Liu *et al.* (1994) showed that immobilised endothelial cells resist shear stress within a flowcell through surface tension. In addition, the slope and curvature of the cell membrane indicated that the static pressure inside the cell was higher than in the flowing fluid. Furthermore, surface tension was transmitted along cells in contact with each other in the direction of flow, leading to the accumulation of tensile stress. These observations may be applicable to solid phase RBC detection in a flowcell. RBCs bound to the surface are exposed to similar shear forces. However, transmission of surface tension can only occur when cells are in contact. Hence, transmission of tensile force may be significant when the cell coverage approaches saturation but is unlikely to be an important factor at low RBC binding levels. Viscoelastic RBCs adsorbed to a surface may resist shear stresses through membrane tension but will deform towards the surface. Deformation of RBCs at the surface may account for the high binding responses observed and the increasing responses observed after termination of the sample injection (e.g. *Figure 4.2.2.1* and *Figure 4.2.2.2*). Heterogeneous association phase curves were observed during BIACORE 1000™ analysis and were characterised by a shoulder as a pseudo-steady state response was approached. This is particularly evident in *Figure 4.2.2.2* and suggests that a rapid conformational change of the bound cells may occur. This apparent conformational change was observed during BIACORE 1000™ analyses and may result from a number of factors including antigen capping, membrane tension, ionic repulsion, shear stress and overcrowding at the surface. However, the possibility that this effect is caused by flow disturbances cannot be dismissed.

A microscopic image of the cells bound to the CM5 sensor probe surface is shown in *Figure 4.2.4.7*. The RBCs appear to be erect on their side in an ordered manner. This conformation may be attributed to the sampling technique. Briefly, the probe is plunged into the sample, which is held in an upright position. Gravity encourages the unstirred RBCs to sediment and to assume a balanced position according to their center of gravity. Hence, cells will tend to collide with the probe surface along their edge resulting in an erect conformation when the probe is viewed in a horizontal position, as observed in *Figure 4.2.4.7*. Alternatively, overcrowding within the sample and/or thermodynamic surface tension, which may result from capping of membrane-associated blood group A antigens, combined with ionic repulsive forces may cause cells to adopt this surface conformation.

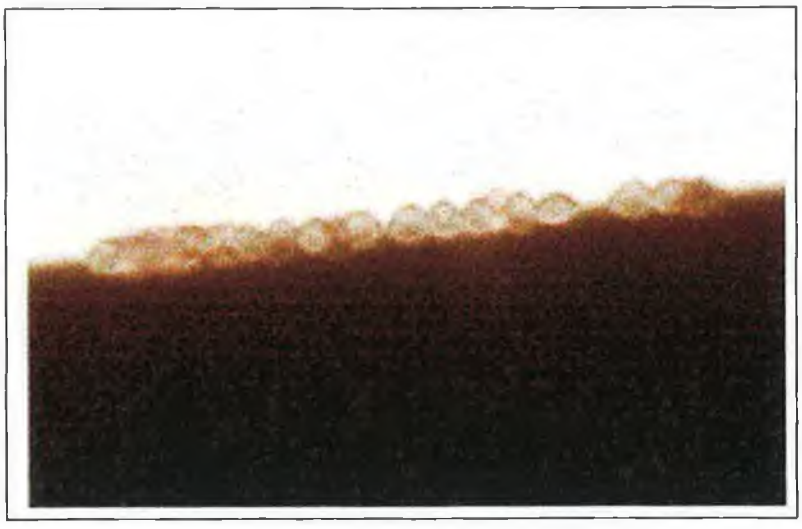

Figure 4.2.4.7. Microscopic image of RBCs bound to the CM5 sensor probe. Interestingly, the RBCs appear to be anchored in an ordered conformation. The cells appear erect on their edge as opposed to their flattened surface.

4.2.4.8 *Saturation Response.* The maximum response observed for a given RBC concentration varies considerably between donors. Hence, accurate binding response comparisons cannot be made between experiments. Complete saturation was not observed for the BIACORE 1000™ analysis, since the force balance at the interaction surface imposed an upper limit on the cell binding response. However, the saturation response should remain constant for both the BIACORE 1000™ and BIACORE Probe™ sensor. The saturation response is dependent on the refractive index of RBCs and the maximum volume fraction that can be occupied by cells outside the hydrogel matrix. The refractive index (n) of a RBC is 1.39, and this corresponds to the refractive index of 47.75 % (v/v) glycerol:water as determined from the equation (n = 0.01207 x (%Gly) + 1.332215) of a calibration curve constructed using an Abbè refractometer (*Figure 5.2.1.5.1*). The expected BIACORE 1000™ response, assuming 100 % surface coverage and a non-dextranated surface, can be calculated from the equation of a calibration curve (RU = 1207 x (%Gly) + 8667.7) constructed using the BIACORE 1000™ and glycerol:water mixtures (*Figure 5.2.3.4.1(b)*). At 100 % surface coverage the response was calculated to be 66,000 RU but the presence of the dextran matrix (100 nm thick) would be expected to lower the expected response to 23,700 RU. However, a maximum experimental response of 18,100 RU was observed using a 'real-time' fibre optic SPR biosensor (*Figure 5.2.2.7*). This response represents 76 % of the theoretical saturation response, assuming that the cells cannot penetrate the hydrogel and that the penetration depth of the evanescent wave is 190 nm (Liedberg *et al.*, 1993). Furthermore, it is unlikely that maximum packing of the RBCs at the surface will approach 100 % occupation of the probed volume located outside the matrix. Hence, 24

% cell-free space outside the hydrogel suggests that the surface must be close to saturation and that RBCs are capable of considerable deformation.

The expected maximum response for the BIACORE Probe™ can be similarly estimated. The SPR response obtained for the fibre-optic device deviates substantially from linearity since the SPR signal is more sensitive at higher wavelengths. In contrast, the SPR signal for a fixed-wavelength angular-dependent SPR configuration is a linear function of surface mass concentration. The CM5 sensor probe employs the same biointerface as the BIACORE 1000™ and may be expected to yield a comparable coverage at saturation. Furthermore, reduced hydrodynamic resistances combined with vertical sampling may facilitate the cell binding process.

4.2.4.9 Advantageous Properties of the RBC Detection Format Examined. The beneficial properties of the RBC detection format investigated are listed.

1. Crude hybridoma supernatants diluted 400-fold (< 0.2 μg/ml IgG) were employed thus obviating the requirement for affinity purification of the antibody.
2. A high degree of control of IgG immobilisation was possible. (It is essential to adsorb the antibody at the desired surface density in order to avoid high cell binding avidity).
3. Specific retention of RBCs was demonstrated at low antibody concentrations and bound cells could be eluted using shear force by increasing the flow rate.
4. Non-specific binding of RBCs from other blood groups to the hydrogel-coated surface was not detected
5. Protein A can bind a large variety of IgG subtypes from many species. (Hence, antibodies specific for a variety of membrane-associated antigens could be used to capture a variety of cell types from suspension).

4.2.5 ***Dynamics of RBC Binding.*** An approximate steady state (i.e. pseudo-steady state) RBC-binding response was observed during both BIACORE 1000™ analysis (*Figure 4.2.2.1* and *Figure 4.2.2.2*) and fibre optic SPR sensor analysis (*Figure 5.2.2.5*). The RBC binding curves obtained from both systems may be interpreted as described in *Figure 4.2.5*. The sensor surface is free of RBCs at the moment of exposure to the RBC suspension. During the initial injection phase, convective forces transport cells to the surface where they bind via specific interactions with an immobilised ligand. The exponential decay of the binding response and the subsequent pseudo-steady state response may be created by the formation of a cell-free zone at the surface. This may result from the tendency of bound RBCs to repel free RBCs due to charge repulsion. In addition, the presence of excess cells in the bulk may cause the net repulsion force to move cells into the cell-binding zone and thus the pseudo-steady state response will increase with increasing RBC concentration. This increase was non-linear as observed in *Figure 4.2.4.3*. The non-linearity arises from a combination of steric effects and the progressive approach to saturation.

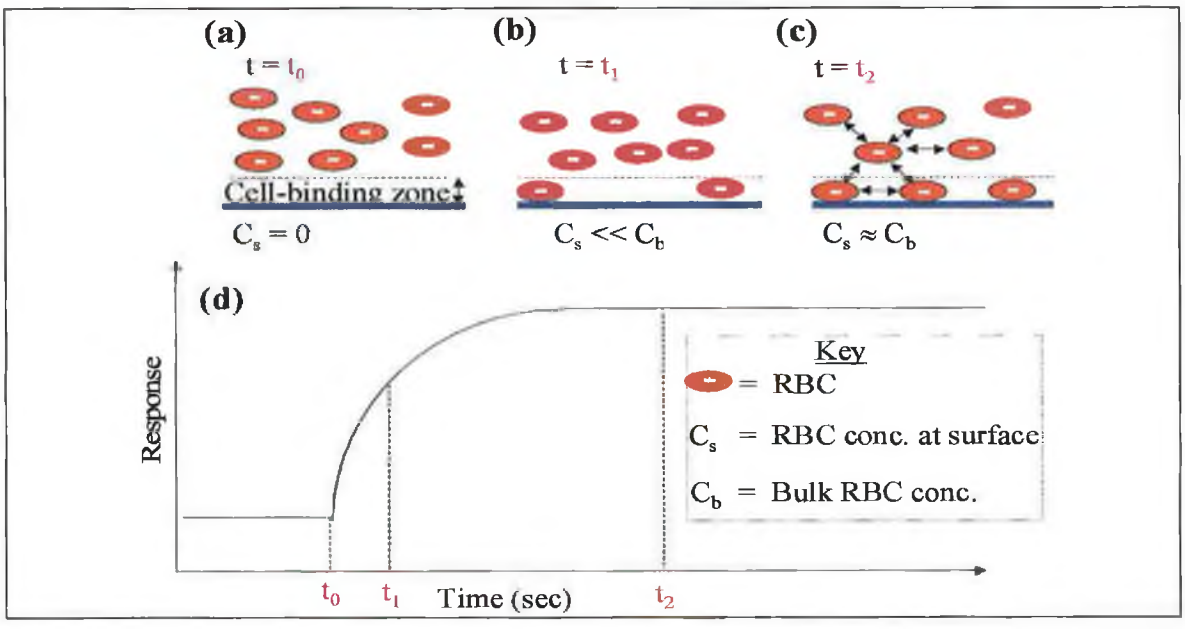

Figure 4.2.5. Illustration depicts the pseudo-steady state mechanism. The sensor surface is coated with a specific antibody that recognises a specific membrane-associated antigen. (a) Point of injection of the RBC suspension. At this instant the cell-binding zone at the sensor surface is free of cells. (b) The cell binding response exponentially declines as binding progresses but the concentration of the cells at the surface is still less than the concentration in the bulk. (c) A pseudo-steady state is reached where cell binding ceases as the concentration of cells at the wall approximates the concentration in the bulk. This may be an oversimplification as the contribution of binding avidity and complex fluid dynamic effects were not considered. Cells at the surface and within the bulk exert ionic repulsive forces on each other that may maximise the distance between cells and thus, prevent free cells from entering the cell-binding zone. (d) Simulation of a RBC interaction curve showing the time-dependent changes of the binding response illustrated in (a), (b) and (c).

4.2.5.1 Qualitative Model for Cell Binding in a Flow Stream. A qualitative model describing the dynamic forces acting within the bulk flow and at the interaction surface will be presented. The cell binding process requires bulk transport of the RBCs to the interaction surface and the generation of sufficient binding avidity to overcome resistive forces. Hence, bulk fluid dynamic and surface binding effects influence the cell binding response. The cell must come into contact with the surface for sufficient time to allow the formation of specific interactions between the immobilised ligand and the membrane-associated antigen. Small cells are more easily retained at the surface because they are less effected by wall shear stress (Zydney and Coulton, 1984). The residence time of the cell at the surface is inversely proportional to the wall shear rate as both the cell-cell collision force and the surface shear stress increase linearly with shear rate.

4.2.5.2 Bulk Transport. The diffusion of small particles is described by the Stokes-Einstein expression for Brownian diffusion and is given by:

$$D = \frac{k\,T}{6\,\pi\,\mu\,r_p}$$

where D = Diffusion coefficient (cm^2/s)

k = Boltzman constant ($erg\ K^{-1}$)

T = Absolute temperature (K)

μ = Viscosity (poise)

r_p = Particle radius (cm)

However, the diffusion of large particles such as RBCs does not obey this expression due to the complex motion exhibited by particles in a shear flow of a concentrated suspension (Zydney and Colton, 1984; Stamatakis and Tien, 1993). Suspended cells rotate producing a rotational flow in the surrounding fluid that exert drag forces on the adjacent cells. Cells travel at different velocities within the fluid streamlines due to the parabolic velocity profile in a flow channel. Collisions occur between these cells causing lateral migration of cells. Hence, the motion of a given cell is the sum of the undisturbed motion expected in the absence of other cells combined with rotational and convective motion induced by the neighbouring cells. Therefore, the motion of the suspended cells is random and can be described by an effective shear-induced diffusivity (D), which is given by the following expression:

$$D = 0.03\,a^2\,\gamma$$

where a = Cell radius

γ = Shear stress

Concentration gradients within the flowcell cause local changes in the viscosity of the suspension

that affect shear-induced diffusion of the cells. Cells moving into a region of high concentration experience greater resistance than particles moving into regions of low concentration, causing a net drift from regions of high concentration to regions of low concentration. Hence, shear-induced diffusion is strongly dependent on the cell concentration and is proportional to shear stress and the square of the cell radius. Furthermore, hydrodynamic forces can result in the establishment of concentration gradients within the flowcell. The tubular pinch phenomenon causes depletion of cells in the region close to the wall (Lokine *et al*, 1992). The tubular pinch effect arises from the curvature of the velocity profile of a fluid within a narrow channel and inertial effects at a solid boundary. Cells assume an equilibrium position between the flow channel axis and the surface, but other forces (e.g. fluid dynamic forces, gravitational force) can distort the position of this concentration gradient.

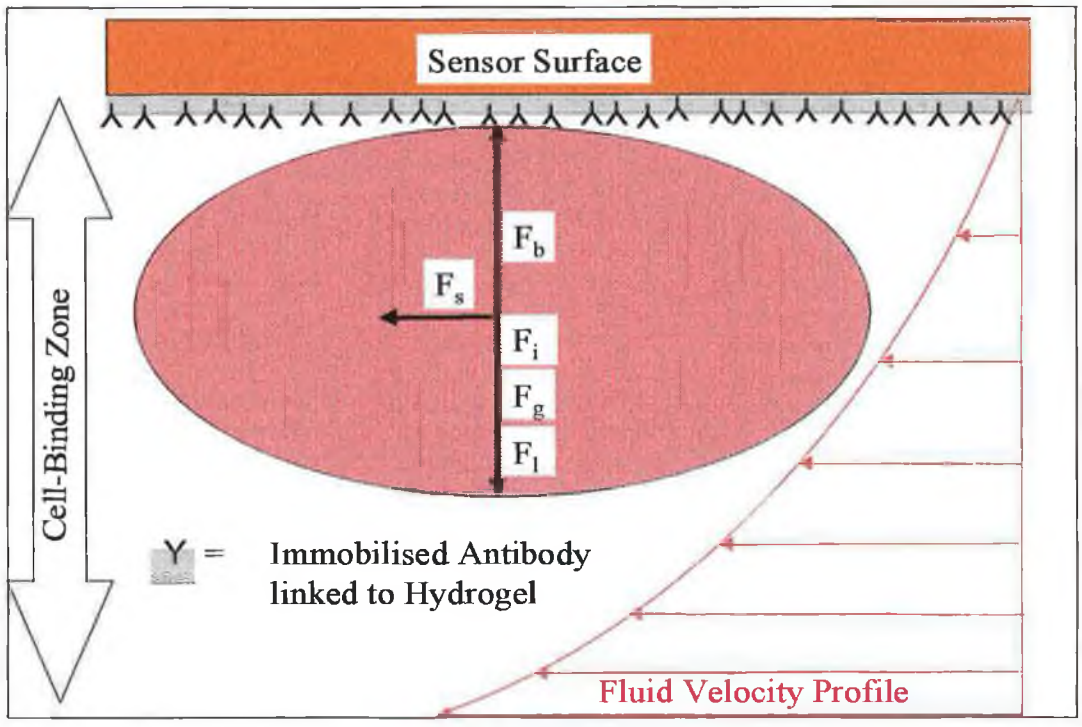

Figure 4.2.5.3. Diagrammatic illustration of the forces acting on the cell at the surface during binding.

4.2.5.3 *Surface Binding Forces.* Particle adsorption is dictated by a number of fluid dynamic and electrochemical forces that have been described for cross-flow microfiltration systems (Hwang *et al.*, 1996). The forces acting within the BIACORE 1000™ are similar, but, in contrast to the microfiltration systems, the adsorption surface is non-porous. Hence, *Figure 4.2.5.3* is a schematic illustration of cell binding to a sensor surface within a fluid stream and the direction of these fluid dynamic forces. After transport of the cell from the bulk to the sensor surface, forces acting on the cell either oppose or promote cell binding and the net result of the force balance

dictates whether the cell will remain at the surface or be released into the bulk. The net binding force (F_{net}) can be written as:

$$F_{net} = F_b - F_s - F_i - F_g - F_l$$

where F_b = Binding avidity force

F_s = Shear-induced force

F_i = Ionic repulsion

F_g = Gravitational force

F_l = Lateral lift force

The binding avidity force results from multiple binding interactions between membrane-associated antigens and the immobilised antibody. The magnitude of the avidity force is dependent on the affinity of the antibody-antigen interaction and the number of specific interactions formed. The affinity of the interaction is a product of hydrogen bonding, hydrophobic interactions, ionic interactions, Van der Waal's forces and topographical complementarity between the antibody and the membrane-associated antigen. Furthermore, the cell must be in contact with the surface for a sufficient period of time to allow a threshold avidity to be generated. The threshold avidity force required for cell retention is greater than the accumulative resistive forces. Furthermore, the binding avidity may be expected to increase with increasing contact time due to capping of membrane-associated antigens.

The shear-induced force (F_s) increases linearly with respect to the fluid velocity and the square of the cell diameter as described by the expression:

$$F_s = 1.276\, \pi\, \rho_f\, d_p^2\, f\, U_f$$

where ρ_f = Fluid density

d_p = Particle diameter

f = Friction factor

U_f = Fluid velocity

Hence, large RBCs (d ≈ 0.7 μm) will be subjected to this force to a much greater degree than microbial cells (< 1 μm). Therefore, low flow rates must be employed to maximise the cell binding response.

Ionic repulsion was found to be the dominant resistive force for suspensions of latex particles (d = 0.021-0.1 μm) during cross-flow filtration experiments (Hwang *et al.*, 1996). It was found that charge repulsion between the particles was dependent on the pH and ionic balance of the solution. The RBC membrane is highly negatively charged due to the presence of sialic acid residues and the resulting ionic repulsion prevents RBCs from adhering to each other or to the negatively charged

CM-dextran hydrogel. In summary, the shear-induced force, sedimentation and ionic repulsion may be expected to significantly influence the pseudo-steady state binding response observed in *Figure 4.2.2.1 and Figure 4.2.2.2.* The cell sample is delivered to the surface via the microfluidic cartridge through a series of flow channels (d = 50 μm). Hence, at low flow rates shear-induced diffusion may not be adequate to prevent sedimentation of the cells. Sedimentation may be expected to reduce the cell binding response as the sensing surface of the BIACORE 1000™ is positioned on the upper surface of the flowcell. Hence, the ideal flow rate represents a compromise that minimises shear forces while preventing sedimentation of the cells. The gravitational force causes sedimentation of the dense RBCs and is given by the following expression:

$$F_g = \frac{\pi}{6}(\rho_c - \rho_f) d_p^3$$

where F_g = Gravitational sedimentation force

ρ_c = Density of the cell

ρ_f = Density of the fluid

Other symbols have their usual meaning

The lateral lift force (F_l) arises from inertial effects at a solid phase boundary and causes cells to migrate away from the interaction surface. It is linearly dependent on the fluid velocity, sample viscosity and the cell diameter. It is described by the following expression:

$$F_l = 3\pi\ \mu\ d_p U_f$$

where μ = Fluid viscosity

Other symbols have their usual meaning

4.2.5.4 Cell Adsorption to Cell-Coated Surfaces. The retention of RBCs colliding with the surface will be affected by the angle of repose (i.e. angle at which the cell strikes the surface). The predominant motion of a cell within the suspension will be in the direction of flow. Lateral migrations of cells due to chaotic shear-induced diffusion may increase the angle of repose for a given cell. However, increasing the flow rate will lower the angle of repose and, thus, the probability of a cell being retained. Furthermore, the presence of previously bound cells at the surface may facilitate the retention of free cells. The force balance of a free cell colliding with these surface protrusions (i.e. bound cells) will vary depending on the angle of contact but these protrusions may increase the probability of cell retention as compared to a smooth surface (Stamatakis and Tien, 1993). Evidence for this co-operative binding effect was observed in *Figure 4.2.1.2.*

The course of a typical RBC interaction curve is characterised by biphasic behaviour (*Figure 4.2.2.1* and *4.2.2.2*). Initially, an exponentially decaying binding rate is observed that reaches a pseudo-steady state response. Dissociation of bound cells was not observed due to the high binding avidity (or masking of the signal due to cell deformation). Hence, if cell dissociation can be neglected, then the cell binding response almost completely ceases during the pseudo-steady state phase as opposed to an equilibrium state where the rate of binding is balanced by the rate of dissociation. The absence of cell binding during this phase may result from the inability of the cells to reach the cell-binding zone and may be predominantly due to charge repulsion that results in the generation of a cell-free zone at the RBC-coated surface.

4.3 Conclusion.

Specific affinity-capture of RBCs onto the Con A-coated surface was demonstrated as a model study using the BIACORE 1000™. An exponential decay in the binding response on approach to a pseudo-steady state was observed. In addition, cells were bound with high avidity since very little dissociation of captured RBCs occurred; hence, conventional regeneration of the surface was not satisfactory. Efforts to optimise regeneration conditions were unsuccessful as complete regeneration of the surface without reducing the biological activity of Con A was not possible.

Solid phase blood grouping was accomplished by immobilising blood group-specific antibodies (anti-A IgG and anti-B IgM) and monitoring the SPR response as RBCs were injected over the sensor surface. In agreement with the Con A experiment, the curves were characterised by a rapid exponentially decaying association phase and the binding rate was proportional to the cell concentration. This phase was followed by a gradual approach to a pseudo-steady state. Dissociation of bound RBCs from the sensor surface proceeded slowly, which is indicative of high avidity between the multivalent IgM and the captured RBCs. RBC binding was found to be specific with negligible non-specific binding during control cycles. However, shear forces within the flowcell combined with ionic repulsion forces may discourage non-specific binding.

The maximum binding response recorded represented 76 % occupation of the volume immediately outside the hydrogel. A free volume of only 24 % suggests that considerable deformation of the bound RBC must occur to enable such high surface coverage. In addition, the positive dissociation phase and the heterogeneous association phase observed provide further evidence for surface deformation. A calibration curve of the binding response against the RBC concentration revealed an exponential dependency of the binding response at low RBC concentrations. However, the cell binding capacity decreased due to a combination of antibody denaturation, stripping of BGAA from cells and the accumulation of residual cellular material. This severely restricted the number of cell-binding-regeneration cycles (i.e. < 20) that could be reliably performed.

The interaction curves for the above analysis showed a pseudo-steady state RBC binding response and may be attributed to the generation of a cell-free zone created by ionic repulsive forces. The cell binding process requires bulk transport of the RBCs to the interaction surface and the generation of sufficient binding avidity to overcome resistive forces. The magnitude of the avidity force required for cell retention must exceed a threshold level that exceeds the accumulative resistive forces. Shear-induced forces, sedimentation and ionic repulsion may be expected to significantly influence the pseudo-steady state binding response. Hence, the ideal flow rate represents a compromise where

shear forces are minimised and sedimentation of the cells is prevented. Furthermore, the presence of previously bound cells at the surface may facilitate the retention of free cells.

Protein A affinity-capture of the specific antibody was introduced to avoid regeneration difficulties. The protein A-coated surface was extremely stable to regeneration with 10 mM HCl, as evidenced by the insignificant loss of IgG binding activity (approximately 5 %). A reduction in the concentration of affinity-captured anti-A IgG and the sample contact time prevented high cell binding avidity. However, regeneration of the surface was not ideal. Furthermore, the binding curves became increasingly erratic at high RBC concentrations. Calibration curves revealed the familiar exponential dependency of the sensor response on the RBC concentration at low RBC concentrations. However, further analysis of the experimental data revealed that the anti-A IgG binding response progressively decreased throughout the course of the analysis due to the accumulation of residual material.

The results demonstrate that sub-optimal surface regeneration seriously hinders solid-phase cell binding studies. Clearly, pH elution was not sufficient to remove cell debris at the surface. Consequently, a two-step regeneration process was introduced. Elution of bound cells while maintaining cell integrity eliminated many of the difficulties observed. In addition, the ability to recover viable cells expands the potential of the technique to include cell isolation. It was possible to elute 82 % of captured RBCs without inducing cell lysis by simply increasing the flow rate. A combination of shear force and non-lytic pH elution (i.e. isotonic buffer) proved successful (99 % recovery of bound material). Hence, a similar approach may be recommended for conventional solid phase cell selection.

It was expected that the use of the BIACORE Probe™ would avoid the sampling difficulties encountered during BIACORE 1000™ analyses since highly viscous samples (100 % (v/v) RBC) can be aspirated without cell damage. Over 40 binding-regeneration cycles were successfully completed for the interaction of anti-A IgG with a protein A-coated CM5 sensor probe surface. Very little variation in the background signal was observed since temperature variations within the laboratory were low (± 0.2 °C). As expected higher antibody levels at the surface promoted higher RBC retention, presumably due to increased binding avidity. The RBC binding response reached a plateau at a given antibody concentration. Furthermore, the antibody concentration required to establish the plateau was dependent on the RBC concentration. The cell binding response represents cells that are bound with sufficient avidity to withstand the shear forces generated by buffer aspirations during the washing step. However, almost complete recovery of bound cells was accomplished by shear force elution thus avoiding the accumulation of residual material.

A sigmoidal RBC titration curve was observed for the interaction of increasing concentrations of RBCs with affinity-captured anti-A IgG. In contrast to the BIACORE 1000™ studies, concentrated RBC suspensions (i.e. 100 % (v/v) RBC) could be analysed, allowing a complete calibration curve to be constructed. The sigmoidal curve indicated that the binding response accelerated with respect to RBC concentrations less than 50 % (v/v) and decelerated at higher concentrations. The initial acceleration phase may be attributed to steric co-operativity effects while the deceleration at high RBC concentrations may be attributed to saturation of the surface. The presence of a non-specific sub-population extended the dynamic range for detection of the target RBC population. This effect was attributed to charge repulsion and the proportional increase in crowding within the mixed RBC samples as compared to the homogenous population. Significant donor variation in the RBC binding response occurred between samples from eighteen individuals. However, all donor samples gave a reliable binding response and the non-specific binding response was negligible. In contrast to previous analyses, the protein A-coated probe was found to be stable for at least 100 cell binding-regeneration cycles without deterioration of the RBC binding response.

Non-specific binding of plasma from multiple donors to a protein A-coated CM5 sensor probe was found to be reversible and reproducible and the surface was successfully regenerated after each binding cycle. Hence, whole blood grouping was examined. An additional plasma-blocking step was incorporated into the affinity-capture format in order to prevent masking of the cell binding signal due to adsorption of plasma components on exposure to whole blood samples. Specific retention of group A RBCs contained in whole blood was demonstrated and, hence, confirmed that solid phase whole blood grouping can be accomplished.

High RBC binding responses were observed during these investigations and may be attributed to the ability of adsorbed RBCs to deform when in contact with a surface. The CM5 sensor probe employs the same biointerface as the BIACORE 1000™ and, hence, may be expected to yield a comparable saturation response. Evidence for rapid conformational changes at the surface was found during BIACORE 1000™ analyses and may result from a number of factors including antigen capping, membrane tension, ionic repulsion, shear stress and overcrowding at the surface. A microscopic image of the cells bound to the CM5 sensor probe surface showed RBCs erect on their side in an ordered manner. This conformation may be attributed to the sampling technique or due to a combination of forces as outlined for the BIACORE 1000™ analyses.

In conclusion, the investigations outlined in this chapter show that solid-phase blood grouping can be accomplished using washed RBCs or whole blood samples. In addition, adsorbed cells yielded

high binding responses and were eluted efficiently at high flow rates without inducing lysis. Furthermore, 'real-time' sensing allowed the development of a simple model describing the dynamic process of cell adsorption. In principle, this blood-grouping format could be combined with an inexpensive image analysis interrogation system and automated sample analysis to create an alternative to agglutination techniques. However, the cell detection formats investigated are complex and are unlikely to compete with simple agglutination based analysers. Nevertheless, similar principles could be used to build an affordable alternative to fluorescence activated cell sorting technology. However, the biointerfacial chemistry may require tailoring for each application as it is unlikely that a simple hydrogel-based interface will be universally applicable.

Chapter 5

Development of SPR-Based Biosensors for 'Real-Time' Biomolecular Interaction Analysis.

5.1 Introduction.

This chapter is concerned with the development of two SPR-based sensors capable of 'real-time' biomolecular interaction analysis. The development of these devices was considered in terms of providing a sensitive, inexpensive and portable alternative to the bench-top analysers currently available. In particular, it was envisaged that these sensors would facilitate 'real-time' interaction analysis of whole cell-ligand interactions since the sampling mechanism could be specifically tailored to accommodate viscous samples. Both devices employ SPR-based sensing to enable visualisation of the progress of the biomolecular interaction, and hence, a brief introduction to the theory of SPR is presented (see review by Yeatman, 1996).

5.1.1 Surface Plasmon Resonance. Surface plasmons are longitudinal oscillations of free charges on the surface of a plasma (e.g. metal surface). The dense plasma of free electrons in a metal allows plasma oscillations at high frequencies (visible-near infrared wavelengths). SPR can be excited by plane polarised light travelling through an optically dense material onto a thin (50 nm) metal (e.g. gold, silver) film. Resonance occurs in the plasmon when the wave vector and the frequency of the incident light coincide with those of the surface plasmon. The dispersion of the charge density wave is dependent on the dielectric constant of both the metal and the sample medium. Hence, if the dielectric properties of the metal and the high refractive index material remain constant then the resonance condition changes with respect to changes in the dielectric properties of the sample medium. The wave vector (k_{sp}) of the surface plasmon at the metal-sample medium interface is described by:

$$k_{sp} = \frac{\omega}{c}\left(\frac{\varepsilon(\omega)\varepsilon_a}{\varepsilon_a + \varepsilon(\omega)}\right)^{1/2}$$

where

	$\varepsilon(\omega)$	=	Dielectric function of metal
	ε_a	=	Dielectric constant of sample medium
	c	=	Speed of light in a vacuum
	ω	=	Frequency of incident light

The wave vector of incident light (k_a) is described by:

$$k_a = \frac{\omega}{c}\sqrt{\varepsilon_s}$$

SPR can only occur when the wave vector of the surface plasmon at the metal-sample medium interface is equal to the wave vector of incident light. A high refractive index waveguide material (e.g. glass, plastic) and total internal reflection of the incident light are required to achieve this condition. An evanescent wave couples with the wave vector of the surface plasmon when the incident light (at a specific angle) is totally internally reflected at the high refractive index material-metal film interface, thus inducing SPR (Figure 5.1.1). This occurs for a specific angle of incidence (θ_{sp}) at a given wavelength (ω) and is a function of the dielectric properties of the sample medium (i.e. refractive index). The wave vector of the evanescent wave (k_{ev}) is the same as the lateral component of the incident lightwave vector (k_g) within the high refractive index material:

$$k_{ev} = k_g \sin\theta = \frac{\omega}{c}\sqrt{\varepsilon_g}\sin\theta$$

where ε_g = Dielectric constant of the high refractive index material

θ = Angle of incidence

Hence, during SPR the wave vector of the evanescent wave is equal to the wave vector of the surface plasmon and a fraction of the light is absorbed thereby diminishing the intensity of the reflected light. The penetration depth of the evanescent wave is the distance at which the electric field strength has decayed to ~ 37 % of that at the surface (Stenberg *et al.*, 1991). The x and z-components of the electric field decay exponentially into the sample medium and the electric field (E_z) of the z-component is described as:

$$E_z = E_z(0)\ exp[-k_z z]$$

and

$$k_z^2 = k_x^2 - \frac{\omega^2}{c^2}\varepsilon_a$$

where k_z = Wave vector of electric field in z-direction

k_x = Wave vector of electric field in x-direction

The wave vector of the evanescent electric field in the x-direction must equal the wave vector of the surface plasmon during SPR. Hence, the z-component of the evanescent electric field can be approximated by:

$$E_z(z) = E_z(0)\ exp[-z/\delta_z]$$

where δ_z = Penetration depth of evanescent field
(e. g. ~ 190 nm for BIACORE 1000™)

This implies that the technique is sensitive to refractive index changes within the volume probed by the evanescent wave. Therefore, the progress of a biomolecular interaction can be visualised by monitoring the change in refractive index within this layer during the interaction. The refractive index change can be directly related to the protein concentration (Stenberg *et al.*, 1991) by:

$$\Delta c = \Delta n \, (\delta c / \delta n)$$

where $\delta c/\delta n$ = 5-7 g/cm^3
n = Refractive index of sample medium
c = Protein concentration

The incorporation of an extended hydrogel (~ 100 nm) at the surface maximises the surface capacity by utilising a significant fraction of the volume probed by the evanescent wave as compared to a planar monolayer (< 10 nm) biointerface. The SPR phenomenon is not a recent discovery (Turbadar, 1964) and has previously been employed for surface analysis of metals (Raether, 1967). Kretschmann (1969) excited SPR by generating an evanescent field using a high refractive index prism, light under conditions of total internal reflection and an optical angle-scanning system. However, Matsubara *et al.* (1988), refined the technique by employing a divergent light source which was polarised and collimated as a wedge-shaped beam incident through the prism onto the gold surface. A photodiode array detects the reflected light and the position of the intensity minimum is determined. The BIACORE 'real-time' BIA analysers (Liedberg *et al.*, 1993) employ a similar optical configuration.

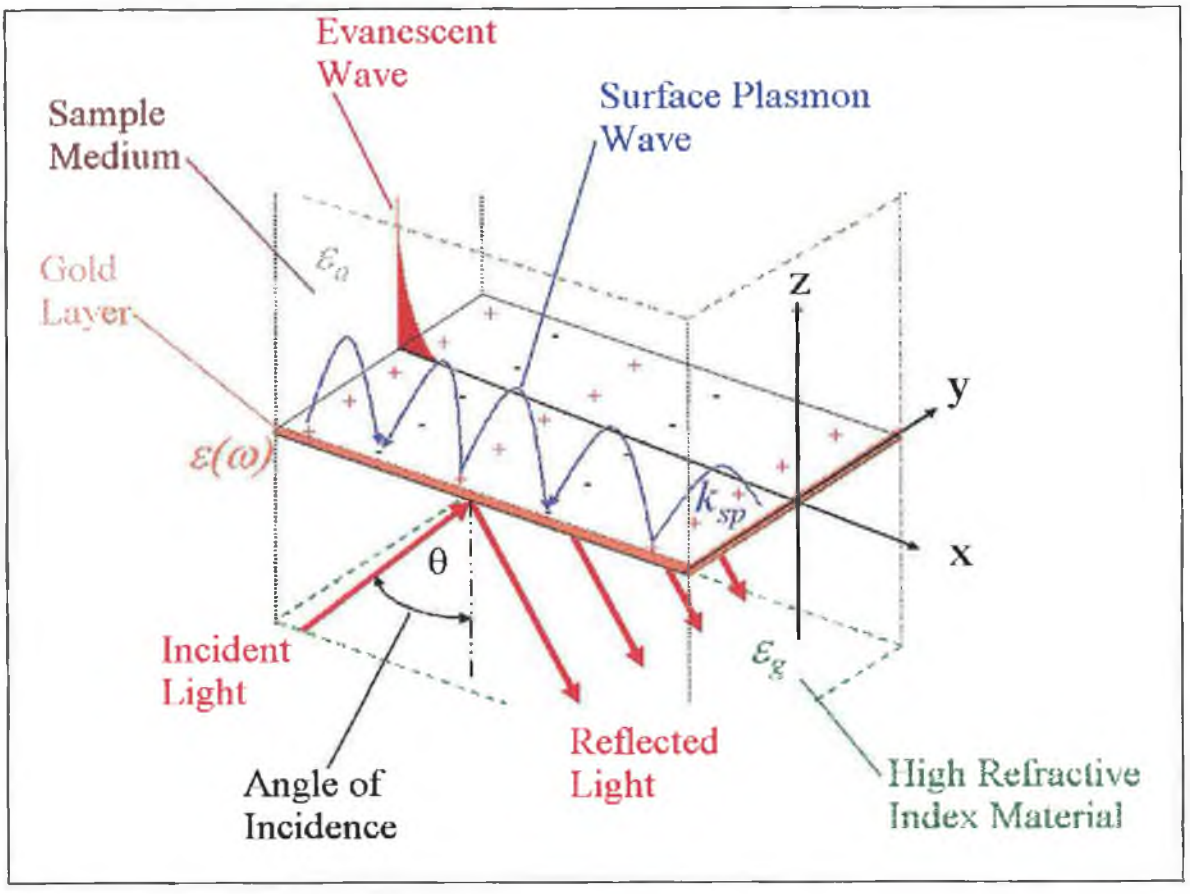

Figure 5.1.1. Schematic illustration of the SPR phenomenon.

5.1.2 ***Overview of Chapter.*** A fibre-optic SPR-based biosensor was constructed to allow the acquisition of 'real-time' interaction data in contrast to the BIACORE Probe™. In addition, a miniaturised version of the 'Kretschmann' optical system (available from Texas Instruments) was modified to facilitate biosensing applications. Both devices were calibrated and applied to the detection of red blood cell-ligand interactions.

5.2 Results and Discussion

5.2.1 Fibre Optic SPR-Based Sensor.

5.2.1.1 Principle of Operation. The Kretschmann configuration is the most widely employed SPR optical configuration (Liedberg *et al.*, 1993) and employs prism-coupled monochromatic light. Bulky optical components are expensive and result in a large device that is not suitable for remote-sensing applications. A less expensive alternative that eliminates the requirement for prism coupling through the use of monochromatic light at variable incident angles (requires a rotation stage) and fibre-optic technology was recently developed (Ronot-Trioli *et al.*,

1996; Abdelghani *et al.*, 1997). However, fixed-angle polychromatic light can also generate an SPR response when combined with a waveguiding substrate The non-'real-time' BIACORE Probe™ system employs this SPR configuration and has been used for the detection of antibody-antigen interactions (Nelson *et al.*, 1997). This system was successfully applied to the study of whole cell-ligand interactions (section 4.2.4), but was limited to point measurements. A similar system was constructed to enable 'real-time' monitoring of biomolecular interactions. The sensing element (CM5 probe) was composed of a gold-coated (~ 50 nm layer) fibre optic with a mirror deposited at the tip. A carboxymethylated dextran (CM-dextran) hydrogel was grafted onto the gold surface via an alkanethiol self-assembled monolayer. These were obtained from BIACORE AB (Uppsala, Sweden) and fitted to our sensor system. In contrast to angle dependent SPR, the wavelength-dependent SPR response is non-linear with respect to the refractive index at the interaction surface.

The fibre optic accommodates multiple light modes giving rise to a range of incident angles that propagate through the fibre (Jorgenson and Yee, 1993). The dielectric function of the gold ($\varepsilon(\omega)$) changes with respect to the wavelength of the propagated light for a given refractive index (i.e. dielectric constant (ε_a)) at the sensing surface. Hence, an increase in the refractive index at the hydrogel layer will cause a shift (i.e. response) in the resonance spectrum that can be monitored using a miniature spectrometer (*Figure 5.2.1.1*). The resonance spectrum represents an accumulated spectrum for the entire range of propagating angles. A custom-written LabVIEW program was employed for data acquisition, processing and presentation. The position of the reflectance minimum was found in 'real-time' (i.e. 0.4 sec intervals) by fitting a high order polynomial curve to the experimental resonance spectrum. The resonance spectral shift was automatically plotted against time giving a 'real-time' interaction curve.

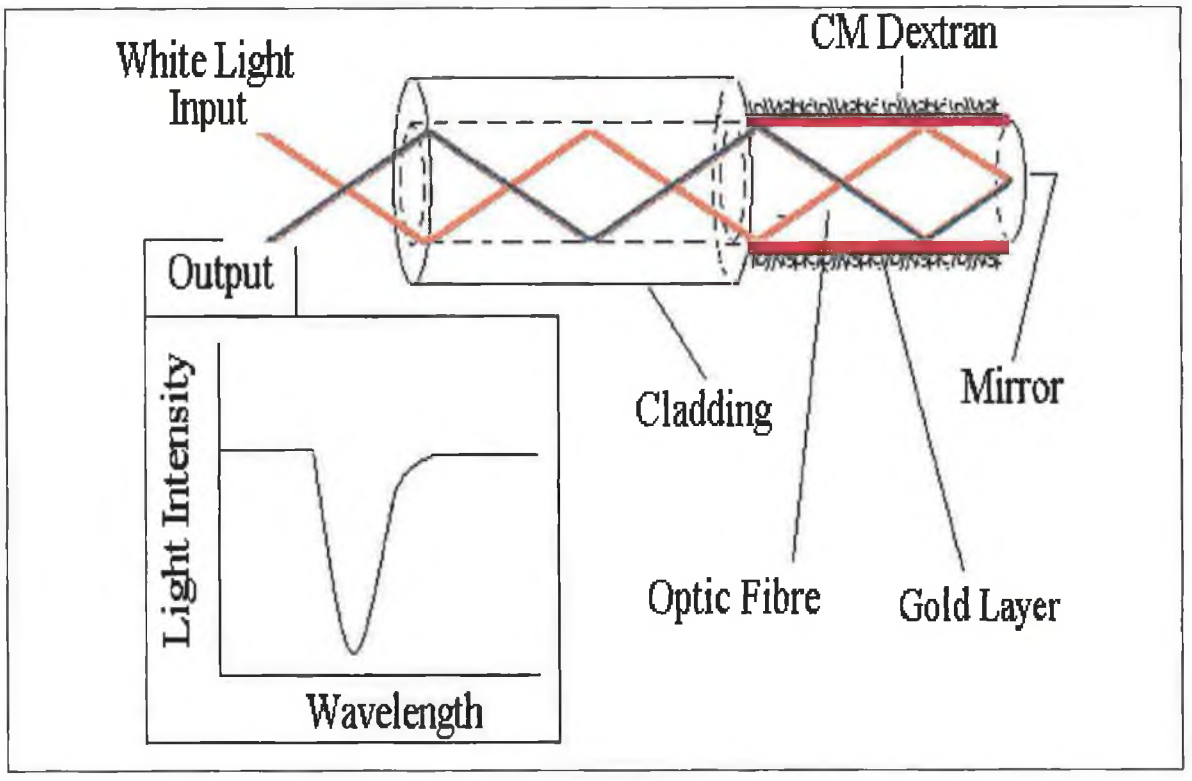

Figure 5.2.1.1. Schematic representation of the fibre optic sensing element.

5.2.1.2 *Sensor Construction.* The configuration of the fibre optic SPR-based sensor is shown in *Figure 5.2.1.2* and is similar to that developed by Jorgenson and Yee (1993). White light from a tungsten-halogen lamp (LS-1) is coupled into the fibre optic waveguide (Fibre Optic Probe RS00-7 (Ocean Optics, Dunedin, Florida, USA)) and is propagated along the fibre optic to the sensing element (connected via a customised fibre optic connector designed by Aiden Doyle, School of Physical Sciences, Dublin City University)) by total internal reflection. The light is reflected via the microfabricated mirror at the tip of the sensing element (CM5 Probe) and is detected by the miniature S2000 spectrometer (Ocean Optics). Light is adsorbed by the SPR phenomenon at specific wavelengths giving a characteristic resonance spectrum. The signal is relayed to the laptop computer where a custom-written LabVIEW program finds the spectral shift of the reflectance minimum and generates a 'real-time' interaction curve.

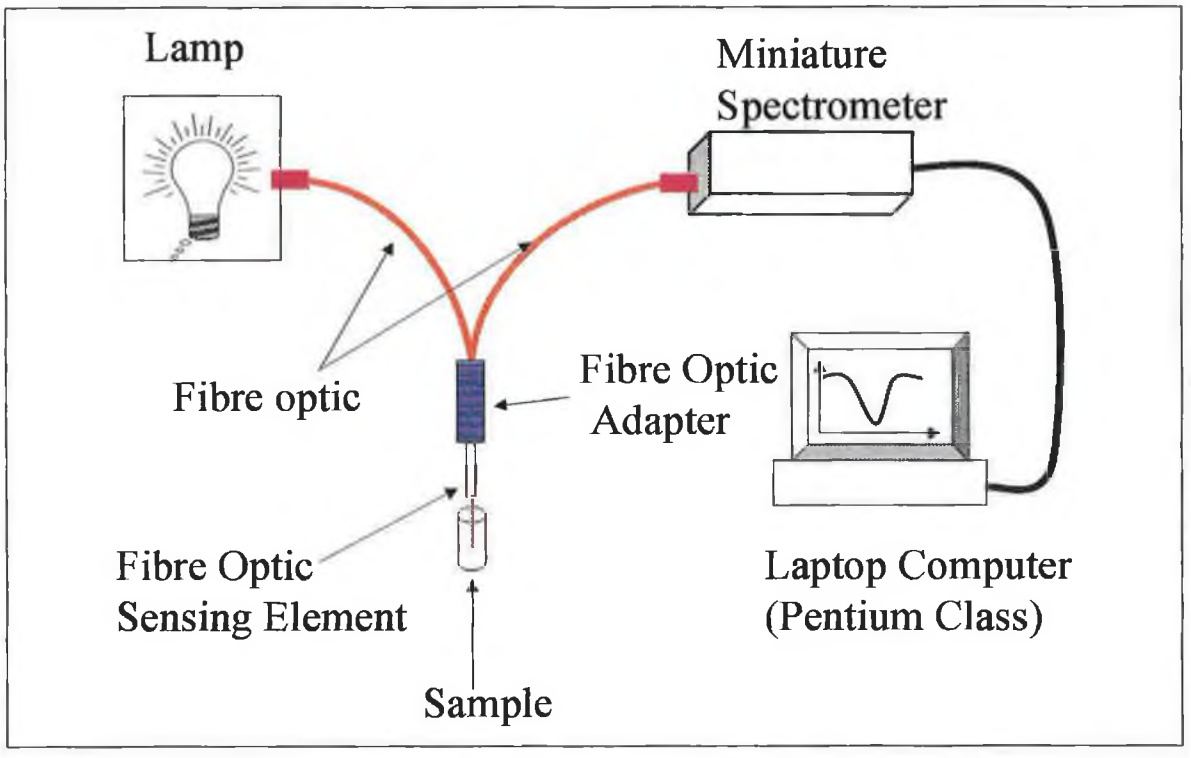

Figure 5.2.1.2. Illustration of the fibre optic SPR-based biosensor.

5.2.1.3 *Data Acquition, Processing and Display.* A custom written software program was developed by Shane O'Neill (Department of Chemistry, Dublin City University) to accommodate 'real-time' interaction analysis (O'Neill, 1999). The LabVIEW (National Instruments) programme consisted of a visual user interface that allowed user-control via a virtual control panel. The actual coding is performed graphically using a block diagram. Data acquisition was performed using a National Instruments Daq-700 PCMCIA I/O card. The LabVIEW software automatically recognises the I/O card, allowing data to be collected from the spectrometer and stored in the computer memory. As stated earlier, the resonance spectrum is characterised by a wavelength-dependent minimum that shifts to higher wavelengths during the progress of a biomolecular interaction. The position of the resonance spectrum minimum was detected by fitting a 30^{th}-order polynomial to the entire curve. The 'Householder' curve fitting algorithm (code supplied with LabView) gave a stable fitting. The minimum of the fitted curve was determined using the Peak-Find algorithm (supplied with LabVIEW Software). This entire process was repeated at 0.4 sec intervals and a 'real-time' plot of the response (i.e. minimum position) against time was continuously updated and displayed on the virtual control panel (*Figure 5.2.1.3.1*). After completion of the biomolecular interaction, the interaction curve was stored as an ASCII text file. In addition, an option to save and store the resonance spectra at any point during the analysis was incorporated.

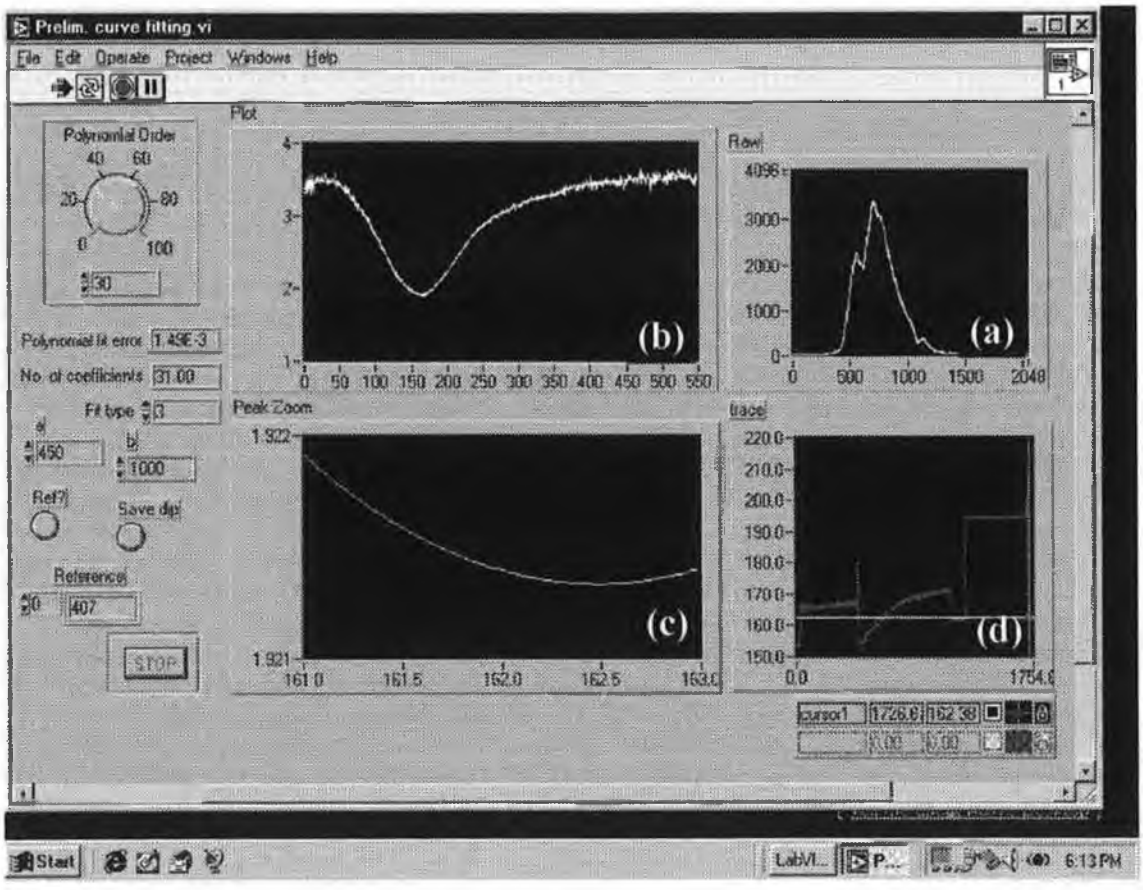

Figure 5.2.1.3.1. LabView virtual control panel and data display. (a) Intensity profile (wavelength against intensity) of reflected light. It was important to control the intensity of the light coupled into the fibre optic since the spectrometer is very sensitive and moderate intensities can easily saturate the SPR signal. The intensity profile shows that the SPR minimum occurs at ~ 612 nm. (b) Resonance spectrum. The actual wavelength at the minimum is the value at the x-axis plus 450 (start of range, i.e. zero). A ~ 46 % intensity drop was observed for the SPR minimum at ~ 612 nm. (c) Magnified view of the resonance minimum. (d) 'Real-time' interaction curve showing the progress of an immobilisation sequence (cross wires employed to find response values at any point).

A 30th order polynomial fitted the resonance spectra better than higher order or lower order polynomials (*Figure 5.2.1.3.2*). Visual inspection of overlaid curves reveals that they are superimposable indicating a reasonable goodness of fit.

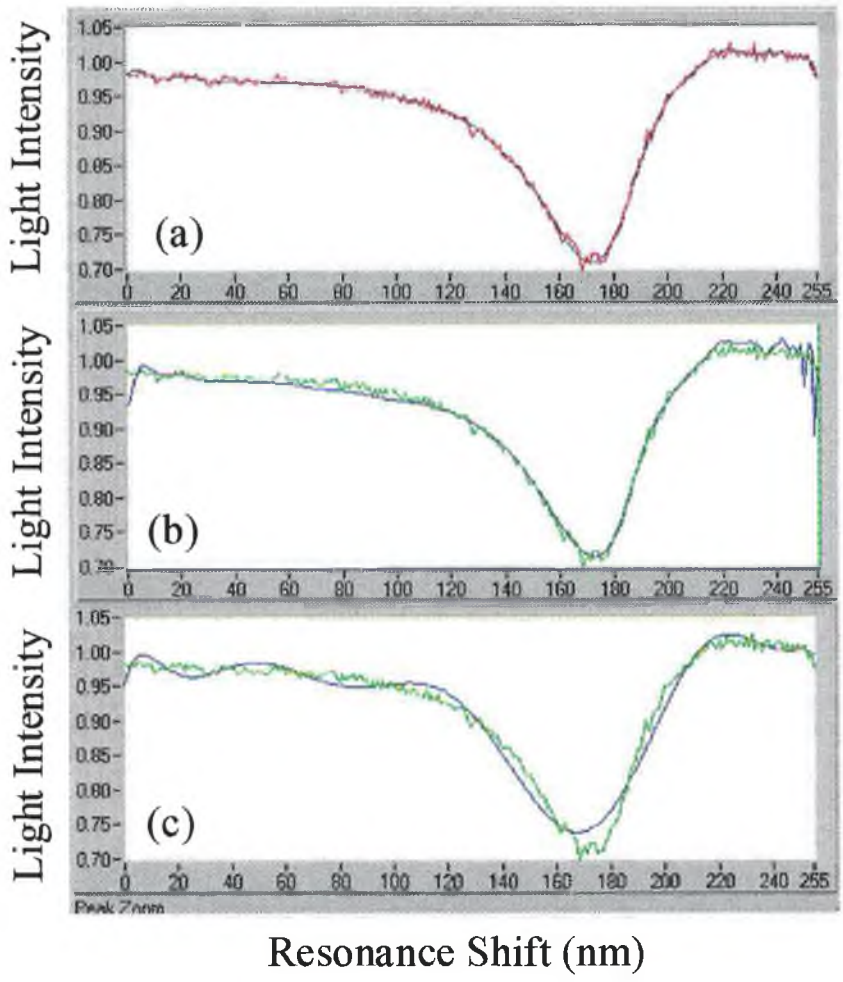

Figure 5.2.1.3.2. Typical resonance spectra with polynomial fitting. The smooth curves are the fitted polynomial curves superimposed on the resonance spectra. The fitting was performed using LabView software. The 'Householder' curve fitting algorithm (code supplied with LabView) fitted the polynomial to the data. The calculated curve was superimposed onto the experimental curve and the position of the minimum of the calculated curve was obtained using the Peak-Find algorithm (supplied with LabVIEW Software). (a) Optimal fitting using a 30th order polynomial. (b) Reasonable fitting using an 80th order polynomial. (c) Poor fitting using 10th order polynomial.

An 80th order polynomial gave a reasonable approximation of the resonance spectrum but clear deviations from the actual curve were apparent. A 10th order polynomial completely misfitted the resonance minimum and was found to be unsuitable for this analysis. The polynomial fitting procedure is a rough fitting procedure and resulted in sub-optimal sensitivity. Fitting a polynomial to a subset of data about the minimum would be expected to considerably enhance the fitting.

However, the polynomial fitting was adequate, since high sensitivity was not essential for the proposed RBC analysis.

5.2.1.4 *Temperature Induced Response Drift.* Generic refractive index sensors are sensitive to temperature fluctuations in the sample due to the thermal expansion of matter. The sample temperature was not thermostatically controlled during sample analysis. Hence, the BIACORE 1000™ was employed to estimate the signal drift expected under normal laboratory conditions.

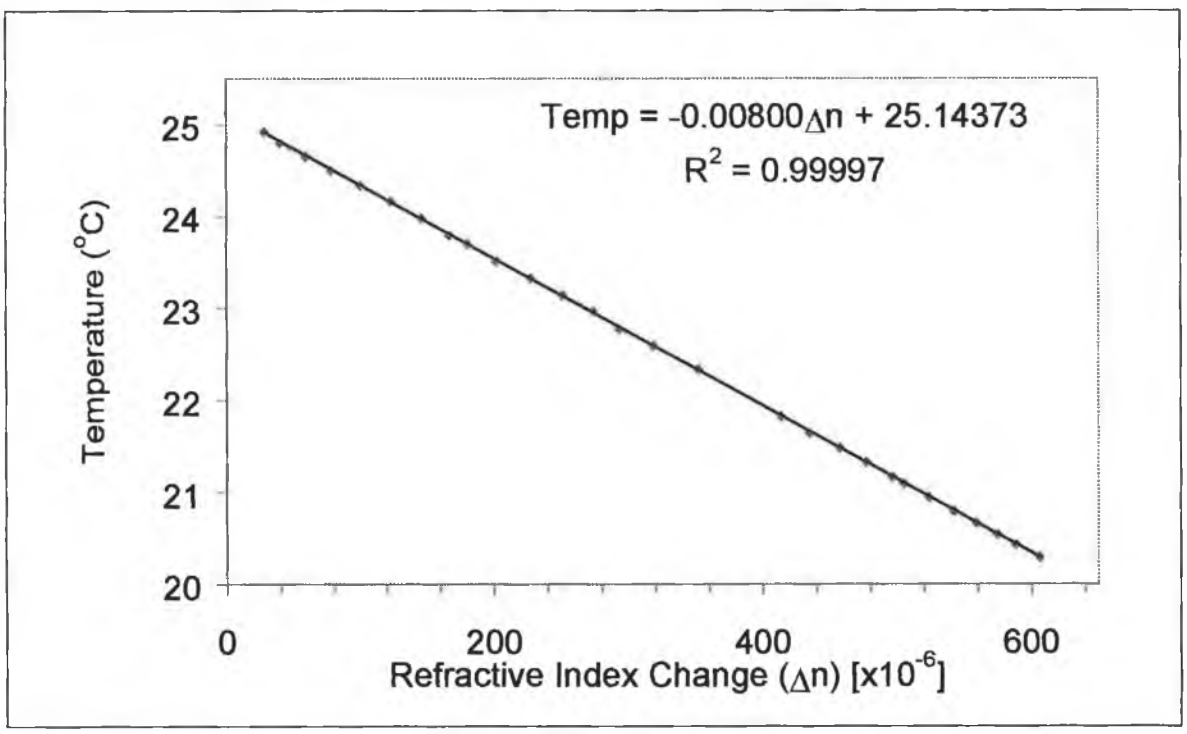

Figure 5.2.1.4. Variation in refractive index due to temperature. The BIACORE 1000™ was primed with HBS running buffer and set to a flow rate of 5 µl/min. The thermostatically controlled temperature was adjusted from 25 °C to 20 °C. The change in the baseline response (RU) and the temperature (°C) were recorded at intervals during the time required to reach the lower temperature. The change in the baseline response was related to the refractive index (i.e. 1000 RU ≈ 0.001 Δn) and plotted against the temperature. A linear regression line fitted the data (R^2 = 0.99997) and the equation of the line is shown above. This equation can be rewritten as ΔT = 8000 Δn.

The refractive index was found to be linearly dependent on the temperature and can be related by the simple expression ΔT = 8000 Δn. Accordingly, a change in temperature of 1 °C will cause a significant change in refractive index of 1.25 x 10^{-4} (i.e. 125 RU). However, the environmental temperature of the laboratory fluctuated by < 0.016 °C giving an insignificant refractive index drift of 2 x 10^{-6}/min. In addition, samples for analysis were allowed to equilibrate at room temperature before analysis.

5.2.1.5. *Sensor Calibration.* The sensor was calibrated using glycerol solutions (prepared in ultrapure water) of known refractive index. The refractive index of the glycerol:water solutions was determined using an Abbé refractometer (Milton Roy Tabletop Refractometer 3L) (*Figure 5.2.1.5.1*). The expression for the calibration curve was applied to calibrate the fibre optic SPR sensor response.

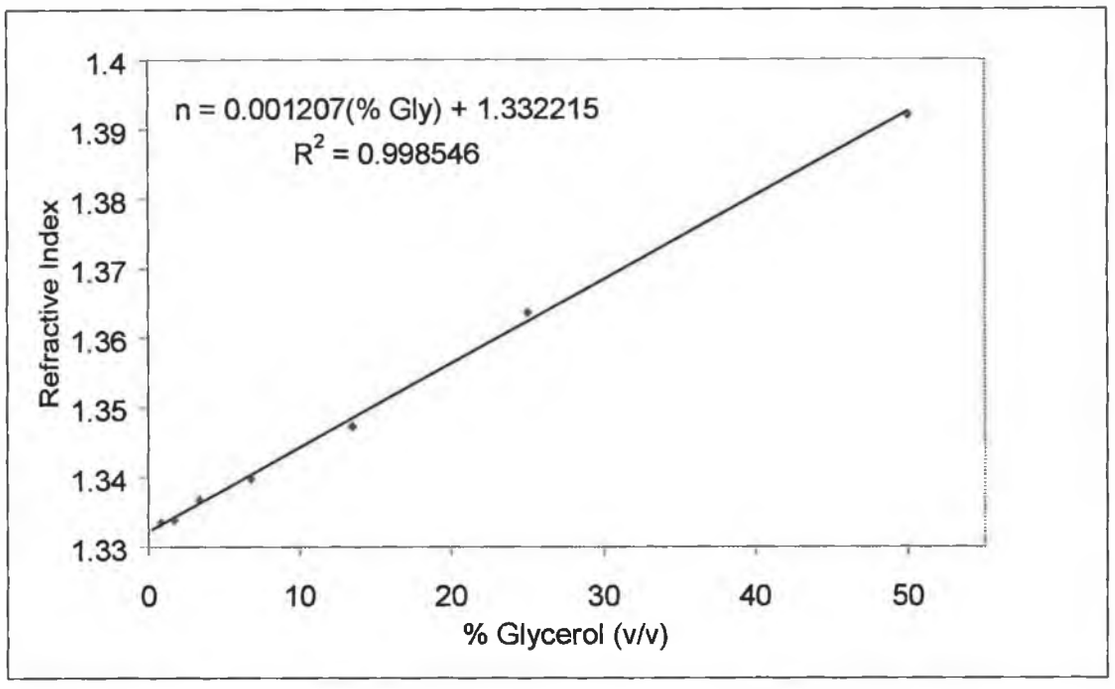

Figure 5.2.1.5.1. Calibration curve to determine the refractive index of glycerol:water solutions. Glycerol:water solutions were prepared in ultrapure water. The refractive index of each sample was recorded (room temperature of 24.3 °C) using an Abbé refractometer. A regression line was fitted to the data and the resulting calibration equation is shown above. This analysis was conducted in collaboration with Colm Mc Atamney (School of Physical Science, Dublin City University).

An overlay of the resonance spectra recorded for increasing glycerol:water solutions is shown in *Figure 5.2.1.5.2.* The resonance spectra appear broad and become broader at higher wavelengths. The width of the SPR minima is a function of the propagation angle within the fibre optic. The smaller the angle (low-order mode) the greater the number of reflections that mode encounters along the SPR surface (~ 1 cm long), resulting in a broad SPR minimum. Narrower SPR minima may be produced by using low diameter optical fibres and high-order modes. However, the SPR response was ideal since ~ 50 % of the available light was absorbed at the SPR minimum, indicating that the surface area of the SPR region was optimal. Complete absorption of light cannot occur as both transverse electric and transverse magnetic polarisations of light propagate through the multimode fibre. Only transverse magnetic polarisations can excite SPR, hence, the expected reflectance minimum cannot exceed 50 % of the total light intensity (Jorgenson and Yee, 1993).

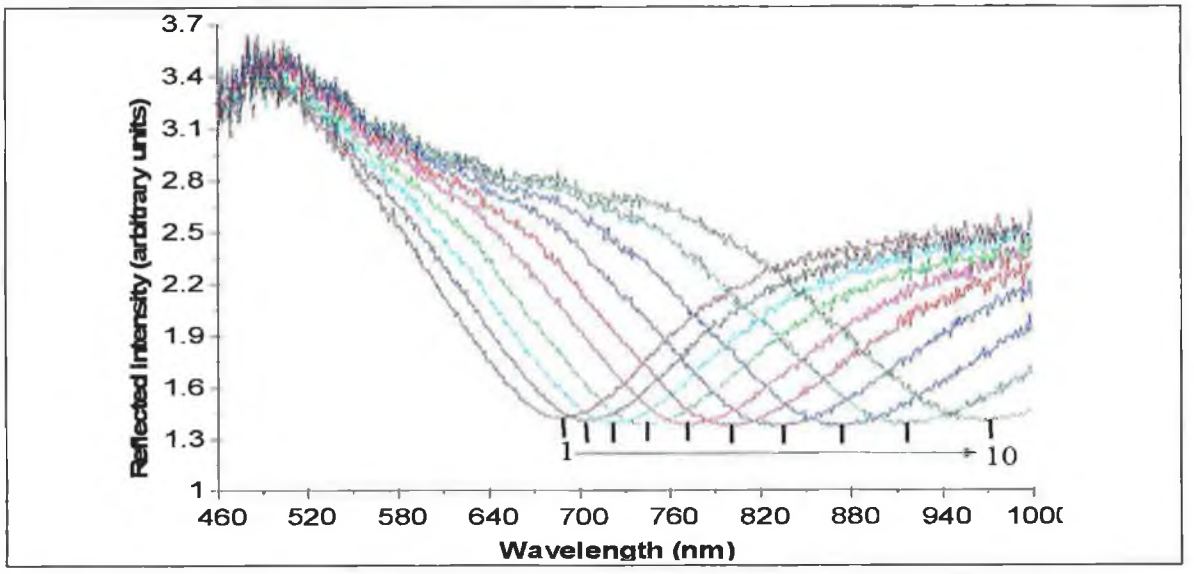

Figure 5.2.1.5.2 Overlaid resonance spectra for Glycerol:water solutions. Glycerol:water solutions were prepared from 5 to 50 % (v/v) glycerol in ultrapure water at 5 % increments (see 1-10 above). The resonance minimum shifts to higher wavelengths with increasing refractive index (sample 1-10). The sensing element of the sensor was immersed in the sample for 1 min and the spectrum recorded. The sensing tip was then rinsed with ultrapure water and the procedure repeated for the remaining samples.

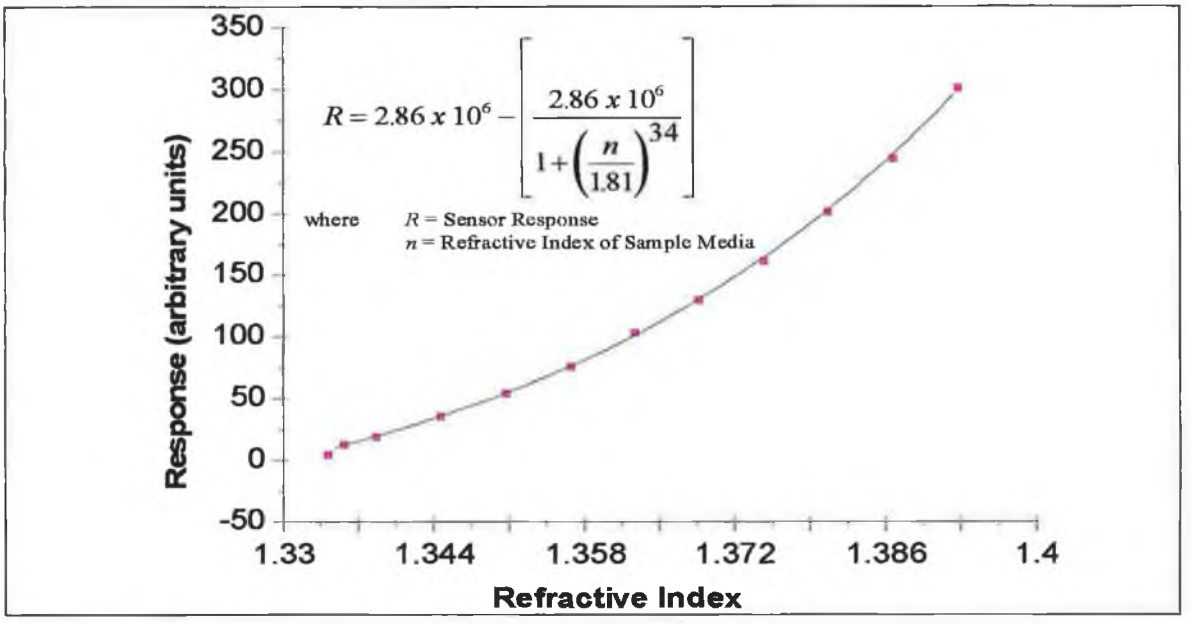

Figure 5.2.1.5.3. Calibration curve of the refractive index against the sensor response. The experiment was conducted as outlined in *Figure 5.2.1.5.2*. The refractive indices of the glycerol:water solutions were determined from the calibration curve in *Figure 5.2.1.5.1*. A 4-parameter equation (see section 3.2.5.2) was fitted to the data and the resulting expression relating the refractive index at the interaction surface to the sensor response is given above.

The position of the resonance minima is related non-linearly to the refractive index of the glycerol:water solutions. The refractive indices of the glycerol:water solutions was determined from *Figure* 5.2.1.5.1 and were plotted against the shifts in the resonance minima obtained from *Figure 5.2.1.5.2*. The resulting calibration curve is shown in *Figure 5.2.1.5.3*. As expected, the sensor response is non-linear and shows an increase in sensitivity to refractive index with increasing response (i.e. increasing wavelength). Hence, the interaction curves obtained with this device will reflect the progress of the biomolecular interaction as distorted by the increasing sensitivity at higher responses. Consequently, a direct comparison of the response obtained from this sensor and angle-dependent SPR systems, which employ monochromatic light, cannot be performed. Hence, the fibre optic sensor response will be referred to in arbitrary response units (AU) to avoid confusion with BIACORE response units (RU). However, the expression given in *Figure 5.2.1.5.3* can be used to estimate the corresponding BIACORE response (RU) from the fibre optic SPR response. The dynamic range of the sensor extends from a refractive index of 1.33 to 1.39. The signal noise varied from $\pm$ 2.5 x 10^{-5} to $\pm$ 1.5 x 10^{-5} (corresponds to $\pm$ 25 to $\pm$ 15 RU) from low to high response values. Therefore, the background noise level is 30 to 50-fold higher than that of the BIACORE 1000™.

5.2.2 ***'Real-Time' Detection of Whole RBCs Employing the Fibre Optic SPR Sensor***. It was expected that the use of the 'real-time' fibre optic SPR sensor would enable detection of whole RBCs in a similar manner to the BIACORE probe™ (section 4.2.4). However, this sensor combines the desirable sampling attributes of the BIACORE Probe™ with 'real-time' sensing capability. The BIACORE Probe™ employs a hand-held micropipette to introduce the sample to the sensing element (held within the pipette tip), a reliable sampling mechanism that requires low sample volumes. A simple immersion approach was employed using the 'real-time' fibre optic SPR sensor. Once coated with a biomolecule, the sensing element was stored in PBS buffer to prevent drying. In addition, the sensing element was incubated in PBS buffer before and after each sample interaction allowing reliable binding response measurements to be recorded from the interaction curve.

5.2.2.1 *Immobilisation of Protein A.* A protein A affinity-capture format was selected for the analysis because of the desirable characteristics outlined in section 4.2.4.9. In particular, it was thought that the stability of a protein A-coated surface would prolong the utility of the expensive sensing element (CM5 Probe) and allow storage for an extended period (1-2 months at 4 °C). Retention of biological activity of a protein A-coated CM5 probe was greater during dry storage (4 °C with desiccant) than in liquid storage (4 °C in HBS buffer containing 0.01 % (w/v) sodium azide). Protein A was immobilised (8.0 AU) onto the CM5 probe using conventional amine coupling and the resulting sensorgram is shown in *Figure 5.2.2.1*. It is apparent that the background

noise level is much greater than that obtained from the BIACORE 1000™ from visual inspection of the sensorgram. Response spikes occurred due to manual sampling but did not interfere with the reliability of the interaction curves obtained.

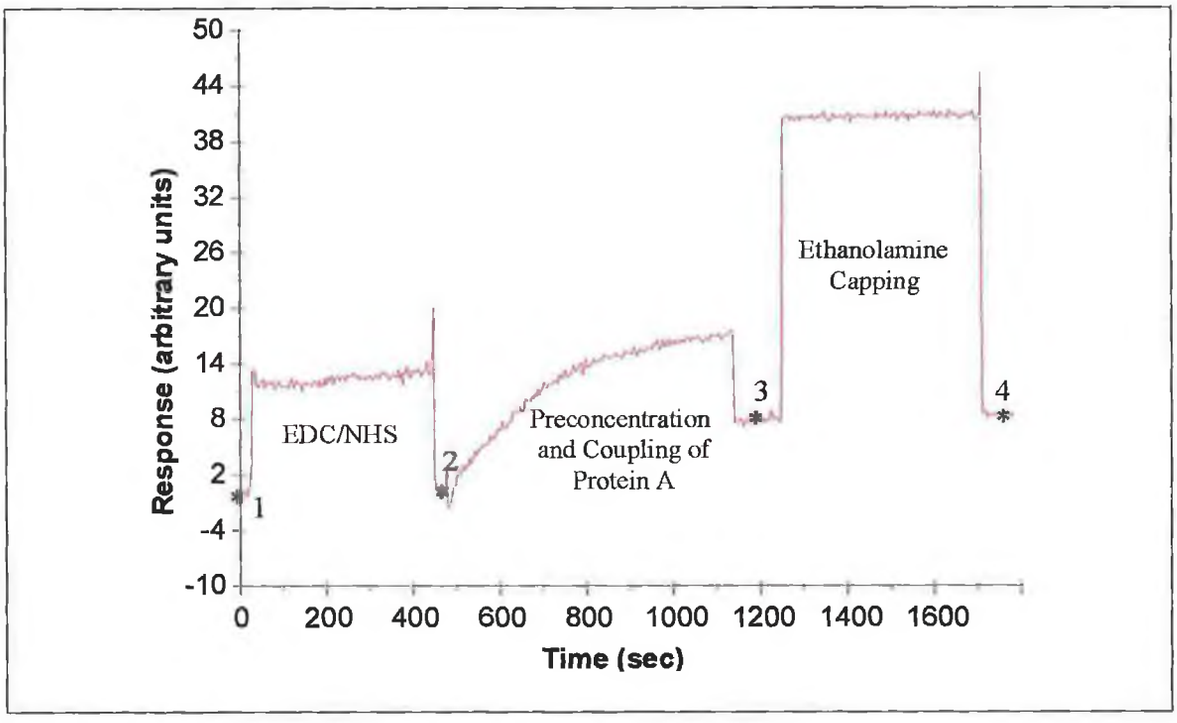

Figure 5.2.2.1. Sensorgram for the immobilisation of protein A using amine coupling. The probe was incubated in PBS (numbered points) buffer, before and after exposure to sample, to eliminate bulk refractive index variations between solutions. Thus, the numbered points refer to the actual change in mass at the surface. (1) Baseline response (0 AU) for the sensor in PBS buffer. (2) Slight increase in the baseline response (0.66 AU) after 7 min exposure to EDC/NHS activation solution (due to matrix contraction). The sensor was exposed to a protein A solution (50 μg/ml, in 10 mM sodium acetate buffer, pH 4.3) for 11 min allowing preconcentration of the positively charged protein onto the negative hydrogel. (3) This process facilitated covalent (8.0 AU) coupling to the activated surface. (4) Residual activated groups on the matrix were quenched (capped) using 1 M ethanolamine, pH 8.5, resulting in a final protein A-coating response of 8.8 AU. The apparent increase in mass (0.8 AU) during capping can be attributed to matrix contraction and does not represent an increase in the immobilised protein A concentration.

5.2.2.2 *Protein A Affinity-Capture Format.* Prior to RBC analysis the sensor performance was evaluated by generating a standard curve for the quantitative detection of rabbit IgG. An overlay of interaction curves recorded for different concentrations of IgG is shown in *Figure 5.2.2.2.* A bulk refractive index effect can be observed immediately after the response spike at the end of sample exposure. This bulk refractive index change is due to the variable NaCl concentration that resulted from serial dilution of the antibody stock solution (PBS containing 0.3 M NaCl) in

normal PBS (containing 0.15 M NaCl) during sample preparation. Regeneration of the surface was ideal; the response returned to the initial baseline response. It is important to point out that analyses conducted with this sensor cannot be extended to kinetic analysis of homogenous interactions because of the non-linear dependence of the response on the refractive index at the interaction surface. In addition, the sample is contained in a non-stirred reservoir causing the binding process to be limited by mass-transfer rates rather than kinetic binding rates. However, the interaction curves are free from spurious effects that may occur due to manual sampling.

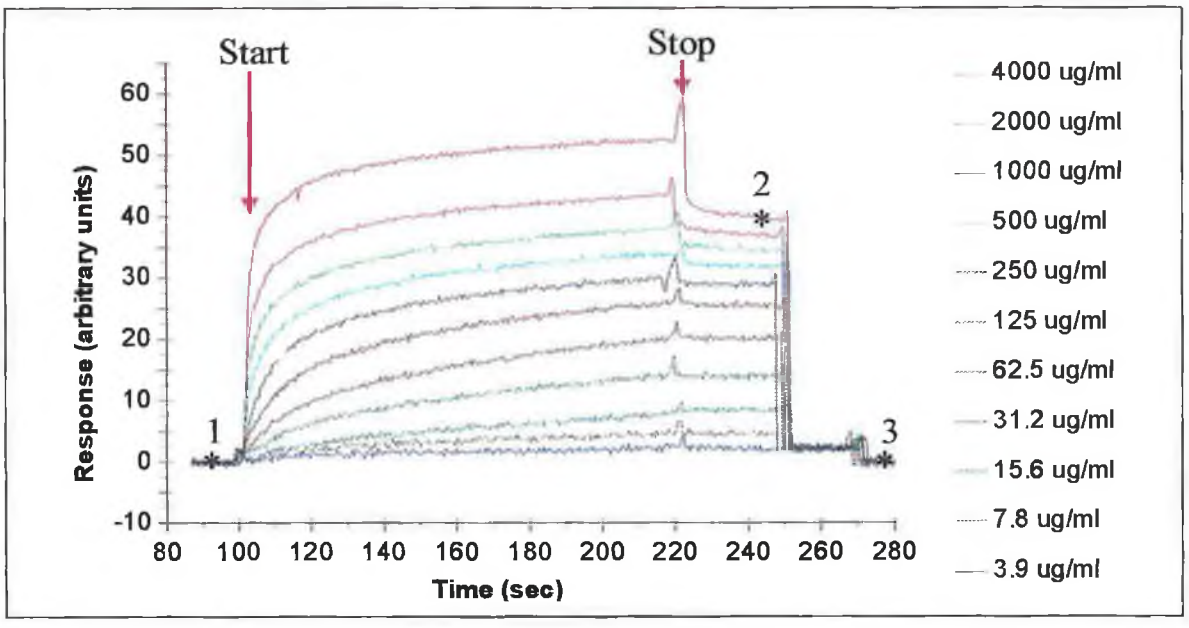

Figure 5.2.2.2. (a) Overlaid interaction curves for increasing concentrations of rabbit IgG. Affinity purified (protein A-affinity chromatography) rabbit IgG (4.0 mg/ml) was serially diluted in PBS buffer. (1) Baseline (in PBS buffer) for the protein A-coated CM5 probe surface before sample addition. The sensing element was exposed to the sample (Start) for 2 min at room temperature. (2) The sensing element was exposed to PBS buffer and the antibody binding response was recorded. These values were used to construct a calibration curve (*Figure 5.2.2.3*). The sensing element was then exposed to 20 mM HCl for 30 sec to remove affinity-captured antibody. (3) Finally, the sensor was exposed to PBS and the response returned to the initial baseline level, indicating complete regeneration of the surface after each analysis. This procedure was repeated for each sample.

5.2.2.3 Antibody Titration Curve. A calibration curve was constructed from the response values (obtained from *Figure 5.2.2.2*) and is shown in *Figure 5.2.2.3*. The sigmoidal calibration curve was fitted by a 4-parameter equation. The maximum response was ~ 40 AU and corresponds to a BIACORE response value of ~ 16,800 RU. This estimate was obtained by converting the fibre optic SPR response into % glycerol:water using a calibration expression (*Figure 5.2.1.5.3*). The %

glycerol value was converted into an equivalent BIACORE response using a similar calibration curve constructed for the BIACORE 1000™ (*Figure 5.2.3.4.1(b)*). The calibration curve does not reach a complete plateau due to the dramatic increase in sensitivity of the sensor at higher response values as expected from the non-linear response (*Figure 5.2.1.5.3.* In conclusion, the 'real-time' biosensing capability of the fibre optic biosensor was successfully demonstrated.

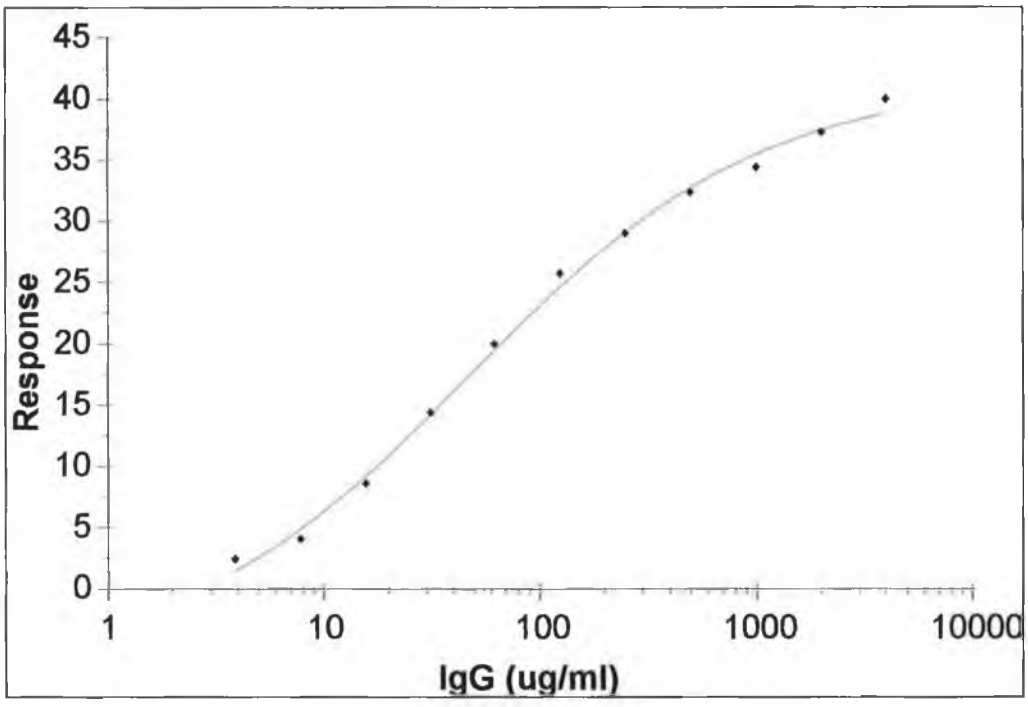

Figure 5.2.2.3. Calibration curve for the interaction of rabbit IgG with a protein A-coated sensor element. The response values at different IgG concentrations were obtained from *Figure 5.2.2.2* and were plotted against the sample concentration. A 4-parameter equation was fitted to the data.

5.2.2.4 Red Blood Cell Detection. RBC detection was performed using affinity-capture as illustrated in *Figure 5.2.2.4.* Anti-A IgG was affinity-captured by the protein A-coated sensing element and enabled specific retention of group A RBCs. Complete regeneration of the surface was possible employing pH elution (20 mM HCl) and a detergent wash (PBS containing 0.1 % Triton-100).

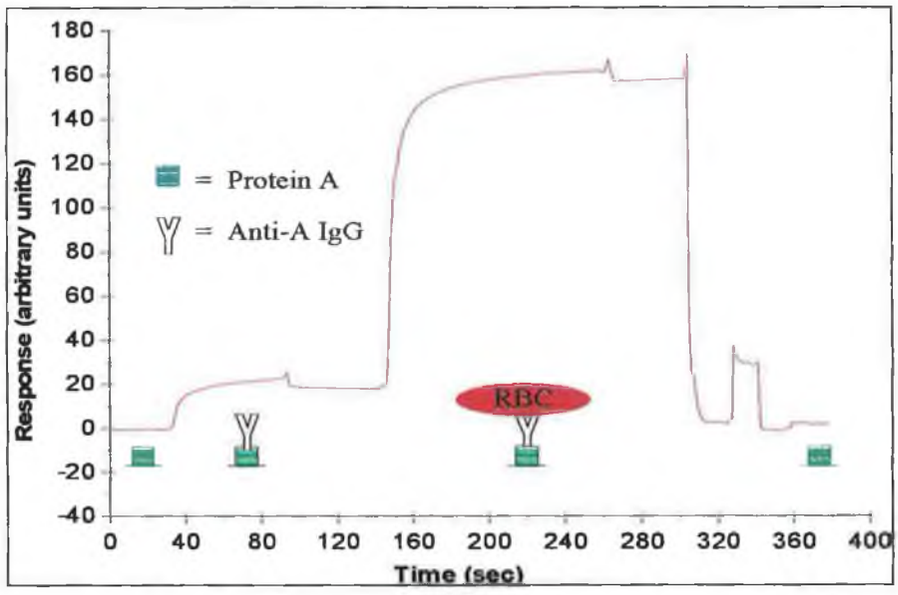

Figure 5.2.2.4. Complete interaction curve for the detection of RBCs using the fibre optic SPR sensor. Protein A was immobilised onto a CM5 sensor probe surface as described in *Figure 5.2.2.1*. The probe was maintained in PBS buffer throughout the analysis other than during exposure to the sample. The sensing element was exposed to neat hybridoma supernatant (serum-free) containing anti-A IgG_{2b} for 1 min giving a binding response of 18.5 AU. The probe was then exposed to 100 % (v/v) washed group A RBCs for 2 min giving a cell-binding response of 139.5 AU. The sensing element was regenerated (98.5 % efficiency) by a 20 sec exposure to 20 mM HCl, a 15 sec exposure to PBS containing 0.1 % Triton-100 and a further 15 sec exposure to 20 mM HCl.

5.2.2.5 RBC Calibration Curve. This procedure was repeated for five RBC concentrations and the cell-binding phase of the interaction curves is shown in *Figure 5.2.2.5*(a). The curves are similar to those observed during BIACORE 1000™ analysis (*Figure 4.2.2.1* and *Figure 4.2.2.2*). The anti-A IgG capture step was reproducible (18.63 ± 0.46 μg/ml). A steady-state response developed rapidly for high RBC concentrations (e.g. 100 % (v/v)) whereas lower concentrations caused a rapid initial binding phase followed by a much slower binding phase. These interaction curves are similar to those observed during BIACORE 1000™ analyses (*Figure 4.2.2.1* and *Figure 4.2.2.2*) and agree with the proposed dynamics of the interaction (section 4.2.5). The change in the binding response with respect to the RBC concentration is shown in *Figure 5.2.2.5*(b). The binding response increases approximately exponentially with the RBC concentration. However, the curvilinear relationship observed from fitting a 4-parameter equation indicates that the binding rate reaches a plateau, presumably due to saturation of the surface at higher coverages (i.e. high sample concentration). Furthermore, a more pronounced plateau may be expected if the data was correcting for the increasing sensitivity of the sensor with increasing response. A similar relationship was

observed for the change in the binding rate as a function of RBC concentration (*Figure 5.2.2.5*(c)). Hence the response for the 100 % (v/v) RBCs may represent the maximum response attainable.

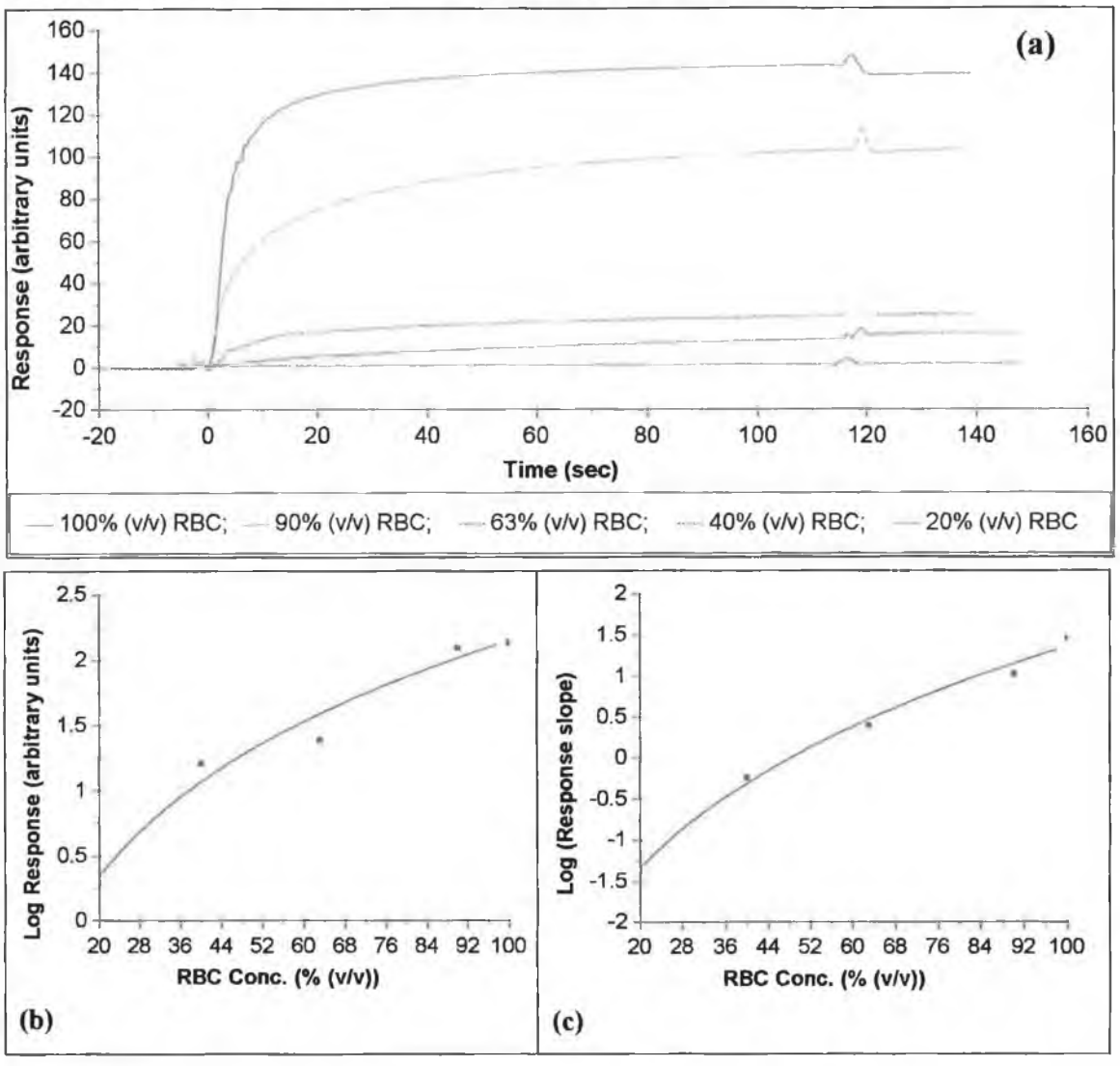

Figure 5.2.2.5. **(a)** Overlay of the RBC interaction curves. The analysis was conducted as outline in *Figure 5.2.2.4* for 5 group A RBC concentrations. The overlaid curves displayed above were normalised with respect to the initial baseline response. Non-specific binding of RBCs to the protein A-coated interaction surface was not detectable when the antibody capture step was omitted (*Figure 5.2.2.6*). **(b)** The log of the binding response against RBC concentration. The RBC-binding responses were obtained from (a). **(c)** Binding rate as a function of RBC concentration. (N.B. A 4-parameter equation was fit to both curves). The curve becomes negative because the binding rates were less than 1unit and the log of a fraction is always negative.

5.2.2.6 Non-Specific Binding. The interaction of the group A RBCs was found to be highly specific since RBC retention did not occur during analysis of 100 % (v/v) group A RBC in the absence of anti-A IgG (*Figure 5.2.2.6*). However, the interaction curve indicates that a fraction of the RBCs were within the range of the evanescent field. These cells may not be interacting with the matrix

and are detectable because of RBC packing against the sensor surface. This is expected as greater than 95 % of the available free space is occupied by RBCs. Consequently, these cells do not remain at the surface when the sensing element is immersed in PBS buffer after sample exposure. This was confirmed by the return of the response to the initial baseline (-0.23 AU).

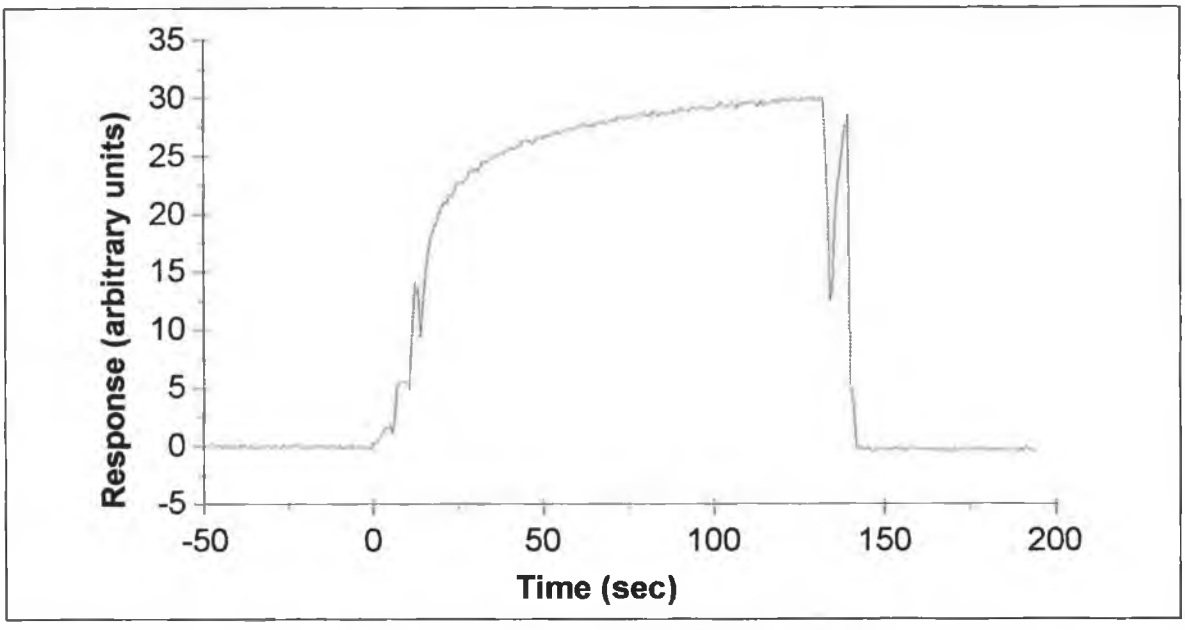

Figure 5.2.2.6. 'Control' interaction curve. The protein A-coated sensing element was exposed to 100 % (v/v) washed group A RBCs for ~ 2 min in the absence of anti-A IgG. The sensing element was returned to PBS buffer and the response returned to the baseline (-0.23 AU). The response spikes are associated with manual sampling and can be ignored.

5.2.2.7 Response Correction for Non-Linearity. As outlined earlier (section 4.2.4.8), the expected BIACORE 1000™ response, assuming 100 % surface coverage was estimated to be 66,000 RU but the presence of the dextran matrix (100 nm thick) will lower the expected response to 23,700 RU. An equivalent saturation response may be expected from the 'in house' built fibre optic probe, since the CM5 sensor probe possesses identical surface chemistry to the CM5 sensor chip. Interaction curves obtained using the fibre optic SPR sensor are not directly comparable to interaction curves from BIACORE analysers due to the non-linearity of the fibre optic SPR response. However, the interaction curves may be corrected by expressing the response (arbitrary units) in terms of refractive index (using the expression given in *Figure 5.2.1.5.3*). The response given in terms of refractive index can be converted to BIACORE response units (using expression in *Figure 5.2.3.4.1*(b)) and plotted as a sensorgram (*Figure 5.2.2.7*(a)). This sensorgram shows that the antibody-binding response was similar to that obtained using the BIACORE probe. In addition, the RBC binding response (18,100 RU) is almost identical to the maximum binding response obtained

for the BIACORE Probe (18, 172 RU, (*Figure 4.2.4.4*). This represents 76 % of the theoretically expected saturation response assuming 100 % coverage. Hence, the void volume at the surface is 24 % and further confirms the ability of RBCs to deform to occupy a large fraction of the space outside the hydrogel surface. Removal of the hydrogel may be expected to increase this response to ~ 28,300 RU.

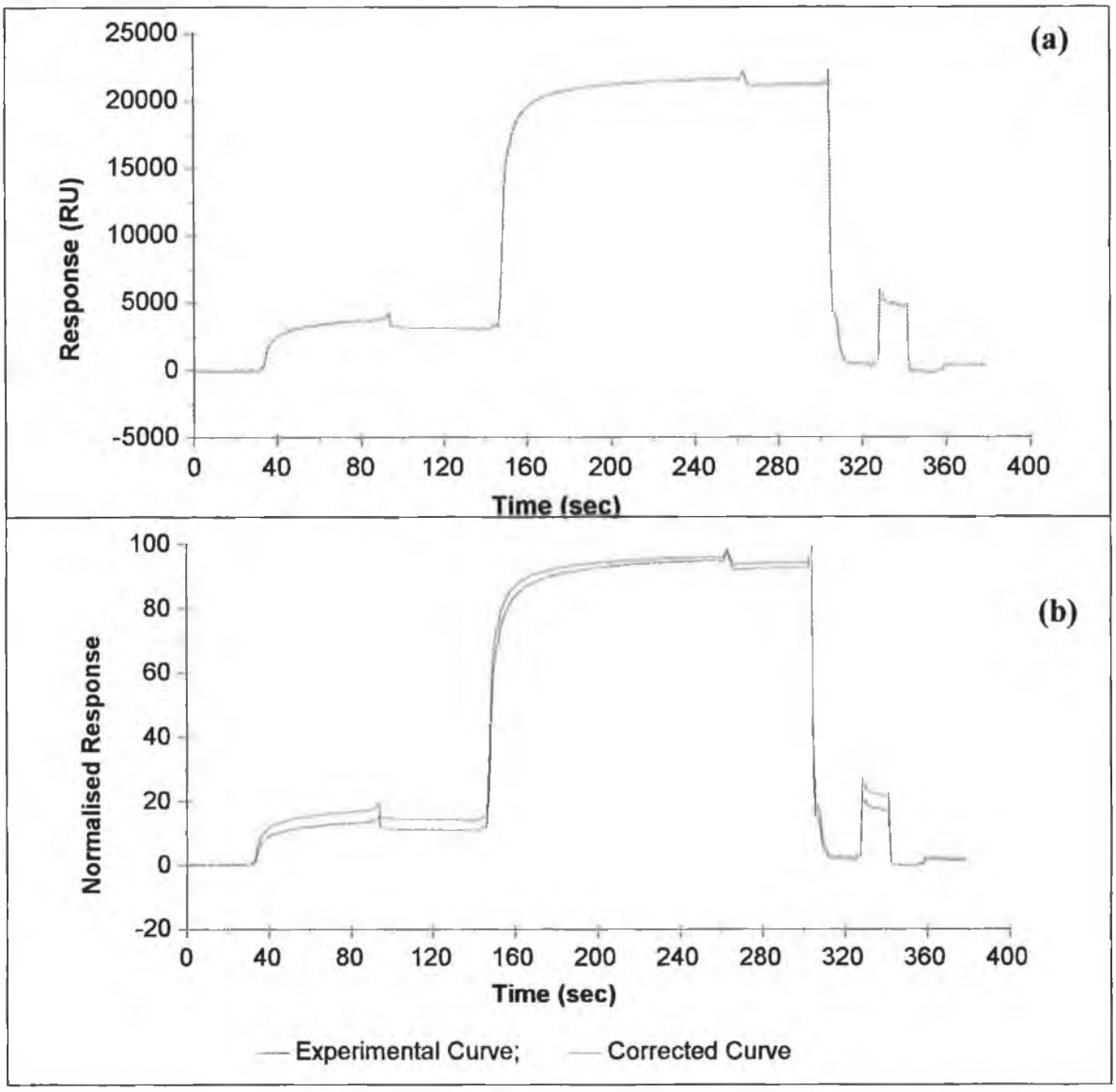

Figure 5.2.2.7. **(a)** Fibre optic SPR interaction curve transformed into an equivalent BIACORE interaction curve. The interaction curve show in *Figure 5.2.2.4* was converted to an equivalent BIACORE sensorgram using refractive index calibration curves. The antibody binding response was 3,100 RU and the RBC binding response was 18,100 RU. **(b)** Overlay of the complete interaction curve obtained for 100 % (v/v) RBCs (Experimental curve) (*Figure 5.2.2.4*) with the equivalent BIACORE sensorgram (corrected curve) (*a*). The curves have been normalised with respect to the respective maximum response values to enable the identification of distortions.

The corrected curve (*Figure 5.2.2.7*(a)) was compared to the original fibre optic SPR curve (*Figure 5.2.2.4*) in *Figure 5.2.2.7*(b). The curves were normalised with respect to the maximum response to facilitate the identification of deviations induced by the non-linearity of the fibre optic SPR response. Visual inspection reveals considerable distortion from the corrected curve, which represents the actual progress of the interaction. The original curve represents the progress of the interaction as distorted by the increasing sensitivity at higher response values. However, the data obtained from the fibre optic SPR sensor may be corrected in 'real-time' by incorporating the calibration expressions into the signal processing software. Hence, it should be possible to conduct kinetic experiments by simply including a means of generating high mass transfer rates during sample analysis. This might be accomplished by employing a rotating cylindrical flowcell. In addition, a more accurate means of determining the position of the SPR minimum from resonance spectra is required to enhance sensitivity.

5.2.2.8 Finding the Position of the Reflectance Minimum. Determination of the zero-crossing point for the first derivative of the resonance spectrum (*Figure 5.2.2.8*) may be a suitable alternative to fitting high-order polynomials. In contrast to other fitting procedures (e. g. first moment of resonance (section 5.2.3.3.1), this technique is insensitive to wavelength-dependent changes in the shape of the resonance minim

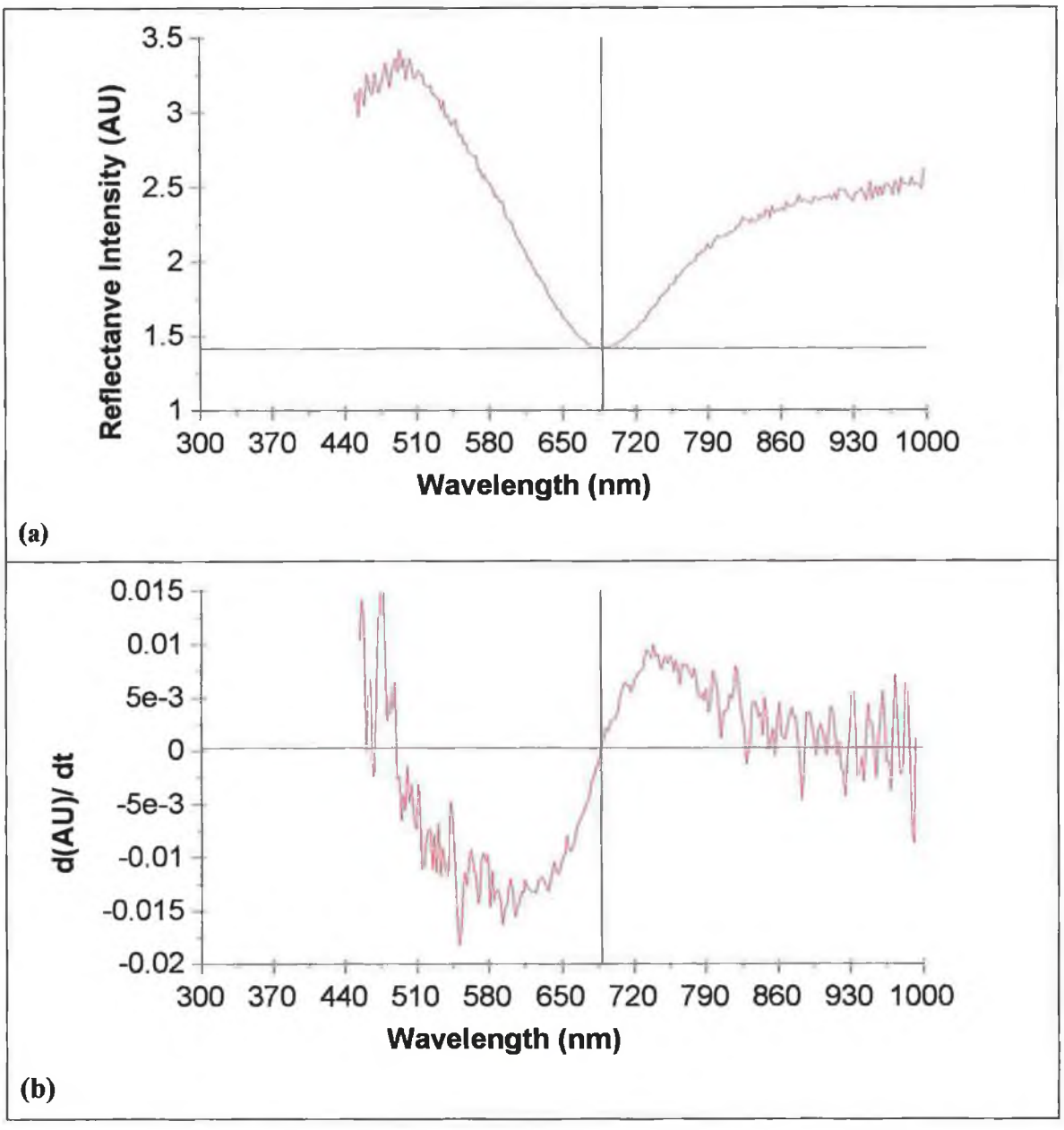

Figure 5.2.2.8. ***(a)*** Resonance spectrum with zero-crossing of the first derivative (cross-wires) about the resonance minimum. **(b)** First derivative of the resonance spectrum. The zero-crossing point about the resonance minimum occurs at 686 nm.

5.2.3 Miniature SPR Sensor.

5.2.3.1 ***Principle of Operation***. The Kretschmann optical configuration for SPR typically requires expensive optical components. However, Texas Instruments (Dallas, Texas, USA) have designed a novel miniature SPR transducer capable of 'real-time' refractive index sensing that is manufacturable in high volume at low cost. Essentially, the device consists of miniature electro-

optical components mounted on a single platform using conventional semi-conductor-based opto-electronic manufacturing techniques (Melendez *et al.*, 1996). The single platform is encapsulated in an optically transparent plastic (i.e. Epoxy) using cast moulding, and it provides a substrate for the deposition of the SPR sensing layer and reflective mirrors. A schematic illustration of the device is shown in *Figure 5.2.3.1*(a). The device weighs ~ 7 g and has a volume of ~ 7 cm^3. A narrow band infrared light emitting diode (LED) is housed in a structure that includes a silicon chip to monitor intensity variations of the LED. A narrow aperture with a polarising film at the top of the housing controls the width of the emerging light beam and reduces the emission of transverse electric radiation. The wedge-shaped beam reflects from the SPR surface under conditions of total internal reflection and is directed onto a linear photodetector array (128 pixels) by a mirror (i.e. gold film). The active sensing surface is 4.5 mm long and 0.025 mm wide. An SPR-induced minimum will occur for the reflected light and the position of the minimum is determined by processing the signal from the diode array. A temperature sensor is incorporated and can be used to correct the response for temperature fluctuations during analysis. A control box interfaces with the device and can be installed on a personal computer. Dedicated software (SPR-MINI MS-Windows Software) allows user control, along with data acquisition, processing and display via a virtual control panel. The complete system is shown in *Figure 5.2.3.1*(b).

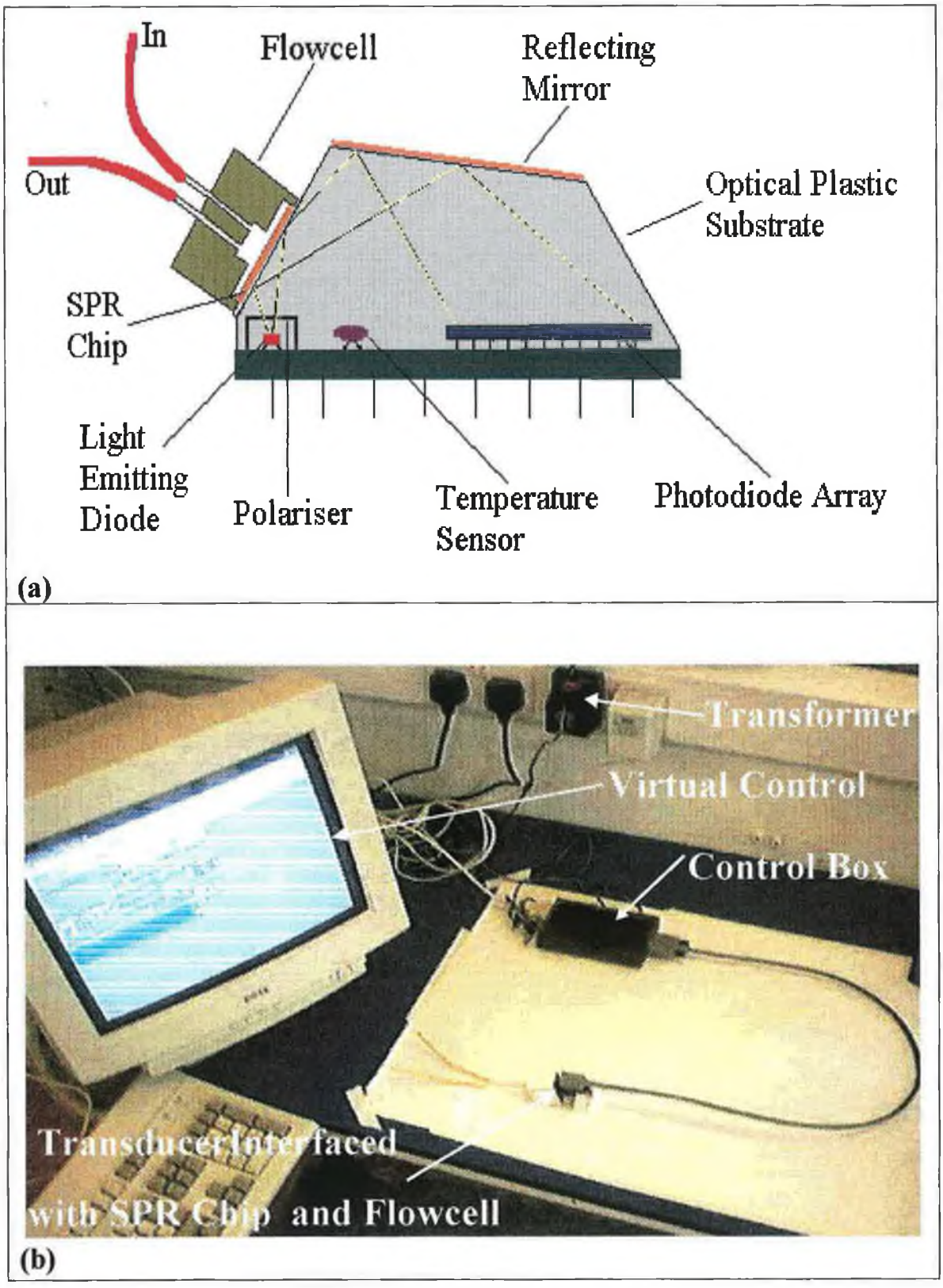

Figure 5.2.3.1. (a) Digital image of the miniature SPR sensor system. (b) Schematic of the single-platform miniature SPR transducer interfaced with the SPR chip and flowcell.

5.2.3.2 ***Data Acquition, Processing and Display***. The reflectivity as detected by each pixel is give by:

$$R = \frac{S - B_S}{A - B_A}$$

where

R	=	Reflectivity
S	=	Signal in liquid
A	=	Air reference
B_A	=	Background reference in air
B_s	=	Background reference in water

The software employs this expression when generating the SPR curve. The background reference is performed with the LED turned off to account for the dark response of the LED. The background reference also subtracts ambient light that may reach the detector. However, this effect has been minimised as the device is covered with an opaque black paint, with the exception of the sensing surface. An air reference is taken to ensure that the above factors are eliminated and the reflectance plot (reflectance intensity against pixel number) should show a uniform straight line as SPR cannot occur in air using this optical configuration. The air reference cannot be taken after immobilisation of the biomolecule because repeated drying may decrease the biological activity of the immobilised ligand. Consequently, this reference was stored before ligand immobilisation and recalled from the computers memory when required. The use of this sensor as a refractometer and biosensor has been demonstrated (Furlong *et al.*, 1996; Melendez, 1996; Texas Instruments, 1998). However, the sensor performance is restricted by the signal/noise ratio that is defined by the systems electronic components (e.g. 8-bit analogue/digital converter in the readout box). This limits the systems sensitivity to the pixel position of reflectance minimum giving a high background noise of $\pm$ 1 x 10^{-4} Δn (equivalent to $\pm$ 100 RU).

5.2.3.3 SPR Curve Analysis. The position of the SPR reflectance minimum can be found by a number of mathematical fitting routines. The first moment method calculates the first moment of the SPR minimum below a set baseline and is described by:

$$1^{st}\ moment = \frac{\sum_{i=1}^{256} \left| SPR\ signal_i - Baseline \right| * i}{\sum_{i=1}^{256} \left| SPR\ signal_i - Baseline \right|}$$

where the data above a pre-set baseline is excluded.

This technique was employed as it reliably found the minimum giving a low background noise level. A typical SPR minimum displaying the 1st moments is shown in *Figure 5.2.3.3.1*.

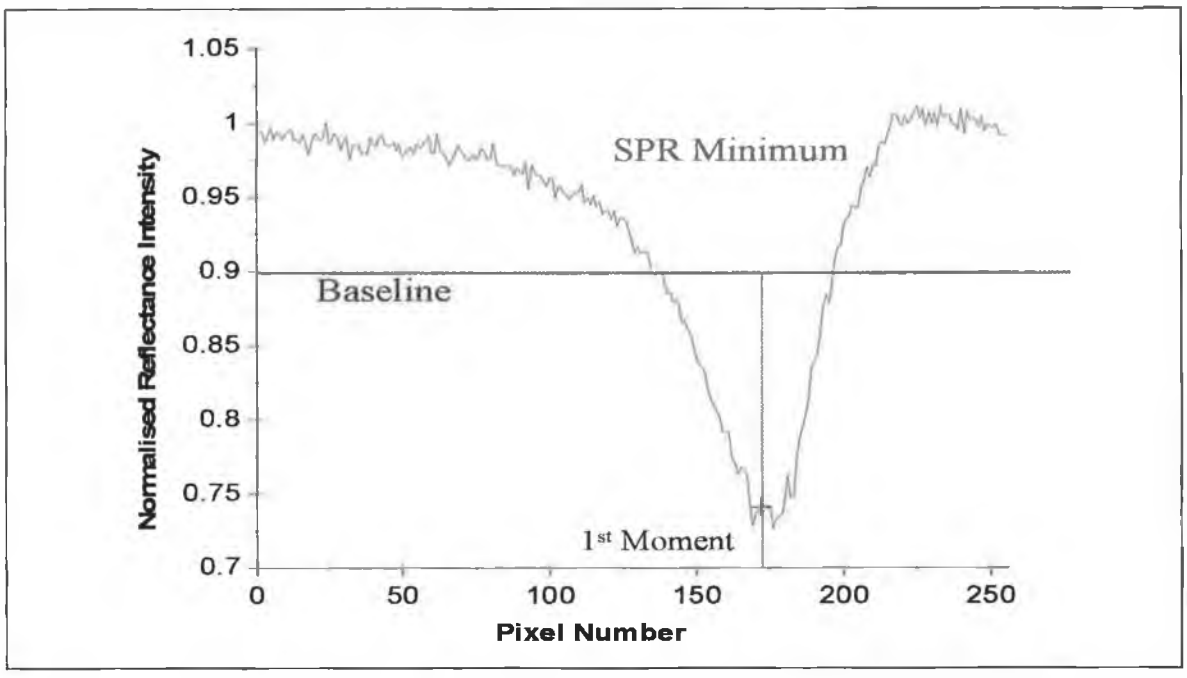

Figure 5.2.3.3.1. Locating the position of the SPR minimum using the 1st moment method. The SPR curve was recorded using the modified miniature SPR sensor. The baseline was set to 90 % reflectance intensity. It is important that the baseline intersects the minimum at two points. The technique is sensitive to changes in the shape of the SPR minimum. It is not suitable for polychromatic fibre optic SPR systems where both the shape and position of the resonance minimum are wavelength-dependent.

The sensor response is generated by finding the position of the SPR minimum over a range of angles of incidence. The map between pixel position and angle of incidence is fixed by the geometry of the sensor. Hence, the following calibration expressions are employed. The refractive index is given by:

$$n = (-4.764515\,x\,10^{-1})(Pn)^2 + (-3.791882\,x\,10^{-4})(Pn) + 1.417017$$

where n = Refractive index
Pn = Pixel number

also

$$Al = (2.599303\,x\,10^{-5})(Pn)^2 + (-0.0670907)(Pn) + 77.13167$$

where Al = Angle of incidence (degrees)

However, the sensor elements are manually placed onto the platform during fabrication causing variation between devices. Hence, the response is normalised using water (known refractive index of 1.3327) to adjust the calibration curve of refractive index versus pixel position along the pixel-axis. The virtual control panel is shown in *Figure 5.2.3.3.2* and displays an interaction curve together with an SPR minimum curve.

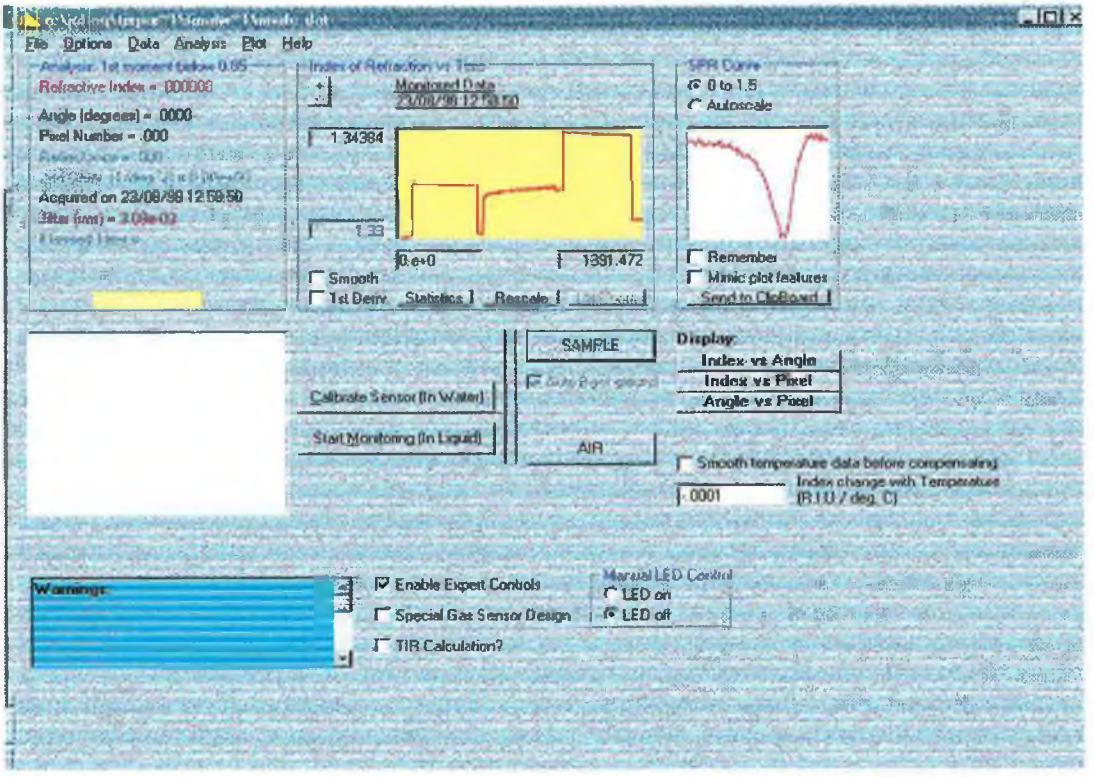

Figure 5.2.3.3.2. Virtual control panel supplied by Texas Instruments (SPR-Mini software). The sensor was not in use when this image was captured. The interaction curve and SPR minimum are from stored data.

5.2.3.4 Sensor Performance without a Disposable SPR Chip.

5.2.3.4.1 Calibration. The performance of the sensor was validated by comparing refractive index calibration curves (produced using glycerol:water solutions) determined using the miniature SPR sensor and an Abbé refractometer. The refractive index measurements recorded for glycerol:water solutions are shown in *Figure 5.2.3.4.1*(a). As expected, the angle dependent SPR sensing configuration resulted in a linear dependence on the refractive index of the sample medium. In addition, the data from the sensor is reliable as both calibration curves are superimposable. Furthermore, the calibration expressions are almost identical giving very similar regression coefficients.

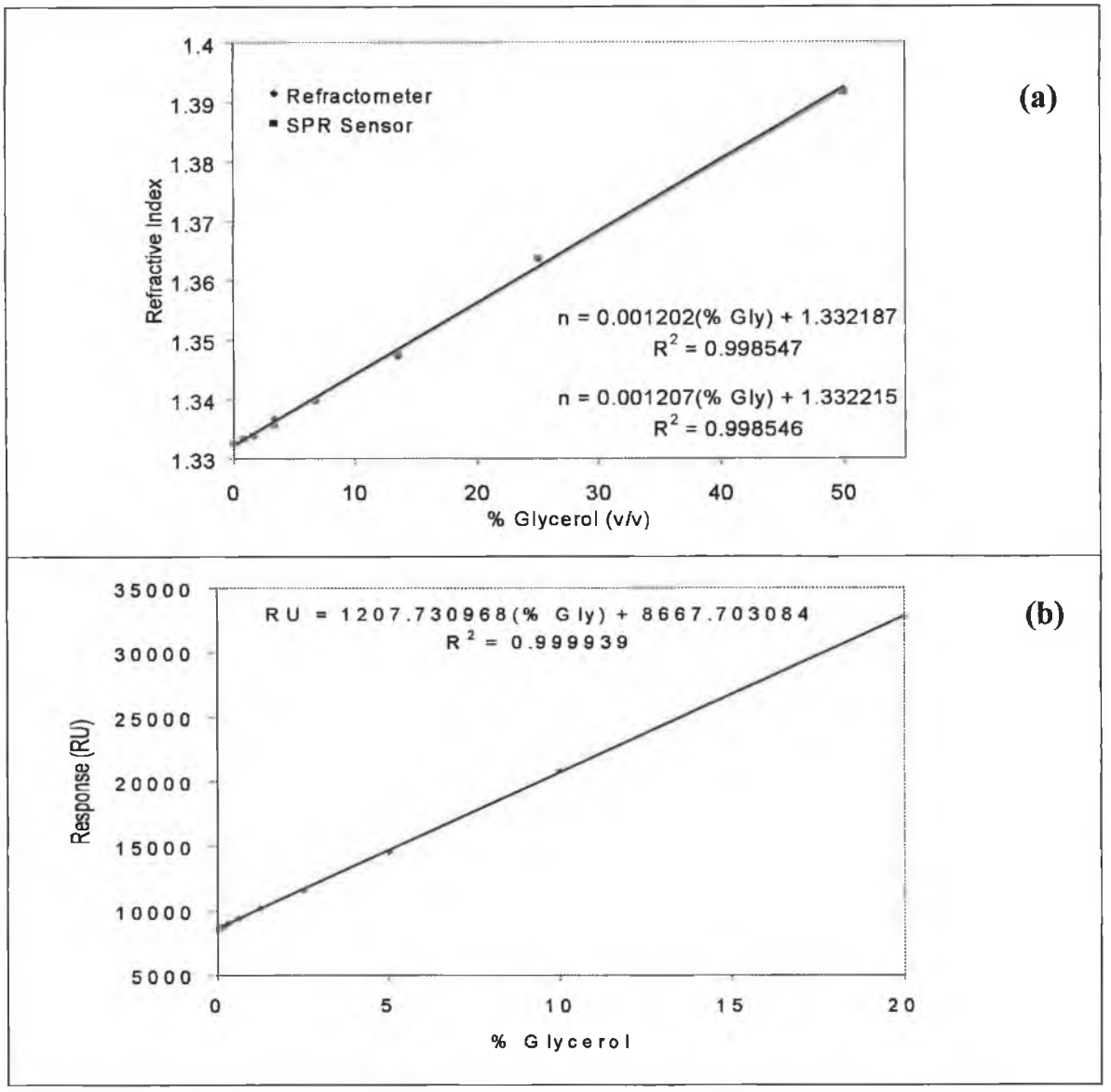

Figure 5.2.3.4.1. (a) Overlay of refractive index calibration curves determined using an Abbé Refractometer and the miniature SPR device. A linear regression analysis was fitted to both sets of data and the resulting calibration equations and regression coefficients (R^2) are displayed. **(b)** Response calibration curve as determined using BIACORE 1000™. The BIACORE response is directly related to the refractive index change at the surface (1000 RU = 0.001 Δn). Hence, the slope is virtually identical to that obtained from the miniature SPR device calibration. Therefore, the calibration curves obtained for both biosensing systems are essentially identical

A calibration curve determined using the BIACORE 1000™ should yield the same calibration equation as it employs angle-dependent SPR and a monochromatic light source (*Figure 5.2.3.4.1*(b)). The slope obtained for the BIACORE 1000™ analysis was 1,207 RU/% Gly. However, the BIACORE response is directly related to the refractive index at the surface as 1,000

RU is equal to 0.001 Δn. Hence, the slope can be expressed in terms of refractive index (0.001207 Δn /% Gly) and is identical to that obtained for the miniature SPR sensor (i.e. 0.001207 Δn/%Gly). Therefore, the calibration curves are almost identical. The dynamic range of the miniature SPR device is greater than the BIACORE 1000™ system. However, the sensitivity of the BIACORE 1000™ system dramatically exceeds (100-fold) that of the miniature device.

5.2.3.4.2 Surface Derivatisation. The device supplied by Texas Instruments possesses a gold-coated SPR surface. Immobilisation of proteins onto this surface can be accomplished by simply allowing the protein to adsorb directly onto the metal surface. However, this strategy leads to deformation and denaturation of the adsorbed protein. In particular, a large fraction of the adsorbed molecules may be poorly orientated at the surface, producing steric hindrance of some binding sites. The incorporation of a CM-dextran hydrogel avoids these difficulties. Firstly, a self-assembled monolayer was generated on the gold-coated surface by submerging the surface in an alkanethiol solution (1 mg/ml mercapto-undecanol in ethanol). This layer serves two purposes.
(a) It provides a linker layer through which the hydrogel can be anchored to the surface.
(b) By insulating the surface it prevents non-specific adsorption to the gold layer.

A proportion of the hydroxyl groups were activated (epoxy groups) using 0.6 M epichlorohydrin under basic conditions. The surface was then exposed to a concentrated solution of dextran (M.W. 500 kDa) under basic conditions in order to achieve covalent attachment of dextran via hydroxyl groups. Carboxyl groups were introduced onto the hydrogel by reacting the hydroxyl groups of the dextran with bromoacetic acid under basic conditions. This procedure produces a biointerface similar to the CM5 SPR chip (Löfås and Johnsson, 1990). The assembly of the biointerface was confirmed by performing a preconcentration test. Essentially, the presence of the CM-dextran at the surface will induce preconcentration of positively charged proteins causing a reversible increase in response. Preconcentrated protein can be removed from the surface by simply increasing the ionic strength of the solution. A solution of bovine serum albumin (BSA) was prepared in 10 mM sodium acetate buffer, pH 4.5, and exposed to the sensor surface. The interaction curve is shown if *Figure 5.2.3.4.2.*

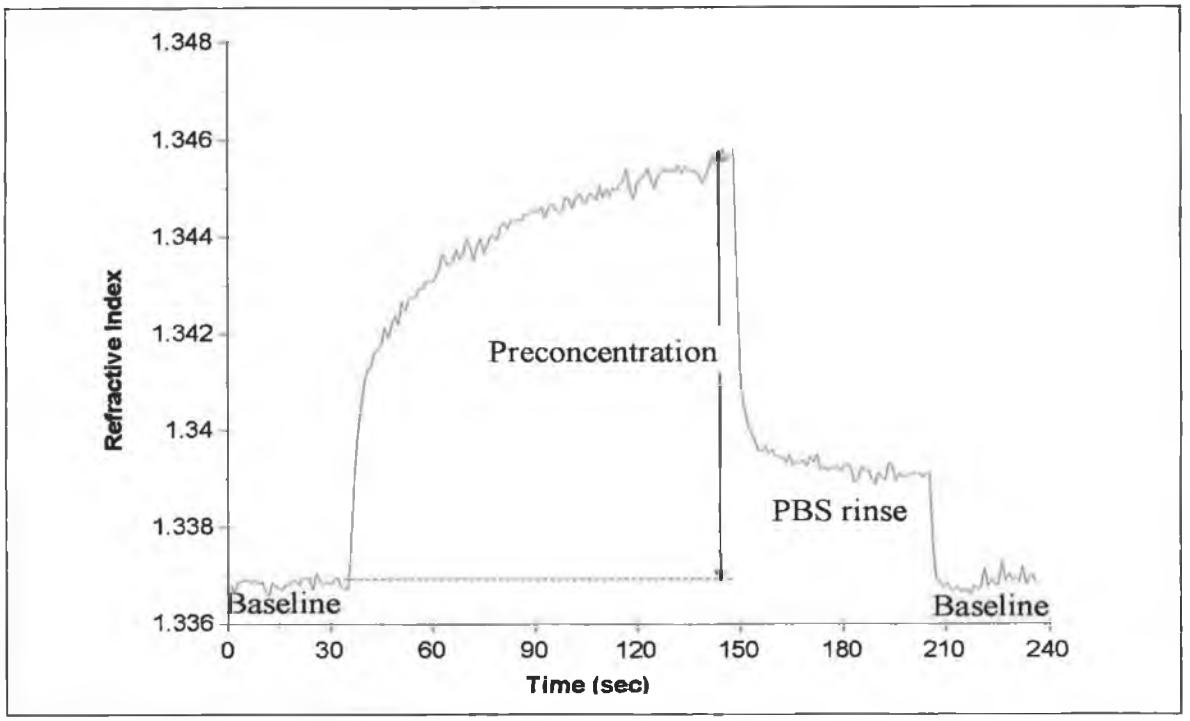

Figure 5.2.3.4.2. Preconcentration of BSA onto the CM-dextran biointerface. A flowcell was attached to the miniature SPR sensor and was primed with ultrapure water. The initial baseline is the response during exposure to water. The BSA solution (100 μg/ml in 10 mM sodium acetate, pH 4.5) was injected into the flowcell and preconcentration of the positively charged protein onto the negatively charged matrix was observed (2 min incubation). The bulk refractive index change due to the dilute acetate buffer can be neglected. Hence, the refractive index change due to preconcentration was approximately 0.009 Δn (i.e. 9,000 RU). The preconcentrated protein was removed by injecting PBS into the flowcell to disrupt the ionic interactions. The refractive index of PBS is high due to the presence of 0.15 M NaCl. Consequently, water was injected into the flowcell to return the signal to the initial baseline response.

The preconcentration effect gave a high refractive index change of 0.009 Δn, whereas repetition of the experiment using the BIACORE 1000™ gave a refractive index change of 0.0206 Δn. The lower preconcentration effect observed for the miniature system may be attributed to size exclusion effects (due to a high density of dextran) or a lower number of carboxylic groups. The response was totally reversible indicating that non-specific binding of BSA to the hydrogel-based biointerface was negligible. The presence of the biointerfacial layer was further confirmed by monitoring the increase in the refractive index at the surface. The self-assembled monolayer has a thickness of ~ 1.3 nm (with a refractive index of 1.59) while the CM-dextran layer is approximately 100 nm thick (dn/dc (dextran) of 0.15) (Stenberg *et al.*, 1991). The refractive index contribution of the monolayer can be neglected due to its extreme thinness. Therefore, the refractive index increase due to the presence of the hydrogel was determined to be 0.004412 Δn.

The change in refractive index (Δn) due to the CM5 dextran matrix was calculated by removing the dextran from a normal CM5 chip by exposing the surface to 5 M NaOH for 10 min and recording the baseline response before and after the exposure. Almost complete removal of the dextran was determined as preconcentration of BSA (1 mg/ml in 10 mM sodium acetate buffer, pH 4.55) was reduced to 2.6 % of the normal response. In addition, the self-assembled monolayer remained intact as complete insulation of the gold layer was validated by the negligible adsorption (21.6 ± 1.39 RU) of BSA (10 mg/ml in HBS buffer) onto the planar surface. The dextran matrix of the CM5 chip was found to give a refractive index contribution of ~ 0.001660 Δn. Therefore, the biointerface generated on the surface of the miniature SPR device possesses 2.6-fold more dextran than the CM5 SPR chip. However, removal of the flowcell revealed that the gold layer was severely corroded. This may be attributed to poor adhesion of the gold layer to the epoxy surface and exposure to extremes of pH (0.2 M NaOH) during derivitisation of the sensor surface. In contrast, the CM5 chip was stable when exposed to 5 M NaOH for 10 min. The enhanced stability of the CM5 chip may be related to the use of 16-mercapto-hexa-undecanol (16-carbon atom chain) rather than mercaptoundecanol (10-carbon atom chain). The longer hydrocarbon chain promotes tight packing within the monolayer due to hydrophobic interactions. However, the quality of the deposited gold layer is likely to be the most important factor, as pinholes in the layer (i.e. due to dust particles) may decrease the stability of the surface. Consequently, the SPR transducer was used in conjunction with disposable SPR chips.

5.2.3.5 Sensor Performance Using Disposable SPR Chip

5.2.3.5.1 Sensor Modifications. The miniature SPR transducer requires specific modifications to facilitate biosensing applications. The gold layer is deposited directly onto the optical device. Consequently, only a single biomolecular interaction can be studied for a given device. In addition, the number of binding-regeneration cycles that can be performed is limited by the stability of the immobilised ligand. Furthermore, the gold layer was found to be unstable. These considerable limitations seriously hinder the utility of the device as a biosensor. Hence, it was decided to modify the device by removing the gold layer and interfacing the device with an SPR chip using a refractive index matching fluid (Lens oil). The CM5 SPR chip is commercially available from BIACORE AB (Uppsala, Sweden) and was used for RBC detection. However, a similar SPR chip was fabricated 'in house' (Mark Hyland, NIBEC, University of Ulster, Co. Antrim, Ireland) and was compared to the CM5 SPR chip. The CM5 sensor chip possesses a hydrogel-based biointerface that significantly increases (> 10-fold) the surface capacity thereby counteracting the effect of the high background noise level. A flow cell was custom fabricated to facilitate docking a

CM5 SPR chip with the device since the flow cell kit supplied by the manufacturers was found to be unsuitable. The assembly of the modified miniature SPR biosensor is shown in *Figure 5.2.3.5.1*.

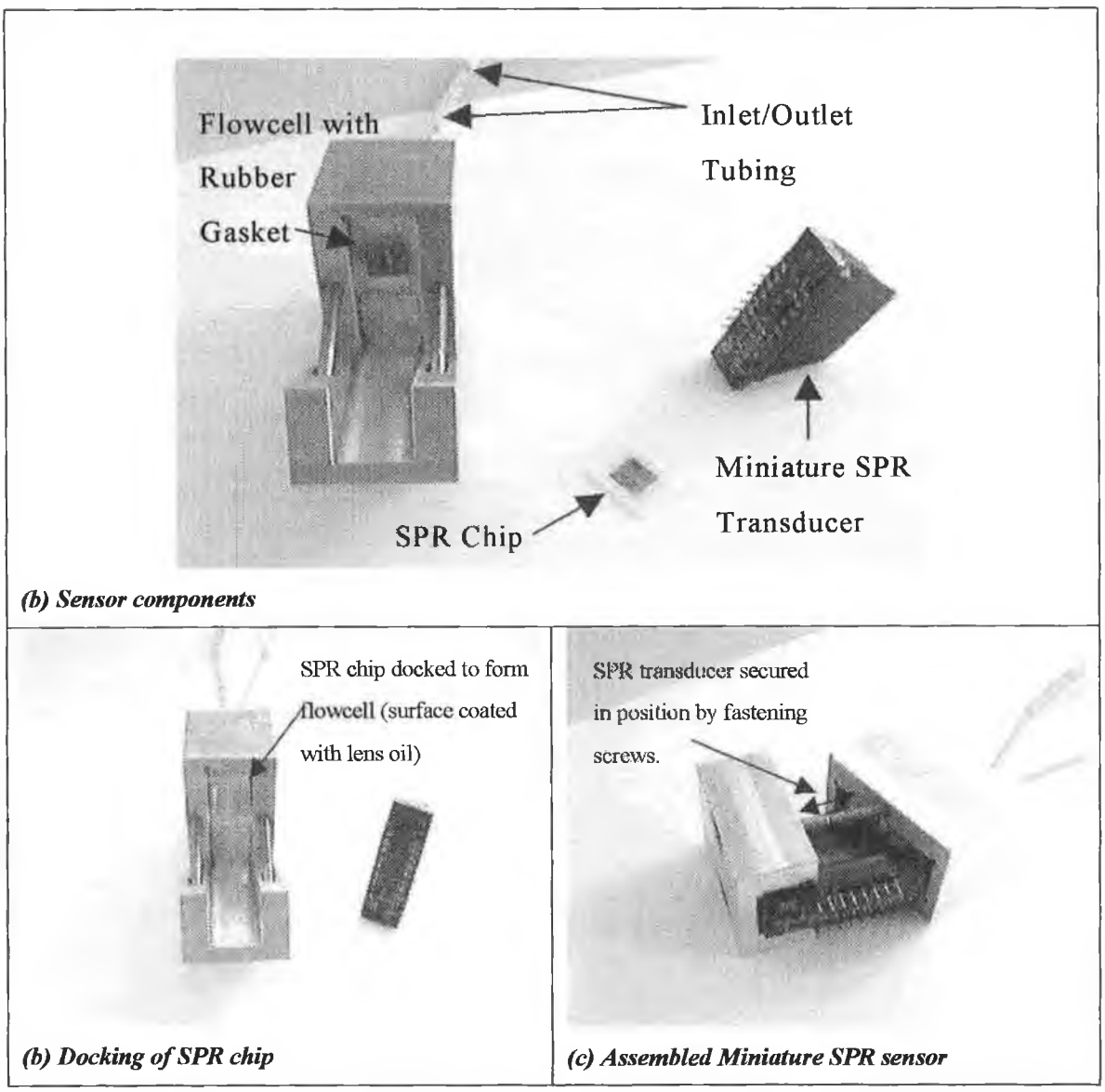

(b) Sensor components

(b) Docking of SPR chip

(c) Assembled Miniature SPR sensor

Figure 5.2.3.5.1. Assembly of miniature SPR sensor employing a disposable SPR chip. The assembled device is then connected via a communications cable to the control box. A personal computer serial communications cable (9-pin D connector) interfaces the control box with a computer that runs SPR-mini software. The sensor, complete with flowcell, was clamped so that the interaction surface was positioned along the roof of the flowcell (similar to BIACORE 1000^{TM} configuration).

5.2.3.5.2 *Sensor Calibration.* A 'real-time' interaction curve for the calibration of the miniature SPR device interfaced with a CM5 chip and flowcell is shown in *Figure 5.2.3.5.2*. Increasing concentrations of glycerol (prepared in ultrapure water) were injected into the flowcell

and incubated for ~ 30 sec. The noise level (± 5 x 10^{-5} Δn) was found to be 100-fold higher than the BIACORE 1000™ system (5 x 10^{-7} Δn). Hence, this system is not suitable for the study of low molecular weight interactants and limits the system to applications that are compatible with very high surface-protein concentrations. Hence the incorporation of dextran matrix onto the chip is recommended in order to enhance the surface capacity for the detection of macromolecular interactions. However, the detection of large particles such as whole RBCs is not enhanced by the presence of a hydrogel due to size exclusion. Nevertheless, high RBC-binding responses (i.e. 0.018 Δn) were observed during fibre optic SPR analysis (*Figure 5.2.2.7*(a)). A similar binding response was expected using the miniature SPR biosensor since identical biointerfacial chemistry was employed (i.e. CM5 SPR chip).

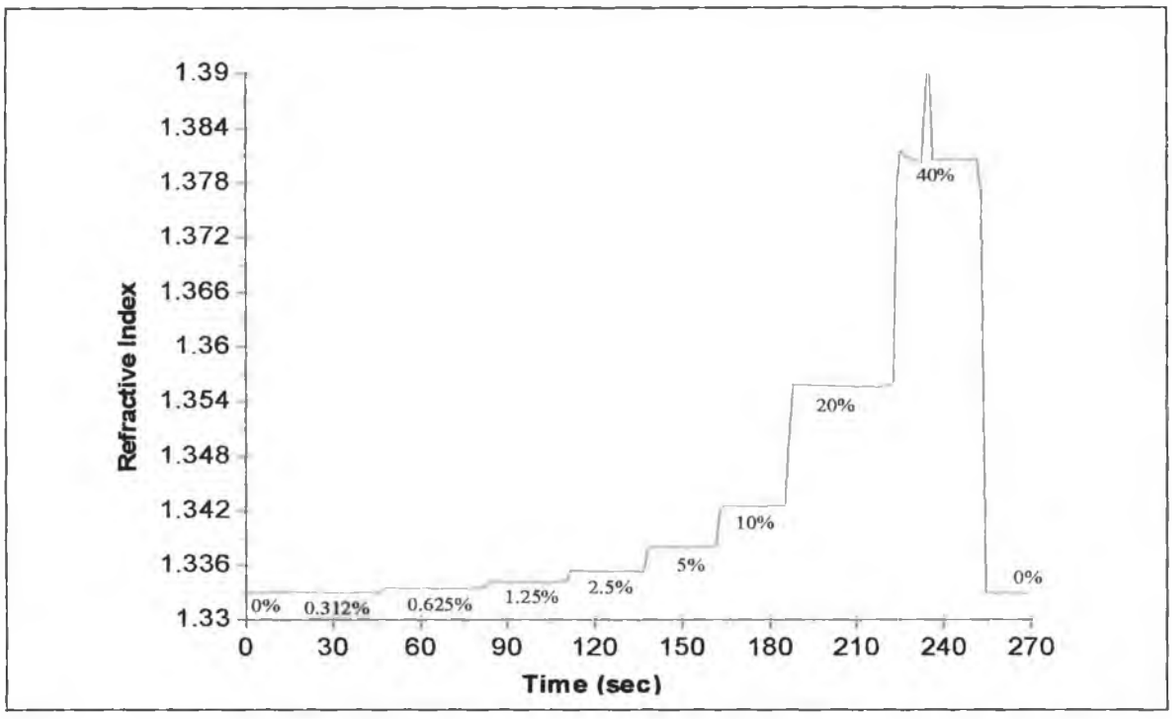

Figure 5.2.3.5.2. Interaction curve for increasing glycerol concentrations using the miniature SPR device interfaced with a CM5 sensor chip and customised flowcell. Glycerol:water solutions were prepared by serially diluting a 40 % (v/v) glycerol solution with ultrapure water. The samples were manually injected into the flowcell and were exposed to the surface for > 30 sec.

A refractive index calibration curve was constructed from the refractive index measurements of *Figure 5.2.3.5.2.* The following calibration equation was determined from linear regression analysis: n = 0.001216(%Gly) + 1.33230 (R^2 = 0.998). This expression correlates with the calibration determined using the unmodified sensor (*Figure 5.2.3.4.1*). A wide refractive index range was observed (1.33 to 1.39) making it particularly suitable for the detection of high MW

macromolecules at high surface binding capacities. An 'in house' alternative to the expensive CM5 chip was developed. This chip was fabricated by deposition of a thin adhesion layer (silicon oxide) onto the glass slides and subsequent deposition of the gold (~ 50 nm layer). A monolayer of mercapto-undecanol was self-assembled on the gold surface to prevent exposing the gold layer to aqueous environments.

5.2.3.5.3 *SPR Chip Comparison.* The performances of the CM5 SPR chip and the 'in house' fabricated SPR chip ('planar' chip) were assessed by examining the SPR minima given by each chip as determined using the miniature SPR biosensor.

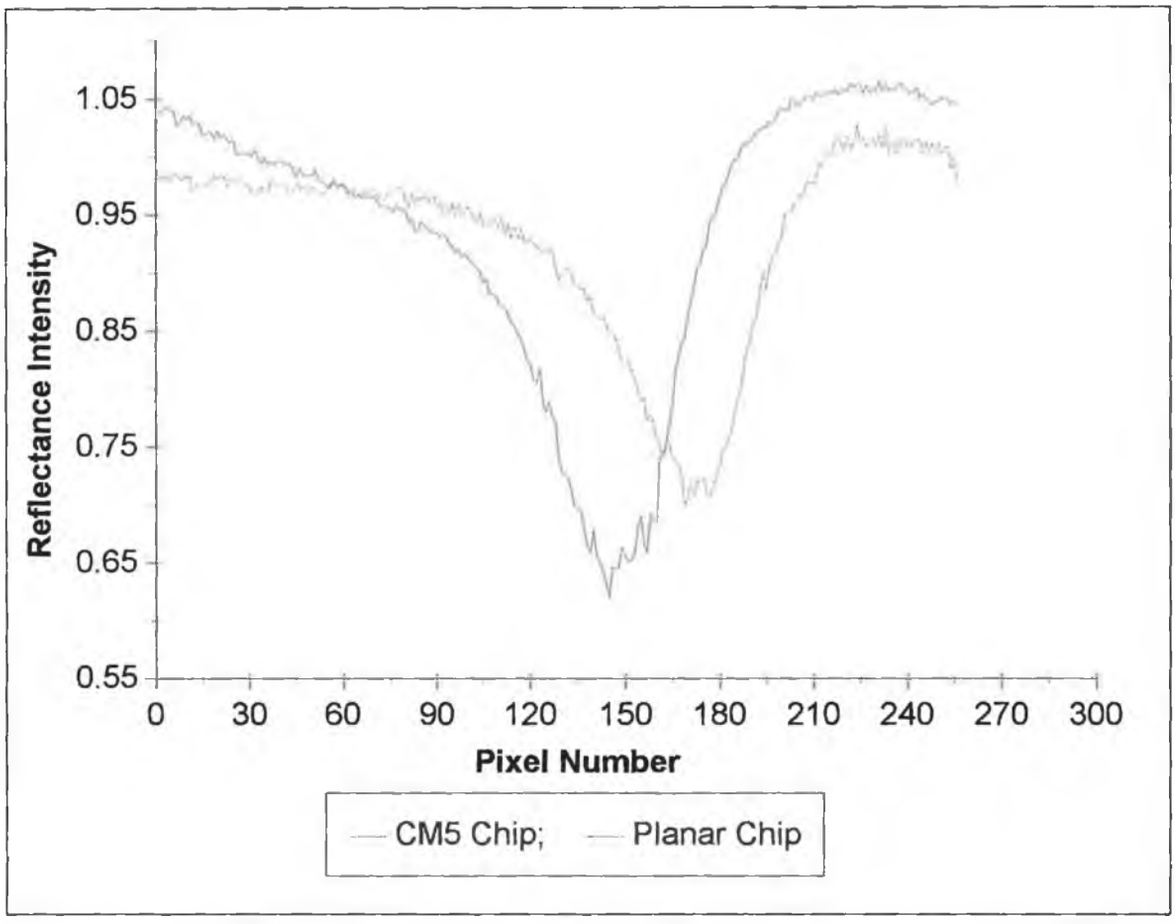

Figure 5.2.3.5.3 Overlay of SPR curves for the CM5 chip and 'planar' chip using the miniature SPR sensor. Both SPR minima were recorded in PBS buffer. The gold layer of the miniature SPR sensor was removed by polishing with fine-grain sandpaper. The reflectance minima of both the CM5 and 'planar' SPR chips were compared by docking either chip against the miniature SPR sensor. Microscope lens oil was used to match the refractive indices of the glass slide and the epoxy plastic of the SPR transducer. Serial dilutions of glycerol in water were prepared and the refractive index was calculated automatically by the mini-SPR software provided.

An overlay of the SPR curves obtained for the CM5 SPR chip and the 'planar' SPR chip is shown in *Figure 5.2.3.5.3.* It is obvious that both SPR curves differ with respect to the intensity of the SPR minimum and the SPR angle. The CM5 and 'planar' sensor chips gave a 40 % and 30 % drop in reflected light intensity, respectively. The depth of the SPR minimum is related to the thickness of both the gold layer and the adhesion layer. The 'planar' chip was fabricated by depositing a thin (10 Å) layer of silicon oxide onto a clean glass slide. This provides an adhesion layer for subsequent deposition of the gold layer (50 μm). A self-assembled monolayer was constructed on the gold surface to insulate the surface from the aqueous environment. The thickness of the adhesion layer is minimized in order to reduce the SPR dampening effect induced by this layer. The composition of the adhesion layer of the CM5 chip is unknown. Hence, the shallower SPR minimum observed for the 'planar' chip may be caused by the silicon oxide adhesion layer. However, both curves are of similar width indicating that the thickness of the gold layer is similar for both chips (~ 50 nm). The offset with respect to the pixel number (i.e. SPR angle) is due to the presence of an extended (~ 100 nm) CM-dextran hydrogel on the CM5 chip as opposed to a thin (~ 1.0 nm) self-assembled monolayer on the 'planar chip'. Hence, the increased mass the surface of the CM5 chip shifts the SPR minimum to lower pixel numbers. In conclusion, the 'planar' SPR chip is suitable for biosensing applications but further optimization of the fabrication procedure is required.

5.2.3.6 ***Detection of Whole RBCs.*** The miniature SPR biosensor was employed for 'real-time' detection of whole RBCs (group A) binding to an anti-A IgG-coated surface. Samples were injected and incubated within the flowcell before flushing the flowcell with PBS buffer. Goat anti-mouse Fc IgG was immobilised (~ 0.00278 Δn, i.e. 2,780 RU) onto the CM-dextran hydrogel using conventional amine coupling and the interaction curve is shown in *Figure 5.2.3.6.1.* This antibody-coated surface affinity-captured anti-A IgG from dilute hybridoma supernatants via the Fc region and resulted in directed orientation of the anti-A IgG within the hydrogel.

Specific retention of RBCs was demonstrated by exposing this surface to group A RBCs. A typical interaction curve is shown in *Figure 5.2.3.6.2.* It is obvious that the background noise level (± 5 x 10^{-5} Δn) exceeds that observed for both the BIACORE 1000™ system and the fibre optic SPR system. Exposure to the hybridoma supernatant resulted in a rapid bulk refractive index change followed by a gradually increasing binding curve. The high bulk refractive index change was due to the presence of a high salt concentration (0.3 M) in the hybridoma supernatant. The high salt concentration was employed to prevent precipitation of the antibody during storage at 4 °C. Nevertheless a satisfactory concentration (i.e. 4.1 mg per ml of hydrogel) of anti-A IgG was captured. The RBC association curve is very steep indicating that a steady state RBC binding

response (0.0027 Δn (i.e. 2,700 RU)) was established immediately after sample injection. Hence, the shear forces generated during sample injection did not hinder cell binding. However, the injection flow rate is unknown as manual syringe injection was employed. Once injected the RBC sample was incubated within the flowcell for 6 min. In addition, very little further binding of RBCs occurred during this period. This is in agreement with previous observations as outlined in section 4.2.5.

However, sedimentation of the cells within the stagnant bulk fluid may also influence the binding response by preventing cells from contacting the interaction surface (positioned on roof of flowcell). The flowcell was flushed with 1 ml of PBS to remove free cells and loosely attached cells. However, the binding response did not decrease, indicating high binding avidity between the affinity-captured anti-A IgG and the RBCs. The surface was regenerated using pH elution (i.e. 20 mM HCl) and a detergent wash (1 % Triton-100 in PBS). Regeneration of the surface was sub-optimal as 14 % of residual mass remained at the surface. Elution using shear force generated by flushing PBS through the flowcell at high velocity may be a more effective alternative.

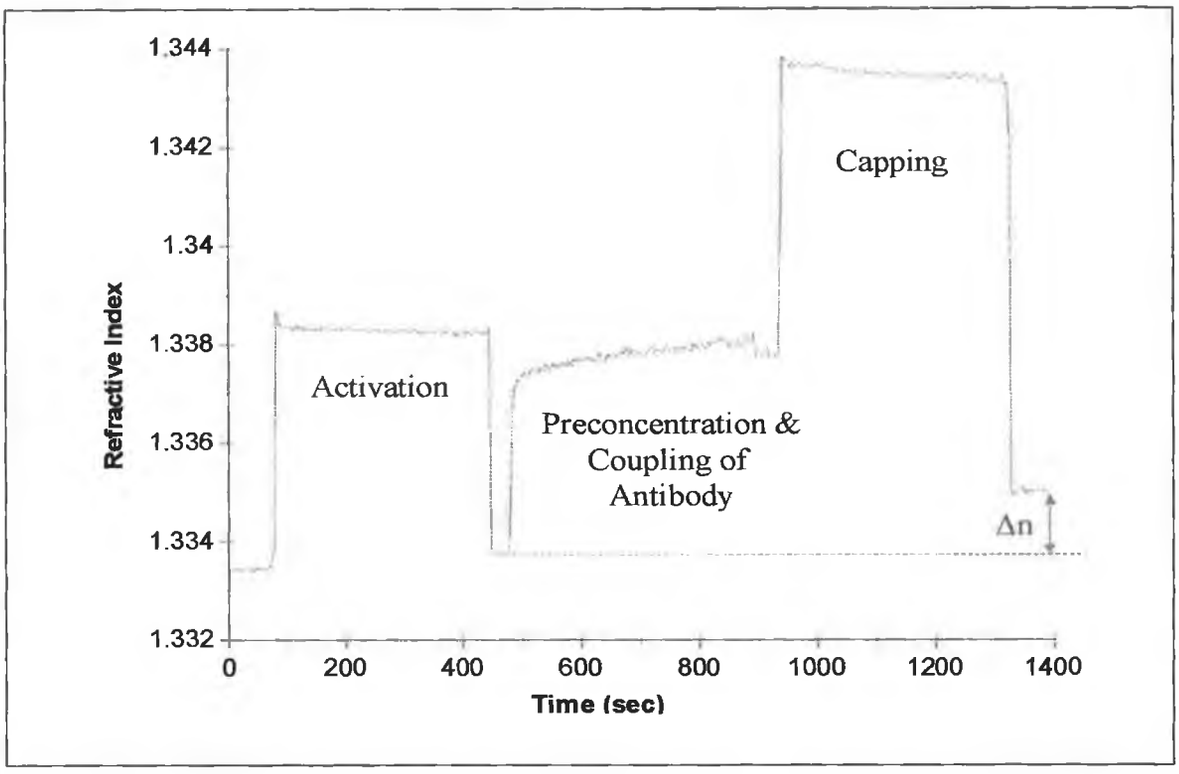

Figure 5.2.3.6.1. Immobilisation of anti-mouse Fc IgG. The sensor was assembled as outlined in *Figure 5.2.3.5.1*. Ultrapure water was injected into the flowcell to give a steady baseline. The CM-dextran hydrogel was activated by injecting a 1:1 mixture of 0.4 M EDC and 0.1 M NHS, allowing a contact time of 6 min. The flowcell was flushed with water and polyclonal goat-anti-mouse Fc IgG (100 μg/ml, in 10 mM sodium acetate, pH 4.5) was injected. The antibody solution was incubated in the flowcell for 6 min to allow preconcentration and covalent coupling and the flowcell was then flushed with water. The response obtained at this point represents both preconcentrated and covalently attached antibody. 1 M ethanolamine was injected to cap residual activated groups. This solution also removed non-covalently adsorbed antibody present in the matrix, because the high ionic strength of this solution negated the ionic preconcentration effect. After 6 min, the flowcell was rinsed with water and the response at this point ($\Delta n \approx 0.00278$ = 2,780 RU) represents covalently attached antibody.

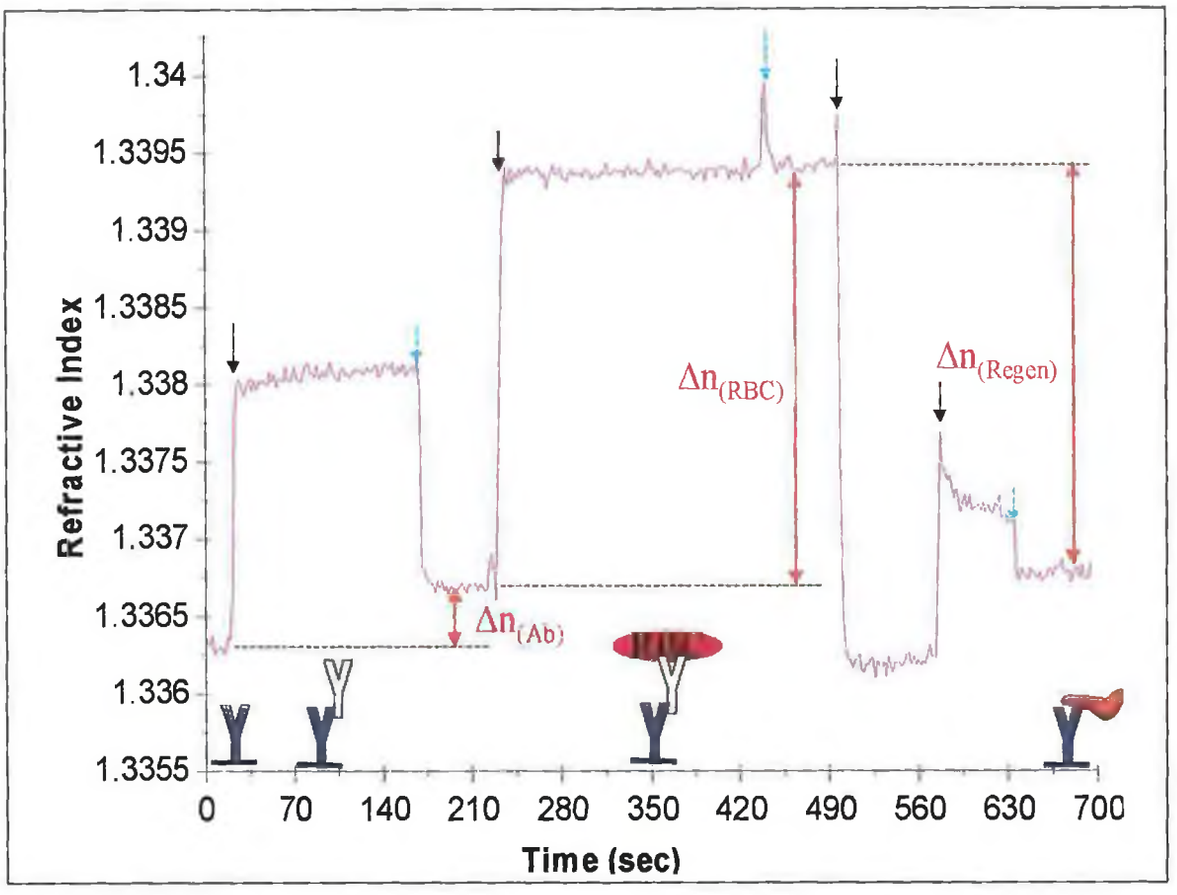

Figure 5.2.3.6.2. Interaction curve for RBC detection using the miniature SPR biosensor. The illustrations depict the interaction sequence. The black arrows correspond to the injection point while the blue arrows correspond to the end of sample contact (i.e. PBS flush). The binding response (i.e. Δn) at each stage is given by the red arrows. The goat-anti-mouse Fc-coated surface was exposed to PBS to obtain a steady baseline. Hybridoma supernatant containing anti-A IgG (containing 0.3 M NaCl) was injected and remained in contact with the surface for 2 min. The flowcell was flushed with PBS and the resulting antibody binding response (0.00041 Δn, i.e. 410 RU) was obtained. Washed group A RBCs (66 % (v/v)) were injected and remained in contact with the surface for 3.5 min. The flowcell was flushed with PBS and the response (0.00271 Δn, i.e. 2,710 RU) due to cell binding was recorded. The surface was regenerated (86 % efficiency) using a 1 min exposure to 20 mM HCl followed by a 40 sec exposure to 1 % Triton-100. The remaining material may be residual membrane fragments.

The analysis was repeated for three RBC concentrations and *Figure 5.2.3.6.3* is an overlay of the RBC interaction phases. The 50 % (v/v) RBC association curve is similar to the 66 % (v/v) RBC association curve but increases slightly with increasing contact time. The binding response for the 33 % (v/v) RBC sample was significantly lower; in agreement with the RBC binding calibration

curve obtained using the BIACORE Probe (*Figure 4.2.4.3*). The control curve shows that non-specific binding of RBCs to the surface was negligible (2 x 10^{-5} Δn (i.e. 20 RU)). In addition, the curve increased significantly with increasing contact time due to the casual association of RBCs to the antibody-coated surface in the absence of specific anti-A IgG. As previously observed (*Figure 5.2.2.6*), these weak interactions are not sufficient to withstand shear forces generated during the flushing procedure.

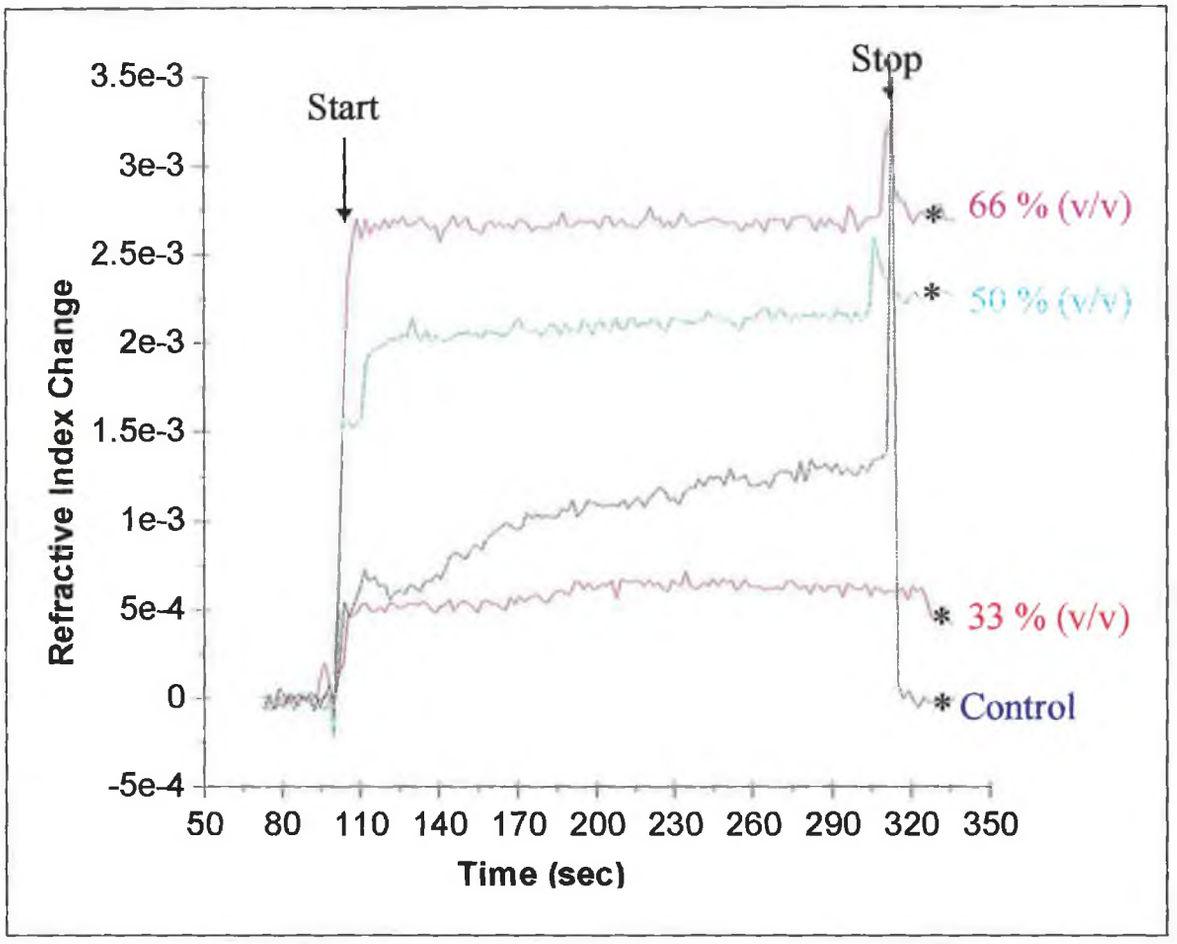

Figure 5.2.3.6.3. Overlaid interaction curves for the interaction of whole group A RBCs with affinity-captured anti-A IgG. The analysis was conducted at three RBC concentrations and performed as outlined in *Figure 5.2.3.6.2.* The anti-A IgG binding step was omitted during the control interaction, resulting in negligible retention of RBCs (66 % (v/v)). The binding response for the control, 33 % (v/v), 50 % (v/v) and 66 % (v/v) RBCs were 2 x 10^{-5} Δn (i.e. 20 RU), 4.33 x 10^{-4} Δn (i.e. 433 RU), 2.278 x 10^{-3} Δn (i.e. 2,278 RU) and 2.7 x 10^{-3} Δn (i.e. 2,700 RU). Regeneration of the surface was non-ideal as ~ 1,700 RU of residual mass accumulated at the surface, decreasing it's biological activity.

5.3 *Conclusions.*

Two biosensors were developed for 'real-time' interaction analysis of biomolecular interactions. Both biosensing systems employed non-invasive SPR detection to monitor the progress of biomolecular interactions. SPR-based sensors are generic refractive index sensors, and hence, fluctuations in the sample temperature cause baseline drift. This effect was not problematic since the environmental temperature of the laboratory was stable and samples were allowed to equilibrate at room temperature before analysis. The miniature SPR sensor possesses a temperature sensor to enable 'real-time' temperature compensation of the response. However, the sensor is embedded within the device and does not reflect the temperature at the sensing surface.

The fibre optic SPR-based biosensor employed a polychromatic light source, fibre optic waveguiding and a miniature spectrometer. These components were commercially available at low cost. However, the fabrication of the sensing element requires considerable expertise to enable deposition of high quality homogenous gold layers onto the glass surface of a fibre optic. Hence, the sensing elements (CM5 Probe) were supplied by BIACORE AB. The optical configuration of the sensor was similar to the BIACORE Probe but 'custom-written' software allowed 'real-time' data acquisition, processing and display. The miniature SPR-based biosensor was constructed by modifying a miniature SPR transducer available from Texas Instruments Inc. The device was interfaced with a disposable SPR chip and customised flowcell. The required hardware and software were supplied by Texas Instruments, with the exception of the personal computer.

Both biosensors were calibrated using glycerol water solutions and gave a similar dynamic range for refractive index measurement (i.e. 1.333-1.400 approximately). However, the sensitivity of both instruments was considerably less than the BIACORE 1000^{TM} system. The background noise of the fibre optic system was 15 to 25-fold higher while the background noise level of the miniature SPR system was ~ 100-fold higher. Lowering the background noise level of the miniature SPR system would require alteration of the optical configuration of the transducer, but this was not possible and seriously limited the potential of the device. However, the background noise level of the fibre optic system may be reduced by 10-fold by optimising both the procedure for determining the position of the SPR minimum and the optical configuration. The fibre optic system revealed an increasing sensitivity with respect to increasing refractive index. Hence, interaction curves produced by this device reflected the progress of the biomolecular interaction as distorted by the increasing sensitivity at higher responses (i.e. wavelengths). The calibration curve for the miniature SPR sensor was almost identical to similar calibration curves from an Abbé refractometer and the BIACORE 1000^{TM}, thus validating the sensor response. A hydrogel-based biointerface, similar to

the CM5 chip, was assembled on the gold layer of an unmodified miniature SPR sensor and preconcentration of BSA onto the CM-dextran matrix was demonstrated. However, the derivatised surface was highly unstable and the gold layer eroded rapidly. Hence, the sensor was used in conjunction with disposable SPR chips. An 'in house' fabricated SPR chip compared favourably with the expensive CM5 SPR chip when interfaced with the miniature transducer. The biosensing capability of the fibre optic system was demonstrated using a protein A-coated CM5 sensor probe. Affinity-capture of rabbit antibody was successfully performed and a calibration curve constructed. Anti-A IgG was affinity-captured from crude hybridoma supernatant using the protein A-coated sensing element and was shown to specifically retain group A RBCs. In addition, RBCs were not retained in the absence of affinity-captured anti-A IgG. A steady state RBC binding response developed in agreement with previous observations. However, the interaction profile did not reflect the progress of the interaction alone. Therefore, the distortions introduced by the variable sensitivity of the fibre optic system were corrected by converting the interaction curve (100 %(v/v) RBC) into an equivalent BIACORE response using refractive index calibration expressions for both systems. The maximum RBC binding response obtained from the corrected curve correlated well with previous point-measurements determined using the BIACORE probe™. Furthermore, this correction procedure may be incorporated into the data processing software to correct the response in 'real-time'. When combined with the optimisation of both the optical system and data processing software, this inexpensive system possess potential for kinetic analysis of molecular interactions. RBC detection was successfully demonstrated using the modified miniature SPR system. A goat anti-mouse Fc-coated sensing element was used for directed affinity-capture of anti-A IgG via the Fc region. Group A RBCs were specifically retained by this functionalised surface. Similar to the fibre optic system, RBCs were not retained in the absence of the anti-A IgG. However, regeneration of the surface was non-ideal and a high background noise level was apparent from the interaction curves.

In conclusion, further analyses were not conducted with the miniature SPR system due to its low sensitivity, which is inherent due to the performance-limitations of the optical components used during fabrication of the device. However, given the rapid developments in the semi-conductor industry, the sensitivity of this sensor may be increased within the near future. The fibre optic biosensor provides a real alternative to the expensive analysers currently available. The sensitivity of the device may not rival the BIACORE analysers, but several applications do not require high sensitivity. The system was ideal for the analysis of crude samples and provided a means of monitoring RBC-ligand interactions in 'real-time' at high concentrations (100 % (v/v) RBC). In particular, the analysis revealed that the RBC binding response rapidly reached a steady state in agreement with the principles outlined previously (section 4.2.5).

Bibliography

Abdelghani, A., Chovelon, J.M., Jaffrezic-Renault, N., Ronot-Trioli, C., Veillas, C., and Gagnaire, H. (1997). Surface plasmon resonance fibre-optic sensor for gas detection. Sensors and Actuators B, **38-39**, 407-410.

Abel, A.P., Weller, M.G., Duveneck, G.L., Ehrat, M., and Widmer, H.M. (1996). Fiber-optic evanescent wave biosensor for the detection of oligonucleotides. Anal. Chem., **68**, 2,905-2,912.

Ahluwalia, A., De Rossi, D., Ristori, C., Schirone, A., and Serra, G. (1991). A comparative study of protein immobilization techniques for optical immunosensors. Biosensors and Bioelectronics, **7**, 207-214.

Åkerström, B., Brodin, T., Reis, K., and Björck, L. (1985). Protein G: a powerful tool for binding and detection of monoclonal and polyclonal antibodies. J. Immunol., **135**(4), 2,589-2,592.

Åkerström, B., and Björck, L. (1986). Physicochemical Study of Protein G, a Molecule with Unique Immunoglobulin G-binding Properties. J. Biol. Chem., **261**(22), 10,240-10,247.

Andle, J.C., Weaver, J.T., Vetelino, J.F., and McAllister, D.J. (1995). Selective acoustic plate mode DNA sensor. Sensors and Actuators B, **24-25**, 129-133.

Arevalo, J.H., Taussig, M.J., and Wilson, I.A. (1993). Molecular basis of crossreactivity and the limits of antibody-antigen complementarity. Nature (London), **365**, 859-863.

Asensio, J.L., Dosanjh, H.S., Jenkins, T.C., and Lane, A.N. (1998). Thermodynamic, kinetic, and conformational properties of a parallel intermolecular DNA triplex containing 5' and 3' junctions. Biochem., **37**, 15,188-15,198.

Baca, M., Presta, L.G., O'Connor, S.J., and Wells, J.A. (1997). Antibody humanization using monovalent phage display. J. Biol. Chem., **272**(16), 10,678-10,684.

Bain, C. D., Troughton, E.B., Tao, Y.T., Evall, J., Whitesides, G.M., and Nuzzo, R.G. (1989). Formation of monolayer films by the spontaneous assembly of organic thiols from solution onto gold. J. Amer. Chem. Soc., **111**, 321-335.

Barnes, C. (1991). Development of quartz crystal oscillators for under-liquid sensing. Sensors and Actuators A, **29**, 59-69.

Bender, F., Meimeth, F., Dahint, R., Grunze, M., and Josse, F. (1997). Mechanisms of interaction in acoustic plate mode immunosensors. Sensors and Actuators **B, 40**, 105-110.

Bertilsson, L., Butt, H-J., Nelles, G., and Schlereth, D. D. (1997). Cibacron Blue F3G-A anchored monolayers with biospecific affinity for NAD(H)-dependent lactate dehydrogenase: characterization by FTIR-spectroscopy and atomic force microscopy. Biosensors and Bioelectronics, **12(8)**, 839-852.

BIACORE AB (1995), Biomolecular interaction analysis with cells and vesicles. Biotechnology note 105.

BIACORE AB. (1995). Supported polar lipid monolayers for BIA. Biotechnology Note 106.

Bier, F. F., and Schmid, R.D. (1994). Real time analysis of competitive binding using grating coupler immunosensors for pesticide detection. Biosensors and Bioelectronics, **9**, 125-130.

Björck, L., and Kronvall, G. (1984). Purification and some properties of Streptococcal protein G, a novel IgG-binding reagent. J. Immunol., **133(2)**, 969-973.

Blackshear, P. L., and Anderson, R. J. (1977). Hemolysis thresholds in microporus structures. Blood Cells, **3**, 377.

Blake, D. A., and Goldstein, I. J. (1982). Resolution of carbohydrates by lectin affinity chromatography. Meth. Enzymol., **83**, 127-131.

Bondeson, K., Frostell-Karlsson, Å., Fägerstam, L., and Magnusson, G. (1993). Lactose repressor-operator DNA interactions, kinetic analysis by a surface plasmon resonance biosensor. Anal. Biochem., **214**, 245-251.

Bowles, M.R., Hall, D.R., Pond, S.M., and Winzor, D.J. (1997). Studies of protein interactions by biosensor technology: An alternative approach to the analysis of sensorgrams deviating from pseudo-first-order kinetic behavior. Anal. Biochem., **244**, 133-143.

Bøyum, A. (1984). Separation of lymphocytes, granulocytes, and monocytes from human blood using iodinated density gradient media. Meth. Enzymol., **108**, 88-109.

Brecht, A., and Gauglitz, G. (1995). Optical probes and transducers. Biosensors and Bioelectronics, **10**, 923-936.

Brecht, A., and Gauglitz, G. (1997). Recent developments in optical transducers for chemical or biochemical applications. Sensors and Actuators B, **38-39**, 1-7.

Brennan, M., Davison, P. E., and Paulus, H. (1985). Preparation of bispecific antibodies by chemical recombination of monoclonal IgG1 fragments. Science, **229**, 81-83.

Brigham-Burke, M., and O'Shannessy, D.J. (1993). A microscale method employing surface plasmon resonance detection for the determination of conditions for affinity chromatography of proteins. Chromatographia, **35**, 45-49.

Brinkmann, U., Lee, B. K., and Pastan, I. (1993 (a)). Recombinant Immunotoxins Containing the V_H or V_L Domain of Monoclonal Antibody B3 Fused to *Pseudomonas* Exotoxin. J. Immunol., **150**(7), 2,774-2,782.

Brinkmann, U., Reiter, Y., Jung, S-H., Lee, B., and Pastan, I. (1993(b)). A recombinant immunotoxin containing a disulfide-stabilized Fv fragment. Proc. Natl. Acad. Sci. (USA), **90**, 7,538-7,542.

Brinkmann, U., Di Carlo, A., Vasmatzis, G., Kurochkina, N., Beers, R., Lee, B., and Pastan, I. (1997). Stabilization of a recombinant Fv fragment by base-loop interconnection and V_H-V_L permutation. J. Mol. Biol., **268**(1), 107-117.

Buckle, P.E., Davies, R.J., Kinning, T., Yeung, D., Edwards, P.R., Pollard-Knight, D., and Lowe, C.R. (1993). The resonant mirror: a novel optical sensor for direct sensing of biomolecular interactions. Part II: Applications. Biosensors and Bioelectronics, **8**, 355-363.

Caruso, F., Rodda, E., Furlong, D.N., Niikura, K., and Okahata, Y. (1997). Quartz crystal microbalance study of DNA immobilization and hybridization for nucleic acid sensor development. Anal. Chem. **69**, 2,043-2,049.

Chaiken, I., Rosé, S., Karlsson, B. (1992). Analysis of macromolecular interactions using immobilised ligands. Anal. Biochem., **201**:197-210.

Chaplin, H., Jnr, and Mollison, P.L. (1952). Correction factor for plasma trapped in the red cell column of the hemaocrit. Blood, **7**, 1,227.

Chaudhary, V.K., Queen, C., Junghans, R.P., Waldmann, T.A., FitzGerald, D.J., and Pastan, I. A. (1989). Recombinant immunotoxin consisting of two antibody variable domains fused to *Pseudomonas* exotoxin. Nature (London), **339**, 394-397.

Chen, Q., Sun, P., Prigione, I., Xie, H., and Ferrini, S. (1992). Targeting of T- lymphocytes against human hepatoma cells by a bispecific monoclonal antibody: role of different lymphocyte subsets. Tumori, **78**, 79-86.

Cheng, J,, Sheldon, E.L., Wu, L., Heller, M J., and O'Connel, P. (1998). Isolation of cultured cervical carcinoma cells mixed with peripheral blood on a bioelectronic chip. Anal. Chem., **70**, 2,321-2,326.

Chidsey, C.E.D., Bertozzi, C.R., Putvinski, T.M., and Mujsce, A.M. (1990). Co-adsorption of ferrocene-terminated and unsubstituted alkanethiols on gold: electroactive self-assembled monolayers. J. Amer. Chem. Soc., **112**, 4,301-4,306.

Chothia, C., Lesk, A.M., Tramontano, A., Levitt, M., Smith-Gill, S.J., Air, G., Sheriff, S., Padlan, E.A., Davies, D., Tulip, W.R., Colman, P.M., Spinelli, S., Alzari, P.M., and Poljak, R.J. (1989). Conformations of immunoglobulin hypervariable regions. Nature (London), **342**, 877-883.

Chowdhury, P.S., Vasmatzis, B., Beers, R., Lee, B., and Pastan, I. (1998). Improved stability and yield of a Fv-toxin fusion protein by computer design and protein engineering of the Fv. J. Mol. Biol., **281**, 917-928.

Christensen, L.L.H. (1997). Theoretical analysis of protein concentration determination using biosensor technology under conditions of partial mass transport limitation. Anal. Biochem., **249**, 153-164.

Clerc, D., and Lukosz, W. (1997). Direct Immunosensing with an Integrated-optical Output Grating Coupler. Sensors and Actuators B, **40**, 53-58.

Coloma, M.J., and Morrison, S.L. (1997). Design and production of novel tetravalent bispecific antibodies. Nature Biotechnology, **15**, 159-163.

Cook, A.G., and Wood, P.J. (1994). Chemical synthesis of bispecific monoclonal antibodies: potential advantages in immunoassay systems. J. Immunol. Methods, **171**, 227-237.

Cooper, M.A., Try, A.C., Carroll, J., Ellar, D.J., and Williams, D.H. (1998). Surface plasmon resonance analysis at a supported lipid monolayer. Biochim. Biophys. Acta., **1,373**, 101-111.

Cush, R., Cronin, J. M., Steward, W.J., Maule, C.H., Mollow, J., Goddard, N. J. (1993). The resonant mirror: a novel optical biosensor for direct sensing of biomolecular interactions. Part I Principle of operation and associated instrumentation. Biosensors and Bioelectronics, **8**, 347-353.

Dacie, J.V., Lewis, S.M. and Worlledge, S.M. (1968). Blood groups and the practical aspects of blood transfusion, in: Practical Haematology (4^{th} Edition), Dacie, J.V., Lewis, S.M. (eds.), J. & A. Churchill Ltd, London, pp417-475.

Dahint, R., Grunze, M., Josse, F., and Renken, J. (1994). Acoustic Plate Mode Sensor for Immunochemical Reactions. Anal. Chem., **66**, 2,888-2,892.

Dave, B.C., Dunn, B., and Valentine, J.S. (1994). Sol-gel encapsulation methods for biosensors. Anal. Chem., **66**, 1,120A-1,127A.

Davies, D.R., Sheriff, S., and Padlan, E.A. (1988). Antibody-antigen complexes. J. Biol. Chem., **263**(22), 10,541-10,544.

De Brunn, H.E., Kooyman, R.P.H and Greve, J. (1992). Choice of metal and wavelength for SPR sensors: some considerations. Applied Optics, **31**, 440-442.

De Haard, H.J.W., Kazemier, B., Koolen, M.J.M., Nijholt, L.J., Meloen, R.H., Van Gemen, B., Hoogenboom, H.R., and Arends, J.-W. (1998). Selection of recombinant, library-derived antibody fragments against p24 for human immunodeficiency virus type 1 diagnostics. Clinical and Diagnostic Laboratory Immunology, **5**, 636-644.

Deng, S., MacKenzie, C.R., Sadowska, J., Michniewicz, J., Young, N.M., Bundle, D.R., and Narang, S.A. (1994). Selection of antibody single-chain variable fragments with improved carbohydrate binding by phage display. J. Biol. Chem., **269**(13), 9,533-9,538.

Drapp, B., Peihler, J., Brecht, A., Gauglitz, G., Luff, B.J., Wilkinson, J.S., and Ingenhoff, J. (1997). Integrated optical Mach-Zehnder interferometers as simazine immunoprobes. Sensors and Actuators B, **38-39**, 277-282.

Dubrovsky, T.B., Demcheva, M.V., Savitsky, A.P., Mantrova, Yu. E., Yaropolov, A.I., Savransky, V.V., and Belovolova, L.V. (1993). Fluorescent and phosphorescent study of Langmuir-Blodgett antibody films for application to immunosensors. Biosensors and Bioelectronics, **8**, 377-385.

Ebersole, R.C., Miller, J.A., Moran, J.R., and Ward, M.D. (1990). Spontaneously formed functionally active avidin monolayers on metal surfaces: a strategy for immobilising biological reagents and design of piezoelectric biosensors. J. Amer. Chem. Soc., **112**, 3,239-3,241.

Edwards, P.R., Gill, A., Pollard-Knight, D.V., Hoare, M., Buckle, P.E., Lowe, P.A., and Leatherbarrow, R.J. (1995). Kinetics of protein-protein interactions at the surface of an optical biosensor. Anal. Biochem., **231**, 210-217.

Edwards, P.R., and Leatherbarrow, R.J. (1997). Determination of association rate constants by an optical biosensor using initial rate analysis. Anal. Biochem., **246**, 1-6.

Einspahr, H., Parks, E.H., Suguna, K., Subramanian, E., and Suddath, F.L. (1986). The crystal structure of pea lectin at 3.0-Å resolution. J. Biol. Chem., **261**(35), 16,518-16,527.

Elender, G., Kühner, M., and Sackmann, E. (1996). Functionalisation of Si/SiO_2 and glass surfaces with ultrathin dextran films and deposition of lipid bilayers. Biosensors and Bioelectronics, **11**(6/7), 565-577.

Elgert, K.D. (1996). Antibody structure and function, in: Immunology-understanding the immune system, Elgert, K. D. (eds.), Wiley-Liss, New York, pp58-78.

Fägerstam, L.G., and O'Shannessy, D.J. (1993). Surface plasmon resonance detection in affinity technologies. Handbook of Affinity Chromatography, **63**, 229-252.

Fisher, R. J., and M. Fivash. (1994). Surface plasmon resonance based methods for measuring the kinetics and binding affinities of biomolecular interactions. Curr. Opin. Biotech., **5**, 389-395.

Flanagan, M.T., Sloper, A.N., and Ashworth, R.H. (1988). From electronic to opto-electronic biosensors: an engineering view. Anal. Chim. Acta., **213**, 23-33.

Flavell, D.J., Cooper, S., Morland, B., and Flavell, S.U. (1991). Characteristics and performance of a bispecific $F(ab'\gamma)^2$ antibody for delivering saporin to a $CD7^+$ human acute T-cell leukaemia cell line. Cancer, **64**, 274-280.

Fortune, D. (1993). Binding and kinetics - new dimensions in optical biosensor analysis. Biosensors and Bioelectronics, **8**(7/8), xxxii-xxxiv.

Fratamico, P.M., Strobaugh, T.P., Medina, M.B., and Gehring, A.G. (1998). Detection of *Escherichia coli* O157:H7 using a surface plasmon resonance biosensor. Biotechnology Techniques, **12**, 371-376.

French, R.R., Hamblin, T.J., Bell, A.J., Tutt, A.L., and Glennie, M.J. (1995 (a)). Treatment of B-cell lymphomas with combination of bispecific antibodies and saporin. Lancet, **346**, 223-224.

French, R.R., Penney, C.A., Browning, A.C., Stirpe, F., George, A.J.T., and Glennie, M.J. (1995 (b)). Delivery of the ribosome-inactivating protein, gelonin, to lymphoma cells via CD22 and CD38 using bispecific antibodies. Cancer, **71**, 985-994.

Frey, B.L., Jordan, C.E., Kornguth, S., and Corn, R.M. (1995). Control of the specific adsorption of proteins onto gold surfaces with poly(L-lysine) monolayers. Anal. Chem., **67**, 4,452-4,457.

Friguet, B., Chaffotte, A.F., Djavadi-Ohaniance, L., and Goldberg, M.E. (1985). Measurements of the true affinity constant in solution of antigen-antibody complexes by enzyme-linked immunosorbent assay. J. Immunol. Methods., **77**, 315-319.

Fujita, K., Kimura, S., and Imanishi, Y. (1994). Bilayer formation of streptavidin bridged by bis(biotinyl) peptide at the air/water interface. J. Amer. Chem. Soc., **116**, 5,479-5,480.

Fujiwara, K., Saita, T., and Kitagawa, T. (1988). The use of *N*-[β-(4-diazophenyl)ethyl]maleimide as a coupling agent in the preparation of enzyme-antibody conjugates. J. Immunol. Methods., **110**, 47-53.

Furlong, C.E., Woodbury, R.G., Yee, S.S., Chinowsky, T., Carr, R., Elkind, J.L., Kukanskis, K.A., Bartholomew, D., and Melendez, J.L. (1996). Fundamental system for biosensor characterisation, application to surface plasmon resonance. SPIE., **28/36**, 208-215.

Gabricius, N., Ganglitz, G., Ingenhoff. J. (1992). A gas sensor based on an integrated optical Mach-Zehnder interferometer, Sensors and Actuators B, **7**, 672-676.

George, A.J.T., French, R.R., and Glennie, M.J. (1995). Measurement of kinetic binding constants of a panel of anti-saporin antibodies using a resonant mirror biosensor. J. Immunol. Methods., **183**, 51-63.

Gershon, P.D. and Khilko, S. (1995). Stable chelating linkage for reversible immobilization of oligohistidine tagged proteins in the BIAcore surface plasmon resonance. J. Immunol. Methods., **183**, 65-76.

Ghetie, V. and Sjöquist, J. (1984). Separation of cells by affinity chromatography on protein A gels. Meth. Enzymol., **108**, 132-138.

Glaser, R.W. (1993). Antigen-antibody binding and mass transport by convection and diffusion to a surface: A two-dimensional computer model of binding and dissociation kinetics. Anal. Biochem., **213**, 152-161.

Glennie, J.W. (1987). Preparation and performance of bispecific $F(ab\gamma)_2$ antibody containing thioether-linked Fab'γ fragments. J. Immunol., **138**, 2367-2375.

Goding, J.W. (1978). Use of Staphylococcal protein A as an immunological reagent. J. Immunol. Methods., **20**, 241-253.

Gōrōg, G., Gandolfi, A., Paradisi, G., Rolleri, E., Klasen, E., Dessi, V., Strom, R., and Celada, F. (1989). Use of bispecific hybrid antibodies for the development of a homogeneous enzyme immunoassay. J. Immunol. Methods., **123**, 131-140.

Griffiths, A.D., Malmqvist, M., Marks, J.D., Bye, J.M., Embleton, M.J., McCafferty, J., Gorick, B.D., Hughes-Jones, N.C., Hoogenboom, H.R., and Winter, G. (1993). Human anti-self antibodies with high specificity from phage display libraries. EMBO J., **12**, 725-732.

Griffiths, D., and Hall, G. (1993). Biosensors – what real progress is being made? Trends in Biotechnology, **11**, 122-130.

Gruber, M., Schodin, B.A., Wilson, E.R., and Kranz, D.M. (1994). Efficient tumor cell lysis mediated by a bispecific single chain antibody expressed in *Escherichia coli*. J. Immunol., **152**(11), 5,368-5,374.

Gruen, L.C., McKimm-Breschkin, J.L., Caldwell, J.B., and Nice, E.C. (1994). Affinity ranking of influenza neuraminidase mutants with monoclonal antibodies using an optical biosensor Comparison with ELISA and slot blot assays. J. Immunol. Methods., **168**, 91-100.

Hall, D.R., Cann, J.R., and Winzor, D.J. (1996). Demonstration of an upper limit to the range of association rate constants amenable to study by biosensor technology based on surface plasmon resonance. Anal. Biochem., **235**, 175-184.

Hartman, N.F., Campbell D. and M. Gross. (1988). Waveguide interferometer configurations. Proc. IEEE-IEOS (Laser Electro Optics Soc. Ann. Meet.) Santa Clara, CA, USA, 298-299.

Hellström, U, Hammerström, S., and Perlmann, P. (1984). Fractionation of human lymphocytes on *Helix pomatia*, A hemegglutinin-sepharose and wheat germ agglutinin-sepharose. Meth. Enzymol., **108**, 153-168.

Hengsakul, M., and Cass, A.E.G. (1997). Alkaline phosphatase-strep tag fusion protein binding to streptavidin: Resonant mirror studies. J. Mol. Biol., **266**, 621-632.

Hladky, S.B., and Rink, T.J. (1982). The use of ion transporters, pH measurement and light scattering with RBCs, in: Red cell membranes, A methodological approach, Chapter 21, Academic press New York.

Holliger, P., Prospero, T., and Winter, G. (1993). "Diabodies": Small bivalent and bispecific antibody fragments. Proc. Natl. Acad. Sci. (USA), **90**, 6,444-6,448.

Homola, J., Ctyroky, J., Skalsky, M., Hradilova, J., and Kolarova, P. (1997). A surface plasmon resonance based integrated optical sensor. Sensors and Actuators B, **38-39**, 286-290.

Hoogenboom, H.R. (1997). Designing and optimizing library selection strategies for generating high-affinity antibodies. Trends in Biotech., **15**(2), 62-70.

Horbett, T.A., and Brush, J.L. (1987). Proteins at interfaces: Current issues and future prospects, in: Proteins at interfaces, Physicochemical and biochemical studies, Horbett, T.A., and Brush, J.L. (eds.), J. Amer. Chem. Soc.,1-33.

Hoshi, T., Anzai, J., and Osa, T. (1995). Controlled deposition of glucose oxidase on platinum electrode based on an avidin/biotin system for the regulation of output current of glucose sensors. Anal. Chem., **67**, 770-774.

Houghten, R .A. (1993). Peptide libraries: criteria and trends. Trends in Genetics. **9**(7), 235-239.

Hubbard, R.A., Schluter, S.F., and Marchalonis, J.J. (1983). Separation of lymphoid cells using immunoadsorbent affinity chromatograph. Meth. Enzymol., **108**, 139-149.

Huse, W.D., Sastry, L., Iverson, S.A., Kang, A.S., Alting-Mees, M., Burton, D.R., Benkovic, S.J., and Lerner, R.A. (1989). Generation of a large combinatorial library of the immunological repertoire in phage Lambda. Science, **246**, 1,275-1,281.

Huston, J.S., Levinson, D., Mudgett-Hunter, M., Tai, M-S., Novotný, J., Margolies, M.N., Ridge, R.J., Bruccoleri, R.E., Haber, E., Crea, R., and Oppermann, H. (1988). Proc. Natl. Acad. Sci. (USA), **85**, 5,879-5,883.

Hutchinson, A.M. (1994). Characterization of glycoprotein oligosaccharides using surface plasmon resonance. Anal. Biochem., **220**, 303-307.

Hutchinson, A.M. (1995). Evanescent wave biosensors. Molecular Biotechnol., **3**, 47-54.

Hwang, S., Chang, D.J., and Chen, C. (1996). Steady state permeate flux for particle cross-flow filtration. Chem. Eng. J., **61**, 171-178.

Ito, W., and Kurosawa, Y. (1993). Development of an artificial antibody system with multiple valency using an Fv fragment fused to a fragment of protein A. J. Biol. Chem., **268**(27), 20,668-20,675.

Jendeberg, L., Nilsson, P., Larsson, A., Denker, P., Uhlén, M., Nilsson, B., and Nygren, P-A. (1997). Engineering of Fc_1 and Fc_3 from human immunoglobulin G to analyse subclass specificity for staphylococcal protein A. J. Immunol. Methods., **201**, 25-34.

Jones, P.T., Dear, P.H., Foote, J., Neuberger, M.S., and Winter, G. (1986). Replacing the complementarity-determining regions in a human antibody with those from a mouse. Nature (London), **321**, 522-525.

Jordan, C.E., and Corn, R.M. (1997). Surface plasmon resonance imaging measurements of electrostatic biopolymer adsorption onto chemically modified gold surfaces. Anal. Chem., **69**, 1,449-1,456.

Jordan, J.D., Dunbar, R.A., and Bright, F.V. (1996). Aerosol-generated sol-gel-derived thin films as biosensing platforms. Anal. Chim. Acta., **332**, 83-91.

Jorgenson, R.C., and Yee, S.S. (1993). A fiber-optic chemical sensor based on surface plasmon resonance. Sensors and Actuators B, **12**, 213-220.

Kang, S-W., Sasaki, K., and Minamitani, H. (1993). Sensitivity analysis of a thin-film optical waveguide biochemical sensor using evanescent field absorption. Applied Optics, **32**(19), 3,544-3,549.

Karlsson, R., Fägerstam, L., Nilshans, H., and Persson, B. (1993). Analysis of active antibody concentration. Separation of affinity and concentration parameters. J. Immunol. Methods, **166**, 75-84.

Karlsson, R., Roos, H., Fägerstam, L., and Persson, B. (1994). Kinetic and concentration analysis using BIA technology. Methods: A Companion to Meth. Enzymol., **6**, 99-110.

Karlsson, R., and Ståhlberg, R. (1995). Surface plasmon resonance detection and multispot sensing for direct monitoring of interactions involving low-molecular-weight analytes and for determination of low affinities. Anal. Biochem., **228**, 274-280.

Karlsson, R., and Fält, A. (1997). Experimental design for kinetic analysis of protein-protein interactions with surface plasmon resonance biosensors. J. Immunol. Methods., **200**, 121-133.

Kataoka, K., Sakurai, Y., and Tsuruta, T. (1987). Affinity selection of cells on solid-phase matrices with immobilised proteins, in: Proteins at interfaces, Comstock, M. J. (eds.), Amer. Chem. Soc., pp603-614.

Katayose, Y., Kudo, T., Suzuki, M., Shinoda, M., Saijyo, S., Sakurai, N., Saeki, H., Fukuhara, K., Imai, K., and Matsuno, S. (1996). MUC1-specific targeting immunotherapy with bispecific antibodies: Inhibition of xenografted human bile duct carcinoma growth. Cancer Research., **56**, 4,205-4,212.

Kazemier, B., de Haard, H., Boender, P., van Gemen, B., and Hoogenboom, H. (1996). Determination of active single chain antibody concentrations in crude periplasmic fractions. J. Immunol. Methods., **194**, 201-209.

Keinänen, K., and Laukanen, M-L. (1994). Biosynthetic lipid-tagging of antibodies. FEBS Letters., **346**, 123-126.

Kempen, L.U., and Kunz, R.E. (1997). Replicated Mach-Zehnder interferometers with focusing grating couplers for sensing applications. Sensors and Actuators B, **38-39**, 295-299.

Killard, A.J., Deasy, B., O'Kennedy, R., and Smyth, M.R. (1995). Antibodies: production, functions and applications in biosensors. Trends in Anal. Chem., **14(6)**, 257-265.

Kim, B.B., Dikova, E.B., Sheller, U., Dikov, M.M., Gavrilova, E.M., and Egorov, A.M. (1990). Evaluation of dissociation constants of antigen-antibody complexes by ELISA. J. Immunol. Methods., **131**, 213-222.

Kipriyanov, S.M., Little, M., Cropshofer, H., Breitling, F., Gotter, S., and Dobel, S. (1996). Affinity enhancement of a recombinant antibody: Formation of complexes with multiple valency by a single-chain Fv fragment-core streptavidin fusion. Protein Engineering., **9**, 203-311.

Klotz, A., Brecht, A., and Gauglitz, G. (1997). Channel waveguide mode beat interferometer. Sensors and Actuators B., **38-39**, 310-315.

Kohler, G., and Milstein, C. (1975). Nature (London), **256**, 495.

Kooyman, R.P.H., Lenferink, A.T.M., Eenink, R.G., and Greve, J. (1991). Vibrating mirror surface plasmon resonance immunosensor. Anal. Chem., **63**, 83-85.

Kretschman, E. (1969). Die bestimmung der optischen konstanten dunner schichten in der nähe der plasmafrequenz aus kurvenfeldern konstanter transmission. Z. Phys. **221**, 346.

Kriz, D., Olof, R., Svensson, A., and Mosbach, K. (1995). Introducing biomimetic sensors based on molecularly imprinted polymers as recognition elements. Anal. Chem., **67**, 2,142-2,144.

Krone, J.R., Nelson, R.W., Dogruel, D., Williams, P., and Granzow, R. (1997). BIA/MS: Interfacing biomolecular interaction analysis with mass spectrometry. Anal. Biochem., **244**, 124-132.

Kuziemko, G.M., Stroh, M., and Stevens, R.C. (1996). Cholera toxin binding affinity and specificity for gangliosides determined by surface plasmon resonance. Biochemistry., **35**, 6,375-6,384.

Ladbury, J. E., Lemmon, M. A., Zhou, M., Green, J., Botfield, M. C., Schlessinger, J. (1995) Measurement of the binding of tyrosylphosphopeptides to SH2 domains, a reappraisal. P.N.A.S, USA, **92**, 3199-3203.

Langone, J.J. (1982). Applications of immobilized protein A in immunochemical techniques. J. Immunol. Methods., **55**, 277-296.

Laukanen, M-L., Alfthan, K., and Keinänen, K. (1994). Functional immunoliposomes harboring a biosynthetically lipid-tagged single-chain antibody. Biochemistry, **33**, 11,665-11,670.

Lehtonen, O.P., and Eerola, E. (1982). The effect of different Ab affinities on ELISA adsorbance and titer. J. Immunol. Methods., **54**, 233.

Lessin, L.S., and Bessis, M. (1978). Morphology of the erythron, in: Hematology, 2nd edition, Williams, W.J., Beutler, E., Erslev, A.J., and Rundles, R.W. (eds.), Mc Graw-Hill, Inc., London, pp103-134.

Lev, O., Tsionsky, M., and Rabinovich, L. (1995). Organically modified sol-gel sensors. Anal. Chem., **67**, 22A-30A.

Levi, M., Sällberg, M., Rudén, U., Herlyn, D., Maruyama, H., Wigzell, H., Marks, J., and Wahren, B. (1993). A complementarity-determining region synthetic peptide acts as a miniantibody and neutralizes human immunodeficiency virus type 1 *in vitro*. Proc. Natl. Acad. Sci. (USA). **90**, 4,374-4,378.

Liedberg, B., Lundström, I., and Stenberg, E. (1993). Principles of biosensing with an extended coupling matrix and surface plasmon resonance. Sensors and Actuators B, **11**, 63-72.

Lin, J., and Brown, C.W. (1997). Sol-gel glass as a matrix for chemical and biochemical sensing. Trends in Anal. Chem., **16**(4), 200-211.

Lindbladh, C., Mosbach, K., and Bülow, L. (1993). Use of genetically prepared enzyme conjugates in enzyme immunoassay. Trends in Biol. Sci., **18**, 279-283.

Liu, S. Q., Yen, M., and Fung, Y.C. (1994). On measuring the third dimension of cultured endothelial cells in shear flow. Proc. Natl. Acad. Sci. USA., **91**, 8,782-8,786.

Löfås, S., and Johnsson, B. (1990). A novel hydrogel matrix on gold surfaces on surface plasmon resonance sensors for fast and efficient covalent immobilization of ligands. J. Chem. Soc., Chem. Communications., **21**, 1,526-1,528.

Löfås, S., Johnsson, B., Tegendal, K., and Rönnberg, I. (1993). Dextran modified gold surfaces for surface plasmon resonance sensors, immunoreactivity of immobilized antibodies and antibody-surface interaction studies. Colloids and Surfaces B: Biointerfaces, **1**, 83-89.

Löfas, S., Malmqvist, M., Rönnberg, I., Stenberg, E., Liedberg, B., and Lundström, I. (1991). Bioanalysis with surface plasmon resonance. Sensors and Actuators B, **5**, 79-84.

Lokine, M.H., Field, R.W., and Howell, J.A. (1992). Crossflow microfiltration of cell suspensions: A review of models with emphasis on particle size effects. Trans. I. Chem. E., **70(c)**, 149-161.

Longstaff, M., Newell, C.A., Boonstra, B., Strachan, G., Learmonth, D., Harris, W.J., Porter, A.J., and Hamilton, W.D.O. (1998). Expression and characterisation of single-chain antibody fragments produced in transgenic plants against the organic herbicides atrazine and paraquat. Biochim. Biophys. Acta., **1,381**, 147-160.

Lowman, H.B., and Wells, J.A. (1993). Affinity maturation of human growth hormone by monovalent phage display. J. Mol. Biol., **234**, 564-578.

Lu, B., Smyth, M.R., and O'Kennedy, R. (1996). Oriented immobilization of antibodies and its applications in immunoassays and immunosensors. Analyst, **121**, 29R-32R.

Lu, B., Wu, C.R., Yang, W.Y., and Wei, Y. (1993). The binding of bifunctional reagents to silanized silicon surfaces studied by angle-dependent X-ray photoelectron spectroscopy. Applied Surface Science, **72**, 125-132.

Lukosz, W. (1991). Principles and sensitivities of integrated optical and surface plasmon sensors for direct affinity sensing and immunosensing. Biosensors and Bioelectronics, **6**, 215-225.

Lukosz, W. (1995). Integrated optical chemical and direct biochemical sensors. Sensors and Actuators B, **29**, 37-50.

Lukosz, W., Clerc, D., Nellen H.M. (1991(a)). Input and Output Grating Couplers as Integrated Optical Biosensors. Sensors and Actuators A, **25-27**, 181-184.

Lukosz, W., Clerc, D., Nellen, Ph.M., Stamm, C., and Weiss, P. (1991(b)). Output grating couplers on planar optical waveguides as direct immunosensors. Biosensors and Bioelectronics, **6**, 227-232.

Lukosz, W., Stamm, C., Moser, H.R., Ryf, R., and Dübendorfer, J. (1997). Difference interferometer with new phase-measurement method as integrated-optical refractometer, humidity sensor and biosensor. Sensors and Actuators B, **38-39**, 316-323.

Mack, M., Riethmüller, G., and Kufer, P. (1995). A small bispecific antibody construct expressed as a functional single-chain molecule with high tumor cell cytotoxicity. Proc. Natl. Acad. Sci. (USA), **92**, 7,021-7,025.

MacKenzie, C.R., Hirama, T., Deng, S.J., Bundle, D.R., Narang, S.A., and Young, N.M. (1996). Analysis by surface plasmon resonance of the influence of valence on the ligand binding affinity and kinetics of an anti-carbohydrate antibody. J. Biol. Chem., **271**, 1,527-1,533.

Mage, M.G. (1984). Separation of lymphocytes on antibody-coated plates. Meth. Enzymol., **108**, 118-124.

Mallender, W.D., and Voss, E.W. (1994). Construction, expression, and activity of a bivalent bispecific single-chain antibody. J. Biol. Chem., **269**(1), 199-206.

Malmborg, A-C., and Borrebaeck, C.A.K. (1995). BIAcore as a tool in antibody engineering. J. Immunol. Methods., **183**, 7-13.

Malmborg, A-C., Dueñas, M., Ohlin, M., Söderlink, E., and Borrebaeck, C.A.K. (1996). Selection of binders from phage displayed antibody libraries using the BIAcore™ biosensor. J. Immunol. Methods., **198**, 51-57.

Malmborg, A-C., Michaëlsson, A., Ohlin, M., Jansson, B., and Borrebaeck, C.A.K. (1992). Real-time analysis of antibody-antigen reaction kinetics. Scandinavian J. Immunol., **35**, 643-650.

Malmqvist, M. (1994). Kinetic analysis on engineered antibody-antigen interactions. J. Molecular Recognition, 7, 1-7.

Mani, J. C., Marchi, C., Cucurou, C. (1994). Effect of HIV-1 peptide presentation on the affinity constants of two monoclonal antibodies determined by BIAcore technology. Molecular Immunology, **31(6)**, 439-444.

Marks, J.D., Griffiths, A.D., Malmqvist, M., Clackson, T.P., Bye, J.M., and Winter, G. (1992). By-passing immunization: building high affinity human antibodies by chain shuffling. Biotechnology, **10**, 779-783.

Masson, L., Mazza, A., and Brousseau, R. (1994). Stable immobilization of lipid vesicles for kinetic studies using surface plasmon resonance. Anal. Biochem., **218**, 405-412.

Masson, M., Yun, K., Haruyama, T., Kobatake, E., and Aizawa, M. (1995). Quartz crystal microbalance bioaffinity sensor for biotin. Anal. Chem., **67**, 2,212-2,215.

Matsubara, K., Kawata, S., and Minami, S. (1988). Optical chemical sensor based on surface plasmon measurement. Applied Optics., **27(6)**, 1,160-1,163.

Matveev, S.V. (1994). Controlled modification of the quartz surface by amino groups. Biosensors and Bioelectronics, **9**, 333-336.

Mayes, A.G., and Mosbach, K. (1997). Molecularly imprinted polymers: useful materials for analytical chemistry. Trends in Anal. Chem., **16**(6), 321-332.

McCall, A.M., Amoroso, A.R., Sautés, C., Marks, J.D., and Weiner, L. (1998). Characterization of anti-mouse Fc-gamma-RII single-chain Fv fragments derived from human phage display libraries. Immunotechnology, **4**, 71-87.

McLean, M.A., Stayton, P.S., and Sligar, S.G. (1993). Engineering protein orientation at surfaces to control macromolecular recognition events. Anal. Chem., **65**, 2,676-2,678.

Melendez, J., Carr, R, Bartholomew, D.U., Kukanskis, K., Elkind, J. Yee, S., Furlong, C., and Woodbury, R. (1996). A commercial solution for surface plasmon sensing. Sensors and Actuators B, **35-36**, 212-216.

Melendez, J., Carr, R., Bartholomew, D.U., Kukanskis, K., Elkind, J., Yee, S., Furlong, C., and Woodbury, R. (1996). A commercial solution for surface plasmon sensing. Sensors and Actuators B, **35-36**, 212-216.

Merkle, R.K., and Cummings, R.D. (1984). Lectin affinity chromatography of glycoproteins. Meth. Enzymol., **138**, 232-259.

Milstein, C., and Cuello, A.C. (1984). Hybrid hybridomas and the production of bi-specific monoclonal antibodies. Immunology Today, **5**(10), 299-304.

Minunni, M., and Mascini, M. (1993). Detection of pesticide in drinking water using "real-time" biospecific interaction analysis (BIA). Analytical Letters, **26**(7), 1,441-1,460.

Mirsky, V.M., Riepl, M., and Wolfbeis, O.S. (1997). Capacitive monitoring of protein immobilization and antigen-antibody reactions on monomolecular alkylthiol films on gold electrodes. Biosensors and Bioelectronics, **12**(9), 977-989.

Mishell, R.I., and Mishell, B.B. (1984). Use of sephadex G-10 to separate macrophages and lymphocytes. Meth. Enzymol., **108**, 303-307.

Mooney, J.F., Hunt, A.J., McIntosh, J.R., Liberko, C.A., Walba, D.M., and Rogers, C.T. (1996). Patterning of functional antibodies and other proteins by photolithography of silane monolayers. Proc. Natl. Acad. Sci. (USA)., **93**, 12,287-12,291.

Moreno, M.B., Titus, J.A., Cole, M.S., Tso, J.Y., Le, N., Paik, C.H., Bakács, T., Zacharchuk, C.M., Segal, D.M., and Wunderlich, J.R. (1995). Bispecific antibodies retarget murine T cell cytotoxicity against syngeneic breast cancer in vitro and in vivo. Cancer Immunology and Immunotherapy, **40**, 182-190.

Morrison, S.L. (1992). In vitro antibodies: Strategies for production and application. Ann. Rev. in Immunol., **10**, 239-265.

Morton, T.A., Myszka, D.G., and Chaiken, I.M. (1995). Interpreting complex binding kinetics from optical biosensors: a comparison of analysis by linearization, the integrated rate equation, and numerical integration. Anal. Biochem., **227**, 176-185.

Mosier, D.E. (1984). Separation of macrophages on plastic and glass surfaces. Meth. Enzymol., **108**, 294-297.

Mrksich, M., and Whitesides, G.M. (1995). Patterning self-assembled monolayers using microcontact printing: a new technology for biosensors. Trends in Biotech., **13**, 228-235.

Müller, D.J., Engel, A., and Amrein, M. (1997). Preparation techniques for the observation of native biological systems with the atomic force microscope. Biosensors and Bioelectronics, **12**(8), 867-877.

Muramatsu, H., Dicks, J.M., Tamiya, E., and Karube, I. (1987). Piezoelectric Crystal Biosensor Modified with Protein A for Determination of Immunoglobulins. Anal. Chem., **59**, 2,760-2,763.

Muratsugu, M., Ohta, F., Miya, Y., Hosokawa, T., Kurosawa, S., Kamo, N., and Ikeda, H. (1993). Quartz crystal microbalance for the detection of microgram quantities of human serum albumin: relationship between the frequency change and the mass of protein adsorbed. Anal. Chem., **65**, 2.933-2,937.

Myszka, D.G. (1997). Kinetic analysis of macromolecular interactions using surface plasmon resonance biosensors. Current Opinion in Biotechnology, **8**, 50-57.

Nakamura, R., Muguruma, H., Ikebukuro, K., Sasaki, S., Nagata, R., Karube, I., and Pedersen, H. (1997). A plasma-polymerized film for surface plasmon resonance immunosensing. Anal. Chem., **69**, 4,649-4,652.

Nakanishi, R., Muguruma, H., and Karube, I. (1996). A novel method of immobilizing antibodies on a quartz crystal microbalance using plasma-polymerized films for immunosensors. Anal. Chem., **68**, 1,695-1,700.

Nelson, R.W., and Krone, J.R. (1997). Surface plasmon resonance biomolecular interaction analysis mass spectrometry. 1. chip-based analysis. Anal. Chem. **69**, 4,363-4,368.

Nelson, R.W., Krone, J.R. and Jansson, O. (1997). Surface plasmon resonance biomolecular interaction analysis mass spectroscopy. 2. Fibre-optic-based analysis. Anal. Chem., **69**, 4,369-4,374.

Nice, E., Lackmann, M., Smyth, F., Fabri, L., and Burgess, A.W. (1994). Synergies between micropreparative high-performance liquid chromatography and an instrumental optical biosensor. J. Chromatography A, **660**, 169-185.

Nice, E., Layton, J. Fabri., L., Hellman, U., Engström, Å., Perrson, B. Burgess, A. W. (1993). Mapping of the Ab and receptor domains of G-CSF using an optical biosensor: Comparison with ELISA: Competition studies. J. Chromatography, **646 (1)**, 159-168.

Nicholls, I.A., Andersson, L.I., Mosbach, K., and Ekberg, B. (1995). Recognition and enantioselection of drugs and biochemicals using molecularly imprinted polymer technology. Trends in Biotech., **13**, 47-51.

Nicolini, C., Adami, M., Dubrovsky, T., Erokhin, V., Facci, P., Paschkevitsch, P., and Sartore, M. (1995). High-sensitivity biosensor based on LB technology and on nanogravimetry. Sensors and Actuators B, **24-25**, 121-128.

Nieba, L., Krebber, A., and Plückthun, A. (1996). Competition BIAcore for measuring true affinities: Large differences from values determined from binding kinetics. Anal. Biochem., **234**, 155-165.

Nieba, L., Nieba-Axmann, S. E., Persson, A., Hämäläinen, M., Edebratt, F., Hansson, A., Lidholm, J., Magnusson, K., Karlsson. Å. F., Pluckthun, A. (1997). BIACORE analysis of histidine-tagged proteins using a chelating NTA sensor chip. Anal. Biochem., **252**, 217-228.

Nilsson, P., Persson, B., Uhlén, M., and Nygren, P-Å. (1995). "Real-time" monitoring of dna manipulations using biosensor technology. Anal. Biochem., **224**, 400-408.

Nissim, A., Hoogenboom, H. R. Tomlinson, I. M., Flynn, G., Modgley, C., Lane, D., Winter, G. (1994). Antibody fragments from a single pot phage display library as immunological reagents. EMBO J., **13(3)**, 692-698.

Noel, D., Bernardi, T., Navarro-Teulon, I., Marin, M., Martinetto, J-P., Ducancel, F., Mani, J-C., Pau, B., Piechaczyk, M., and Biard-Piechaczyk, M. (1996). Analysis of the individual contributions of immunoglobulin heavy and light chains to the binding of antigen using cell transfection and plasmon resonance analysis. J. Immunol. Methods., **193**, 177-187.

Nolan, O., and O'Kennedy, R. (1990). Bifunctional antibodies: concept, product and applications. Biochim. Biophys. Acta., **1040**, 1-11.

Oddie, G.W., Gruen, L.C., Odgers, G.A., King, L.G., and Kortt, A.A. (1997). Identification and minimization of non-ideal binding effects in BIAcore analysis: Ferritin/anti-ferritin Fab' interaction as a model system. Anal. Biochem., **244**, 301-311.

O'Neill, S. (1999). Rapid analytical methods based on monitoring colour changes. Ph.D.Thesis, Dublin City University, Ireland.

O'Shannessy, D.J., and Winzor, D.J. (1996). Interpretation of deviations from pseudo-first-order kinetic behavior in the characterization of ligand binding by biosensor technology. Anal. Biochem., **236**, 275-283.

Pack, P., and Plückthun, A. (1992). Miniantibodies: Use of amphipathic helices to produce functional, flexibly linked dimeric F_v fragments with high avidity in *Escherichia coli*. Biochemistry, **31**(6), 1,579-1,584.

Pack, P., Müller, K., Zahn, R., and Plückthun, A. (1995). Tetravalent miniantibodies with high avidity assembling in *Escherichia coli*. J. Mol. Biol., **246**, 28-34.

Panayotou, G., Waterfield, M.D., and End, P. (1993). Riding the evanescent wave. Current Biology, **3**(12), 913-915.

Parham, P. (1983). On the fragmentation of monoclonal IgG_1, IgG_{2a}, IgG_{2b} from BALB/c mice. J. Immunol., **131**(6), 2,895-2,902.

Parsons, I.D., and Stockley, P.G. (1997). Quantification of the *Escherichia coli* methionine repressor-operator interaction by surface plasmon resonance is not affected by the presence of a dextran matrix. Anal. Biochem., **254**, 82-87.

Parsons, I.D., Persson, B., Mekhalfia, A., Blackburn, G.M., and Stockley, P.G. (1995). Probing the molecular mechanism of action of co-repressor in the *E.coli* methionine repressor-operator complex using surface plasmon resonance (SPR). Nucleic Acids Research, **23**(2), 211-216.

Peacock, J. S., Colsky, A.S., and Pinto, V.B. (1990). Lectins and antibodies as tools for studying cellular interactions. J. Immunol. Methods., **126**, 147-157.

Persson, B., Stenhag, K., Nilsson, P., Larsson, A., Uhlén, M., and Nygren, P.-Å. (1997). Analysis of oligonucleotide probe affinities using surface plasmon resonance: A means for mutational scanning. Anal. Biochem., **246**, 34-44.

Piehler, J., Brecht, A., and Gauglitz, G. (1996(a)). Affinity detection of low molecular weight analytes. Anal. Chem., **68**, 139-143.

Piehler, J., Brecht, A., Geckeler, K.E., and Gauglitz, G. (1996(b)). Surface modification of direct immunoprobes. Biosensors and Bioelectronics, **11**(6/7), 579-590.

Piehler, J., Brecht, A., Giersch, T., Kramer, K., Hock, B., and Gauglitz, G. (1997). Affinity characterization of monoclonal and recombinant antibodies for multianalyte detection with an optical transducer. Sensors and Actuators B, **38-39**, 432-437.

Plant, A.L., Brigham-Burke, M., Petrella, E.C., and O'Shannessy, D.J. (1995). Phospholipid/alkanethiol bilayers for cell-surface receptor studies by surface plasmon resonance. Anal. Biochem., **226**, 342-348.

Plückthun, A. (1990). Antibodies from *Escherichia coli*. Nature (London), **347**, 497-498.

Porstmann, T., and Kiessig, S.T. (1992). Enzyme immunoassay techniques. An overview. J. Immunol. Methods., **150**, 5-21.

Prime, K.L., and Whitesides, G.M. (1991). Self-assembled organic monolayers: model systems for studying adsorption of proteins at surfaces. Science, **252**, 1,164-1,167.

Quinn, J.G., O'Kennedy, R., Smyth, M., Moulds, J., and Frame, T. (1997). Detection of blood group antigens utilising immobilised antibodies and surface plasmon resonance. J. Immunol. Methods., **206**, 87-96.

Raether, R. (1967). Surface plasmon oscillations as a tool for surface examinations. Surf. Sci., **8**, 233.

Ray, T. (1989). Antibodies in HLA serology, in: Antibodies volume II, a practical approach, Catty, D. (eds.), IRL Press, Oxford New York Tokyo, pp31-75.

Rehàk, M., Šnejdárková, M., and Otto, M. (1994). Application of biotin-streptavidin technology in developing a xanthine biosensor based on a self-assembled phospholipid membrane. Biosensors and Bioelectronics, **9**, 337-341.

Reid, M.E., and Lomas-Francis, C. (1997). The blood group antigen facts book, Academic press, New York.

Reinartz, H.W., Quinn, J.G., Zanker, K. and O'Kennedy, R. (1996). Bispecific multivalent antibody studied by "real-time" interaction analysis for the development of an antigen-inhibition enzyme-linked immunosorbent assay. Analyst, **121**, 767-771.

Reiter, Y., Brinkmann, U., Kreitman, R.J., Jung, S-H., Lee, B., and Pastan, I. (1994). Stabilization of the Fv fragments in recombinant immunotoxins by disulfide bonds engineered into conserved framework regions. Biochemistry, **33**, 5,451-5,459.

Renken, J., Dahint, R., Grunze, M., and Josse, F. (1996). Multifrequency evaluation of different immunosorbents on acoustic plate mode sensors. Anal. Chem., **68**, 176-182.

Rickert, J., Weiss, T., Kraas, W., Jung, G., and Göpel, W. (1996). A new affinity biosensor: Self-assembled thiols as selective monolayer coatings of quartz crystal microbalances. Biosensors and Bioelectronics, **11**(6/7), 591-598.

Robert, B., Mach, J-P., Mani, J-C., Ychou, M., Folli, S., Artus, J-C., and Pèlegrin, A. (1996). Cytokine targeting in tumors using a bispecific antibody directed against carcinoembryonic antigen and tumor necrosis factor α_1. Cancer Research, **56**, 4,758-4,765.

Roberts, S., Cheetham, J.C., and Rees, A.R. (1987). Generation of an antibody with enhanced affinity and specificity for its antigen by protein engineering. Nature (London), **328**, 731-734.

Robinson, G.A. (1993). Optical immunosensing systems – are they meeting market needs? Biosensors and Bioelectronics, **8**, xxxvii-xxxx.

Roden, L. D., and Myszka, D. G. (1996). Global analysis of the macromolecular interaction recorded on BIAcore. Biochem. Biophys. Research Communications, **225**, 1073-1077.

Rodrigues, M.L., Presta, L.G., Kotts, C.E., Wirth, C., Mordenti, J., Osaka, G., Wong, W.L.T., Nuijens, A., Blackburn, B., and Carter, P. (1995). Development of a humanized disulfide-stabilized Anti-$p185^{HER2}$ Fv-β-lactamase fusion protein for activation of a cephalosporin doxorubicin prodrug. Cancer Research, **55**, 63-70.

Ronot-Trioli, C., Trouillet, A., Veillas, C., and Gagnaire, H. (1996). Monochromatic excitation of surface plasmon resonance in an optical-fibre refractive-index sensor. Sensors and Actuators A, **54**, 589-593.

Sakai, G., Saiki, T., Uda, T., Miura, N., and Yamazoe, N. (1995). Selective and repeatable detection of human serum albumin by using piezoelectric immunosensor. Sensors and Actuators B, **24-25**, 134-137.

Sakai, G., Saiki, T., Uda, T., Miura, N., and Yamazoe, N. (1997). Evaluation of binding of human serum albumin (HSA) to monoclonal and polyclonal antibody by means of piezoelectric immunosensing technique. Sensors and Actuators B, **42**, 89-94.

Samuelson, A., Yari, F., Hinkula, J., Ersoy, O., Norrby, E., and Persson, M.A.A. (1996). Human antibodies from phage libraries: neutralizing activity against human immunodeficiency virus type-1 equally improved after expression as Fab and IgG in mammalian cells. European J. Immunol., **26**(12), 3,029-3,034.

Sandhu, J.S. (1992). Protein engineering of antibodies. Critical Reviews in Biotechnology, **12**(5/6):437-462.

Savage, P., Rowlinson-Busza, G., Verhoeyen, M., Spooner, R.A., So, A., Windust, J., Davis, P.J., and Epenetos, A.A. (1993). Construction, characterisation and kinetics of a single chain antibody recognising the tumour-associated antigen placental alkaline phosphatase. Cancer. **68**, 738-742.

Scalice, E. R., Sharkey, D. J., and Daiss, J. L. (1994). Monoclonal antibodies prepared against the DNA polymerase from *Thermus equaticus* are potent inhibitors of enzyme activity. J. Immunol. Methods., **172**, 147-163.

Schmitt, H.-M., Brecht, A., Piehler, J., and Gauglitz, G. (1997). An integrated system for optical biomolecular interaction analysis. Biosensors and Bioelectronics, **12**(8), 809-816.

Scholthof, K.B.G., Zhang, G., and Karu, A.E. (1997). Derivation and properties of recombinant Fab antibodies to the phenylurea herbicide diuron. J. Agricultural Food Chem., **45**(4), 1,509-1,517.

Schott, M.E., Frazier, K.A., Pollock, D.K., and Verbanac, K.M. (1993). Preparation, characterization, and in vivo biodistribution properties of synthetically cross-linked multivalent antitumor antibody fragments. Bioconjugate Chemistry, **4**, 153-165.

Schuck, P. (1996). Kinetics of ligand binding to receptor immobilized in a polymer matrix, as detected with an evancescent wave biosensor. I. a computer simulation of the influence of mass transport. Biophysical Journal, **70**, 1,230-1,249.

Schuck, P., and Minton, A.P. (1996). Analysis of mass transport-limited binding kinetics in evanescent wave biosensors. Anal. Biochem., **240**, 262-272.

Schuster, S.C., Swanson, R.V., Alex, L.A., Bourret, R.B., and Simon, M.I. (1993). Assembly and function of a quaternary signal transduction complex monitored by surface plasmon resonance. Nature (London), **365**, 343-347.

Schwarz, F.P., Puri, K.D., Bhat, R.G., and Surolia, A. (1993). Thermodynamics of monosaccharide binding to concanavalin A, Pea (*Pisum sativum*) lectin, and lentil (*Lens culinaris*) lectin. J. Biol. Chem., **268**(11), 7,668-7,677.

Sedgwick, J.D., and Holt, P.G. (1986). The ELISA-plaque assay for the detection and enumeration of antibody-secreting cells. J. Immunol. Methods., **87**, 37-44.

Severs, A.H., and Schasfoort, R.B.M. (1993). Enhanced surface plasmon resonance inhibition test (ESPRIT) using latex particles. Biosensors and Bioelectronics, **8**, 365-370.

Shinohara, Y., Kim, F., Shimizu, M., Goto, M., Tosu, M., and Hasegawa, Y. (1994). Kinetic measurement of the interaction between an oligosaccharide and lectins by a biosensor based on surface plasmon resonance. European Journal of Biochemistry, **223**, 189-194.

Skerra, A., and Plückthun, A. (1988). Assembly of a functional immunoglobulin Fv fragment in *Escherichia coli*. Science, **240**, 1,038-1,041.

Skibo, G.G., Koval, L.M., and Zhulin, I.B. (1988 (a)), Biotechnological aspects of lectins, in: Lectins: Biology, Biochemistry, Clinical Biochemistry, Kocourek, J., and Freed, L.J. (eds.), vol 7, PART X, Sigma Chemical Company, pp417-426.

Skibo, G.G., Koval, L.M., and Zhulin, I.B. (1988 (b)), Effective method of cell agglutination analysis by lectins, in: Lectins: Biology, Biochemistry, Clinical Biochemistry, Kocourek, J., and Freed, L.J. (eds.), volume 7, PART IX, Sigma Chemical Company, pp405-409.

Skibo, G.G., Koval, L.M., and Zhulin, I.B. (1988 (c)). Lectins as a tool for the study of developing neurons, in: Lectins: Biology, Biochemistry, Clinical Biochemistry, Kocourek, J., and Freed, L.J. (eds.), volume 7, PART IX, Sigma Chemical Company, pp339-343.

Soderlind, E., Simonsson, A. C. Borrebaeck, C. A. K. (1992). Phage display technology in antibody engineering: Design of phagemid vectors and in vitro maturation systems. Immunological Rev., **130**, 109-124.

Soderlind, E., Simonsson, A. C., Lagerkvist, A. C., Duenas, M., Malmburg, A. C. Ayala, M., Danielsson, L., Borrebaeck, C.A.K. (1993). Chaperonin assisted phage display of antibody fragments on filamentous bacteriophages. Biotechnology, **11**, 503-507.

Spinke, J., Oranth, N., Fattinger, C., Koller, H., Mangold, C., and Voegelin, D. (1997). The bidiffractive grating coupler: application to immunosensing. Sensors and Actuators B, **38-39**, 256-260.

Spooner, R.A., Murray, S., Rowlinson-Busza, G., Deonarain, M.P., Chu, A., Epenetos, A.A. (1994). Genetically engineered antibodies for diagnostic pathology. Human Pathology, **25**(6), 606-613.

Stamatakis, K., and Tien, C. (1993). A simple model of cross-flow filtration based on particle adhesion. AIChE Journal., **39(8)**, 1,292-1,302.

Steegborn, C., and Skládal, P. (1997). Construction and characterization of the direct piezoelectric immunosensor for atrazine operating in solution. Biosensors and Bioelectronics, **12**(1), 19-27.

Stein, T., and Gerisch, G. (1996). Oriented binding of a lipid-anchored cell adhesion protein onto a biosensor surface using hydrophobic immobilization and photoactive crosslinking. Anal. Biochem., **237**, 252-259.

Steinem, C., Janshoff, A., Wegener, J., Ulrich, W-P., Willenbrink, W., Sieber, M., Galla, H-J. (1997). Impedance and shear wave resonance analysis of ligand-receptor interactions at functionalized surfaces and of cell monolayers. Biosensors and Bioelectronics, **12**(8), 787-808.

Stenberg, E., Persson, B., Roos, H., and Urbaniczky, C. (1991). Quantitative determination of surface concentration of protein with surface plasmon resonance using radiolabeled proteins. J. colloid and Interface Science., **143**(2), 513-526.

Su, H., Kallury, K.M.R., and Thompson, M. (1994). Interfacial nucleic acid hybridization studies by random primer ^{32}P labeling and liquid-phase acoustic network analysis. Anal. Chem., **77**, 769-777.

Suresh, M.R., Cuello, A.C., and Milstein, C. E. Langone, J.J. and Van Vunakis, H. (1986). Bispecific monoclonal antibodies from hybrid hybridomas. Meth. Enzymol., **121**, 210-229.

Sychugov, V.A., Tishchenko, A.V., Lyndin, N.M., and Parriaux, O. (1997). Waveguide coupling gratings for high-sensitivity biochemical sensors. Sensors and Actuators B., **38-39**, 360-364.

Tatsuma, T., and Buttry, D.A. (1997). Electrochemical/piezoelectric dual-response biosensor for heme ligands. Anal. Chem., **69**, 887-893.

Terskikh, A.V., Le Doussal, J-M., Crameri, R., Fisch, I., Mach, J-P., and Kajava, A.V. (1997). "Peptabody": A new type of high avidity binding protein. Proc. Natl. Acad. Sci. (USA), **94**, 1,663-1,668.

Texas Instruments (1997), Affinity Analysis. Web site
http, //www.ti.com/research/docs/spr/affinity analysis, © Texas Instruments Incorporated.

Traunecker, A., Lanzavecchia, A., and Karjalainen, K. (1991). Bispecific single chain molecules (Janusins) target cytotoxic lymphocytes on HIV infected cells. EMBO J. **10**(12), 3,655-3,659.

Traunecker, A., Lanzavecchia, A., and Karjalainen, K. (1992). Janusin: new molecular design for bispecific reagents. Cancer, Supplement, **7**, 51-52.

Turbadar, T. (1964). Complete absorption of plane polarized light by thin metallic films. Opt. Acta., **11**, 207.

Turner, A.P.F. (1997). Immunosensors: The next generation. Nature Biotechnology. **15**, 421.

Tutt, A., Stevenson, G.T., and Glennie, M.J. (1991). Trispecific $F(ab')_3$ derivatives that use cooperative signaling via the TCR/CD3 complex and CD2 to activate and redirect resting cytotoxic T cells. J. Immunol., **147**(1), 60-69.

Vadgama, P., and Crump, P.W. (1992). Biosensors: Recent Trends. A Review. Analyst., **117**, 1,657-1,669.

Van Den Heuvel, D.J., Kooyman, R.P.H., Drijfhout, J.W., and Welling, G.W. (1993). Synthetic peptides as receptors in affinity sensors: a feasibility study. Anal. Biochem., **215**, 223-230.

Vaughan, A. and Millner, A. (1989). Fluorescent activated cell sorting, in: Antibodies volume II, a practical approach, Catty, D. (eds.), IRL Press, Oxford New York Tokyo, pp201-222.

Wang, R., Narang, U., Prasad, P.N., and Bright, F.V. (1993). Affinity of anti-fluorescein antibodies encapsulated within a transparent sol-gel glass. Anal. Chem., **65**, 2,671-2,675.

Ward, L.D. (1985). Measurement of ligand binding to proteins by fluorescence spectroscopy. Meth. Enzymol., **117**, 400-414.

Watts, H.J., and Lowe, C.R. (1994). Optical biosensor for monitoring microbial cells. Anal. Chem., **66**(15), 2,465-2,470.

Watts, H.J., Yeung, D., and Parkes, H. (1995). "Real-time" detection and quantification of DNA hybridization by an optical biosensor. Anal. Chem., **67**, 4,283-4,289.

Weetall, H. (1993). The activation of inorganic carriers by silanization. Biosensors and Bioelectronics, **8**(5), x-xi.

Welsch, W., Klein, C., Von Schickfus, M., and Hunklinger, S. (1996). Development of a Surface Acoustic Wave Immunosensor. Anal. Chem., **68**, 2,000-2,004.

Williams, W.V., Moss, D.A., Kieber-Emmons, T., Cohen, J.A., Myers, J.N., Werner, D.B., and Greene, M.I. (1989). Development of biologically active peptides based on Ab structure. Proc. Natl. Acad. Sci. (USA), **86**, 5,537-5,541.

Williams, R.A., and Blanch, H.W. (1994). Covalent immobilization of protein monolayers for biosensor applications. Biosensors and Bioelectronics, **9**, 159-167.

Wink, Th., Van Zuilen, S.J., Bult, A., and Van Bennekom W.P. (1997). Self-assembled monolayers for biosensors. Analyst, **122**, 43R-50R.

Wiseman, T., Willston, S., Brandts, J. F. (1989). Rapid measurement of binding constants and heats of binding using a new titration calorimeter. Anal. Biochem., **179**, 131-137.

Wood, S.J. (1993). DNA-DNA hybridization in real time using BIAcore. Microchemical Journal, **47**, 330-337.

Xiang, J., Pan, Z., Attah-Poku, S., Babiuk, L., Zhang, Y., and Liu, E. (1992). Production of hybrid bispecific antibody recognizing human colorectal carcinoma and CD3 antigen. Molecular Biotherapy, **4**, 15-23.

Yamamoto, K., Ishida, C., Shinohara, Y., Hasegawa, Y., Konami, Y., Osawa, T., and Irimura, T. (1994). Interaction of immobilized recombinant mouse c-type macrophage lectin with glycopeptides and oligosaccharides. Biochemistry, **33**, 8,159-8,166.

Yeatman, E.M. (1996). Resolution and sensitivity in surface plasmon microscopy and sensing. Biosensors and Bioelectronics, **11**(6/7), 635-649.

Yoshitake, S., Imagawa, M., Ishikawa, E., Niitsu, Y., Urushizaki, I., Nishiura, M., Kanazawa, R., Kurosaki, H., Tachibana, S., Nakazawa, N., and Ogawa, H. (1982). Mild and efficient conjugation of rabbit Fab' and horseradish peroxidase using a maleimide compound and its use for enzyme immunoassay. J. Biochem., **92**, 1,413-1,424.

Zhang, C., Feng, G., and Sui, S. (1997). Study on behaviour of QCM sensor in loading variation. Sensors and Actuators B, **40**, 111-115.

Zydney, A.L., and Colton, C.K. (1984). A red cell deformation model for hemolysis in cross flow membrane plasmapheresis. Chem. Eng. Commun., **30**, 191-207.